Design Synthesis Exercise

AERIS: An unmanned aerial vehicle capable of continuous flight by using remote power

DSE TEAM 4

Final Report

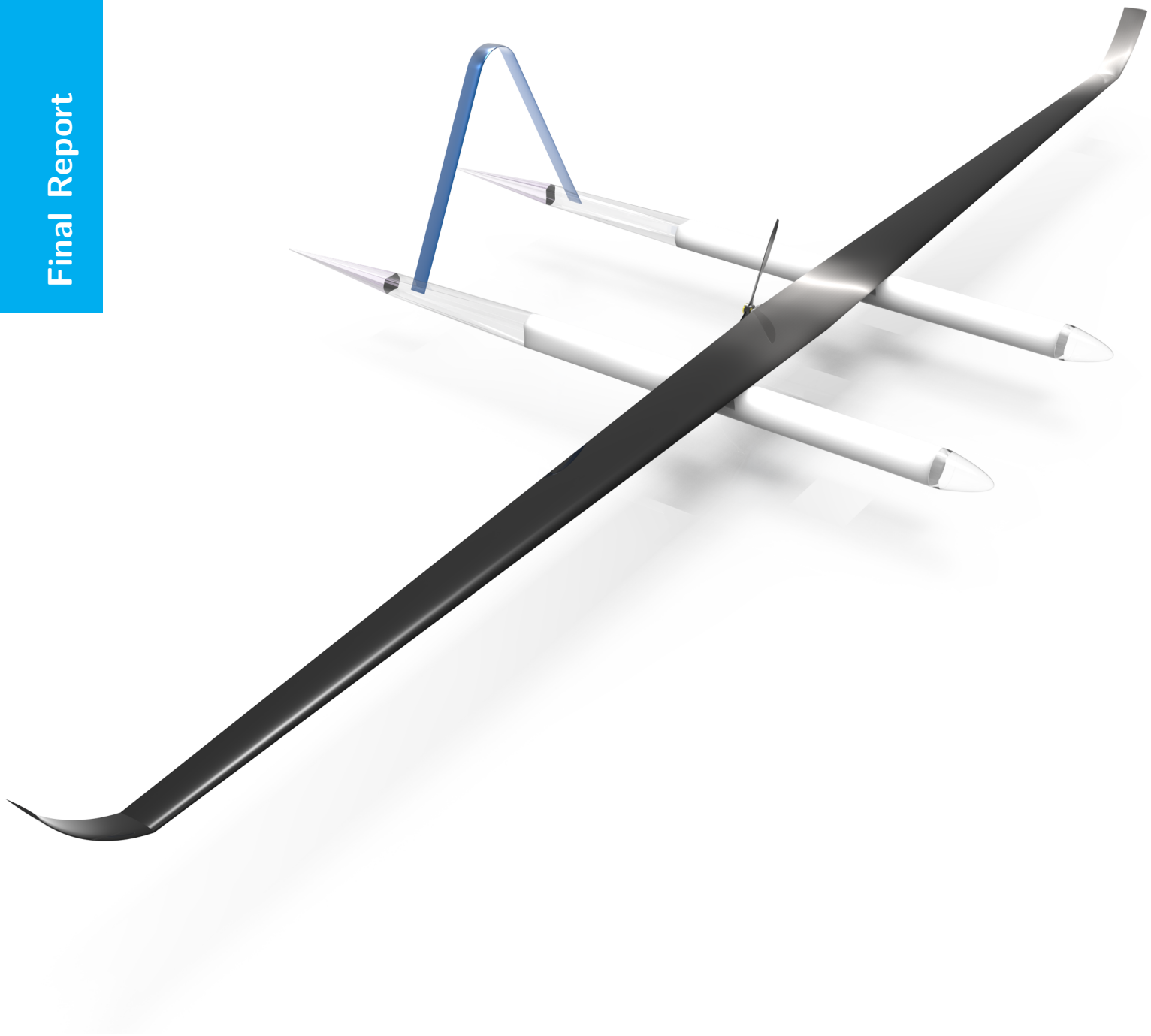

TU Delft Delft University of Technology

Challenge the future

AE3-200 DSE FINAL REPORT

AERIS - REMOTE POWERED UAV

by

Aendekerk, F.J.	**4180022**
Dijk, N. van	**4168143**
Geurts, G.J.H.	**4001877**
Helvoort, D.T.J. van	**4132505**
Mkhoyan, T.	**1527312**
Mobertz, X.R.I.	**4161289**
Rijal, S.	**4124294**
Storteboom, A.G.	**4164814**
Thuijs, J.R.	**4096428**
Winters, B.B.	**4089782**

In partial fulfillment of the requirements for the degree of

Bachelor of Science
in Aerospace Engineering

at Delft University of Technology

Project duration:	*November 10, 2014 – January 30, 2015*	
Principal tutor:	*Dr. R.M. Groves,*	*TU Delft*
DSE coaches:	*S. Minghe, MSc,*	*TU Delft*
	H.W. Ho, MSc,	*TU Delft*

TU Delft Delft University of Technology

PREFACE

L.S.,

This is the Final Report of team four's Design Synthesis Exercise in which a "continuous flying Unmanned Aerial Vehicle (UAV)" is considered. In this report, we explain which methods were used for sizing of the concept that was chosen in the baseline report. These methods will be verified and validated to ultimately present the detailed design of UAV. After presenting the detailed design, AERIS will be subjected to a performance analysis to prove that it is able to meet the requirements as set in the requirement discovery tree that was initially presented in the baseline report.

Next, we elaborate on the business roadmap which explains what steps should be made in order to actually put the design on the market. This is done by performing a market analysis, developing a revenue model and a five-year plan.

We would like to express our gratitude to Dr. R.M. Groves, H.W. Ho MSc, M. Shan MSc and Dr. V. Papadakis for guiding us through the whole DSE project, and hope to see all of you during our final review.

Sincerely,

X.R.I. Mobertz
Project Manager

CONTENTS

List of Figures vii

List of Tables ix

Acronyms xi

List of Symbols xii

1 Introduction 2

2 Project Description 4
- 2.1 Mission Description . . . 4
- 2.2 Requirement Discovery Tree . . . 4
- 2.3 Human Resources Allocation . . . 7

3 Risk Strategy 8
- 3.1 Technical Risk Assessment . . . 8
  - 3.1.1 Context Establishment . . . 8
  - 3.1.2 Risk Identification . . . 9
  - 3.1.3 Risk Assessment and Risk Map . . . 9
  - 3.1.4 Risk Evaluation . . . 9
  - 3.1.5 Risk Treatment . . . 10
  - 3.1.6 Risk Monitoring and Review . . . 11
  - 3.1.7 Updated Context . . . 11
- 3.2 Contingency Management Strategy . . . 11

4 Concept Description 14
- 4.1 Operations and Logistic Concept Description . . . 14
  - 4.1.1 Laser Station . . . 14
  - 4.1.2 Offices . . . 14
  - 4.1.3 Aircraft . . . 14
- 4.2 Functional Breakdown Structure . . . 15
- 4.3 Functional Flow Diagram . . . 15

5 System Design 19
- 5.1 Hardware . . . 19
- 5.2 Software . . . 21
  - 5.2.1 Air Segment . . . 21
  - 5.2.2 Ground Segment . . . 22
- 5.3 Electrical . . . 24

6 System Sizing and Characteristics 28
- 6.1 Engineering Strategy . . . 28
- 6.2 Payload . . . 32
  - 6.2.1 Hyperspectral Imaging . . . 32
  - 6.2.2 Infrared Camera . . . 33
  - 6.2.3 Safety Infrared Camera . . . 33
  - 6.2.4 Data Rate Estimations . . . 33
  - 6.2.5 Data Cube . . . 34
  - 6.2.6 Component Integration . . . 36
  - 6.2.7 Weather Influence . . . 36

6.3 Safety . . . 37
6.4 Communication . . . 38
6.4.1 Background Information . . . 38
6.4.2 Communication Subsystems . . . 39
6.4.3 Link Budget . . . 39
6.5 Aerodynamics . . . 41
6.5.1 Airfoil Selection . . . 41
6.5.2 Wing Characteristics . . . 44
6.5.3 Lift and Drag . . . 44
6.6 Propulsion . . . 45
6.6.1 Basic Equations of Motion . . . 45
6.6.2 Linear Momentum Theory . . . 46
6.6.3 Propeller Radius . . . 46
6.6.4 Blade Design . . . 46
6.6.5 Engine Power . . . 48
6.6.6 Engine Hardware . . . 48
6.7 Stability and Control . . . 49
6.7.1 Determination of Mass Distribution . . . 50
6.7.2 Tail Sizing . . . 53
6.7.3 Vertical Tail Sizing . . . 55
6.8 Power Subsystem . . . 58
6.8.1 Energy Harvesting . . . 58
6.8.2 Battery Pack . . . 58
6.8.3 Voltages . . . 59
6.8.4 Cables . . . 59
6.8.5 Checks . . . 60
6.9 Structures . . . 61
6.9.1 Manufacturing Process . . . 61
6.9.2 General Approach . . . 62
6.9.3 Structural Design of the Wing . . . 63
6.9.4 Fuselage Design . . . 64
6.10 Flight Control . . . 65
6.10.1 Flaperons . . . 65
6.10.2 Ruddervator . . . 66
6.11 Ground System . . . 66
6.11.1 Laser Station . . . 66
6.11.2 Laser Fundamentals . . . 66
6.11.3 Pointing and Tracking System . . . 69
6.11.4 Communication . . . 71
6.11.5 Office . . . 71

7 Results: The Bigger Picture **72**
7.1 Non-Iterative Results . . . 72
7.1.1 Camera Output . . . 72
7.1.2 Communications . . . 73
7.1.3 Safety . . . 74
7.1.4 Overview Non-Iterative Parameters . . . 74

7.2 Iterative Results . . . 74
7.2.1 Aerodynamics . . . 74
7.2.2 Propulsion Results . . . 75
7.2.3 Power Subsystem . . . 77
7.2.4 Structures . . . 78
7.2.5 Summary of the Iterative Process . . . 78
7.3 Remarks on Results . . . 78
7.3.1 Take-off . . . 78
7.3.2 Landing . . . 79

8 System Analysis **81**
8.1 Verification . . . 81
8.1.1 Aerodynamics . . . 81
8.1.2 Propulsion . . . 81
8.1.3 Tailsizing . . . 82
8.1.4 Power . . . 84
8.1.5 Structural Verification . . . 85
8.2 Validation . . . 88
8.2.1 Subsystem Validation . . . 88
8.2.2 Flight Performance of AERIS . . . 89
8.3 Sensitivity Analysis . . . 90
8.3.1 Univariate Sensitivity Analysis of the Main Input Parameters . . . 91
8.3.2 Multivariate Sensitivity Analysis of the Main Input Parameters . . . 92
8.4 Performance Analysis . . . 93
8.4.1 Range . . . 94
8.4.2 Rate of Climb . . . 95
8.4.3 Solar Power . . . 96
8.4.4 Noise Characteristics . . . 96
8.4.5 Turn Radius . . . 97
8.5 Mission Analysis . . . 98
8.5.1 Wind and Gust Speed . . . 98
8.5.2 A Day with AERIS . . . 99
8.6 Reliability, Availability, Maintainability, and Safety Characteristics . . . 101
8.6.1 Reliability . . . 101
8.6.2 Availability . . . 102
8.6.3 Maintainability . . . 102
8.6.4 Safety . . . 103

9 Business Roadmap **105**
9.1 Market Analysis . . . 105
9.1.1 Market Potential . . . 105
9.1.2 Competitors . . . 106
9.1.3 Market Trend . . . 107
9.1.4 SWOT Analysis . . . 107
9.1.5 Possible Extensions Markets . . . 108
9.2 Cost Break-Down Structure . . . 108
9.2.1 Development Cost . . . 108
9.2.2 Production Cost . . . 109
9.2.3 Operation Cost . . . 110

9.3 Revenue Model . . . 111
9.3.1 Key Selling Points . . . 111
9.3.2 Government . . . 112
9.3.3 Commercial . . . 112
9.4 Five-Year Plan . . . 112

10 Discussing the Requirements **115**
10.1 Management Requirements . . . 115
10.2 Sustainability Requirements . . . 115
10.3 Equipment Requirements . . . 115
10.4 Safety Requirements . . . 115
10.5 General Mission Requirements . . . 116
10.6 Security Requirements . . . 116
10.7 Government Requirements . . . 116
10.8 Flight Performance Requirements . . . 116
10.9 Energy and Powerhouse Requirements . . . 117
10.10 Other Requirements . . . 117

11 Conclusion **118**

12 Recommendations **119**
12.1 Safety . . . 119
12.2 Payload . . . 119
12.3 Communications and Ground Station . . . 119
12.4 Aerodynamics . . . 119
12.5 Propulsion . . . 119
12.6 Power Subsystem . . . 120
12.7 Structures . . . 120
12.8 Stability . . . 120

Bibliography **121**

A Risk Matrix **126**

B Technical Drawings **127**

List of Figures

2.1 Requirement Discovery Tree (1/2) . . . 5
2.2 Requirement Discovery Tree (2/2) . . . 6
2.3 Schematic Representing the Organizational Breakdown Structure where White Blocks Represent Managerial Teams and Blue Blocks Represent Technical Teams . . . 7

3.1 Trivial Risk Assessment Process . . . 8
3.2 Table of Risks Identified and Assessed for Likelihood and Consequence . . . 12
3.3 Risk Map with the Identified Risks Assessed . . . 13
3.4 Risk Bow-Tie Likelihood and Consequence Management . . . 13

4.1 Functional Breakdown Structure . . . 16
4.2 Functional Flow Diagram for the Airborne Part . . . 17
4.3 Functional Flow Diagram for the Ground Part . . . 18

5.1 Hardware Block Diagram Air Segment . . . 20
5.2 Hardware Block Diagram Ground Station . . . 21
5.3 Software Connections of the Air Segment . . . 23
5.4 Software Connections of the Ground Segment . . . 24
5.5 Electrical System of the Air Segment . . . 26
5.6 Electrical System of the Ground Segment . . . 27

6.1 The N^2 Chart for the Final Conceptual Design . . . 31
6.2 Spectral Data Cube Obtained by Scanning the Ground . . . 35
6.3 Two Different Reflectance Profile of Spinach . . . 35
6.4 Line of Sight . . . 38
6.5 Actual Radio Datalink Hardware . . . 39
6.6 Antennae of the Unmanned Aerial Vehicle and Ground Station Respectively . . . 40
6.7 Coveragemap for the 2.4 $[GHz]$ and 430 $[MHz]$ Up- and Downlink Respectively For Unique Values of Tx . . . 41
6.8 Analysis of Lift Coefficient vs α of the Four Airfoils in XFLR5 with $Re = 500,000$ . . . 42
6.9 Analysis of Moment Coefficient vs α of the Four Airfoils in XFLR5 with $Re = 500,000$ . . . 42
6.10 Analysis of the Lift over Drag Ratio vs α of Four Airfoils in XFLR5 with $Re = 500,000$ . . . 43
6.11 NACA 2210 Airfoil Obtained from XFLR5 . . . 44
6.12 Effects of adding Winglets on Tip Vortices . . . 45
6.13 Illustration of Lift Distribution over the Span of the Wing . . . 45
6.14 The Lift over Drag Ratio of the Clark Y Airfoil as a Function of the Angle of Attack . . . 47
6.15 Visual Representation of the Actuator Disc . . . 47
6.16 Visual Representation of a Propeller Blade Section . . . 47
6.17 Example of a Composite Blade Cross Section . . . 49
6.18 Definitions of Two Coordinates Systems Definitions and the Margin Allowed For YCG Location . . . 50
6.19 Payload and System Components with 20 Battery Packs as an example with the Coordinate System indicated 51
6.20 3D MATLAB Plot of the Battery Layout for 39 Batterypacks . . . 52
6.21 Plot Showing Wing Loading Diagram With Most Aft and Most Forward Centre of Gravity Points Resulting From Battery and Payload Weight Margins . . . 55
6.22 Plot Showing The Optimum Wing Setting and Horizontal Tail Surface Area for the Required Centre of Gravity Range . . . 55
6.23 Quick Estimation Method of Vertical Tail Volume from Torenbeek . . . 57

6.24 Digitalised Version of Fast Estimation Graph from Torenbeek Translated to MATLAB . . . 57
6.25 Visualization of the Usage of Titanium and ABS . . . 62
6.26 Flow Chart of the Structural Optimization . . . 63
6.27 Visualization of the Change in the Skin Thickness of the Airfoil . . . 65
6.28 Components of a Typical Laser: 1. Gain Medium 2. Laser Pumping Energy 3. High Reflector 4. Output Coupler 5. Laser Beam . . . 66
6.29 Electrons and their Energy Levels around an Atom . . . 66
6.30 Wavelengths of Commercially Available Lasers. . . . 67
6.31 Received Power at AERIS for Different Visibilities and Charging Ranges with a 0.09 $[m^2]$ Panel and an Output Power of 2 $[kW]$ with a Wavelength of $\lambda = 1064[nm]$ . . . 69
6.32 Example of a Laser with a Pointing and Tracking System. . . . 69
6.33 Schematic Overview of the Possible Distances of Charging . . . 70
6.34 Minimum and Maximum Horizontal Range of Charging . . . 70

7.1 IR Raw Data Rate for the Velocity Range at Optimal Height . . . 72
7.2 IR Raw Data Rate in the Velocity and Altitude Range . . . 73
7.3 HSI Pixel Resolution in the Velocity and Altitude Range . . . 73
7.4 Safety Lights Planform . . . 74
7.5 Lift Distribution Over the Semi-Span of the Wing . . . 76

8.1 Six Data Points on Control and Stability Curves Generated in MATLAB . . . 83
8.2 Overlay of Two Plots: MATLAB vs Original From Torenbeek . . . 84
8.3 Simplified Load Case Used for Structural Verification . . . 86
8.4 Shear Force Diagram Used for Structural Verification . . . 86
8.5 Moment Diagram Used for Structural Verification . . . 87
8.6 Torque Diagram Used for Structural Verification . . . 87
8.7 AERIS as Created in X plane's Plane Maker . . . 90
8.8 Univariate Sensitivity of AERIS to the Design Cruise Velocity . . . 91
8.9 Univariate Sensitivity of AERIS to the Design Endurance . . . 92
8.10 Univariate Sensitivity of AERIS to the Maximum Allowable Normal Material Stress . . . 92
8.11 Univariate Sensitivity of AERIS to the Main Wing's Aspect Ratio . . . 93
8.12 Univariate Sensitivity of AERIS to Effective Material Density . . . 93
8.13 Multivariate Sensitivity of AERIS to Cruise Velocity, Aspect Ratio and Endurance (1 of 2) . . . 94
8.14 Multivariate Sensitivity of AERIS to Cruise Velocity, Aspect Ratio and Endurance (2 of 2) . . . 95
8.15 Visualisation of the Rate of Climb as a Function of Speed and Altitude . . . 96
8.16 The Load Factor Plotter Against the Speed in Meters per Second . . . 97
8.17 The Turn Radius Plotter Against the Speed in Meters per Second . . . 98
8.18 Maximum Daily Mean Wind Velocities . . . 98
8.19 Maximum Daily Gust Velocities . . . 98
8.20 Solar Radiation Power $[MJ/m^2]$ over Five Years . . . 99
8.21 The Flight Path Points of AERIS of One Day. . . . 100

9.1 Strength, Weakness, Opportunity and Threat Matrix . . . 107
9.2 Visual Representation of the Revenue Model of the Five-Year Plan . . . 113
9.3 Project Gantt Chart for the Six-Year Period after the Design Synthesis Exercise . . . 114

A.1 General Risk Matrix used for Risk Assessment . . . 126

B.1 Technical Drawing of AERIS' Main Wing . . . 127

LIST OF TABLES

2.1 The Stakeholders, Their Values and Their Norms . . . 4
2.2 Organizational Roles Within the Group with a Distinction Between Function, Responsibilities and Responsible 7

6.1 Preliminary Trade-Off to Select Configuration Type . . . 29
6.2 Rayleigh Fading Model . . . 40
6.3 Main Results Link Budget . . . 41
6.4 Obtained Airfoil Values . . . 43
6.5 Operating voltages for subsystems . . . 60
6.6 Cable Thicknesses for Subsystems . . . 60
6.7 AWG Cable Sizes . . . 61
6.8 Properties of Materials Used for the Structural Design . . . 62
6.9 Specifications of the Ground Station Laser . . . 68
6.10 Total Power Delivery at AERIS for Different Parameters . . . 68

7.1 Non-Iterative Results . . . 75
7.2 Initial Parameters . . . 75
7.3 Non-Iterative Engine Parameters . . . 76
7.4 Overview of the Park 450 Specifications . . . 76
7.5 Overview of the Power 15 Specifications . . . 77
7.6 Chord Length of Each Element of the Propeller Blade . . . 77
7.7 Blade Angle of Each Element of the Propeller Blade . . . 77
7.8 Variation of the Most Important Parameters During the Iterations . . . 79
7.9 Trade-Off Table of the Take-Off System . . . 79
7.10 Trade-Off Table of the Landing System . . . 79

8.1 Overview of the Analytical and Numerical Values Calculated of the Aerodynamics Script . . . 81
8.2 Overview of the Analytical and Numerical Values Calculated of the Propulsion Script . . . 82
8.3 Verification of Stability and Control Module: Coefficients . . . 83
8.4 Verification of Stability and Control Module: CG Locations . . . 83
8.5 Verification of Stability and Control Module: Coefficients . . . 83
8.6 Verification Values for Power Verification . . . 85
8.7 Shear Flow Verification . . . 88
8.8 The Total Distance, Time, Data Rate of Hyperspectral Imager, Power Used and Imager Covered Area per Section Respectively . . . 100

9.1 Extension Markets . . . 108
9.2 Total Development Costs for the AERIS project . . . 108
9.3 Total Initial Aerial Subsystem Costs for One and Any Extra Unmanned Aerial Vehicle . . . 109
9.4 Total Initial Ground Station Costs . . . 110
9.5 Total Operational Costs per Year . . . 111
9.6 Total Cost per Province per Year . . . 112
9.7 Total Revenue and Costs for Five Year Plan . . . 113

10.1 Compliance Table on Project Management Requirements . . . 115
10.2 Compliance Table on Sustainable Development Requirements . . . 115
10.3 Compliance Table on Sustainable Development Requirements . . . 116
10.4 Compliance Table on Safety Requirements . . . 116

10.5 Compliance Table on Mission Profile Requirements 116
10.6 Compliance Table on Security Requirements 116
10.7 Compliance Table on Government Requirements 117
10.8 Compliance Table on Flight Performance and Flight Envelope Requirements 117
10.9 Compliance Table on Energy and Powerhouse Requirements 117
10.10 Compliance Table on Other Requirements 117

ACRONYMS

a.c. aerodynamic centre. 53, 56
ABS Acrylonitrile butadiene styrene. 61, 78
AC Alternating Current. 59
AERIS AErial Research, Inspection, and Surveillance. 2–4, 14, 15, 19, 21, 24, 25, 28, 29, 32–34, 36–41, 43–45, 50–52, 54, 58, 59, 61, 65–74, 77–79, 81, 84, 88–91, 93, 94, 96–103, 105, 108–113, 115–117, 119, 120
AWG American Wire Gauge. 60, 78
BeNeLux Belgium, Netherlands and Luxembourg. 107
BLR Baseline Report. 2
BOL Beginning Of Life. 59, 78
CCD Charge-Coupled Device. 32
CFAR Constant False-Alarm Fate. 35
CMOS Complementary Metal–Oxide–Semiconductor. 32
CPU Central Processing Unit. 19, 21, 22, 25, 41, 59–61, 109
DC Direct Current. 25
DOT Design Option Tree. 2
DSE Design Synthesis Exercises. 4, 7, 108, 111, 113, 119
ELT Emergency Locator Transmitter. 37
EOL End Of Life. 59, 78, 95
ESC Electronic Speed Control. 21, 22, 85
FBS Functional Breakdown Structure. 14, 15
FFD Functional Flow Diagram. 14, 15
FPS Frames Per Second. 33
FSPL Free Space Path Loss. 40
GNSS Global Navigation Satellite System. 19
GPRS General Packet Radio Service. 106
GPS Global Positioning System. 22, 25, 60, 61, 101, 109
HR Human Resources. 7
HSI Hyperspectral Imager. 2, 15, 19, 22, 25, 32–36, 38, 39, 50, 60, 61, 72, 74, 75, 100, 105, 106, 109, 119
i.e. Id est. 28, 43, 51, 59, 85, 90, 92
ILT Inspectie Leefomgeving en Transport. 10, 111, 116
InGaAs Indium Gallium Arsenide. 19, 58, 67
IR Infrared. 2, 19, 22, 32–34, 39, 50, 70, 72, 74, 75, 100, 105, 109, 110
ISR Intelligence, Surveillance, and Reconnaissance. 107
KNMI Koninklijk Nederlands Metereologisch Instituut. 98
LED Light-Emitting Diode. 37, 74
LiDDS Live Disaster Detection System. 112
LiPo Lithium Polymer. 58
LiS Lithium Sulfur. 58, 59, 78
LoS Line of Sight. 14, 38, 40, 41, 66, 73
m.a.c. mean aerodynamic chord. 52, 54
MTR Mid-Term Report. 2, 14, 28, 32, 37, 38, 45, 58, 74, 98, 109
N^2 Systems Engineering Overview Chart of Complete System. 2, 28–30, 34, 119
NDT Non Destructive Testing. 103
OBS Organisational Breakdown Structure. 7
OCT Optical Coherence Tomography. 103
PMS Power Management System. 10, 19, 21, 24, 25, 58–60, 78
RAMS Reliability, Availability, Maintainability and Safety. 81, 101
RC Radio Controlled. 42
RDT Requirements Discovery Tree. 4, 9, 81, 101, 115, 117
RoC Rate of Climb. 44, 46, 93, 95
RPAS Remotely Powered Aerial System. 10
RPM Revolutions per Minute. 45, 46, 48, 49, 76, 77, 96, 120
RPS Revolutions per Second. 46–48, 82
SM Static Margin. 54
SMS Short Messaging Service. 106
SWIR Short-Wavelength Infrared. 32
SWOT Strength, Weakness, Opportunity and Threat. 107
UAV Unmanned Aerial Vehicle. ii, 2, 4, 8–11, 14, 15, 19, 21, 22, 24, 25, 32, 34, 36–39, 45, 48–53, 55, 58, 59, 63, 69, 71–74, 78, 79, 81, 84, 85, 88–90, 95–97, 100, 102, 103, 105–113, 116–120
UHF Ultra High Frequency. 38, 109
USA United Stated of America. 106
USB Universal Serial Bus. 33, 39
VAT Value Added Tax. 109, 110
VNIR Visible Near-Infrared. 32

List of Symbols

Greek Symbols

α_i	[rad]	Induced angle of attack	47
α_h	[deg]	Angle of attack of the horizontal tailplane	53
α	$[deg]$	Angle of attack	42–44
β	[deg]	Sideslip angle	53
η_{earo}	[-]	Airfoil efficiency	53
η_{prop}	[-]	Propulsive efficiency	46, 48, 77
μ	$[\frac{m}{s}]$	Bank angle	98
ϕ	[rad]	Angle of incidence	47, 48
π	[-]	Transcendental number	46–48, 77
ψ_{inv}	[deg]	Dihedral angle of the inverted v-tail tailplane	57
ρ_{air}	[-]	Density of air	46, 47, 97
ρ_i	$\left[\frac{kg}{m^3}\right]$	Density of the material used in section i	63
σ_{max}	[Pa]	Ultimate shear strength of the wing material	62, 64
σ_y	[Pa]	Highest occurring longitudinal stress (y-direction)	64
τ_{max}	[Pa]	Ultimate shear force	62, 88
ω	$[\frac{rad}{s}]$	Angular speed of propeller blade	48

Alphanumeric Symbols

A_{cross}	$[m^2]$	Cross-sectional area of the airfoil	64
A_{encl}	$[m^2]$	Area enclosed by the structural part of an airfoil section	64
A_i	$[m^2]$	Area of section i	63, 64
b	[m]	Wingspan	45
b_f	$[m^2]$	Width of the fuselage	53
$\bar{c}$	$[m]$	Chord length of the mean aerodynamic chord	54
C_D	[-]	Drag coefficient	43, 47, 48
g_0	$[m/s^2]$	Gravitational acceleration	97
C_{D_0}	[-]	Profile drag coefficient	45
$C_{D_{0_w}}$	[-]	Profile drag coefficient on wing	45
$C_{D_{min}}$	[-]	Minimum drag coefficient on wing	45
C_f	[-]	Skin friction drag during laminar flow	45
cg	[m]	Coordinate of the centre of gravity	49–54, 59, 63, 89
CG_{LE}	$[\% \cdot \bar{c}]$	Coordinate system w.r.t. leading edge of mean aerodynamic chord	50, 52, 54
cg_x	[m]	X-coordinate of the centre of gravity	63
cg_z	[m]	Z-coordinate of the centre of gravity	63
c	[m]	Chord length	47, 48
c_i	[-]	Chord length of the i-th element	48
C_{L_0}	[-]	Zero lift coefficient	43, 74
C_L	[-]	Lift coefficient	43, 47, 48, 97
$C_{L_{\alpha_w}}$	[-]	Lift rate coefficient of the wing without the tail	83
$C_{L_{\alpha_h}}$	[-]	Lift rate coefficient of the horizontal tail	54, 83
$C_{L_{\alpha_{wf}}}$	[-]	Lift rate coefficient of the wing and fuselage	54, 83
$C_{L_{max}}$	[-]	Maximum lift coefficient	41–44, 53
C_{L_h}	[-]	Lift coefficient of the horizontal tailplane	54
$C_{L_{wf}}$	[-]	Lift coefficient of the wing and fuselage	53, 54

C_m	$\left[=\frac{M}{\frac{1}{2}\rho {V_h}^2 S_h \bar{c}}\right]$	Coefficient of the aerodynamic moment about the Y-axis, three-dimensional flow	43, 83
C_{m_α}	$\left[=\frac{M}{\frac{1}{2}\rho {V_h}^2 S_h \bar{c}}\right]$	Derivative of the moment coefficient around a.c w.r.t. angle of attack	53, 56, 89
$C_{m_{ac}}$	$\left[=\frac{M}{\frac{1}{2}\rho {V_h}^2 S_h \bar{c}}\right]$	Moment coefficient around the Y-axis and the a.c of the wing, three-dimensional flow	54
$C_{n_{\beta_f}}$	[-]	Contribution of the fuselage to the directional derivative C_{n_β}	56, 83
$C_{n_{\beta_i}}$	[-]	Contribution of the wing setting to the directional derivative C_{n_β}	56
C_{β_n}	[-]	Derivative of the yawing moment coefficient around a.c w.r.t. angle of sideslip	56, 83, 89
$C_{n_{\beta_p}}$	[-]	Contribution of the propeller to the directional derivative C_{n_β}	56, 83
$(\frac{t}{c})_{i+1}$	[-]	Thickness over chord ratio of the i-th + 1 element	48
dD	[N]	Drag force per section	47
dL	[N]	Lift force per section	47
dQ	[Nm]	Propeller element torque	47
dr	[m]	Propeller element size	47, 48
D	[N]	Drag	46
ds	[m]	Element length	64
dT	[N]	Propeller element thrust	47
D_{trim}	[N]	Trim Drag produced by the tail	58
dV	$[m^3]$	Volume one blade element	48
E	$[Pa]$	Young's modulus	64
E	[h]	Endurance in hours	94
V_h	[-]	Speed experienced by the horizontal tailplane after downwash effect of the wing	54
V_∞	[-]	Free stream speed of the wing	54
F_M	[-]	Function of Mach number	45
fov	[m]	Field of view	32–34, 72, 99
f_{tc}	[-]	Function of thickness ratio	45
cg_0	$[\% \cdot \bar{c}]$	Coordinate system w.r.t. fuselage nose and symmetry plane	50
I	[A]	Amperage	60
I_{eng}	$[A]$	Ampere of the engine	77
I_{xx}	$[m^4]$	Moment of inertia around the x-axis	63, 64
I_{xz}	$[m^4]$	Moment of inertia around the xz plane	63, 64
I_{zz}	$[m^4]$	Moment of inertia around the z-axis	63, 64
l	[m]	Cable length	60
$\frac{L}{D}$	[-]	Lift over drag ratio	44
$LEradius$	[m]	Leading edge radius	43
l_h	$[=x_h - x_{c.g.}]$	Tail length of horizontal tail	54, 56
L_{inV}	[N]	Tail lift force generated by the inverted V-tail	58
l_v	$[=x_v - x_{c.g.}]$	Tail length of vertical tail	56
L_y	$[m]$	Distance between symmetry line of AERIS and the section of interest in y-direction	64
$\dot{m}$	[kg/s]	Mass flow of air	46
M_x	[Nm]	Internal moment about the x-axis	63, 64, 86, 87
n	$[\frac{rev}{s}]$	Propeller angular velocity rps	46–48, 77
n	[-]	Maximum load factor	97, 98
P_a	[J/s]	Total power of the aircraft available	46, 48, 95
P_r	[J/s]	Total power of the aircraft required	46, 48, 95
P_{cruise}	[J/s]	The power of the engines in cruise condition	48
P_{max}	[J/s]	The maximum power of the engines	48
Q	[Nm]	Propeller torque	46, 77

q	$[mm^2]$	Cable thickness	60
q_s	$[Pa \cdot m]$	Shear flow	64, 88
R	[km]	Range of the UAV	94
R	$[m]$	Local radius of curvature during bending	64
r	[m]	Propeller element distance from root	47, 48, 64
R	[m]	Propeller blade radius	46–48
R	[m]	Turn radius	97
S	$[m^2]$	Surface of the wing	97
sc_x	[m]	X-coordinate of the shear centre	64
sc_z	[m]	Z-coordinate of the shear centre	64
S_h	$\left[m^2\right]$	Surface of the horizontal tailplane	53, 54, 57, 58
$\frac{S_h}{S}$	[-]	Surface ratio of horizontal tail over wing	54, 83
S_{net}	$[m^2]$	Surface area of wing minus the area projected from central part of fuselage	53
S_{inv}	$\left[m^2\right]$	Surface of the inverted v-tail tailplane	57, 58
n	[%]	Maximum energy loss over cable	60
S_v	$\left[m^2\right]$	Surface of the vertical tailplane	53, 56–58
S_{wet}	[-]	Wetted surface area	45
S_x	[N]	Internal shear load in x-direction	63, 64
S_z	[N]	Internal shear load in z-direction	63, 64, 86
t	[m]	Local airfoil skin thickness	64
$(\frac{t}{c})_i$	[-]	Thickness over chord ratio of the i-th element	48
$\left(\frac{t}{c}\right)_{max}$	[-]	Maximum thickness ratio	45
T	[N]	Thrust produced by engines	46
t_{min}	[m]	Minimum manufacturing thickness	62
$t_{req,}s$	[m]	Local thickness required to withstand shear flow	88
T_y	[Nm]	Internal torsion about the y-axis	63, 64
U	[V]	Voltage	60
V_0	[m/s]	Assumed ground speed for cruise	46–48, 94, 97
V_e	$[\frac{m}{s}]$	Assumed ground speed for cruise	46
V	$[V]$	Voltage of the engine	77
V_{turn}	$[\frac{m}{s}]$	Turn speed	97
W	[N]	Weight of the aircraft	46, 95, 97
$\bar{x}$	$[m]$	X-location of the c.g. of the UAV expressed as percentage of m.a.c.	52
x	[m]	Distance between section centre and iterative grid-wise shear centre in x-direction	64
$x_{\bar{c.g.}}$	[m]	Abscissa of the c.g. expressed in percentage of MAC from leading edge	54
$x_{c.g.}$	[m]	Abscissa of the c.g.	53, 54, 83
$\frac{X_{cg_{LEMAC}}}{l_f}$	$[\% \cdot \bar{c}]$	Ratio of the x-coordinate of the cg location MAC w.r.t. fuselage lenght	51–53
x_i	[m]	Location of airfoil section i in x-direction	63, 64
$x_{p.p.}$	[m]	Abscissa of the n.p.	53, 54
$\bar{x}_{w_{ac}}$	[m]	Abscissa of the a.c. of the wing expressed in percentage of MAC from leading edge	54
$x_{w_{ac}}$	[m]	Abscissa of the a.c. of the wing	54
YCG_0	$[\% \cdot \bar{c}]$	Y-coordinate of the center of gravity location of the entire UAV	50, 51
z	[m]	Distance between section centre and iterative grid-wise shear centre in z-direction	64
z_i	[m]	Location of airfoil section i in z-direction	63, 64

SUMMARY

The Final Report is the last in a series of four reports written by a group of ten undergraduate engineering students of the Delft University of Technology for the Design Synthesis Exercise of their bachelor programme describing the design synthesis of AERIS: an unmanned aerial vehicle capable of continuous flight by using remote power. The final mission need statement of AERIS is defined as follows: "*Mankind needs longer range, more sustainable and more accessible unmanned aerial vehicle(s) to provide accurate and continuous Earth observation*". This report succeeds the Mid-Term Report which had considered a variety of different candidate architectures to carry out the mission. Significant progress has been made in the development of the risk strategy, functional breakdown and flow diagrams, system design, and the development of a new design tool tasked with the iterative sizing of AERIS from the subsystem level. This design tool has also been analysed in univariate and multivariate sensitivity analyses to determine the impact of the major tool inputs and hence the effect that yet undetermined errors might have on the system's design.

The final report's primary focus is to give the reader an insight into the complex design process of a cutting-edge extreme endurance unmanned aerial vehicle. Not only does it provide readers with an account of what the team learned over the duration of the ten week project and how that learning was applied to the creation of a design tool, it also highlights several little-studied areas of knowledge that should be pursued by future researchers and designers working on this topic. One of these areas is the integration of external laser power in the design of future aircraft. Advantages include broadening the fuel mix of those future aircraft in a world in which fossil fuels, as well as other natural resources, are becoming increasingly scarce. Another advantage is the so-called "snowball effect" which comes from removing (part of) the power system from an aircraft. The second is a more robust and detailed analysis of the novel structural design strategy outlined in this report to iteratively add material to a complex shape to bear pre-defined loads until the structure performs adequately.

The design synthesis exercise project description included a number of requirements. They included the ability to fly and monitor the surface between 50 and 100 $[\frac{km}{h}]$ at an operational altitude between 100 and 4000 $[m]$. The case study to be considered by the team was the ability to continuously monitor urban and natural landscapes in the province of South Holland in the Netherlands, and the possibility to cover the whole of the Netherlands five years after its initial production. The payload was initially a single hyperspectral imager, but was later expanded to include an infrared camera for night-time monitoring. AERIS' mission is comprised of three segments: the aircraft, a control centre and a laser station. The latter of the two form the ground station. Every function relevant to the mission were identified and presented in a functional breakdown structure and in functional flow diagrams. Hardware, software and electrical diagrams are also included in this report.

AERIS' design was guided by an comprehensive N^2 systems engineering chart and the value-sensitive design philosophy of the project, which was implemented at every design level since the baseline report. One especially important value was sustainable development. The final systems engineering trade-off was, in part, influenced by the design options' performance with regard to its impact on the environment. This performance parameter was valued particularly high and was often in direct competition with other performance parameters. Nevertheless, the highest-scoring concept was chosen; the report includes its modelled performances, stability and control characteristics, and its projected market potential according to an analysis on Western markets all of which are performed by the team.

The result of running the new iterative MATLAB design tool is an aircraft with a calculated mass of 12.54 $[kg]$, and a wingspan 9.05 $[m]$. Though its design was modelled and successfully flown in X plane, this "final" design is far from final, and requires a significant amount of physical tests to validate the numerical model (the design tool). Furthermore, the team identified several lesser-studied areas of knowledge of particular interest to any similar future projects.

1. INTRODUCTION

Ever since the very first flight in 1903, aircraft and their missions have been limited in endurance. Since then, technologies have proven effective, yet the world flight endurance record for an unmanned aircraft stands at just over 336 $[hrs]$ after more than one hundred years of progress. [1] Take-offs and climbs are mission segments that are particularly fuel intensive; to increase aircraft endurance, it is best to minimize the impact of these mission segments, or eliminate them entirely. From the perspective of any business-minded individual, frequent ground activities such as re-fuelling and carrying out maintenance is time consuming as well as costly and inconvenient.

This team was given the opportunity to come up with a partially laser powered UAV design capable of continuous flight. In recent years, technological breakthroughs in lasers have widened their applications; they are no longer limited to cutting or welding, and may be considered as a way to wireless transmit power. Combined with other energy harvesting technologies, using lasers may increase the aircraft's endurance, range and business potential. The final report is the last in a series of four reports whose primary focus is to give the reader an insight into AErial Research, Inspection, and Surveillance (AERIS)' complex design process. Not only does it provide readers with an account of what the team learned over the duration of the ten week project, and how that learning was applied to the creation of a design tool for, it also highlights several little-studied areas of knowledge that should be pursued further by researchers and designers alike (another design synthesis exercise, for example).

The name AERIS was chosen for this UAV project; Aeris is latin for 'air' and an acronym, for ***AE**rial **R**esearch, **I**nspection, and **S**urveillance* as well as a reference to Iris, an ancient personification of rainbows and a messenger of the gods in Greek mythology. The case study to be considered by the team was the ability to continuously monitor urban and natural landscapes in the province of South Holland in the Netherlands, as well as evaluating what it would take to cover the whole of the Netherlands five years after its initial production. The payload was initially comprised of a single Hyperspectral Imager (HSI) in the project description, but was later expanded by the team to include an Infrared (IR) camera for night-time activities. AERIS' mission is made up of three segments: the UAV, a control centre and a laser station.

The requirements from the project description and several additional indirect and direct stakeholder requirements the team created were documented in the Baseline Report (BLR); these essentially limiting the UAVs design space. Following their discovery, these requirements were categorized according to the norms and values that they represented. They will be restated in Chapter 2 of this reports. Those requirements were then further broken down in to what the team considered key, killer, and a variety of performance requirements. The Design Option Trees (DOTs) of the BLR were the results of an extensive and effective brainstorm session performed by the team, with each design option being a possible solution for each specific function. Each main DOT category was traded off according to the importance ratings of the performance parameters. This eventually lead to the elimination of the non-feasible design options which formed the basis for the Mid-Term Report (MTR).

In the MTR, a top-down approach was utilized to get the remaining design options from the BLR to narrow the scope of the design further. Although the number of design options significantly reduced with respect to the DOT as presented in BLR, many solutions to the design problem remained. These options - or candidate architectures - were: a high aspect ratio glider, a flying wing, a Pandlt wing and a Zeppelin. A more detailed analysis was done to gather the additional information that was required to trade off the options to choose the final candidate architectures. The analysis included the general sizing of those candidate architectures, which was done by choosing typical values for each architecture, which in turn required the team to research each architecture. The sizing process was based on a systems engineering Systems Engineering Overview Chart of Complete System (N^2) chart which essentially gave an overview of how the subsystems were related to each other in the overall system and took the form of a MATLAB design tool. Each architecture was sized according to the same fixed payload and communication mass and power rating. Wiring and actuators were only taken into account by assuming an additional mass block to account for these unknowns.

After each of the four remaining candidate architectures were sized, they were traded off according to several fuzzy mathematical choice models. This trade-off indicated that the high aspect ratio powered glider performed the best with enough margin to convince the group that it was the right choice. Following this decision, the theoretical performance of the glider concept was also examined more closely in the MTR: its approximate range, climb performance, noise characteristics and stability and control qualities were all estimated. The sensitivity analysis of the design tool was also performed, which showed that script used for the initial sizing and trade-off for the final concept was stable. The final technical contribution of the MTR was the generation of several powered glider configurations to be analysed further in the Final Report. Next to these technical feats, a preliminary market investigation was performed in the MTR as well, which identified possible clients as well as the expected costs and annual revenues of the project in the Netherlands, accompanied by a risk map. The risk

map provided the team with an overview of all of the risks associated with the project, and orders them in severity. Combined with a comprehensive contingency management strategy that is used throughout the design and in its development phase.

The structure of this Final Report is as follows: the project analysis - including the mission need statement, mission statement, project requirements and human resource management scheme - is presented in Chapter 2. The updated risk strategy and contingency management plan is then given in Chapter 3, which gives an overview of each of the identified threats to the project, as well as their possible consequences for the design. It was particularly important to perform this updated risk analysis before developing AERIS' design further. Following this, Chapter 4 gives an overview of the entire system as well as each of its subsystems. Combined with the requirements in Chapter 2, this overview helped to visualize the physical connections between each of the component (sub-) systems in Chapter 5. Following this, the approach to develop AERIS further is discussed in Chapter 6; this is done at the subsystem level and was finally implemented in a new MATLAB design tool. The results of this sizing process is presented in Chapter 7. To ensure that the script performed as expected, each part was also verified, as discussed in Chapter 8 by comparing that component of the design tool's results to analytical solutions to some problem. In addition to the tool's verification, its results were traded off to obtain AERIS' final conceptual design, whose theoretical performance was then analysed further and finally validated in the X plane simulator. Once the precise performance and mission capabilities were known, a business roadmap could then be planned out, and is given in Chapter 9. This roadmap accounts for the design's continued growth to mature as AERIS expands its reach from Zuid-Holland to cover the whole Netherlands within five years. Hereafter, Chapter 10 shows the extent to which each specific requirement is met. Finally, this report is concluded with the conclusion and recommendations for future work as they are presented in Chapters 11 and 12 respectively.

2. PROJECT DESCRIPTION

This chapter describes the project provided to the team four in November 2014 and discusses the initial set of tasks. The chapter is structured in such a way that it analyses the project's assignment and defines the mission need statement and the mission statement that was used during the complete Design Synthesis Exercises (DSE) in Section 2.1. Hereafter, both the requirements set by the client and by the project team are presented by means of a Requirements Discovery Tree (RDT) in Section 2.2. Finally, it concludes with an overview of the management of human resources in Section 2.3.

2.1. MISSION DESCRIPTION

The mission description as provided to the project team in November 2014 described the deliverable of a case study to design a wireless powered UAV for monitoring of the waterways of Zuid-Holland in the Netherlands. In addition to this pilot case, the project description also outlined the need for the design to be scalable such that the system could monitor urban and natural landscapes in the Netherlands as a whole. In addition to the initial mission description, several requirements have been set by the client on performance, safety and reliability, sustainability, engineering budgets and costs. These requirements will be presented in more detail in the succeeding section.

In order to give shape to the challenge the team is facing, a mission need statement has been specified as follows: *Mankind needs longer range, more sustainable and more accessible UAVs to provide accurate and continuous earth observation.* The mission need statement was the desire from the market for the product to be designed by this team. It describes the niche that AERIS will operate in, after it has been successfully designed.

Using the mission need statement, it is possible to define the mission statement of AERIS as follows: *The UAV shall provide a reliable, sustainable and accessible system capable of accurate and continuous monitoring urban areas, natural landscapes, coastlines and weather in the Netherlands from 2016 onwards.* The mission statement is the foundation for the continuation of this report and has been the basis for this project team during the duration of the DSE.

2.2. REQUIREMENT DISCOVERY TREE

Before the design phase can start, a more thorough and deeper analysis was performed on the requirements to get a more complete insight on those aspects that prove to be vital for the design. The result of this analysis is presented in this section. Before presenting the requirements in a RDT, which is a consistent manner to identify requirements of all different types, all stakeholders and their respective values and norms are inventoried. The stakeholders that have been identified and their respective values and norms are presented in Table 2.1.

Table 2.1: The Stakeholders, Their Values and Their Norms

Direct stakeholders	***Values***	***Norms***
Employees	Reputation, finance	Job security
Company owners	Reputation, finance, safety, security	Market-competitiveness
Clients	Performance, sustainable development, safety	High coverage capabilities, low down-time, "no-gap" coverage, fail-safe operation use of renewable energy, low-impact use of materials, low energy consumption
Government	Human welfare	Laws & legislation respected, economic growth
Shareholders	Finance, reputation, economic efficiency	Market-competitiveness
Investors	Finance, economic efficiency	Market-competitiveness
Suppliers	Finance, reputation	Product availability
Indirect stakeholders		
Local communities	Privacy, sensory experience, safety	Fail-safe operation, privacy protection, minimize sensory impact
Companies	Privacy, (negative) reputation	Privacy protection
Environmentalists	Animal welfare, sustainable development	Minimise health risks to wildlife, minimize sensory impact, use of renewable energy use of renewable energy, use of low-impact/renewable materials

The norms and values in Table 2.1 form the basis of the RDT. Two main categories are used; requirements that originate from the stakeholders and requirements that strongly relate to the system itself. The values are presented next, after which the different norms are selected for each value. Looking at the norms, requirements are generated. An overview of the RDT is presented in Figures 2.1 to 2.2. A legend of both figures is included in Figure 2.2. Both figures are, in essence, part of the same RDT, but to make it readable, they are split up in to two parts. It should be noted that the compliance of these requirements with respect to the end result is presented in Chapter 10.

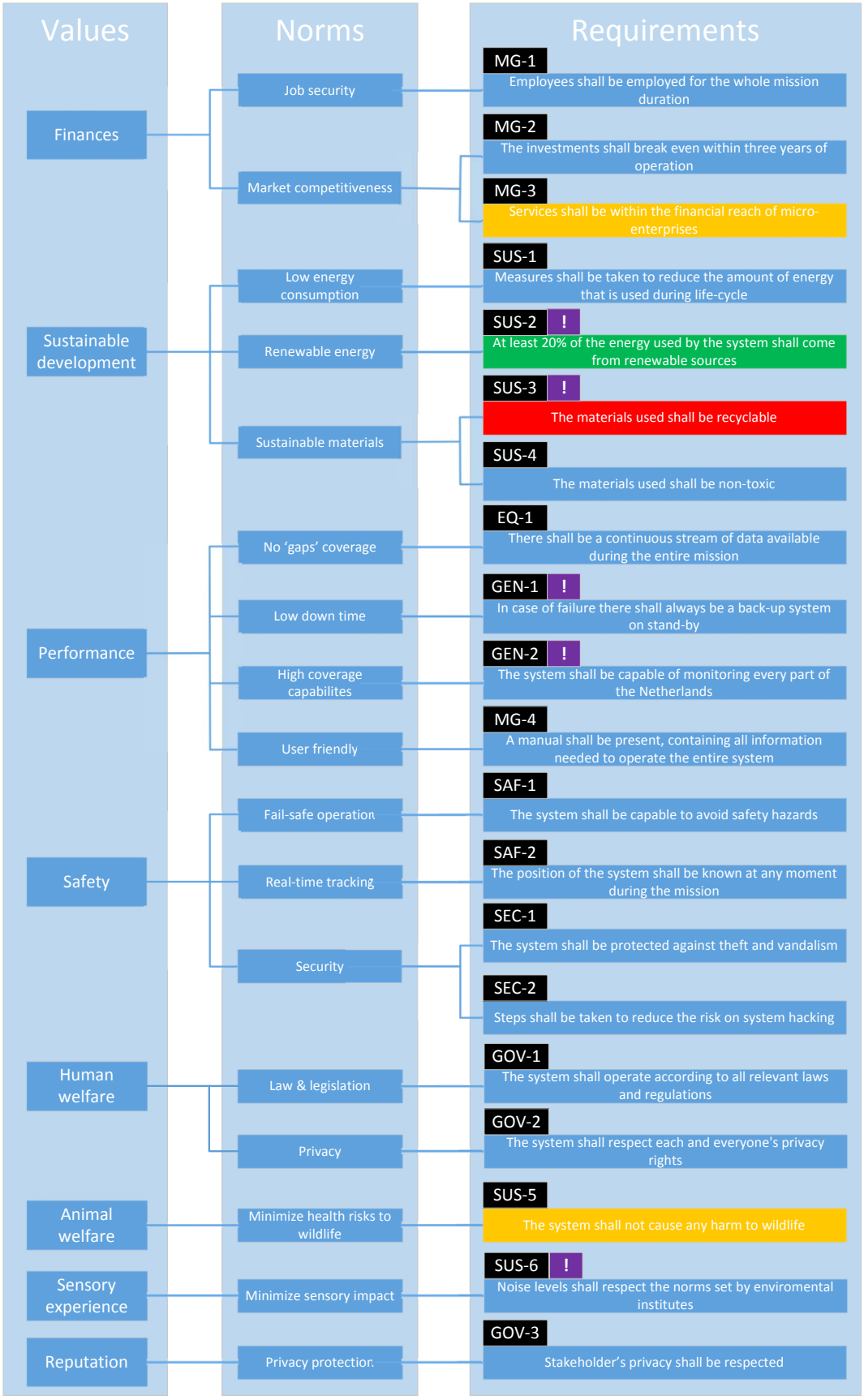

Figure 2.1: Requirement Discovery Tree (1/2)

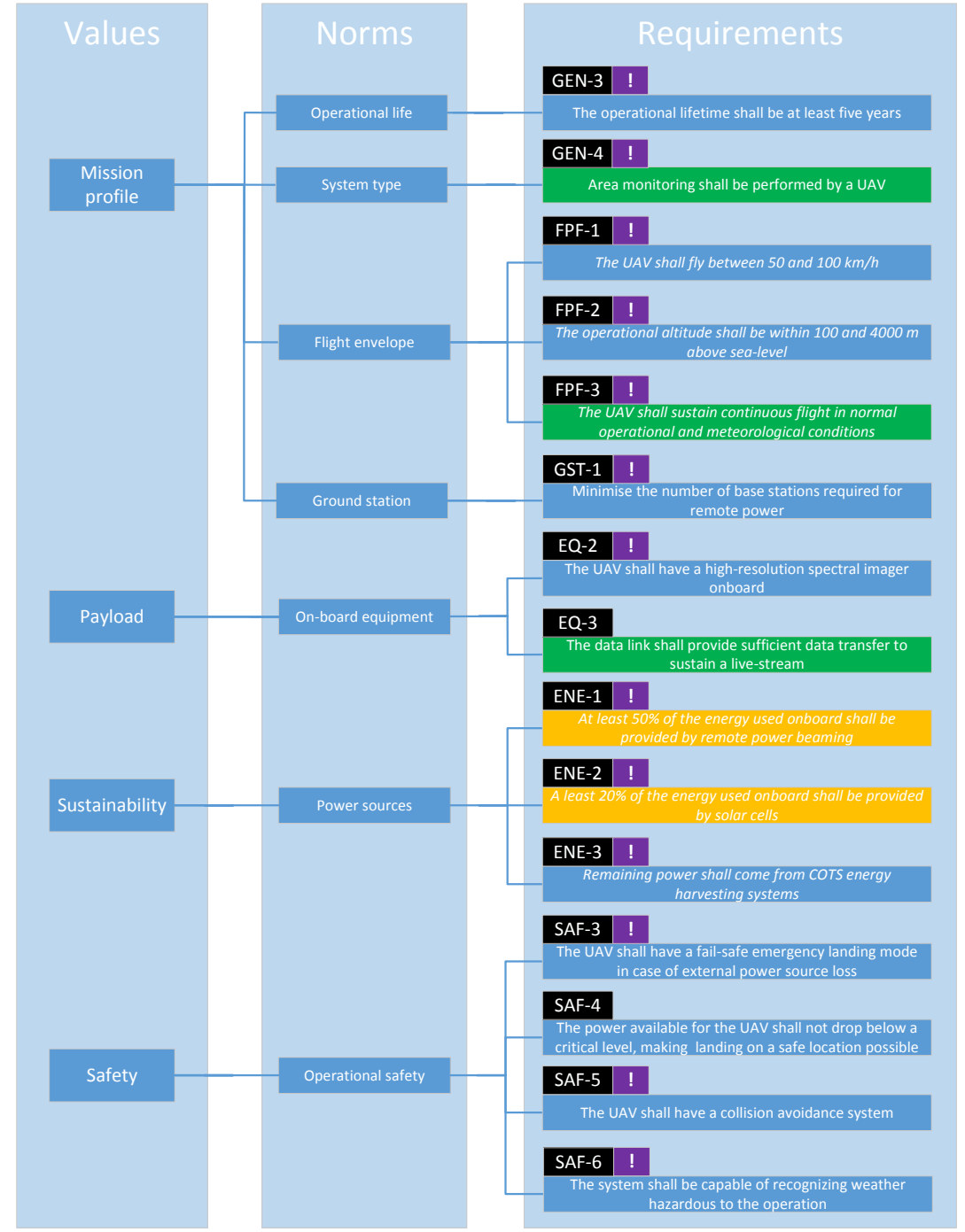

Figure 2.2: Requirement Discovery Tree (2/2)

2.3. HUMAN RESOURCES ALLOCATION

Several organisational and technical tasks have been defined and divided over the members of the project team. This section presents the Human Resources (HR) allocation and the Organisational Breakdown Structure (OBS) that was in effect during the DSE. The organisational and managerial structure of the project team is presented in Table 2.2 and the OBS is presented.

Table 2.2: Organizational Roles Within the Group with a Distinction Between Function, Responsibilities and Responsible

Function	***Responsibilities***	***Responsible***
Project Manager	Assign organisational and departmental roles to team members; Guide team members by providing general overview of the entire project; Assign resources to the designated project tasks; Monitoring the progress of the project; Manage deadlines; Chair meetings and keep proper communications with tutor and coaches.	X.R.I. Mobertz
Systems Engineer	Organising the entire design process; Ensuring that the design philosophy is strictly observed during the entire process Take care of the communication between engineering departments;	D.T.J. van Helvoort
Chief Editor	Keeping consistency in latex reports and deliverables; check spelling and grammar and general layout; Checking for plagiarism; Ensuring that the report meets the technical and quality standards	T. Mkhoyan
Chief Operations	Responsible for operations, business and marketing; Risk assessment	B.B. Winters
Secretary	Taking minutes of meetings; Maintaining the logbook Chair meetings and keep proper communications with tutor and coaches	G.J.H. Geurts

In Figure 2.3, blue blocks (if printed in black and white, the grey blocks) represent the technical task distribution amongst team members. Each member responsible for the particular technological function can be identified with help of this diagram. Despite these divisions in roles, all the team members have been providing assistance, supervision, and recommendations to each other during the entire project to improve the quality of the overall work. White blocks represent the managerial task distribution that some group members had over the course of the DSE.

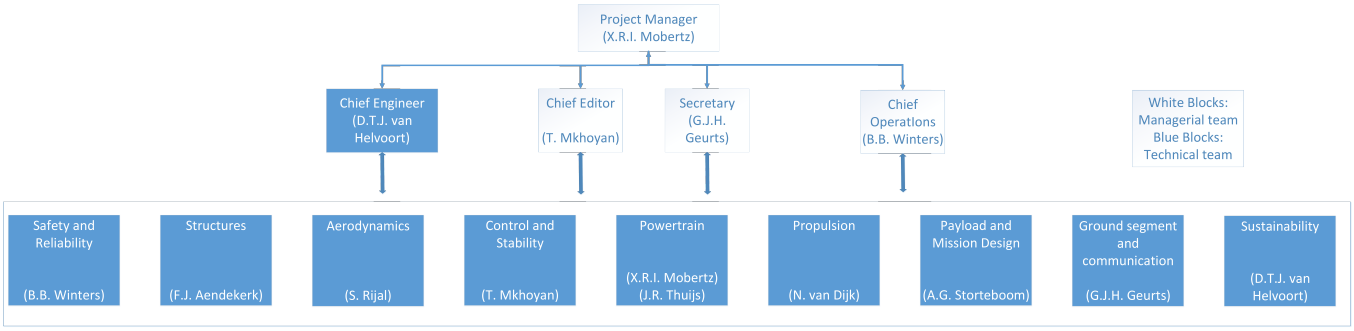

Figure 2.3: Schematic Representing the Organizational Breakdown Structure where White Blocks Represent Managerial Teams and Blue Blocks Represent Technical Teams

3. Risk Strategy

In each design and any operation one is involved in, risks exist. The design and operations of novel technology, in which one wants to power a continuous semi-autonomous UAV over rural areas with laser-light, especially possesses several severe threats. Therefore this project can only continue with a proper risk strategy in mind.

The foundation of every risk strategy is based on the definition of risk. Risk is defined as the product of the likelihood of an event to occur and the consequence this effect has. [2] To have an effective risk strategy one is first required to identify the risks and assess them accordingly. The complete process of the technical risk assessment is described in Section 3.1. However, identifying all possible risks is impossible. For this reason, a proper contingency management strategy is required. It is a strategy and philosophy this team is continuously aware of and improves the overall resilience of the project. The contingency management strategy will be presented in Section 3.2.

3.1. Technical Risk Assessment

Julian Talbot and Miles Jakeman have written an extensive body of knowledge covering the topics of security risk management. This report uses the foundation laid down by Talbot and Jakeman to assess the technical risks involved in this project. This book is the foundation of many risk assessments in the security and safety domain and the theories described in this book are applicable to our design situation. [2]

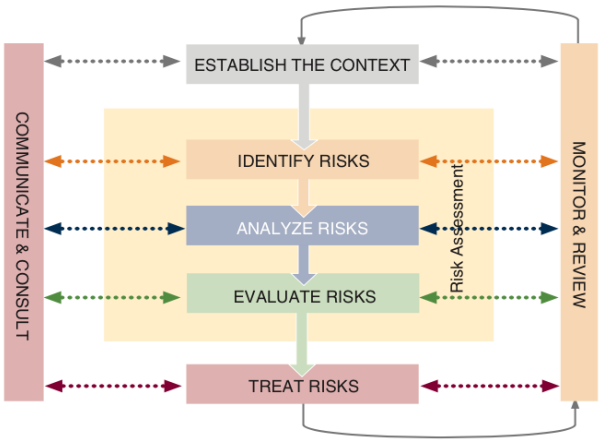

Figure 3.1: Trivial Risk Assessment Process [2]

At the highest level of abstract the risk assessment process should at least cover the following: establishment of organisational context, risk identification, risk analysis, risk evaluation, development of a treatment plan, monitoring, and the establishment of a new context. This process is visualised in Figure 3.1. It should be noted that a proper risk assessment thus already presents some, but most likely not all, barriers and/or controls for the contingency management that is treated later in this report.

For the assessment and evaluation of risk there exists a proven tool. This tool is commonly used for technical risk analysis in many industries and is called the risk matrix. A visualisation of the risk matrix is found in Appendix A. This tool will eventually be used to assess all identified risks. At any point of the design, only a limited level of risk assessment is possible since at each stage of the design new specific risks arise. As the design progresses towards production and operations, more specific and detailed risks shall be identified and assessed using this strategy.

3.1.1. Context Establishment

Context establishment helps to establishes the context of the strategic, organizational, and threat domain in which the assessment takes place. [3] It is helpful to define criteria in which the threat/risk will be evaluated against, as well as the structure of this evaluation. The context will be defined by collecting information on the project's internal and external environments. Analysing this information combined with focussed intelligence on these environments is the basis for a solid context assessment. After the context has been defined, it is possible to identify risks. This topic is covered in the succeeding section.

It is possible to make a distinction between external and internal context. Externally one needs to take into account the business environment, social environment, regulatory environment, competitive environment, financial environment, political environment, and external stakeholders. In order to identify these environments for this project, the RDT is used and described in Chapter 2. Using this visualisation it can easily be seen what values (or environment/stakeholder) are of importance and what norms and requirements are relevant for the key external environments.

The internal environments that require research are those environments in which this project operates. One should consider topics like: people, information, property & equipment, reputation, financial, and capability. Accordingly it is possible to detect threats on these assets. This is described in the next section.

3.1.2. RISK IDENTIFICATION

With the assets of this project, and more importantly, the context of these assets known, it is possible to identify the risks involved. It should be noted that risk identification is always limited to the creative spirit of the risk manager. To cover risks not identified by the risk manager it is important to have a proper resilience build into the culture and technology of the system. This contingency management will be elaborated in more detail in Section 3.2.

Furthermore, looking at the RDT, it is possible to identify critical areas in the system. A region is denoted as critical, as soon as this region fails and key requirements are not met. The two regions in which occur risk in this project are the UAV and ground station. They are thereby also the most vulnerable large objects at the moment this system is operational. Risks that impose a threat for critical regions are likely to have a larger consequence in the risks assessment later on. For now it aids the risk manager in a creative process; to focus on risks that have consequences on those regions.

Risks can be found in many different categories. Typical risk categories are: disaster, financial, reputation, legal & compliance, market, environment, expansion, human resources, project, reporting & oversight, fraud, and information technology. Risks are structured with a unique identifier (ID), a risk number, which is composed out of the product of chance and likelihood of that event, and a risk category. Each event, or risk, is described along with its possible cause and consequence. The result of the current state of our risks identification process is presented in Figure 3.2.

3.1.3. RISK ASSESSMENT AND RISK MAP

After the risk identification, the next step in the technical risk assessment is to actually asses the identified risks. Risks are assessed by looking at two parameters, their respective likelihood and consequence. Likelihood is distinguished between the qualitative likelihood and quantitative likelihood and ranges from rare to almost certain. For consequences the team looked at different assets, such as: people, information, property & equipments, reputation, financial, and capabilities. Consequences vary from insignificant to extensive. A typical risk assessment tool is the risk matrix shown in Appendix A. To properly analyse the identified risks, each risk needs to be properly assessed with the risk matrix tool. Problems arise when identifying the likelihood and consequence. To prevent going into too much detail at this stage, engineering experience and fast research on the internet are used to asses the different parameters. Ideally, when entering the in depth analysis, this assessment is completed with more background information and research. To be conservative, risks have been rounded upwards.

The result of the risk assessment is visible in Figure 3.2 and is visualised in the risk map, Figure 3.3. With each risk properly assessed, it is possible to say 'how high' a certain risk is. This information is practical since the higher a risk is, the more attention it deserves to maintain the consequences. But first, before risks are treated, they need to be evaluated. The highest risk at this stage is loss of contact (ID:28). At this stage this event is actually made up from different underlying causes. For instance, the communication system can be both distorted at the ground station as in the air and this again can have several reasons. Again, to be conservative, this event has been assessed as likely if no measures are taken. Also the consequence is very high if nothing is done to minimise it. The evaluation and treatment of these risks is discussed in the succeeding sections.

3.1.4. RISK EVALUATION

Risk evaluation focusses on if the risks are acceptable. It is required to know how tolerant this project and its systems are to risks. With sufficient adequate barriers the project should be able to cope with the risks involved. This involves a high level of resilience when one wants to cover most risks. It might be acceptable, for instance, to do not have specific barriers set up for earthquakes when the ground station operates on a location where earthquakes are very unlikely to occur. On the other hand, for instance, a barrier for a different risk, such as flooding which is more likely, might impose alterations to the system on such a level that the system is able to cope with earthquakes too. So it should be kept in mind that there exists overlap between several risks.

Losing contact with the drone can be seen as unacceptable and not tolerable. Idem for the risk of losing power in the air. However, being hit by lightning, should be tolerable since prevention can be very difficult with unpredictable weather conditions. This is also the case for terrorists that want to do harm to the system. They can hardly be controlled and an attack on the system and thus losing hardware by a terrorist attack can be seen as acceptable on a risk management point of view.

3.1.5. RISK TREATMENT

With risk treatment we look for the possibility of applying treatments to 'cope' with the risk. It is possible to lower a risk by either decreasing the likeliness of an event or by decreasing the consequence of an event. For instance, it is impossible to prevent flooding of rivers, but by placing the ground system on higher grounds the consequences are minimised.

In general it is preferable to reduce, rather than to eliminate the risk. Risks can be: avoided, reduced, accepted or even exploited to create opportunities. For instance, a market shift can initially be a threat for the system but with slight alterations to the system a new market may present itself. This is visualised when finishing the risk assessment cycle, by redefining the context, which should be updated after a market shift.

The last part of this section presents an appropriate treatment for the highest risks identified yet.

ID28: LOSS OF CONTACT

Probable causes should be minimised. Since most likely causes are failing communication systems either on-board or on the ground. They should be designed with redundancy and safety margins in mind. It should be considered to increase redundancy in the air by having a second communication systems on-board to be fail-safe. Additionally, to decrease the consequence of a failing communication system, the UAV can be programmed in such a way that whenever communication fails the system continues with an emergency procedure and initiate an emergency landing on a predefined location. This greatly reduces direct fatal consequence for the hardware but still reduces mission capabilities. Finally, this can be solved by having a second backup UAV ready for flight to save the mission. It is preferable to know the reliability of the system to guarantee that in a high percentage no third UAV is required. Also it is preferable that maintenance is made not labour intensive, such that the UAV that is out of order is repaired quick and easy.

ID31: LOSS OF POWER IN THE AIR

Causes are technically related, or bad power management on-board. Redundancy in wiring and including safety margins in the design treat direct technical related causes. Reducing the probability of flying the batteries empty is assured by installing a proper Power Management System (PMS) in the software. As a minimum requirement, the UAV should always be able to have enough battery power to reach a ground station or an emergency landing location. One option is a multitude of these zones and locations is required to increase mission applications by covering a larger area. Allowing the system to have sufficient power to reach an emergency landing location whenever it is failing to reach a ground station, minimises the consequences. Preferable, there is enough power for communications after the emergency landing to send a beacon to the controller with its location. With very sudden bad weather it might even be the case that the emergency landing location is not met. The beacon still allows the system to not go lost and thereby wasting the hardware and polluting the environment.

ID:25 PERMITS OF OPERATIONS

This event is currently noted as a very high risk. At this time there exists only limited knowledge on legislation that can be applied on UAVs. Currently Dutch legislation describes that no commercial flights with Remotely Powered Aerial System (RPAS) are allowed for anyone, unless an exemption is made by theInspectie Leefomgeving en Transport (ILT). [4] Additionally, to be allowed to fly, no autonomous operations are allowed and flight shall be conducted by two pilots at all time. This regulation is a direct result from the lack of legislation concerning RPAS. Causes can be managed by initially increasing the knowledge on legislation. Hereafter, the consequences can be managed by acting accordingly. If it can be assured beforehand that our mission profile is not viable before a certain date, the set-up of the project can be delayed. A second option is to move the mission to other countries, for example the United States of America, where legislation on drones is less strict, to perform the mission and gain experience in operating the system there.

A preferred approach for the case study is to work in close contact with governmental instances such as the ILT and Rijkswaterstaat. The inspection states that exemptions are made as they are convinced that flying will be safe and orderly. In other words, that only happens if the applicant (us) makes it likely that the flights will be carried out safely because the aircraft is reliable, the pilot(s) are properly trained and they work in a well organised company or organisation. A contract that is signed by both parties after agreement on the operations of the system is a preferred solution. This contract clearly

describes the responsibilities of both parties. Having contact with the instances at an early stage it should be considered to have this major client as stakeholder in this company to make the system operational in the Dutch airspace.

3.1.6. RISK MONITORING AND REVIEW

This is a general step in risk management, at all times shall the risk manager keep an overview of the risks and steps in the process. Also, whenever risks have gone through the loop, the last step of the loop before redefining the context, it is required to monitor the risks. This requires the risk manager to write down the actions that have been taken to treat the risks and basically helps him to keep an overview of all identified risks in the defined context and adds to the general risk awareness of the manager. At this point in the design, no effort is put in the further assessment of risks. As soon as more details are known about the design the technical risk assessment will be applied in more detail.

3.1.7. UPDATED CONTEXT

After risks have been treated and monitored by the risk manager, it might be possible that the context of the system has changed. Therefore it is always possible to check whether the context has changed. If the context is changed, it is required to go through the technical risk assessment cycle once again. This step in the technical risk assessment also allows for the possibility of opportunities to arise out of risks. It might very well be that a risk after it has been treated or after the context has been updated, new opportunities can be found for the system. An example is the case of a flooding, when parts of Holland are flooding, our UAV is already in the air and capable of direct monitoring and/or warn the ground system. Also a market change is a threat for our future operations, but a changing market might also present opportunities to operate in. Eventually, with correct and (semi-)continuous monitoring of risks, success of the project is increased.

3.2. CONTINGENCY MANAGEMENT STRATEGY

This section describes the contingency management strategy applied in this project. An effective contingency management strategy increases the overall resilience of the project. The amount of resilience in a system describes the ability of the system to cope with disruptions of any kind. Looking at the bow-tie diagram in Figure 3.4 it is possible to increase resilience by two means. There is likelihood management, on the left-hand side of the bow-tie, prior to the event. In likelihood management one wants to have barriers and escalation controls to minimize the amount of risk sources causing a noteworthy event. On the right-hand side of the bow-tie, succeeding the event, consequence management is effective to reduce the consequence of the event. Consequence management consists of direct consequence barriers and escalation controls.

An example case is the event of a lightning strike causing a short circuit in a house. There are threat barriers such as circuits breakers and lightning rods in the likelihood management part of the bow-tie. Escalation factors may be dust that has surrounded the circuit that set fire easily. A proper escalation control would be to remove dust actively around such circuits. However when the barriers and control fail, an event, such as a fire, can occur. The consequence can be managed by having proper fire detection systems and a fire suppressing system, limiting the consequence of the event.

In this project the team tries to have a high level of situational awareness in every design phase. Each design phase has known and still presents different threats and risks and it is the team's job to set up capable threat barriers, escalation controls, consequence barriers, and escalation controls. Besides that, we should be aware of existing escalation factors and try to minimise and manage them accordingly. Regarding safety and reliability a key system requirement is the ability to fail safely. In case of loss of external power sources the system should be capable of landing safely. Hence when the UAV requires external power, and no power is provided from the ground station, the UAV should have enough power left in the batteries to reach a safe location to execute the emergency landing. This is a sub-requirement that directly can be linked to the initial safety requirement. Additionally it should be considered to have sufficient amount of safety margins in the complete system. The safety margins shall be determined at a sufficient level to account for uncertainties in operations. Whenever the quality of the threat is uncertain, the risk margin should increase accordingly.

At this point in the design several crucial regions of the design are known. Both the ground system and aerial system as a whole can be noted as crucial. However, when more information is known about the subsystems and their importance to the mission and their respective contingency strategy (for instance fail-safe capabilities) the risk strategy is applied to that system in more detail. Especially Chapters 4 and 5 allow us to gain a deeper insight in the different subsystems. In order to create effective barriers and controls in the system it is smart to look at both high risks and specifically also focus on risks that influence the key regions. When the design progresses, the iteration process of identifying new risks is continued. Accordingly, the threats that imply the highest risk should be treated using the risk assessment technology described before and documented for increased awareness. Finally, the use of safety margins and fail-safe policies further increases the reliability of the system.

Risk ID	Chance	Impact	Risk	Risk Category	Event	Cause	Consequence
1	1	5	5	Environment	Terrorist Attack	Terrorist feeling spied by the system and want this to stop by any means	The UAV can be shot down or the ground system may be attacked leaving the UAV without it's major power source or hijack of personell
2	5	2	10	Disaster	Flooding	Flooding of dykes, or more downpour than anticipated	Ground station can be short circuited or destroyed, or under water. UAV will be without major power source
3	5	2	10	Environment	Theft	Mischievousness, or intentional in order to profit from stolen equipment	Loss of resources
4	1	3	3	Disaster	Earthquake	Shifting continental plates	Ground station can be destroyed, UAV will be without major power source
5	4	2	8	Disaster	Wildfire	Fire	Ground station can be destroyed. Smoke can decrease efficiency of laser. UAV will be without major power source and in worst case UAV can catch fire
6	4	2	8	Human Resources	Long term Illness	Illness	Inefficient use of resources
7	1	2	2	Disaster	Tornado	Combination of environmental factors	The UAV cannot be controlled and may crash or be destroyed. The ground station may suffer from damage.
8	1	5	5	Disaster	Solar Flare	Natural phenomenon.	If strong enough X class flare, electronics onboard the UAV or in the ground station are destroyed.
9	3	4	12	Information Technology	Espionage	Interest from competative companies or governments in intellectual property.	Detailled information about the UAV is leaked, making it vulnarable for hacking. Also, potential development is rendered useless since competition knows all details
10	4	1	4	Environment	Vandalism	Mischievousness, or intentional destruction of UAV / Ground station	Inoperational ground stations or UAV's
11	3	4	12	Information Technology	Hacking	Mischievousness, or interest in information	No control of the UAV with potential secondary damage if UAV causes damage.
12	3	5	15	Environment	Collision with other aircraft	Non-situational awareness about UAV or other traffic	Damage to the UAV and other aircraft, potentially with risks for the health of pax of the aircraft. Eventual crash landings can cause secondary damage.
13	3	5	15	Environment	Collision in the air	Non-situational awareness about UAV or other traffic / obstacles	Damage to the UAV and other obstacle, potentially with risks for the health of persons.
14	4	3	12	Legal and Compliance	Privacy	Legal charges against the company because someone feels that privacy is compromised	Damage to the image of the company with risk of financial losses.
15	4	3	12	Reputational	activists	Insufficient or inadequate provision of information	Impact on positive brand awareness and possible reluctancy from companies to invest in UAVs
16	2	3	6	Environment	Bird attacks	UAV looks like a pray.	Damage to the UAV with potential uncontrollable crash landing. The crash landing can cause secondary damage.
17	5	3	15	Disaster	Lightning Strike	Combination of environmental factors	Potential damage to UAV components or UAV in general. This might cause an unvoluntary crash landing with secondary damage.
18	2	3	6	Project	Time management	Failure of having a good overview of the to be executed tasks	Loss of resources and insufficient project progress.
19	3	4	12	Market	Market collapse	Combination of financial factors	Potential customers might be afraid to invest in an UAV
20	2	3	6	Information Technology	virus computer	Mischievousness, or intentional attack on random or targeted computers for benefits to the programmer	Loss of resources on recovery of the information-technology to original state
21	3	3	9	Market	Competition	Competitors see that your product is viable and try to profit from your idea by replication.	A competitor might develope an UAV similar to your own product for a lower price, e.g. because the competitor did not invest in developement.
22	3	4	12	Market	Finance problems (no investors)	The product to be sold has little market potential or one uses wrong channels to find investors	Unsufficient funds are raised for further development of the UAV
23	3	4	12	Project	system error	Technical problem or programming error.	Depending on the system impaired, functions of the UAV will seize to operate. Possible secondary damage if component failure results in crash landing.
24	3	3	9	Legal and Compliance	Pertubation of no fly zones	Piloting error by not checking NOTAM or other published notifications or failure in guidance system	Hazardous situations for aviation or penalties imposed by ATC services. Potential secondary damage to activities or objects in NFZ
25	4	4	16	Legal and Compliance	Permits of operations/costs	Unsufficient insight about which permits are required to perform the intended operations.	Delays before developed product can go in to operation and thus a loss of resources
26	3	4	12	Project	supplier problems	Failure of having a backup supplier and insufficient contact with supplier	Loss of time to production or mainteneance of the components
27	3	3	9	Project	component error	Tecnnical problem	Depending on the component impaired, functions of the UAV will seize to operate. Possible secondary damage if component failure results in crash landing.
28	5	4	20	Project	Loss of contact	Several Reasons; include comms failure due ground and air segment	Operational instructions cannot be send to the UAV, and valuable data from the UAV cannot be transferred to ground.
29	4	3	12	Project	Loss of power on the ground	Technical problem in the ground station or external problem such as broken cable	The UAV doesn't produce enough energy to continue uninterruptive operations and will be forced to land.
30	4	3	12	Project	engine failure	Technical problem	The UAV cannot continue operations and needs to land immediately.
31	4	4	16	Project	Loss of power in the air	Technical problem or insufficient energy reserves	The UAV cannot continue operations and crashes immediately, as backup systems cannot support a soft landing. Possible secondary damage.
32	3	3	9	Project	laser failure	Tecnnical problem	The UAV doesn't produce enough energy to continue uninterruptive operations and will be forced to land.
33	3	3	9	Human Resources	lack of knowledge	Insufficient Training or non-involvement of team members	Waste of resources
34	2	4	8	Project	pilot error	Insufficient piloting knowledge, fatigue or human error. Programming error or technical failure for autopilot	Depends on the piloting error made, consequences range from none to pertubation of NFZ's or crash landings with possible secondary damage.
35	2	4	8	Project	Bad oversight/management	Non-qualified personell	Loss of resources and insufficient project progress.
36	2	4	8	Project	Unintentional Interference of laser	Unsufficient accuracy or unsufficient safety systems on the laser guidance system	Possible secondary damage

Figure 3.2: Table of Risks Identified and Assessed for Likelihood and Consequence

Impact score table	
1	Impacts ground segment with solely small financial consequences
2	Impacts with small financial concequences and minor chance on secondary damage
3	Impacts with small financial concequences and reasonable change on secondary damage
4	Impacts project with large financial consequences, perhaps on long term.
5	Large schale consequences, ranging from financial to brand image.

Risk score table
Very High (15-25)
High (10-14)
Medium (7-9)
Low (4-6)
Very Low (1-3)

Likelihood ->	Consquence -> Insignificant	Negligible	Moderate	Major	Extensive
Almost Certain		2, 3	17	28	
Likely	10	5, 6	14, 15, 29, 30	25, 31	
Possible			21, 24, 27, 32, 33	9, 11, 19, 22, 23, 26	12, 13
Unlikely			16, 18, 20	34, 35, 36	
Rare		7	4		1, 8

Very High (VH)	Immediate action required by the Executive with detailed planning, allocation of resources, and regular monitoring
High (H)	High risk, senior management attention needed
Medium (M)	Management responsibility must be specified
Low (L)	Monitor and manage by routine procedures
Very Low (VL)	Managed by routine procedures

Figure 3.3: Risk Map with the Identified Risks Assessed

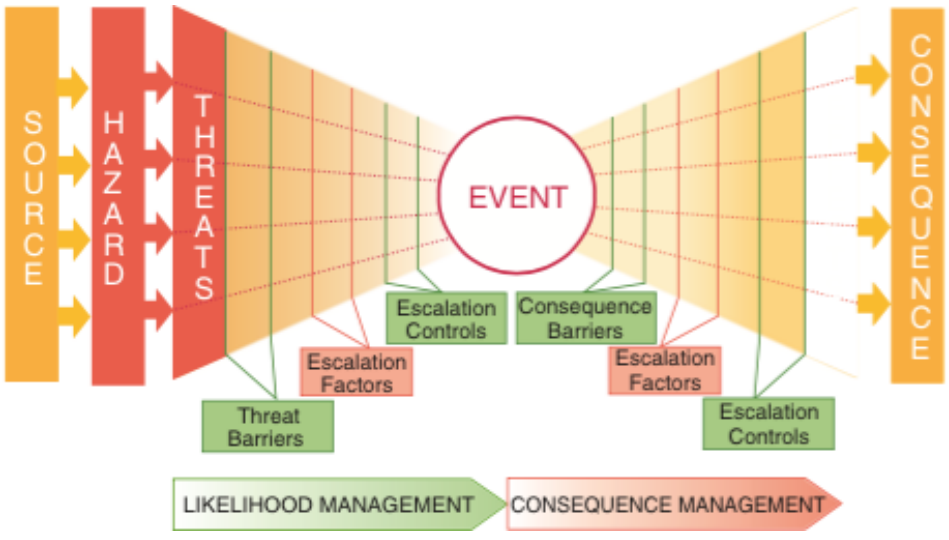

Figure 3.4: Risk Bow-Tie Likelihood and Consequence Management [2]

4. Concept Description

With the risk strategy in mind, it is possible to look forward to the actual concept and functional breakdown and flow diagrams. This chapter serves to provide overview to the variety of functions that each (sub-)system is required to perform for a successful execution of the mission. But first the concept is explored in Section 4.1. Hereafter, the set requirements are used to determine all functions needed to perform a generic mission. All these functions are presented with help of a Functional Breakdown Structure (FBS) and is treated in Section 4.2. With this knowledge it is possible to define the Functional Flow Diagram (FFD) and this diagram chronologically presents the mission functions in Section 4.3. These diagrams are the basis for the detailed design of the AERIS, and are especially useful for Chapter 5 where, amongst others, the hardware and software diagrams are presented.

4.1. Operations and Logistic Concept Description

This section describes the conceptual operations and logistics of the AERIS project. Using the results from previous reports, this section will describe the operations and logistics behind this concept, which is the basis for the further analysis and development in the succeeding of this report.

Starting with the analysis of the requirements, several design options for multiple system levels have been defined. When the knowledge on these systems grew, the design space became smaller. Both by means of performing trade-offs, backed-up by extensive research on different subsystem technologies and by engineering guts. Eventually, with an effective system engineering strategy and integrative work, it was possible to present the concept in the MTR. [5] The concept, in short, is a continuous flying high aspect ratio lightweight single motor UAV with two booms, which is partially powered by a laser whilst in flight. The fact that this aircraft is designed to fly continuously makes this whole project a prestige project. In addition, powering an aircraft with laser power is a juvenile, but proven technology. Several working prototypes exist making this technology very trustworthy for the near future as depicted already in 2010. This is also supported by Dr. Jordin Kare who is a top expert in the field of laser propulsion and power beaming. [6] The operations and logistics of the AERIS concept can be described by making a distinction between the ground station, which consists of a laser station, offices, and the aircraft itself. For a more detailed analysis of the functions of each system please refer to the descriptions provided in Sections 4.2 and 4.3 on the FBS and FFD respectively.

4.1.1. Laser Station

The laser station is a location where the laser system is housed and the communication system is sited. For reasons concerning energy losses through the atmosphere of the laser light as it travels to the aircraft, and the fact that the communication system works on a Line of Sight (LoS) basis, locating the laser station at an higher altitude is advantageous. Moreover, the AERIS project team experiences good relations with the Delft University of Technology network allowing them to locate an initial laser station on top of the EWI-faculty building. This will be used in the pilot case as described in more detail in Chapter 9, where the business roadmap of the AERIS project is presented.

Operations wise, all locations defined for the laser station should be accessible enough for maintenance. Also, the laser system requires the site to have access to a power source of sufficient strength. The laser system has a shielding device to shield the device from the environment such as rain and hail. Furthermore, there are wild-life protection systems installed and a pointing system is present with a high pointing accuracy to focus the laser light on the laser panel of the aircraft. The laser station will be sized in more detail in Section 6.11.

4.1.2. Offices

The concept that is developed by the AERIS project team include offices that are needed for operations. The sizing of the offices, which is part of the ground station, takes place in Section 6.11, whereas the budget breakdown is presented in Chapter 9. To cut costs, eventual maintenance on the aircraft should take place in the offices. It is for this reason that a feasible landing and take-off site is preferred near the location of the office. As the location differs from the laser station, an internet link with the communication system and laser station is a logistic requirement. Another requirement is that the office should be big enough to accommodate at least ten people working at the same time where at least two people should be present to serve as safety pilots in case of an emergency. Requirements are elaborated upon in Section 8.6.

4.1.3. Aircraft

The concept that is presented in this report is initially based on the pilot case in which the concept should cover the province of Zuid-Holland. It can be read in the business roadmap of this project, Chapter 9, that this pilot project is just the start of

a presumably bright future for AERIS. Part of this success will be the decision to start with two identical aircraft for the pilot case. Using two aircraft allows the team to quickly adapt and change subsystems on the aircraft and also execute maintenance on the laser system whilst maintaining operations alive, as will be elaborated on in Section 8.6.

Furthermore, Chapter 6 will elaborate on all subsystems on-board this aircraft. Operations wise, the aircraft will harvest at least 50% of its energy from laser power beaming and the remaining energy is generated by solar panels on-board of the aircraft. The mission scope will primarily focus on the detection of discrepancies in surface water, such as oil, and scanning of the farmers ground with the HSI. Finally, in Chapter 9 the general picture of the exact business case of AERIS is presented.

4.2. FUNCTIONAL BREAKDOWN STRUCTURE

A FBS is a structured, modular breakdown of every function that must be addressed to perform a generic mission. [7] The focus of this type of breakdown structure is to list all functions and operations that should be performed to execute the mission successfully. It differs from the FFD, which is presented in the succeeding section, as it is not limited to any particular architectural or chronological order.

The FBS for the AERIS project is shown in Figure 4.1. In this figure, it becomes clear how the success of the mission is dependent on many different functions that the UAV and ground station (laser station and offices) have to perform. Several time-dependant functions are presented in the FBS but will not be presented in the FFD. These functions are the controllability and stability since they are regarded as continuous standards and that these standards do not change over time. The FBS will serve as a guide in the further development and design of the systems and subsystems engineering activities to help integrate and optimise each discipline for the total system level, thus avoiding optimisation at the element level. In addition, it serves as a framework that will help prevent over or under specified requirements because all functions are identified and all elements are aligned to functions.

4.3. FUNCTIONAL FLOW DIAGRAM

Now that the FBS has been defined and all functions needed to successfully perform the mission are known, the next step will be presenting the different functions in a chronological order. The FFD presents the sequence of functions needed to be performed at a general level of depth. A more detailed analysis of these diagrams is performed in Chapter 5 to present, amongst other, the hardware diagrams. Finally this information is again used to go into more detail with specific subsystem sizing in Chapter 6.

The FFD is split up into two parts. The air segment and the ground segment, visualized in Figures 4.2 and 4.3 respectively. The top-level domain presents the primary functions that need to be performed. Details of those functions are described in the processes. For some processes another level of depth is displayed under the sub-processes. Functions $3 - 8$ represent the mission phase. Concluding the mission is function 9, the landing. Function 13 is one of the most important ones for the AERIS mission, the charging by means of laser power. Taking a closer look at sub-process 13.3, the charge, one can see that a feedback loop is included to continuously check if the laser reaches the UAV and if the laser temperature is still within its operating range.

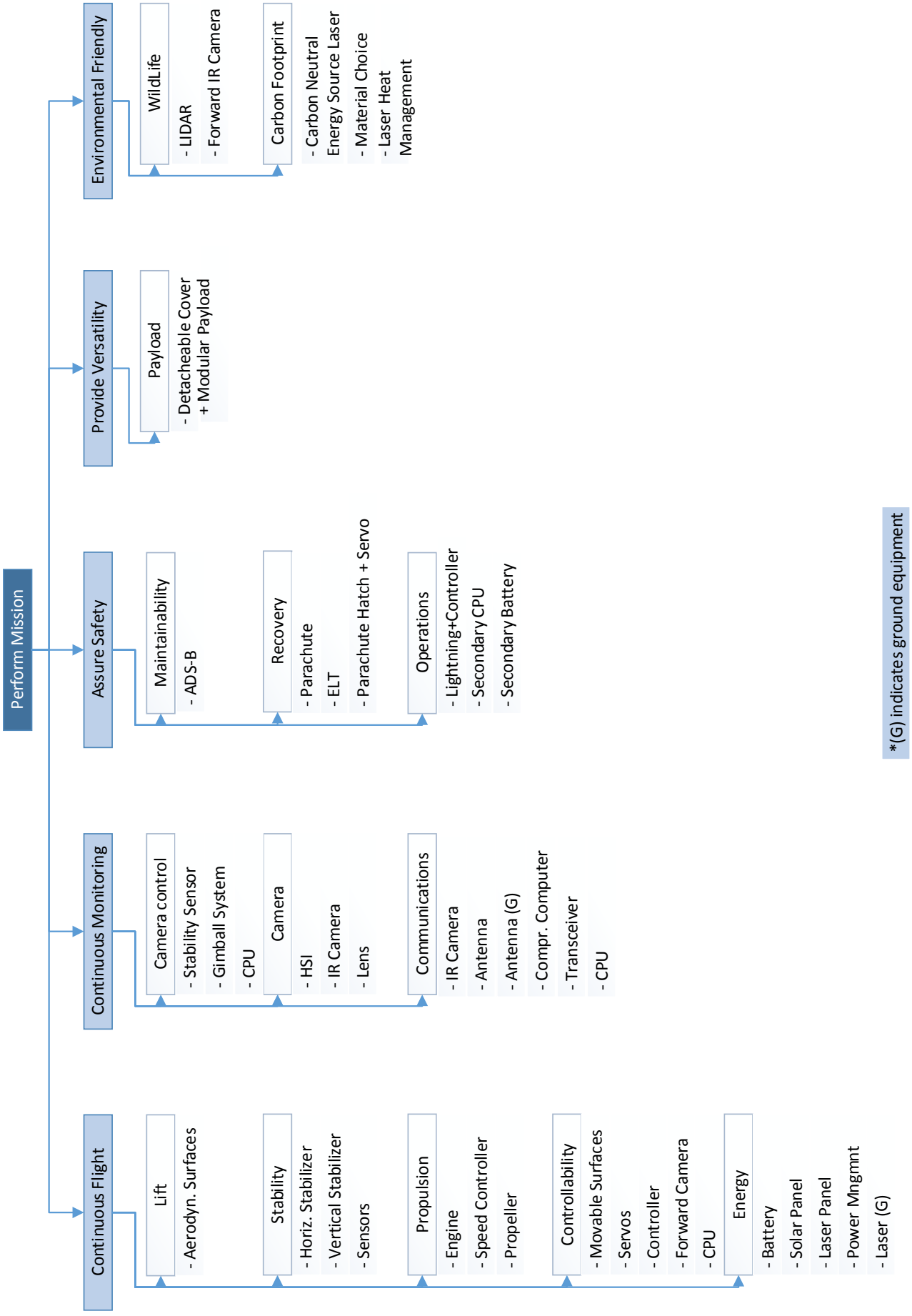

Figure 4.1: Functional Breakdown Structure

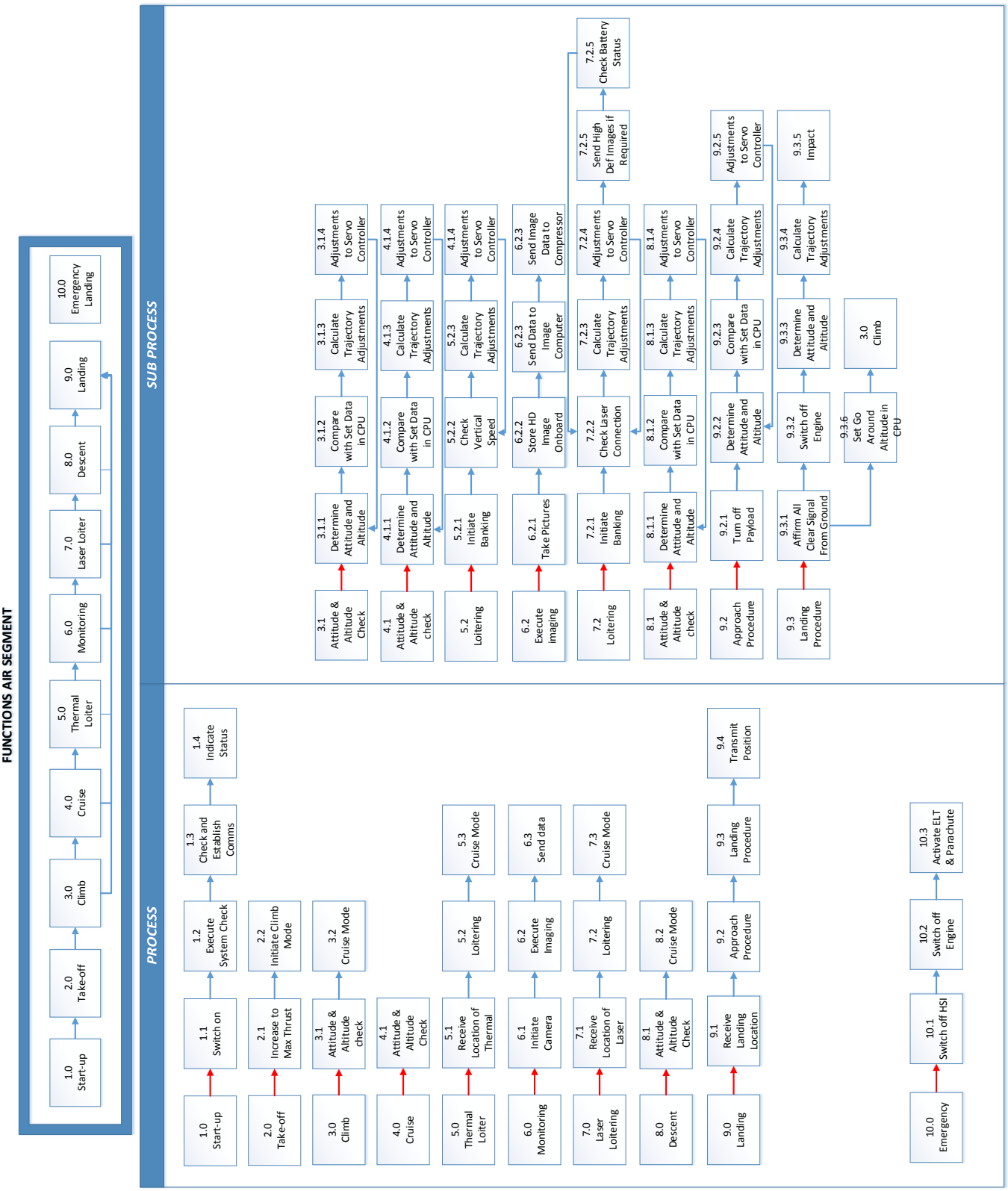

Figure 4.2: Functional Flow Diagram for the Airborne Part

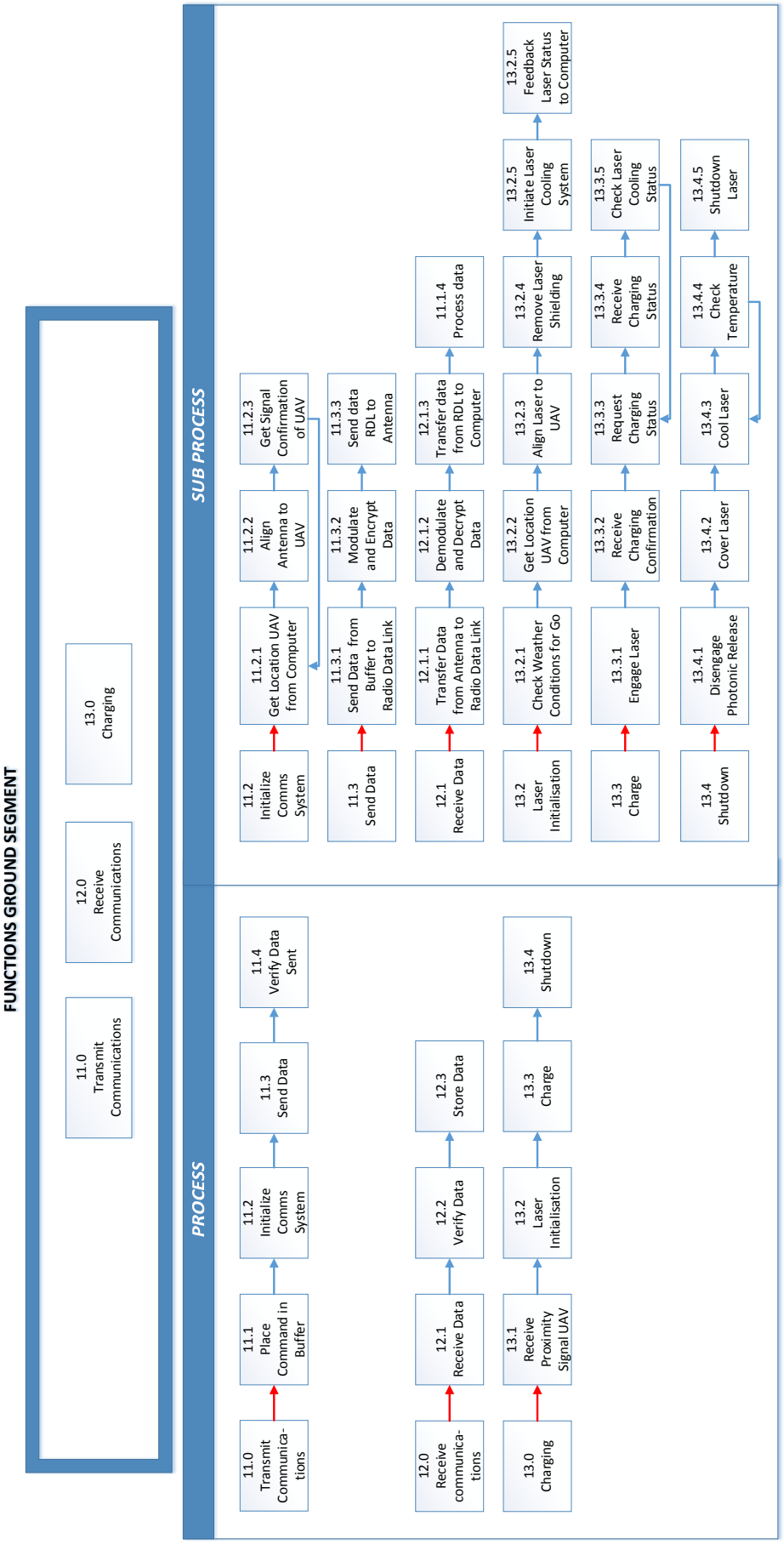

Figure 4.3: Functional Flow Diagram for the Ground Part

5. System Design

In this chapter the physical connection between all different subsystems is presented. These connections show the dependencies of each subsystem, and give an overview of how the network of multiple subsystems form into a complete system. In the first Section, 5.1, the hardware components and their interrelation is explained. After this, Section 5.2 continues with the software block diagrams, which provides more details on communication between the different subsystems. The final section, Section 5.3 shows how the network of electrical cabling connects the hardware to multiple power sources.

5.1. Hardware

This section shows the major hardware blocks AERIS contains and the relation between them. In Figure 5.1 all blocks are shown and the lines show the connection. Each hardware block and its connection is explained below, going from top left to bottom right. The hardware blocks of the ground system are shown in more detail in Figure 5.2. A short description of all the blocks from Figures 5.2 and 5.2 and their connection is listed below.

Laser Panel The first hardware block is the laser panel. This is the part where the laser power in the form of photonic energy coming from the ground station is collected. This block is therefore connected to the ground station but also to the power management system. The laser panel consist of triple-junction Indium Gallium Arsenide (InGaAs) cells which have an efficiency range from 50% to 38%, for a temperature of respectively; 7 - 127 [$^{\circ}C$]. [8]

Solar Panel At the solar panel at least 20% of the total power is collected, which puts through the energy to the power management system. These solar panels consist of single-junction cells which are 25% efficient. [9]

Safety Battery The safety battery is only active when the Central Processing Unit (CPU) receives insufficient power from the PMS. This might occur due to a faulty PMS, faulty solar panel or when there was insufficient charging. When one of the previous situations occur, the safety battery ensures that AERIS can continue flying long enough to perform a safe landing. The safety battery is connected with the power management system, which makes sure the battery is always fully charged (this is a one way connection from the power management system to the safety battery). Note that, in case emergency energy has to be used, energy flows directly from the emergency battery onto the emergency bus without need from the PMS for safety reasons. The lithium polymer safety battery has a voltage of 14.8 [V] and a energy charge of 3000 [mAh].

Power Management System The power management system is the point where the distribution of all electricity starts. When AERIS is in charging mode, it collects all the energy coming from the laser and solar panel and distributes it to the batteries. During daylight flight, AERIS only receives energy from the solar panel. When insufficient photonic energy is received, the power management systems regulates that enough energy travels from the batteries to the main bus. A management system is necessary because different hardware components require different voltages.

Battery The battery, which consist of seven battery packs, provides AERIS enough energy to perform seven hours endurance without charging. These new technology batteries are made of lithium sulfur cells which have a power density of 300[$\frac{Wh}{kg}$] and a voltage of 2.1 [V].

Central Processing Unit The CPU performs most calculations on-board AERIS. It is linked to almost every other hardware block and receives, processes, and sends all necessary data. Responsibilities of the CPU are: auto take-off, auto flight plan execution, auto landing, auto return to base in case of communication failure, and parachute activation in case of emergency.

Sensors The block of sensors provide the CPU with all necessary information, for example: altitude, position and flight angles, that are needed to calculate adaptations to the attitude and flight path. These sensors are combined in one module which has a weight of only 49 [g], where there are three gyroscopes, three magnetometers and three accelerometers around three axis. This module also includes a Global Navigation Satellite System (GNSS) receiver with a 2 meter accuracy.

Communications The communication block is of major importance because it sends the valuable data for the customer, from AERIS to the ground station. The antenna block consists of two antennas to lower the chance of loosing contact, where one antenna receives the command from the ground station while the other sends the data to it. The connection between the antenna and the ground station is shown with a dashed line because it is not a hardware block of the UAV and is shown in more detail in Figure 5.2.

Control To let AERIS be able to change position, it must be able to move the ruddervators and flaperons, which are controlled by servos. These servos are driven by a controller, which receives its command from the CPU.

Payload The pictures coming from the 4.2 [$Mpixel$] HSI camera and the two 0.3 [$Mpixel$] IR cameras, are passed on to the communication block. There is also a link between the payload and the CPU, to initiate imaging when desired. The pictures from the HSI go to a compression computer, which makes sure the data is compressed enough to send the data to the ground station. This computer also contains one Terabyte of memory to store pictures in case of a communication failure, which is sufficient for more than one month of storage.

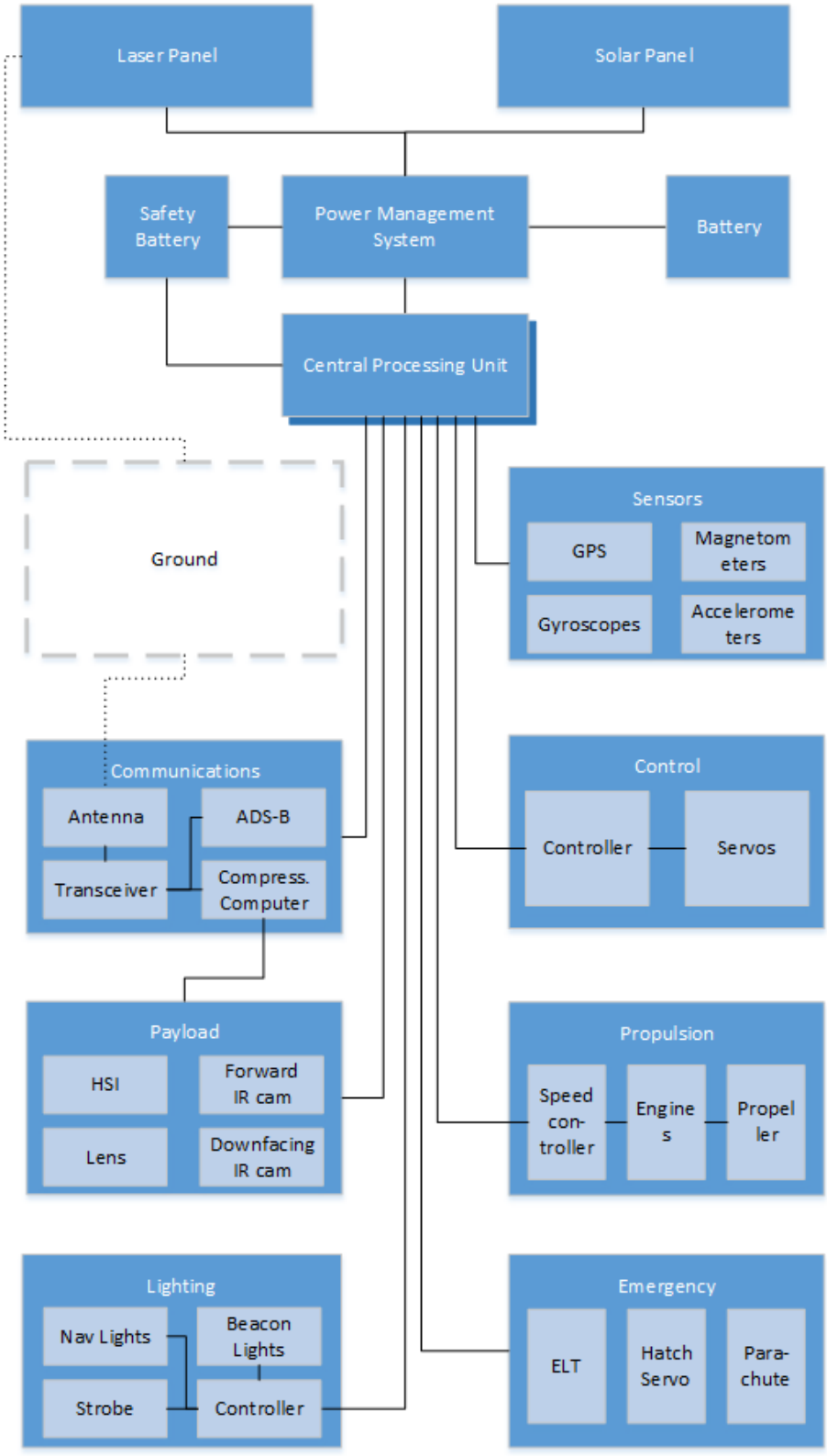

Figure 5.1: Hardware Block Diagram Air Segment

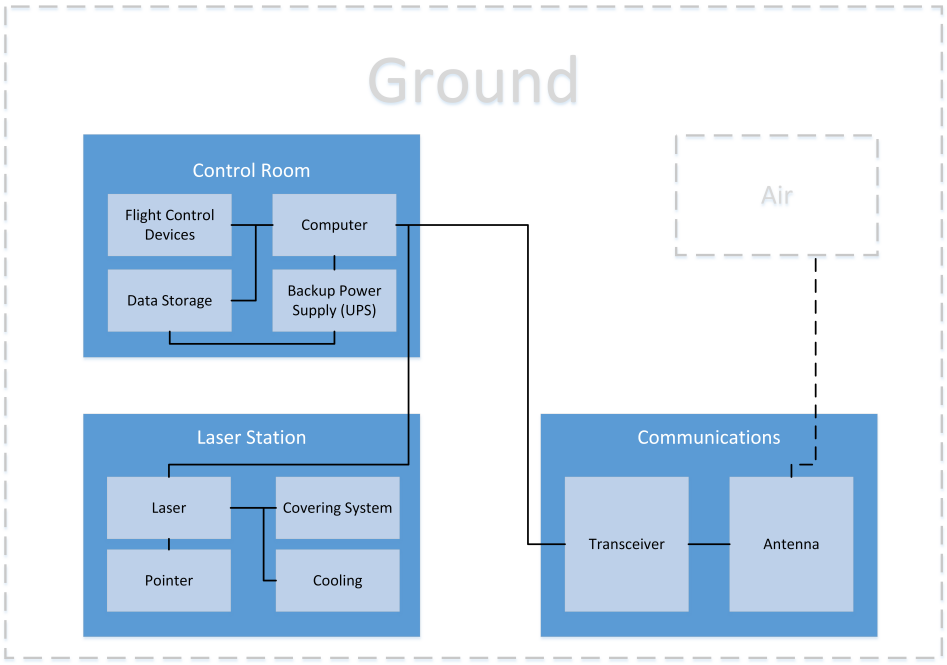

Figure 5.2: Hardware Block Diagram Ground Station

Propulsion In this block, the speed of the propeller which is determined by the CPU is passed on to the Electronic Speed Control (ESC). The ESC then regulates the speed of the engine which turns a fixed gearbox, driving the fixed pitch propeller.

Lighting Like conventional aircraft AERIS will have multiple lights for safety reasons. These 1.4 [W] tri-color leds make sure AERIS is visible for other aircrafts.

Emergency In case a crucial subsystem fails, or the CPU does not respond to the emergency block, the emergency mode will be activated. In this case, an emergency locater transmitter will be active and a "Iris Ultra" parachute deploys to prevent the UAV from crashing. [10]

Ground Control Room In the control room the received data is processed and stored. When necessary, it is possible to take over control of AERIS, although an auto return to base function exist on AERIS. Another component is the backup power, in order to make sure the mission does not fail when the ground station looses external power.

Ground Laser Station The laser station is the connection block to get the power from the ground to AERIS. Since the laser uses a lot of energy, a cooling system is necessary. To protect the laser from the environment there will be a covering system in case the laser is not active. Since the laser is a major part of this report, more details can be found in Section 6.11

Ground Communication This block forms the connection between the ground and the air segment. From here, commands will be sent to AERIS and data is received from it, by making use of a 26 [dBi] antenna.

5.2. SOFTWARE

Following from the hardware block diagram, in this section the software block diagrams are presented. These indicate the communication that takes place between components and subsystems for both the air in Figure 5.3 and ground section in Figure 5.4. To indicate the differences in data handling and communication, black and red lines are used respectively. Data handling refers to complex data transfers, such as telemetry or payload data, whereas communication lines only need to carry an on or off signal. The software connections of all individual components are described into detail below.

5.2.1. AIR SEGMENT

CPU: As the CPU perform most calculations and handles most data, there are a lot of software connections involved. The connections between the CPU and the following subsystems have been identified;

- **Switch**: The CPU sends a signal to the switch in case power from the PMS is lost, which will cause the safety battery to power the emergency bus. One way communication only since on/off signal is determined by the CPU.
- **Transceiver**: The transceiver modulates, encrypts, and decrypts information that is received from the antenna. An example of data from the transceiver to the CPU are mission instructions. Data from the CPU to the transceiver could include current mission statistics. Two way data handling.
- **Forward IR cam**: The forward IR camera is always turned on and data from the camera is send to the CPU for navigational purposes. One way data handling.

- **Lens**: The CPU sends lens setting data to the lens to obtain correct images. One way data handling.
- **Down-facing IR cam**: The down-facing IR camera is turned on, together with imaging instructions by the CPU. One way data handling.
- **HSI**: The HSI is turned on, together with imaging instructions by the CPU. The CPU also sends information to the gimbals to stabilize the HSI based on the data it receives from the sensors. One way data handling.
- **Lighting Controller**: The lighting can be switched on or off by the CPU. One way communication.
- **Emergency subsystem**: The CPU turns the emergency system on when desired. This cannot be undone as the parachute will deploy. One way communication.
- **ESC**: The CPU sends desired engine settings to the ESC and receives engine statistics. Two way data handling.
- **Controller**: The CPU sends desired attitude information to the controller. In turn, the CPU receives servo settings from the controller. Two way data handling.
- **Sensors**: The CPU receives sensor information that, amongst others, is needed for navigational purposes and HSI stabilization.

Antenna: The antenna relays data from the ground to the transceiver and vice versa. It therefore performs two way data handling.

Transceiver: As explained in the CPU section, the transceiver encrypts, decrypts, modulates, and demodulates data for transmission to the ground station. Data that is to be processed comes from the compression computer and from the CPU. Whereas, there is only one way data handling required with the compression computer, two way data handling is required with the CPU for reasons mentioned earlier.

HSI: After receiving instructions from the CPU, the HSI sends captured image data to the compression computer to prepare it for transmission. Note that the compression computer also features a hard drive that stores original, uncompressed data which can be transmitted on request. One way data handling.

Down-facing IR camera: After receiving instructions from the CPU, the down-facing IR camera sends captured image data to the compression computer to prepare it for transmission. One way data handling.

Compression Computer: The compression computer receive instructions from the CPU to send stored, uncompressed data to the ground station if desired. Furthermore, it receives Global Positioning System (GPS) data for geotagging of the pictures and the payload data from the HSI and down facing IR camera. Ultimately, this data is send to the transceiver. All of these data flows are one way.

Controller: After receiving attitude settings from the CPU, the controller calculates desired servo settings and sends these setting to the individual servos. One way data handling.

ESC: After receiving desired engine settings from the CPU, the ESC sends those setting to the engine. One way data handling. Note that the engine is mechanically connected to the propeller, so no data handling takes place.

Lighting controller: The lighting controller is switched on or off by the CPU. The controller itself turns the lights on. All connections are one way communication.

5.2.2. GROUND SEGMENT

Computer: Similarly to the CPU in the airborne segment, the computer performs most calculation and communicates or performs data handling with multiple subsystems and components. The following have been identified;

- **Internet**: Using the internet, the computer communicates with various service including weather providers for the latest forecasts and the data center to store captured data. Two way data handling.
- **Flight Control Devices**: These devices help pilots to control the UAV and range from flight yoke to monitors etc. Two way data handling is here required.
- **Data Storage**: Local data is stored in the control room. Two way data handling.
- **Covering System**: The covering system for the laser is controlled by the computer. It is important that the computer receives feedback of the status of the covering system, therefore two way data handling occurs.
- **Pointer**: The pointer aligns the laser with the UAV. Likewise to the pointer, it is important that the computer receives feedback of the status of the pointer, therefore two way data handling occurs.
- **Cooling**: Cooling removes waste heat from the laser. It is important that the computer receives feedback of the status of the cooler such that the laser can operate safely. It is for that reason that two way data handling is required.
- **Laser**: The laser is switched on after which it transmits status data back to the computer. Two way data handling.
- **Transceiver**: Same as in the UAV, the transceiver modulates, encrypts, and decrypts information that is received from the antenna. An example of data from the transceiver to the UAV are mission instructions. Data from the UAV to the transceiver include payload data. Two way data handling.

Laser: Providing additional safety, the laser should receive confirmation from both the covering system and the cooling that they operate properly before the laser beam is engaged, for which they need one way data handling.

Antenna: The antenna relays data from the UAV to the transceiver and vice versa. Creating a two way data handling.

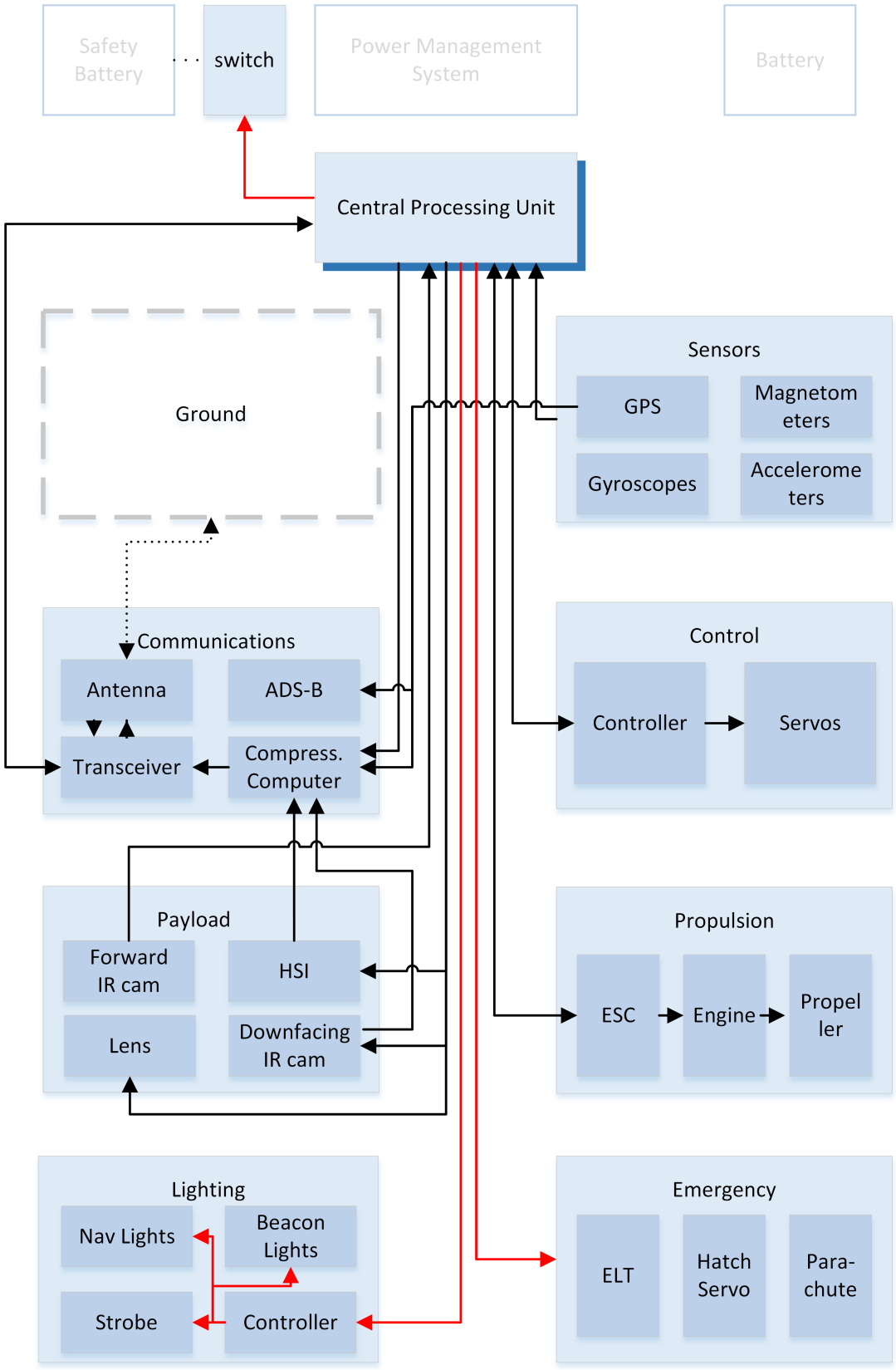

Figure 5.3: Software Connections of the Air Segment

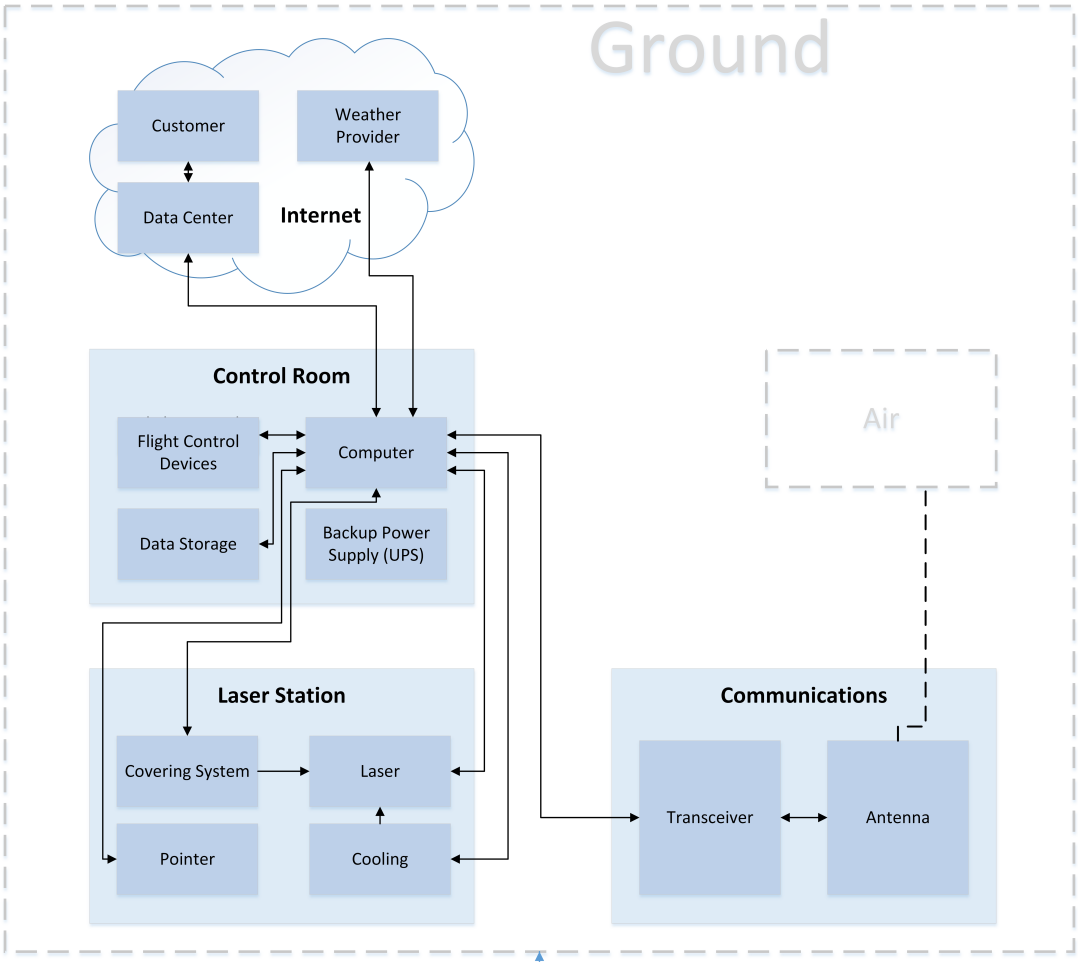

Figure 5.4: Software Connections of the Ground Segment

5.3. ELECTRICAL

The electrical system provides all individual systems of the UAV with a sufficient amount of power. Providing this power however is not enough. The UAV should be protected from, for example power peaks that may harm the system and from other failures. In order to do this, multiple subsystems are required that each have an own function. All of these subsystems should be connected in a well organised way, which is schematically represented in Figures 5.5 and 5.6.

Complimentary to the organisation of the cables, sizing is important too. Large cables are both bulky and heavy whereas too small cables are dangerous since cables heat up and waste energy due to high resistance. Before sizing commences, one has to determine the desired voltage and amperage that is to be transported. This, and the fact why the cable diameters are chosen as indicated in Figures 5.5 and 5.6 is explained into more detail in respectively Sections 6.8.3 and 6.8.4.

The subsystems that are identified will be elaborated on in the succeeding of this section using the analysis of the Figures mentioned earlier. 5.5, 5.6.

Power Supplies In Figures 5.5 and 5.6, a general overview of the electrical system of AERIS is presented. The initial inputs in the system consist of the solar panels and the laser, whereas the Peltier elements have been removed due to reasons mentioned in Section 6.8. All of the elements mentioned can generate power at different voltages. It is for this reason that they will each need a separate connection with the PMS.

Power Management System Since the supplied power constantly varies, it has to be regulated to a constant voltage before it can be used in the system. If this would not be de done, the subsystems will be subject to too many voltage changes, potentially damaging them. Another reason to make use of a PMS is that a part of the energy needs to flow directly onto the main bus, whereas the remainder should be used to charge batteries. If there is no external power available, e.g. during the night and out of range from the laser, the PMS should use energy from the battery to feed the main bus. The PMS is connected to the primary battery, main bus, and power supplies.

Main Bus The main bus is connected with the PMS and transports all energy to the individual subsystems that are attached to the bus. Since all subsystems are attached to the same bus, it supplies one single Direct Current (DC) voltage that all subsystems can handle. Using a bus prevents the use of separate wires that are to be connected to individual systems.

Batteries The UAV has two batteries on-board; the primary (rechargeable) battery and the secondary (emergency) battery. As the primary battery needs to be charged and discharged, the energy flow is regulated by the PMS. In order to prevent dangerous situations that render the UAV inoperable, the emergency battery however is used in case of emergency and needs to be independent from the PMS in case of malfunction. For this reason the secondary battery is only charged by the PMS if the energy level drops below 90%, to always allow for at least 15 minutes of flight time. Once the CPU notices a power loss, the secondary battery is activated. The emergency battery then provides energy to the emergency bus, which is connected to all the subsystems that are also connected to the main bus plus the emergency subsystem.

Central Processing Unit The CPU can be compared to the brain of the UAV, and consists of smaller computers that each have an own task. Receiving data from the sensors such as GPS, gyroscopes, and barometers, the CPU determines attitude, altitude, speed, and position. It uses this data to remain in autonomous flight. Furthermore, it controls command that are received from the communications subsystem and executes these command, controls lighting, triggers emergency system etcetera.

Control System The control system consists of the controller and the servos. The controller receives a command from the CPU, after which it translate it to commands for the servos. These servos translate the commands into actual deflection of control surfaces that manipulate the attitude of the aircraft. Since the control system has to be available at all times it is also linked to the emergency bus.

Communications To be able to send payload data to the ground station and in order to receive navigational commands, a communication system is required. The communication system is connected to both the main- and the emergency bus since a communications link has to be established at all times.

Payload The payload consists of three components; the HSI which performs the spectral imaging during the day and two thermal imagers. One thermal imager is mounted facing forward to detect birds and for navigational purposes. The second thermal imager provides additional imaging data that is outside the operational spectrum of the HSI. The payload is connected to both the main and emergency bus the same holds for the safety camera.

Sensors Sensors measure attitude, speed, and global positional data which are essential for navigational purposes. Furthermore, navigational data is used by the payload to determine the exact location of all the images that are to be processed. The sensors receive energy from both the main and the emergency bus.

Emergency Systems The emergency subsystem includes the emergency transmitter and the parachute. The subsystem is connected to both the emergency bus and the main bus, since all leftover energy of the normal battery could be used as long as it functions.

Propulsion Propulsion of the UAV is required when performing emergency manoeuvres. It is for that reason that this subsystem is connected to both the main and the emergency bus.

Lights The UAV has to be visible during night time operations and therefore requires external lighting. The lighting is controlled by the controller and the required power originates from both the main and the emergency bus.

Note that the ground systems are assumed to work with 230 [V] AC, or 400 [V] AC 3-phase power current but have not been sized since there are no weight limitations. For that reason, it is assumed that this sizing is outside the scope of the AERIS project.

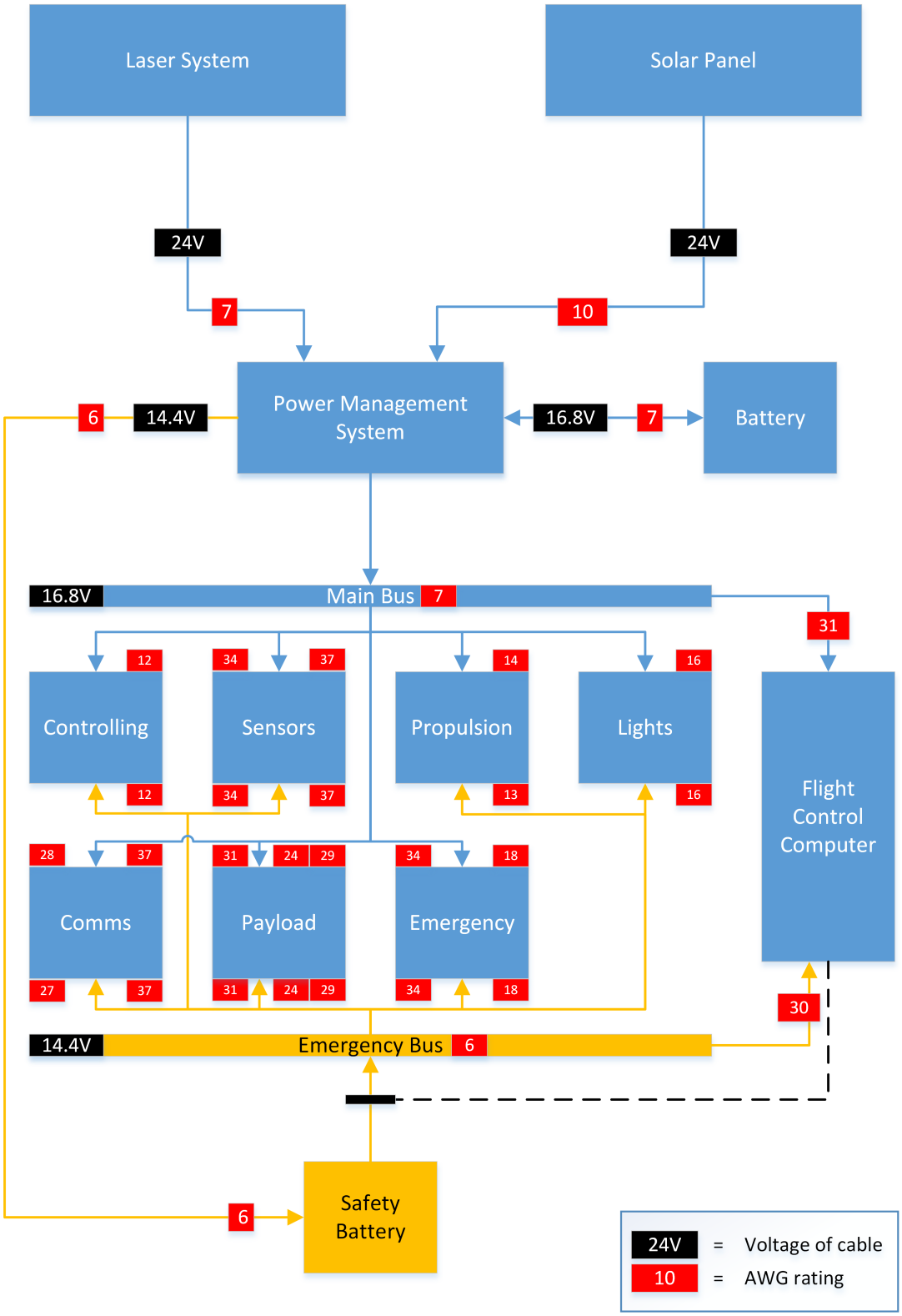

Figure 5.5: Electrical System of the Air Segment

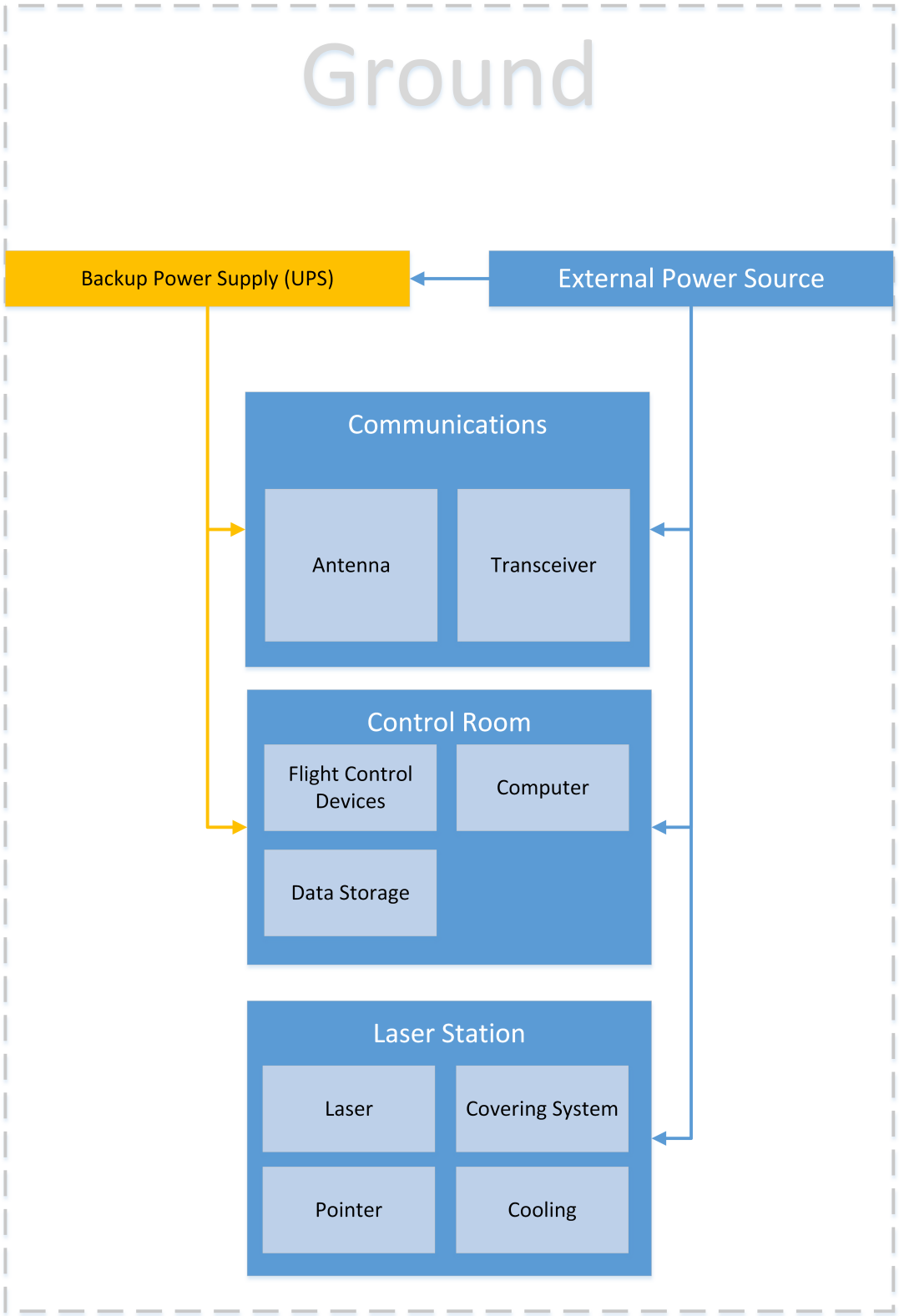

Figure 5.6: Electrical System of the Ground Segment

6. SYSTEM SIZING AND CHARACTERISTICS

This chapter shall present the reader with the new N^2 diagram for AERIS's final design along with a description of the engineering strategy that the team used. Following this, the sizing of the subsystems that make up AERIS are given in the order of the N^2 chart, and finally the sizing of the ground system is explained. The work was then implemented in a MATLAB script which was structured in exactly the same way, and the results were iterated to obtain the final design. These results will be given in the following chapter.

6.1. ENGINEERING STRATEGY

An engineering design strategy is a formal method to allow engineers to explicitly make trade-off decisions. A trade-off strategy should be aligned with the project's design philosophy. The design philosophy of this project values sustainable development, system performance, and human welfare among other values. In other words, these values and norms should also feature in the trade-off; concepts should score higher according to how well they satisfy them. Three common approaches are to select designs according to their standard weighted sum, conservative mindset and/or an aggressive mindset scores. The difference between the latter two is that they evaluate each option's overall performance based on the option's worst attributes and best attributes respectively; the first option has no inherent bias to differentiate between good and bad scores. In all case, the outcomes have fuzzy-mathematical definitions: Equation 6.1 is the standard-weighted sum definition, Equation 6.2 is the conservative definition, and Equation 6.3 is the aggressive design definition. In each of these equations, the subscript i denotes a performance parameter, ω is the importance rating of that parameter, and μ is the score of that performance parameter. Furthermore, $q+n$ is the number of design options. Each of the scores and importance ratings must first be normalized; the entire process can be visualised in the form of a matrix. This matrix is made up of performance parameters with their own importance ratings (Id est (i.e.) weights), and the design parameters' (the candidate architectures') scores on the basis of how well they satisfy those performance parameters. These scores represent a mix of specific data, generalized data and an engineering 'gut-feeling'. The team shall examine all outcomes to obtain a better overall feel for the trade-off.

$$\max_{i\epsilon[1,q+n]} \left(\sum \mu_i \cdot \omega_i\right) \tag{6.1}$$

$$\min_{i\epsilon[1,q+n]} \left[[\mu_i^{\omega_i}]^{1/\max_{i\epsilon[1,q+n]}[\omega_i]} \right] \tag{6.2}$$

$$\max_{i\epsilon[1,q+n]} \left(\prod_{i=1}^{q+n} \mu_i^{\omega_i} \right) \tag{6.3}$$

One might argue that the influence of the subjective engineering gut on this process might easily compromise the integrity of the design. To an extent, this argument is valid as engineers would undoubtedly introduce guess-work, biases and their own experiences into the trade-off. This in turn might lead to sub-optimal choices. It is important to recognise, however, that this subjectivity is also a strength. Including the subjective influence of the engineer may identify any particularly good or bad options in an efficient use of project resources. In addition to this, engineering gut-feeling might also account for some of the wider human values that are more difficult to quantify. It is quickly apparent that mitigating the risk of making a bad choice is crucial in a successful trade-off process. The trade-off itself will motivate the engineers to think about the strengths and weaknesses of each option; incorporating the ability for reflection makes the trade-off a potentially valuable learning process. It makes sense, therefore, to iterate each option's score if need be by re-assessing the importance ratings and/or the component scores as the engineer learns from the trade-off process, thereby mitigating the risk of making a bad choice.

As with the previous trade-offs, small differences in the overall preference between options after a trade-off should be considered negligible. In the event that options have close overall scores, these concepts should all be explored further in a more detailed design; following that, a new trade-off should be performed. This also incorporates what has been learned in the detailed design phase, giving the engineers a better perception and understanding of the design problem, which in turn would lead to a better trade-off.

Compared to the preliminary trade-off performed in the MTR, the performance parameters are even more quantifiable. [5] In other words the engineers' gut senses is used even less than the previous case to arrive at a final decision. The following rules must be respected throughout the trade-off process.

- Performance parameters based solely on one's engineering gut-sense, they may have an importance rating of at most four on a ten point scale;
- Performance parameters based on hard data may have a maximum importance rating (ten on a ten point scale);
- If a performance parameter is unable to distinguish between options it should be removed as a performance parameter;
- Reasons for each performance parameter's importance rating must be clearly documented for future review;
- When hard data exists to compare the candidate architectures, each score is normalised linearly;
- When obvious contradictions exist in the overall scores, the table should at least be re-examined to understand the reason for those contradictions;
- The trade-off can be subject for review if new information comes to light in future work.

In the previous report, the team sized a series of typical design options to trade them off to select the most suitable option to explore further. The zeppelin, Prandtl wing and flying wing were all eliminated in this process, leaving the team with a powered-glider as the best solution.

AERIS's glider configuration was only sized to the expected aspect ratio and airfoil characteristics, giving an approximate expected mass of 11.536 [kg]. [5] The effects of different tail and engine configurations presented after the aforementioned trade-off was then unknown, hence the need for the development of a more intricate and comprehensive design tool to iteratively size what will become AERIS's final conceptual design.

Shortly after starting to build the final design tool, the team realized that the design space was too large with the given resources; the scope of the design tool would be too large and far too complicated to build in a few short weeks. To address the issue, the team spent some time researching the general characteristics of two possible configuration types: a single-boom pull-prop and a double-boom push-prop. This research allowed the team to make a trade-off between the two, and to continue developing the tool with one type of configuration in mind. The results in Table 6.1 show that the double-boom push-prop is a far more promising design to develop.

Table 6.1: Preliminary Trade-Off to Select Configuration Type

Performance Paramater	Importance rating	'Single-boom' pull prop	'Double-boom' push prop
Longitudinal Stability	0.28	0.38	0.62
Lateral Stability	0.21	0.44	0.56
Control Qualities	0.21	0.43	0.57
Landing Capabilities	0.07	0.44	0.56
Market Attractiveness	0.14	0.29	0.71
Design Complexity	0.10	0.43	0.57
Final Scores	Standard weighted sum	0.40	0.60
	Conservative design	0.38	0.62
	Aggressive design	0.40	0.60

A new N^2 Chart is required to provide an overview of this more intricate design. This chart was put together piece by piece after constant communication between the systems engineer and each subsystem engineer. This overview was extremely important to the systems engineer in the start of the tool's development, as it allowed him to efficiently communicate the required inputs and outputs for each part of the design, and thus gave the design tool a structure. In addition to this, it also gave a rather comprehensive view of the effect of each various variables on the design to troubleshoot problems in verification.

The chosen design parameters were aspect ratio, cruise speed at the chosen design altitude of 500 [m], material choice, and endurance. Each combination of those parameters will be sized in the design tool after its completion, and its performance analysed; the variation of those design parameters on the design will thus effectively be measured, so by varying these parameters, one is effectively performing a sensitivity analysis which will be analysed in Section 8.3. The overall score of each design will be determined in an engineering trade-off table and the best design will hence be selected in Chapter 8. Following this, the best design's performance shall be analysed as well as its mission in Section 8.5.

"*Sustainable Development is a development that meets the needs of the present without compromising the ability of future generations to meet their own needs*". [11] Sustainable development is one of the AERIS project's key values in its design philosophy, and will be addressed at the systems engineering level. Sustainability goes beyond minimising pollution; truly sustainable ideas must also consider the economic and social implications that the design might have, and this should also

be reflected in the trade-off table if possible; the team has been wary of various 'greenwashing' statements when researching throughout the project.

These rather wide sustainable development goals are up for interpretation, and it may be challenging to find and use a combination of metrics that give sufficient insight to a design's sustainable qualities. One should realise that there will not be a single 'sustainable performance' parameter to evaluate each option, and that sustainable development performance parameters might not always be present in certain trade-offs. The difference in impact of the materials used between designs may, for example, be quantified with the help of an Ecolizer score would be appropriate as it gauges the environmental impact of its production, use and/or disposal of that material whilst also accounting for its recyclable qualities (if applicable). [12]

The new N^2 Chart can be seen in Figure 6.1; it is far more comprehensive than the previous chart as the level of detail of all systems have all substantially increased.

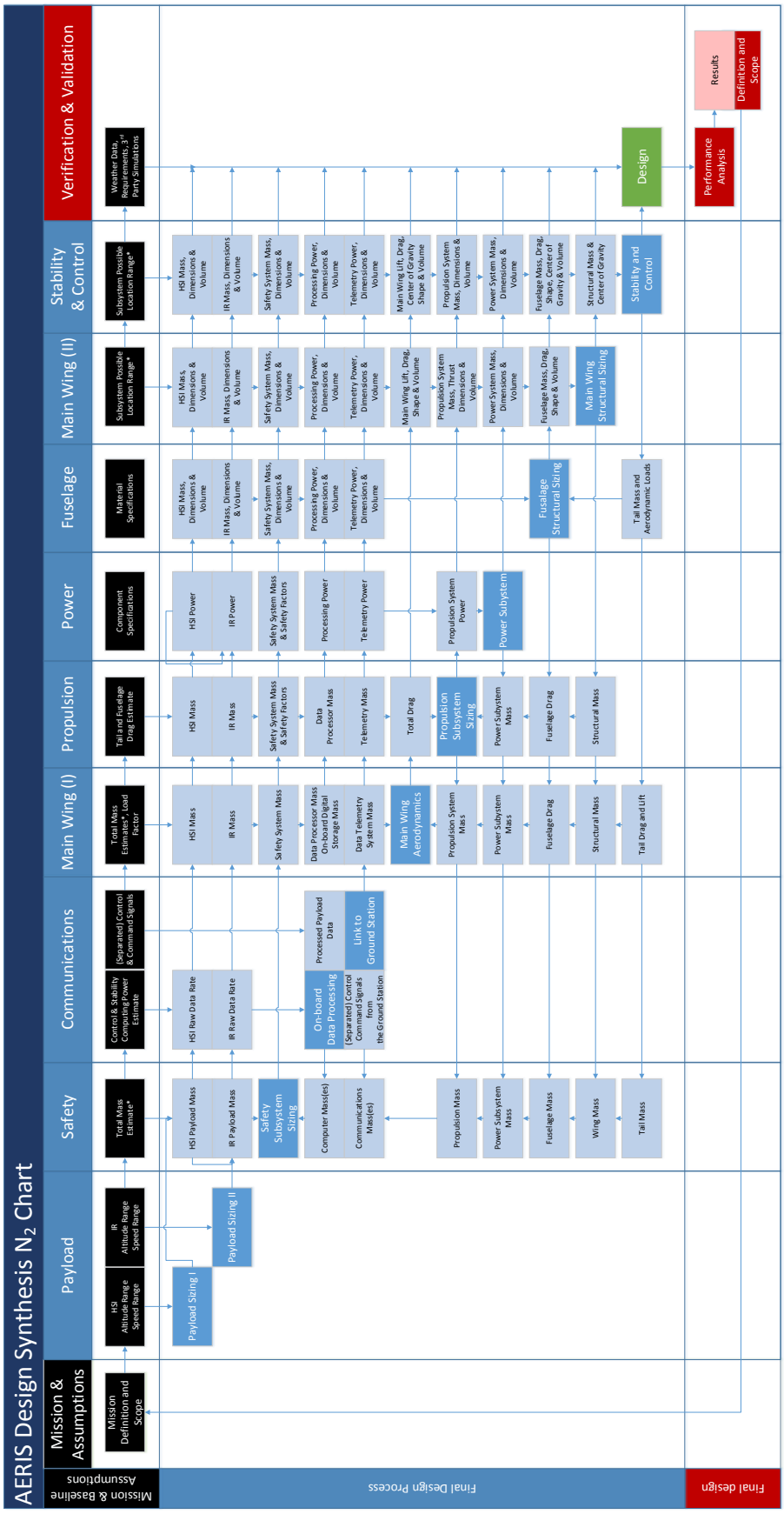

Figure 6.1: The N^2 Chart for the Final Conceptual Design

6.2. PAYLOAD

As the abbreviation implies, AERIS is a system that performs remote sensing whilst in the air. Remote sensing involves the acquiring of information about an object or scene without contacting that object or scene. In the case of AERIS the mission required the use of an HSI. Although the UAV will continuously fly, the HSI produces little to no useful information during the night. It is for this reason, that an IR camera is carried as additional payload. The structure of this section is to first describe the hyperspectral imaging techniques and all technologies that are involved for translating electromagnetic waves to useful data. Secondly the IR camera is described and additional information on expected data rates, system integration and weather influence is discussed.

6.2.1. HYPERSPECTRAL IMAGING

From the MTR it has been learned that hyperspectral imaging is the process of capturing images and gathering information on substances based on their reflectance of frequencies within a large portion of the electromagnetic spectrum. [5] Reflectance is an index that indicates what fraction of the incident light is reflected by a substance. This is measured in a range from zero to one. The range in the spectrum exceeds the range visible by humans. The upper limit of the HSI is usually set to the lower boundaries of IR light and can therefore detect no temperatures lower than 400 [$°C$], hence the use of an additional IR camera as described in the succeeding of this chapter. Commonly, the spectrum is divided in several parts such as Visible Near-Infrared (VNIR) that ranges from $0.4 - 0.97$ [μm] and Short-Wavelength Infrared (SWIR) in the range of $0.9 - 2.5$ [μm]. If one would investigate a narrow part of this spectrum range with only several bands, this is referred to as multispectral imaging. [13] The payload that is carried by AERIS consists of a camera that is able to capture a more significant part of the spectrum whilst using a high spectral resolution. This allows the data handlers to yield more information on the data of the spectrum profile of that imaged object. In fact, each pixel of this image captures not only red, green and blue light, but the entire spectrum range in a multitude of bands.

The camera images the scene line by line using the a so-called Line-Scan scanning mode. One narrow spatial line in the scene is imaged per frame. This line contains all spectral information which is split before the sensor is reached. Then the two-dimensional sensor allows for two dimensions to be captured. Each dimension of this sensor has its own use where one dimension is used for the spatial direction and the other for spectral separation. In our case the movement of the UAV allows for the third dimension to exist. When combined, the result includes every picture of which each contains the complete spectrum to form a two dimensional image for each channel. This visualisation is presented in Figure 6.2. The advantage of this type of imaging is that no movement of parts in the imaging system is required, as the forward motion is provided by the aircraft. This makes the final system more compact, reliable, stable and allows for less maintenance. [14]

HYPERSPECTRAL SENSOR AND FILTER

An image sensor is a device that converts an optical image into an electronic signal. AERIS will use a Complementary Metal–Oxide–Semiconductor (CMOS) imager sensor type from the company Imec. A CMOS imaging chip is a type of active pixel sensor made for constructing integrated circuits using a photodetector in combination with an amplifier. CMOS sensors have an advantage over conventional Charge-Coupled Device (CCD) sensors because all circuit functions can be placed on a single integrated circuit chip. This minimises lead and solder joints which are the main causes of circuit failures. [15] The sensor from Imec is capable processing images in the $600 - 1000$ [nm] VIS to NIR wavelength region with 100 spectral bands which depends on the filter. The resolution of this sensor is 2048×2048 with a pixel pitch of 5.5 [μm]. The spectral resolution, the bandwidth per band, is less than 10 [nm] and is assumed to be 2 [nm] based on reference missions. [16] This means that in each scanned line the width of the line contains 2048 pixels and the spectral information is stored with 2048 pixels as well, making a cube of images.

Customisation of the spectral bands can be achieved by modifying the design of the filter over the CMOS sensor. Additionally, one can tune and design spectral filters such that specific spectral ranges or a number of bands for your camera change, as each camera might have specific applications and needs. In our case the Imec camera comes with a wide enough spectrum to meet the need of our application.

OPTICAL LENS

Lenses are optical components designed to focus or divert light that enable a projection to focus on the sensor to create images. An important output of the lens specification is the FoV. The FoV defines the amount of degrees of how wide the imaging spectrometer can detect in degrees. For practical use, this report sometimes refers to a FoV in respect to the width on the ground that is measured in meters. The FoV is strongly dependant on the focal length of an optical lens. Any camera lens will have a defined focal length, which is the distance where incoming light is focused by the lens into a single point. The focal length, next to sensor specification, will determine the FoV as will be shown further on. The larger the focal length, the smaller the FoV since the angle of view will be narrower.

A sensor is light sensitive. This also implies that both too much and too little light can cause the sensor to be useless in the gathering of useful data. The optical lens will therefore have an Auto Iris mounted on top of it. An Iris controls the incoming light by changing the aperture (diameter) of the lens to maintain the right magnitude of light hitting the sensor. This ensures that images are sharp, clear and with sufficient contrast under a good resolution. An auto Iris uses an analogue signal to control the motor that automatically adjusts the iris according to light levels. As described in Section 6.2.7, weather will influence the performance of the imagers significantly making the Iris control very important. However, for the estimation of data rates an average day with constant light intensity is taken into consideration.

The light that reaches the sensor is dependant on the parameter called exposure time or also called shutter speed. Whenever the objects to be imaged are in low lighting levels, the exposure time will have to be altered to a higher value. Shutter speed goes hand in hand with the frame rate. As an example, if the frame rate is set to 50 Frames Per Second (FPS), the maximum shutter time which can be achieved is 20 $[ms]$. Additionally, varying the shutter speed changes the way movement appears in images. Longer exposure times will therefore blur the images and decrease the spatial resolution. Spatial resolution is an important feature since it determines how small objects can be distinguished from its surroundings in the images by that determining the image resolution. As mentioned before, and as will be shown in the data rate estimation in Section 6.2.4, a constant exposure time is assumed based on an average weather day. The rate of readout is an inverse of the time it takes to digitise one single pixel. A good estimation for the read out time, for one frame rate is often about five percent of the shutter time. Thus, for a shutter time of 100 $[ms]$ the actual shutter time is 95 $[ms]$ where 5 $[ms]$ is required to read the frame. This will not adversely influence the frame rate of the corresponding ten frames per second.

Since the distance between the object of the camera and ground is large, a long focal length is preferred. Longer focal lengths will narrow the field of view which in turn improves spatial resolution. A compact VIS-NIR optical lens compatible with an Auto Iris will have a maximum focal length of around 50 $[mm]$. [17] The length of the HSI lens is 5 $[cm]$ with a Iris lens of six $[cm]$ added to that.

6.2.2. INFRARED CAMERA

As stated before, the HSI makes images based on the reflectance property of materials. This means that external illumination is required to obtain useful data. Since AERIS is continuously flying, hyperspectral imaging is not feasible during night time. For this reason an IR is mounted in the payload as well. For this purpose, a FLIR TAU 640 Core with a narrow field of view lens focal length 50 $[mm]$ and 150 $[g]$ will be used. [18] This type core is light-weight (45 $[g]$), allows for Universal Serial Bus (USB) connection with external devices and supports per-pixel temperature measurement within each recorded frame. The camera parameters settings in each dataset are determined by the software which also enables adjustment for every picture for optimal results.

The resolution of this IR core is 640 by 512 with a pixel pitch of 17 $[\mu m]$. The interesting feature of this IR is the spectral band range of $7.5-13.5$ $[\mu m]$ equivalent to a temperature range of -25 to 160 $[[^{\circ}C]]$ with a minimum sensitivity of 0.05 $[^{\circ}C]$ at high gain settings. The pictures are stored and transferred with eight bits per pixel for highest quality. The data rate equations and results are discussed in Section 6.2.4 and Section 7.1 respectively.

6.2.3. SAFETY INFRARED CAMERA

For safety reasons, it has been specified that an IR is carried that is front viewing to detect heater than air objects such as birds. The body temperatures differ from its surroundings which can hereafter be picked up by the IR. To provide continuous detection, this camera has to stream continuously. The IR used for this purpose will be the same Tau 640 core with the same resolution but now with a 7.5 $[mm]$ lens and a high 90 $[deg]$ field of view. As desired, this camera is able to stream video with optional digital zoom. Compared with the downward IR, the lower focal point results in a larger FoV which will increases impact detection. On the other hand, as will be shown with the equations in the next section, the pixel size will be slightly lower. But as only objects in a relatively short range are considered, this impact is not disastrous compared to the benefits of increased impact detection.

The continuous video stream is processed with eight bits per pixel resulting in a data rate of about 35 $[Mbps]$. This however does not need to be transferred to the ground but will have to be processed with the on-board computer. Software on the computer will analyse the streaming video data for plausible impacts by detecting temperature differences which then can be acted upon with the actuators if needed.

6.2.4. DATA RATE ESTIMATIONS

Using the specifications from the cameras described in the previous sections, this section covers governing equations. These equations are used to determine what the impact of altitude and velocity is on the data rate and resolution of the images.

The equations hold for the HSI as well as the IR but with the inputs from the corresponding specifications as discussed in the preceding sections. The results will be showed and discussed in Section 7.1.

Depending how much light is available during imaging, the shutter speed of the HSI is varied accordingly. The frame rate is as stated before depending on this value. The shutter speed and thus the frame rate will alter the resolution as will be shown later. For the estimation of the data rate, the shutter value is kept constant at the estimated value of 100 $[ms]$. This is done since a lot of parameters have influence on the amount of incoming light as will be described later.

As stated before, the focal length of the lens determines the FoV but also the altitude as can be seen in Equation 6.4. Obviously, a higher altitude will result in a wider camera view.

$$field\ of\ view = \frac{Pixel\ Size \cdot Spatial\ Pixels \cdot Altitude}{Focal\ length}\ [m] \tag{6.4}$$

$$dwell\ time = \frac{FoV}{V_{cruise}}\ [s] \tag{6.5}$$

The IR imaging technique is not the same as Line-scan. The IR camera makes full sized images without making use of the scanning motion. For this reason, the dwell time needs to be determined which is obtained using the FoV. Dwell time is defined as the time required for the UAV to sweep across a full ground segment captured in one frame. The slower the speed, the longer the dwell time is. This allows for a slower frame rate, as shown by Equation 6.5.

For the HSI, the FoV is used to determine the spatial resolution. It can be stated that when a longer period of time is required to cover the same ground length, the dwell time is longer and the frame rate can be reduced. For the HSI the data rate is determined in a different manner since a different imaging technique is used. Here, the scanning motion results in a constant rate of pictures. With the 2048×2048 sensor and the assumed 100 $[msec]$ shutter speed, a bit depth of twelve, the data rate would be 500 $[Mb]$ which is a significant amount of data.

To solve this problem binning is introduced. Binning is the process of registering multiple pixels into one single but larger "super pixel". Since the sensor's spectral resolution is about 2 $[nm]$ and the wavelength region is 400 $[nm]$ from 600 – 1000 $[nm]$, the effective amount of pixels in the spectral resolution is 200 pixels. This means that a binning ratio of eight is sufficient since $2048/8 = 256$ pixels. As a result, the data (63 $[Mb]$) is significantly smaller.

$$Frame\ rate = \frac{1}{Dwell\ time}\ [fps] \tag{6.6}$$

$$Data\ rate = \frac{Frame\ rate \cdot Resolution \cdot Bits/pixel}{1 \cdot 10^6}\ [Mbps] \tag{6.7}$$

The uncompressed (raw) data rate is calculated with Equation 6.7. The frame rate is multiplied with the sensor resolution and the amount of bits per pixel. The images are processed with twelve bits per pixel, which is the bit depth for the HSI and eight bits per pixel for the IR in order to loose as little of information as possible. An advantage of using higher bits of data can be seen when clouds are producing shadows on the ground. The shadowed area are enhanced with the higher bits of data resulting in more detailed images even when the reflection is distorted. [19] The data compression and data handling will be discussed in greater detail in Section 6.4.

Another important aspect to focus on are the dimensions of the pixels, the pixel size. This number gives information on how big objects can be to be distinguished. The pixel size is, as shown by the equations, dependant on the FoV, and thereby the altitude, and velocity. The higher the altitude, the larger FoV and therefore the pixel size. When velocity increases, the length of a pixel will increase when the shutter speed is kept constant. This is the result of a faster dwell time in one shutter time span.

As was shown in the N^2 chart, the payload system data rates outputs that are inputs for the communication system, also the updated masses will contribute to the sizing of the main wing, propulsion, aerodynamics, stability and the power to the power system.

6.2.5. DATA CUBE

Hyperspectral imaging relies on spectral features to detect and identify materials. This detection takes place by comparing the image with spectral signature images of different substances. These spectral signatures have been generated under controlled conditions and are carried on-board the UAV. [20] Once the data is obtained by AERIS, an analogue-to-digital

converter samples the radiance measured in each spectral band and produces digital data at a prescribed resolution. When the two-dimensional images are combined this eventually results in a three-dimensional cube of spectral data. This is often referred to as a spectral data cube. [21] As the images are processed, they are compared to control spectral signature data sets and as soon as the system makes a recognition those pixels are highlighted. [22] An example of a three-dimensional data cube is shown in Figure 6.2.

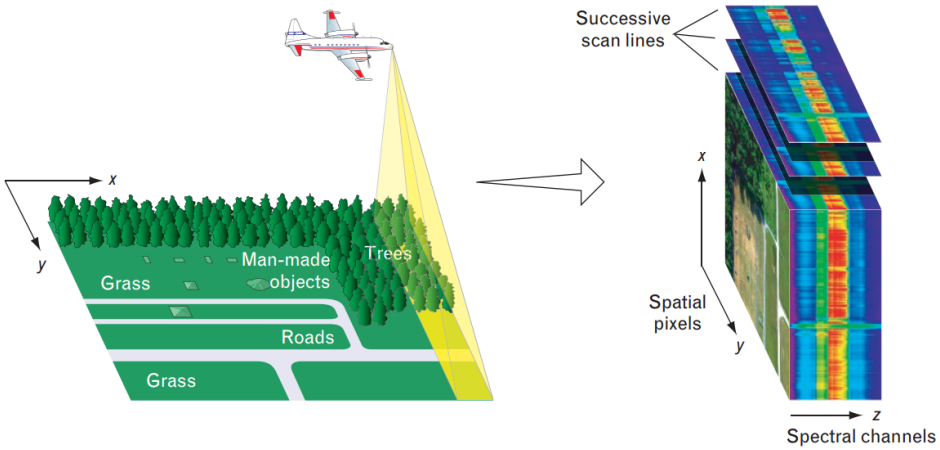

Figure 6.2: Spectral Data Cube Obtained by Scanning the Ground [21]

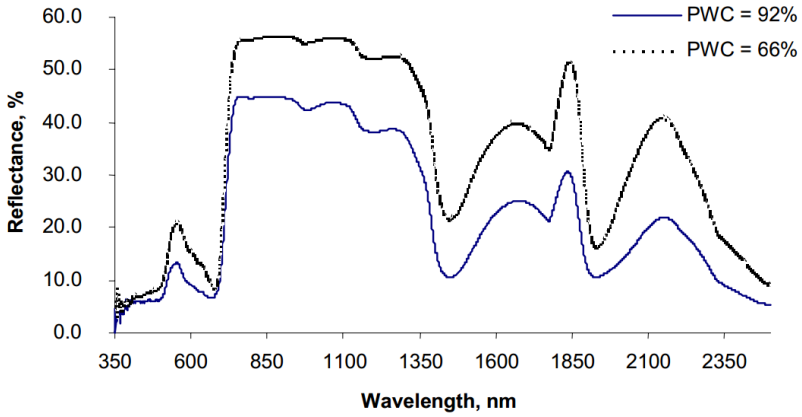

Figure 6.3: Two Different Reflectance Profile of Spinach [23]

Depending on the mission, the acquired data can be used for multiple material detection. In Section 9.1 potential clients will be analysed and discussed. A very promising application of the HSI is vegetation analysis. With data from crops, the development and health can be determined from which the farmers can act upon which otherwise would be impossible. As an example, crops reflectance profile differ when the water content is altered. This can be seen in Figure 6.3 for spinach where higher reflectance is a result of at lower water content. Estimating water content, plant species detection, vegetation classification, fertilizer modelling, crop productivity and more can be studied which will increase the agricultural market's efficiency.

MATERIAL DETECTION

To limit the data coming from the cameras which has to be streamed to the ground, material detection software will be used. The purpose of this is to only store and stream images when certain materials are detected on and or in the ground. This is very beneficial when there are no clients asking for remote sensing of the covered ground. Only images with for example hazardous materials will be send with the rest of the data dissipated.

The detection of materials is based on the identification whether a target exist or does not exist. Common picture classification methods assign one label to each pixel which is called 'hard classification'. However, a more efficient way of classifying pixels containing multiple materials is done with 'soft classification'. Here, multiple labels with an assigned number are used per pixel. These numbers are interpreted with the likelihood of that identification correct thus analysing the presence material in that pixel in more detail. Software algorithms using this way of detection generate target maps at a Constant

False-Alarm Fate (CFAR). These maps hold the information about the observed materials which is then used for the specific applications. [21].

Whenever materials 'targets' are smaller than each picture pixel, which will happen more frequently for increasing altitudes, sub-pixel analysis has to be implemented in the software. Sub-pixel analysis methods are used to determine the amount of material present in an image pixel. This analysis can detect materials which cover one to three percent of the pixel, thus making it important to implement in AERIS system. [24]

6.2.6. COMPONENT INTEGRATION

In this section, the integration of the payload is discussed. As will be shown in Section 6.10, the diameter of the fuselage is mainly based on the dimensions of the payload. For small UAV, often the on-board cameras are combined with turning mirrors. These turning mirrors are used in order to mount the imagers horizontal, 90 $[deg]$, instead of vertical installations since the vertical space is limited. However, the cameras of AERIS will be fit in the fuselage and will thus be placed pointing nadir.

Whenever AERIS is performing manoeuvres, the orientation of the cameras is changed. For this reason a gimbal system will be implemented. A gimbal is a supporting system with integrated servos and the gyroscope which provide yaw, roll and tilt stabilization around the three axis. Nowadays, lightweight gimbals including the servos have weights as less as 120 $[g]$ with dimensions $10x9x8$ $[mm]$ including damping unit with a power input of 7.5 $[W]$. [25] These easy to mount systems gives the freedom to change the payload layout without great effort supporting modularity.

For most aircraft, vibration problems is mechanical fatigue which can have a hazardous impact on fragile parts and electrical components. Blurred pictures and shaky video from the optical equipment are going to cause problems for remote sensing. The most critical reason to implement damping system is therefore to prevent the effect of vibrations for the sensory equipment. [26] The system operated by AERIS is not expected to operate under strong mechanical shocks. This implies that shock absorbers are not needed. On the other hand the system is expected to keep operating under vibrations. These vibrations can be caused by turbulence and are usually small in magnitude and intensity. Along with the periodic nature these vibrations are the most important parameters to design for. The gimbal system will be mounted on a damping unit, gel pads, which is connected to the inner part of the fuselage.

Vibrational impact can be reduced further using the hardware described above combined with software. Software techniques such as filtering and smoothing are used most often to reduce and filter out the imaging errors. Vibration frequencies higher than the shutter time will result in about three percent noise maximum. These vibrations will not be considered disturbing and can be made smooth by software and thereby not influencing the image quality much. [27] When the gimbal, including the damping system and camera with lens are fit in the fuselage, it will be covered with a transparent materials under the fuselage allowing for maximum vision for the cameras.

6.2.7. WEATHER INFLUENCE

Hyperspectral imaging is based on reflectance. So whenever the sunlight is reduced the reflectance profile of materials is lowered for which the HSI has to compensate resulting in in overall decrease in imaging quality.

The cloud ceiling is the altitude of the lowest layer of clouds that are categorized as most cloudy or cloudy. In the last five years, the average cloud ceiling was about 500 $[m]$. [28] Since HSI's are not capable of looking through clouds, AERIS should fly below this ceiling. As will be presented in Section 7.1 the data rate also starts to increase significantly when the altitude is lowered below this value. For this reason, the most optimum altitude for AERIS to fly at is assumed to be at this altitude or lower to prevent significant disturbance. Cloud observation is thus a very important aspect to consider when constant monitoring is required.

As the atmosphere has the property to absorb and scatter light, this influences the images. As light travels from the source, the Sun, towards the Earth's surface the atmosphere modulates the spectrum for the first time. Secondly, after the light is reflected by the surface it is again modulated. Aerosols, such as water vapour and rain, decrease the transmission of atmospheric light. Also parts of the light are scattered, sometimes even directly into the sensor without reaching the ground. This scattered light adds to the conventionally reflected light from the ground that reaches the sensor. This obviously disturbs the image to some degree. Next to this, the light that is diffused by clouds causes it to act as a secondary source of diffused light. This type of light is useful for regions that are normally not in direct sunlight but are now reached by the diffused light. As this light is no longer the full spectrum of the sunlight, this image is disturbed. However, as under normal conditions these shadowed regions were not reached by direct sunlight, this is a positive effect of the diffusion. A final note is that the

light that is reflected from the ground is again travelling through the atmosphere towards the sensor. In this process again some form of distortion takes place and disturbs the data again as scattering occurs. There exist several software programs that allow for compensation of these effects to take place by estimating the atmospheric propagation. [21] This algorithm will be implemented in AERIS' computer as it will improve the overall quality of the images.

6.3. SAFETY

This section describes the overall sizing process and characteristics of dedicated subsystems and key-values for safety. Subsystems that are sized and determined in this section are the back-up battery, anti-collision lights, Emergency Locator Transmitter (ELT) and emergency parachute. Key-values that are determined in this section are the maximum designed wind gust speed to sustain flight in and the system safety margins. The redundancy and resilience of system specific items, such as a back-up communication system, is treated in the respective section of this chapter.

In order to properly size the back-up battery, several parameters need to be determined. First, to get an estimate of the endurance this battery should supply, typical mission profiles of conventional aircraft were investigated. In general, a fuel margin of 45 minutes is brought with. [29] However, since this is an electrical aircraft this endurance should be met by means of battery. The battery with the highest energy density, and hence the lowest overall weight, is a Lithium Thionyl Chloride cell battery designed by Tadiran and has an energy density of 710 $[\frac{Wh}{kg}]$. [30] Unfortunately, these type of batteries have a slow discharge rate and hence do not provide enough power in the timespan needed. Therefore the final battery is chosen to be the Turnigy nano-tech 3000 $[mAh]$ with 14.8 $[V]$. [31] It provides enough Watt-hours to power the engine and on-board electronics and is a separate system to the conventional batteries and is the perfect back-up power supply. Additionally, with an anticipated and expected glide ratio above 30, it is possible to glide for at least 3000 $[m]$ when flying at the minimum altitude of 100 $[m]$. Detailed information on the location and power outputs of this part is found in the power subsystem section (see Section 6.8).

For increased visibility, anti-collision flashing Light-Emitting Diode (LED) lights are used at all times. Furthermore, between sunset and sunrise, additional navigation LED lights are used. This allows the aircraft to partially comply with regulations set by authorities. [32] During day time, on the dedicated locations (wing-tip pointing backwards, up, down) white LED lights flash for one-third of a second. At night the navigation lights (red/green on wing-tip forward, aft) are put on continuously. Each LED requires 1.4 $[W]$ to shine and create 148.5 lumen and operates as low as -40 $[[\circ C]]$. [33] The outline of the safety lights are made visible in Figure 7.4 in Section 7.1.

In order to trace the UAV after a crash landing, the AERIS team will make use of a GPS tracker. Commercial ELTs for aircrafts are designed to withstand flooding and fire, but weigh at least 850 $[g]$ [34], which is too heavy. In order to still be able to locate the UAV after an emergency landing, a Trax GPS locator is used that weighs 25 $[g]$. [35] The device is connected to the emergency bus and possesses an own battery that enables the tracker to work for another day after depletion of the emergency battery. The tracker is able to operate as a stand-alone device without the need of other subsystems since it uses a dedicated communications channel via the cellular network to transmit its location once requested.

The emergency parachute has been sized next. The research performed on recovery systems for fixed wing aircraft has been expanded and a dataset of different sized parachutes and their characteristics was gathered from an expert company on UAV parachutes. [10] Secondly the equation for the speed at which the aircraft falls out of the sky under a parachute was related as found in Equation 6.8. In which the weight is the overall system weight, ρ is the density of the air. Furthermore, the drag coefficient of this type of parachute is relatively high such that the overall weight can be reduced since less surface area is required. The C_{Dpar} is 2.2 $[-]$ and the surface area is determined with a script that chooses the appropriate parachute for the right overall weight. [10] The maximum falling velocity is set to a common 6 $[\frac{m}{s}]$.

$$V_{par} = \sqrt{\frac{2 \cdot W}{\rho \cdot C_{D_{par}} \cdot S_{par}}} \, [\frac{m}{s}] \tag{6.8}$$

In the safety script of the design tool several key-values have been determined that are used in the further design process. These values include the maximum allowed wind gust and safety margins. In the MTR it has already been decided that the aircraft shall be able to fly at wind speeds up to storm force. This implies that the aircraft is able to fly at wind speeds up to 50 $[\frac{km}{h}]$, and hence the maximum one-hour continuous wind speed this aircraft shall be designed for is 14 $[\frac{m}{s}]$. [36] Also, the UAV must be able to sustain gusts of 80 $[\frac{km}{h}]$ which is 22 $[\frac{m}{s}]$. Furthermore, the general safety margin for aerospace structures is applied for generic subsystem calculations. This is found to be and set to 1.5 $[-]$. [37] In Section 8.5 the wind limits will be discussed in greater detail based on statistical data. For subsystems in which there is an increased uncertainty and the quality of the calculations is less, a higher safety margin is applied. This applies mostly for composite structures and 3D printed materials and is found to be and set to 2.0 $[-]$. [38]

6.4. COMMUNICATION

This section describes the approach to define an appropriate communication system on AERIS as well as the ground station. The first step in this approach is to determine the maximum data rate and distance AERIS can deal with. Afterwards, the considered communication topology is presented including a proper link budget.

6.4.1. BACKGROUND INFORMATION

The initial killer requirement for the AERIS mission was to achieve a communication link able to stream the gathered data from the HSI continuously. After analysing several bandwidths in the MTR, it was found that the L band would result in a feasible solution. Now that the design is in a more detailed stage, a new data rate calculation is made in Section 6.2. In here, it can be found that the maximum data rate is increased compared to earlier estimations, and becomes 63 [$Mbps$] occurring in the daytime when the HSI generates pictures at the estimated frame rate during the monitoring phase.

As discussed in the MTR, this amount of data can only be transmitted via radiowaves that reach as far as the LoS. Therefore, it is decided that the antennas gathering and sending data to AERIS will be placed on top of the EWI-building. This building is the highest building in Delft and has a height of 80 [m], which drastically increases the LoS. Placing the antennas at this height, results in a maximum communication distance of 69.5 [km], calculated according to Equation 6.9. However AERIS has an endurance of 7.5 [h], and can therefore have an incredible range. The LoS communication determines the range limit. For the case study, the given distance does not put any limitations to the mission, however when scaling the mission to cover the whole Netherlands, multiple communication systems on ground are required.

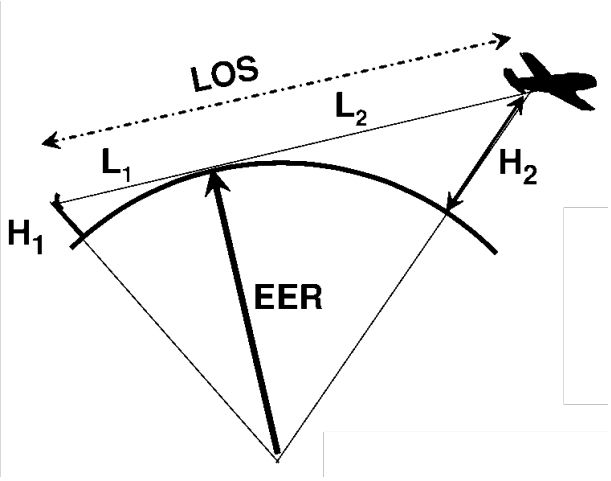

Figure 6.4: Line of Sight

$$Line\ of\ Sight = \sqrt{(2 \cdot (EER) \cdot h_1) + h_1^2} + \sqrt{(2 \cdot (EER) \cdot h_2) + h_2^2} \tag{6.9}$$

Where:

- EER = Equatorial Earth Radius = 6371 [km]
- h_1 = Height of Ground Antenna = 80 [m] (height of the EWI building at the TU Delft)
- h_2 = Height of AERIS = 100 [m] (lowest flying altitude)

To perform a proper link budget calculation, not only the maximum distance is decisive but also the carrier frequency used. Every radio frequency has its own features, e.g. maximum bandwidth and range (that also dependents on the input power). One of the fundamental driving parameters for AERIS was to keep the weight of every subsystem as light as possible. During the research of finding a lightweight radio datalink with a specified bandwidth, it was found that an Ultra High Frequency (UHF) of 2.4 [GHz] is a more suitable solution compared to the L band that was proposed in the MTR. A company specialized in UAV equipment offers an encrypted radio datalink able to send 37 [$Mbps$] over a distance of 50 [km], by making use of the 2.4 [GHz] frequency. [39] Encrypting the communication link between AERIS and the ground is one of the advantages this specific transceiver offers. The second advantage; this transceiver is offered for customer and governmental use. For the link budget calculation, described in Section 6.4.3, the customer edition with a signal power of 600 [mW] is used. However, when the Dutch government supports the mission and a license can be given to the team, a governmental 2 [W] transceiver can be used which allows the maximum range to extend to 200 [km] (in case the antenna is placed on an even higher building).

6.4.2. COMMUNICATION SUBSYSTEMS

From the calculations made in Section 6.2, the bandwidth required to send data coming from the HSI and IR is more than the maximum the radio datalink can handle. At this stage there are two options to overcome this problem. The first option is to use a different bandwidth, the second option is to compress the data on-board. The team has chosen for the latter option, because it is a less power-consuming and more lightweight option. To compress the data from the payload, an extra computer is needed on-board. The computer has six USB connection points, that is sufficient because three USB connections are necessary to connect the HSI and the two IR. It also includes slots for mSATA chips, that can store data in case there is not a proper communication link. On the internal harddrive the team will put software to compress the data from the HSI with a maximum compression ratio of 3 : 1 by making use of specialized HSI software.[40] More specifications for this small computer can be found below. [41]

- **Product name:** Intel NUC Board D54250WYB
- **Processor:** Intel Core i5-4250U Processor
- **Maximum Memory Bandwidth:** 1600 $[GB/s]$
- **Number of USB connections:** 6

Due to the compression ratio of 3 : 1, the data can be send to the ground station without any loss of data. The data will be encrypted by the previous mentioned radio datalink. The radio datalink found has the following properties and the results are shown in Figure 6.5a and 6.5b. [39] Research has shown that the extremely good receiver sensitivity and the multiple modulation techniques make this component able to have a bandwidth of 37 $[Mbps]$ over a large distance. From the safety site of view, the multiple encryption techniques and algorithms also prefer to make use of this specific transceiver.

- **Ultra High Frequency:** 2.4 $[GHz]$
- **Signal to Noise Ratio:** 20, for a bandwidth of 37 $[Mbps]$
- **Output power:** 33 $[dBm]$ = 600 $[mW]$
- **Receiver Sensitivity:** -144 $[dBm]$

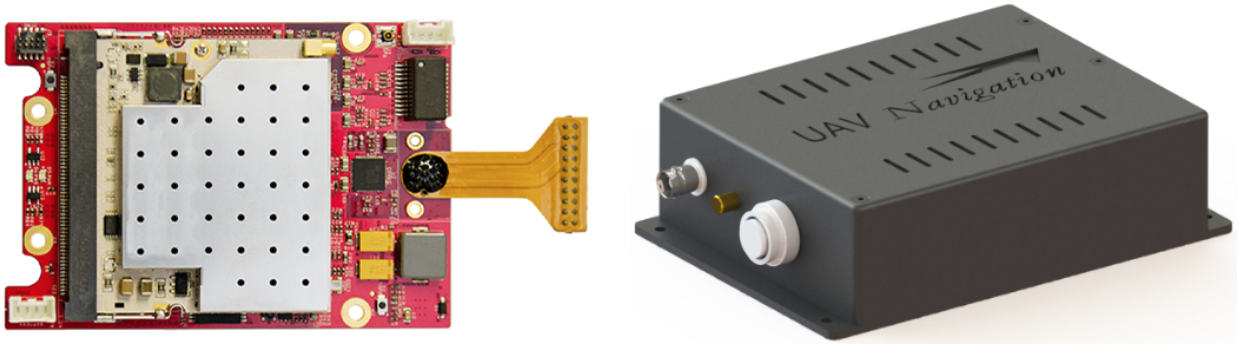

(a) Radio Datalink. [39]

(b) Radio Datalink in Housing. [39]

Figure 6.5: Actual Radio Datalink Hardware

The shown radio datalink is connected to the antenna of AERIS which is responsible for the downlink to the ground station and the uplink from it, shown in Figure 6.6a. This is possible because the antenna can receive and transmit signals at the same time for different frequencies. From the uplink signal, the commands to control AERIS will be received, as from the downlink signal the data from the HSI, and if necessary the front pointing IR imager, will be send. The uplink commands are send by a 430 $[MHz]$ frequency radio signal.

The last communication component is the ADS-B module, that periodically broadcasts a signal so the UAV can be tracked and seen by other aircraft. The signals will be received at the ground station via the auto-tracking ground station antenna shown in Figure 6.6b. This antenna is an auto-tracking antenna, that includes a pan and tilt motor unit allowing the antenna to move in both horizontal and vertical planes.

6.4.3. LINK BUDGET

A link budget is shown in Table 6.2 for the downlink signal. A similar link budget is made for the uplink signal of 430 $[MHz]$ frequency, where for both of the frequencies a coverage map is made, see Figures 6.7a and 6.7b which visualises how well a signal is received at the ground station for a given percentage of time. Due to the height of AERIS, and therefore the antenna, it is assumed that this link has a sufficient Fresnel Zone clearance, meaning that there is no obstruction between the

(a) Omni-Directional 5 [dBi] at 2.4 [GHz] Antenna used on AERIS. [39]

(b) Parabolic 26 [dBi] Twin Grid Tracking Antenna used on the Groundstation. [39]

Figure 6.6: Antennae of the Unmanned Aerial Vehicle and Ground Station Respectively

transmitting and receiving antenna. [42]

The link budget is said to be good when the received power on the ground station, coming from the transmitter of AERIS is sufficient. The Rayleigh Fading model, see Table 6.2 gives an overview for the link margin compared to the time availability of receiving a strong signal.

Table 6.2: Rayleigh Fading Model

Time Availability [%]	***Link Margin [dB]***
90	8
99	18
99.9	28
99.99	38
99.999	48
99.9999	58
99.99999	68

The received power is calculated with Equation 6.10. To start with the losses, by using Equation 6.11 the Free Space Path Loss (FSPL) is calculated. The maximum channel noise can be calculated with Equation 6.12.

$$Received\ Power\ [dBm] = Transmitted\ Power\ [dBm] + Gains\ [dB] - Losses\ [dB] \tag{6.10}$$

$$FSPL\ [dB] = 10 \cdot log\left(\frac{4 \cdot \pi \cdot d \cdot f}{c}\right)^2 \tag{6.11}$$

$$Maximum\ Channel\ Noise\ [dBm] = Received\ Power\ [dBm] - Signal\ to\ Noise\ Ratio\ [dB] \tag{6.12}$$

In the link margin there is an additional loss of 6 [dB], this is done because cabling and connectors introduce extra losses. Choosing 6 [dB] is on the safe site, because a loss of 0.25 [dB] is counted for each connector and an extra 0.1 [dB] loss for each meter of cabling.

This results in the link margin is shown in Equation 6.13:

$$Link\ Margin\ [dB] = Received\ Power\ [dBm] - Receive\ Sensitivity\ [dBm] \tag{6.13}$$

With the given equations, and given inputs, a link budget is made. The main results are summarised in Table 6.3.

As can be seen in Table 6.3 the link margin becomes 61.16 [dB]. Comparing this with the Rayleigh Fading Model in Table 6.2 the link corresponds to an availability of 99.9999% of the time. This percentage of availability is a common percentage in the communication field. [43] To visualize these results, a coverage map, see Figure 6.7a, is made. In this figure the green and yellow colour represent a fade margin of respectively > 20 [dB] and > 10 [dB]. In the coverage map a black line is drawn, it represents a 60 [km] distance, near the edge of LoS flying. In Figure 6.7b the coveragemap for the uplink signal is shown, with a transmitted power signal of 10 [W]. Both figures show the quality of the signal received for 99.9999% of the time. In both figures a line is drawn that represents a distance of 60 [km], these lines are drawn to have a safety margin of 5 [km], before the LoS communication is lost. It is possible to go beyond the LoS without an immediate crash of AERIS,

Table 6.3: Main Results Link Budget

Item	*Value*	*Unit*
Free Space Path Loss	135.62	$[dB]$
Received Power	-82.84	$[dBm]$
Maximum Channel Noise	-102.84	$[dBm]$
Link Margin	61.16	$[dB]$

because the CPU has an integrated software tool that directly sends back AERIS to the ground station in case of a total loss of communication.

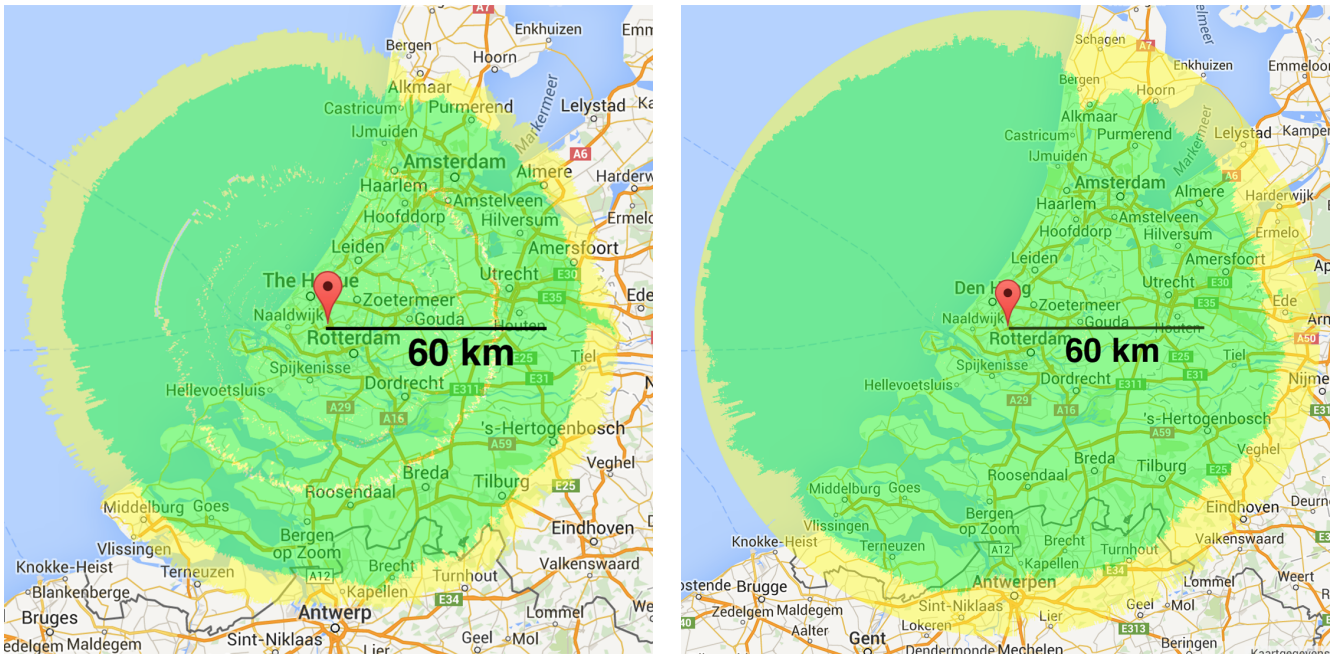

(a) Coverage map for the 2.4 $[GHz]$ Downlink with Tx=0.6 $[W]$

(b) Coveragemap for the 430 $[MHz]$ Uplink with Tx=10 $[W]$

Figure 6.7: Coveragemap for the 2.4 $[GHz]$ and 430 $[MHz]$ Up- and Downlink Respectively For Unique Values of Tx [44]

6.5. AERODYNAMICS

Aerodynamics is the part that makes it possible for AERIS to get and stay airborne. Without a lifting wing, flight is impossible. In the following sections an airfoil will be selected and the wing sizing will be described.

Since the mission of AERIS is to fly continuous, a high lift to drag ratio is desired to have the maximum range and endurance while consuming the least amount of energy. The aerodynamic behaviour of the wing planform, its position and the airfoil's design parameters are analysed to generate the optimum wing that achieves the best aerodynamic performance in order to perform the mission successfully.

6.5.1. AIRFOIL SELECTION

The selection of an airfoil is an important aspect of the aerodynamic design. Basically, the shape of a wing is decided by the shape of the airfoil. The shape of an airfoil provides the sectional geometry of the wing planform. Using this information, the sectional lift and drag can be estimated. The size of the airfoil provides the total volume available in the wing once the span and the chord of the wing are known.

The most important parameters for the selection of an airfoil are $C_{L_{max}}$, stall angle, stall behaviour, thickness ratio, and the capability of storing batteries inside. The stall of the airfoil should be gentle to prevent a dangerous situation when flying at a high angle of attack when a sudden gust increases it above the stall angle. The thickness to chord ratio and the ability to store batteries in the wing go hand in hand. The thickness to chord ratio, together with the chord length, need to provide sufficient space for the batteries.

Using the information stated above, four existing airfoils are selected to further investigate their properties. Two of the selected airfoils are of the NACA system, NACA 2210 and 2410. Furthermore, the Norbert Habe HN 1023 is selected. [45] This airfoil is used on large Radio Controlled (RC) gliders. The SA 7035 is the last one, also a RC glider airfoil. [46] The selected airfoils are simulated in XFLR5 using a Reynolds number of 500,000 to analyse their behaviour with variation in α. The Reynolds number chosen was a guess estimation of flying at an initial velocity of 20 $[\frac{m}{s}]$ at sea level. The obtained plots can be seen in Figures 6.8, 6.9, and 6.10.

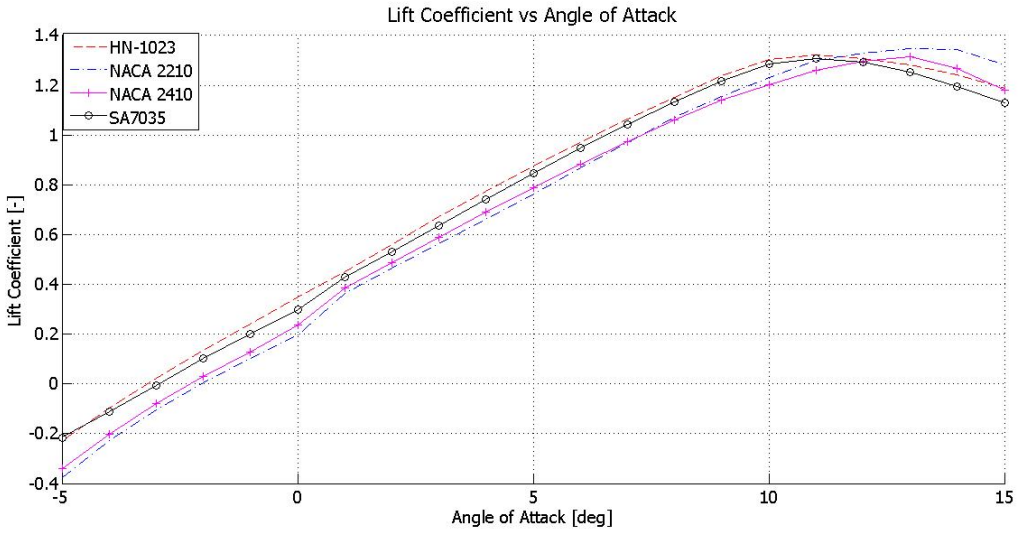

Figure 6.8: Analysis of Lift Coefficient vs α of the Four Airfoils in XFLR5 with $Re = 500,000$

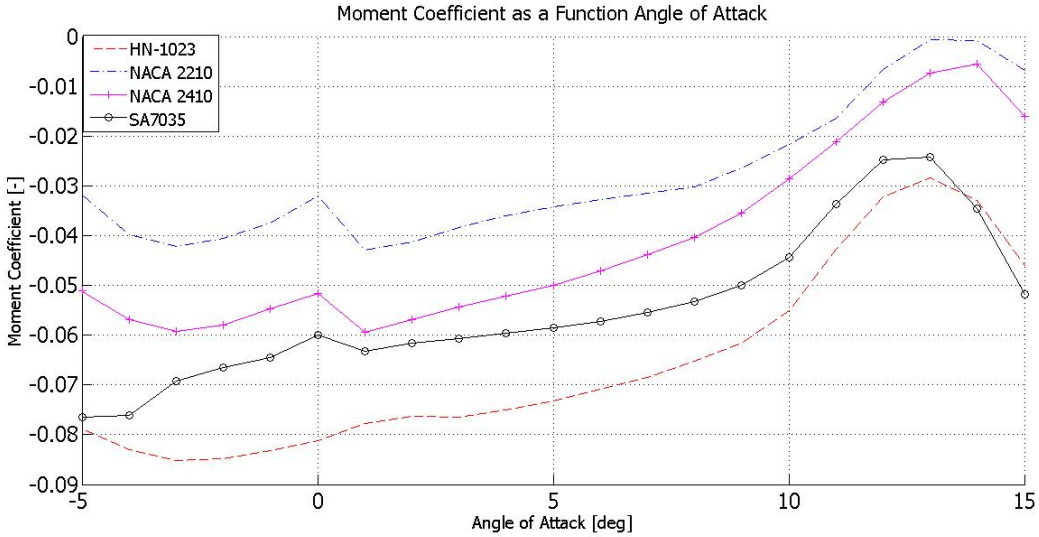

Figure 6.9: Analysis of Moment Coefficient vs α of the Four Airfoils in XFLR5 with $Re = 500,000$

In Figure 6.8 one can see the $C_{L_{max}}$ of the airfoils. The corresponding angle where the airfoil reaches its maximum is the stall angle. A further increase in α beyond the stall angle results in a loss of lift. The maximum lift coefficient of the wing is lower than the maximum of the airfoil. This is because the airfoil is treated as an infinite wing whereas wings, in general, are finite. As a result the slope of the curve decreases, thereby decreasing the maximum lift coefficient. It can be seen that all four selected airfoils have similar stall behaviour as the lift coefficient decreases gradually with increasing α rather than abruptly. This is desirable as it allows safe recovery when the wing stalls. The maximum lift coefficient is inversely proportional to the stall velocity. The airfoil with a higher lift coefficient allows a lower stall velocity which enables the aircraft to fly and land at lower speeds, a property which is preferable.

In Figure 6.9 the variation of the moment coefficient with changing α can be seen. The four curves representing the individual airfoils, have a positive slope. The value of the moment coefficient should be close to zero because the higher the value

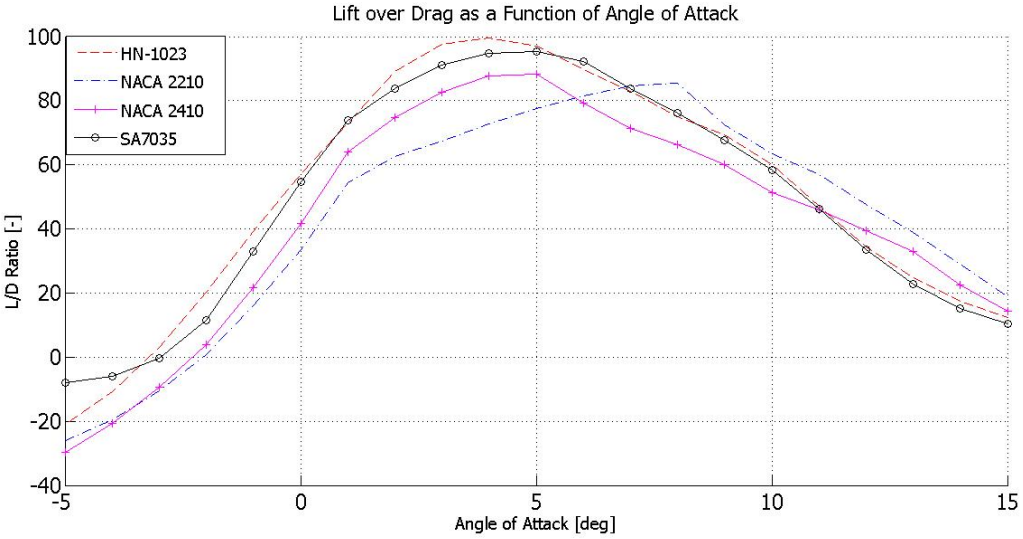

Figure 6.10: Analysis of the Lift over Drag Ratio vs α of Four Airfoils in XFLR5 with $Re = 500{,}000$

of C_m, i.e. more negative, the larger the tail needs to be to counteract this.

In Figure 6.10 the glide ratio is shown. This is the horizontal distance AERIS will cover for each meter it loses in altitude in non- powered gliding flight. The glide ratio is of high importance due to the fact that it has a high impact on the endurance and range of the aircraft. The higher the value, the better AERIS is able to glide. The angle corresponding to the highest glide ratio is the optimum angle for loitering flight. The values in the graph are again for an infinite wing. The glide ratio of the complete aircraft will be less than the values in the graph.

Apart from the obtained graphs, there are other important properties of an airfoil which can affect the design. The properties that influence the design are; the thickness to chord ratio, location of maximum thickness, and $LEradius$. These have a direct impact on drag, maximum lift, stall characteristics, and structural weight. The location of maximum thickness has influence on the nose of the airfoil and affects the lift. If the maximum thickness is located towards the nose, the airfoil generates more lift while pulling up, however, the drag increases due to the transition from laminar to turbulent flow.

The $LEradius$ has a huge impact on the stall characteristics of the wing. An airfoil with a larger $LEradius$ has a more gentle stall than an airfoil with a smaller $LEradius$ which has a sharp and abrupt stall. A higher $LEradius$ restricts the increase in C_D but allows an increase in C_L. Therefore it is helpful in maintaining a good balance between maximum C_L and C_D.

TRADE-OFF

The importance of every aerodynamic aspect is known for the design. Hence, the trade-off is carried out between the selected airfoils. The obtained values of different aerodynamic parameters can be found in Table 6.4.

The selected airfoils are formed into a preliminarily sized wing and simulated in XFLR5 to see the amount of drag experienced by the wing with variation in velocity. As it is expected that AERIS will be flying between 14 $[\frac{m}{s}]$ and 20 $[\frac{m}{s}]$, the preliminary sized wing is simulated within this speed range. The obtained values can be found in Table 6.4.

Table 6.4: Obtained Airfoil Values

Airfoil	***Stall Angle*** $[deg]$	$C_{l_{max}}$	***Maximum*** $\frac{C_l}{C_d}$	$\frac{C_l}{C_d}$ ***at*** $0\,[deg]$ α	C_{L_0}	***Thickness Ratio***	$LEradius$	***Wing Drag*** $[N]$ ***at*** $14\,[\frac{m}{s}]$	***Wing Drag*** $[N]$ ***at*** $20\,[\frac{m}{s}]$
NACA 2210	13.0	1.35	86	35	0.20	0.100	0.1098	2.05	3.20
NACA 2410	13.0	1.31	88	40	0.24	0.100	0.1097	2.05	3.50
SA 7035	14.0	1.30	96	55	0.30	0.092	0.0130	2.00	3.75
HN 1023	11.0	1.32	98	56	0.34	0.102	0.2380	2.20	3.60

During the trade-off, priority is given to certain properties depending on their influence on the design. Important properties are; the wing stall angle, $C_{L_{max}}$, and the drag experienced by the wing with increasing velocity. It can be seen that the NACA

2210 has a higher stall angle, higher $C_{L_{max}}$, and lower drag with increasing velocity. The higher stall angle helps to fly at higher α. Having a higher value of $C_{L_{max}}$ eliminates the need of high lift device which has a huge impact on the structure of the wing as well as the mass of the aircraft. It plays a vital role in decreasing the stall velocity which decreases the approach velocity of the aircraft during landing. It is found that the drag experienced by the wing is lower when the NACA 2210 is used. Having an impact on the energy consumption, endurance, and range of the aircraft.

The glide ratio has a significant impact on the range and endurance of a typical glider. But AERIS is a powered glider, its range and endurance depends on the type and size of the engine. For which, $\frac{L}{D}$ ratio is not considered as one of the determining properties in airfoil selection. Finally, the stall quality of the airfoils are given priorities. The stall quality of all the airfoils are found to be gentle in nature which is desirable. This gentle stall quality allows AERIS more time to recover from a possible stall.

Considering all the arguments and the values obtained, the NACA 2210 is the final airfoil and is represented in Figure 6.11 that will be implement in the design of AERIS.

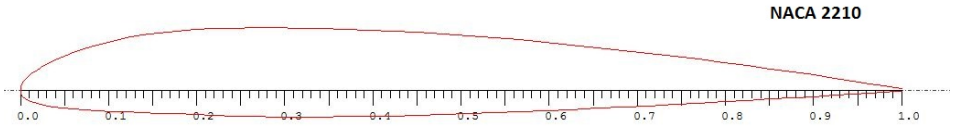

Figure 6.11: NACA 2210 Airfoil Obtained from XFLR5

6.5.2. WING CHARACTERISTICS

Before starting with the estimation of lift, drag, and moment coefficients during various mission phases, a wing needs to be sized. According to the design requirements, AERIS will have a maximum velocity of 100 $[\frac{km}{h}]$ (Mach 0.08) during cruise. This means that it will always fly subsonic, which is less than Mach 0.8 and therefore eliminates the use of wing sweep. The sizing of the wing depends on several wing parameters. The design features a high aspect ratio along with a taper ratio to approach an elliptical lift distribution.

As AERIS is based on a glider type aircraft, it will have a high aspect ratio. Which means that it will have a large span but small chord. Having a large aspect ratio will limit the induced drag which allows it to have a better Rate of Climb (RoC). It is also beneficial for the tail as the downwash is decreased, which increases the stability of AERIS. The disadvantage of a high aspect ratio is the increase in parasite drag as well as the torsion and bending stresses in the wing.

Furthermore, the wing will have a taper ratio of 0.4 $[-]$. By implying this ratio, the lift distribution will approach an elliptical one [47], that also improves the stall behaviour. Furthermore the wing mass will be reduced because the center of gravity gets closer to the fuselage and reduces the bending moment by doing so.

WINGLETS

Winglets are small surface areas located at the wingtip. They are extensions of the wingtip designed to reduce tip vortices. These tip vortices reduces the lift and increase the drag. An example of a winglet can be seen in Figure 6.12. For AERIS the winglet has another purpose next to the reduction of tip vortices, it will be the location of the laser charging panel. Mounting this panel at the wingtip will reduce the bank angle during charging, thereby increasing the wing efficiency and the range.[48]

AERIS will be equipped with a normal winglet. The sizing will be done using data from XFLR5. During validation tests the effectiveness of the winglet will be analysed and, if needed, it will be changed. The size of the winglet is determined by the size of the laser charging panel, as determined in Section 6.8.1, this will be 0.3 $[m] by$ 0.3 $[m]$.

6.5.3. LIFT AND DRAG

The wing shall be able to produce enough lift during various mission phases. The total lift produced by the wing needs to be calculated. The lift produced by the wing depends on the velocity and the density of the air which varies with the change in altitude. Since, it has been decided that NACA 2210 is the airfoil that will be implemented in the wing design, the total lift produced by the wing will be a summation of the sectional lift produced by the wing times the span of the wing. Figure 6.13 shows the lift distribution over the span of the wing. It shows the typical behaviour of using taper ratio in the wing. The lift will be maximum at the root and will be minimum at the tip of the wing. The lift produced and drag experienced by the wing will be discussed further in section 7.2.

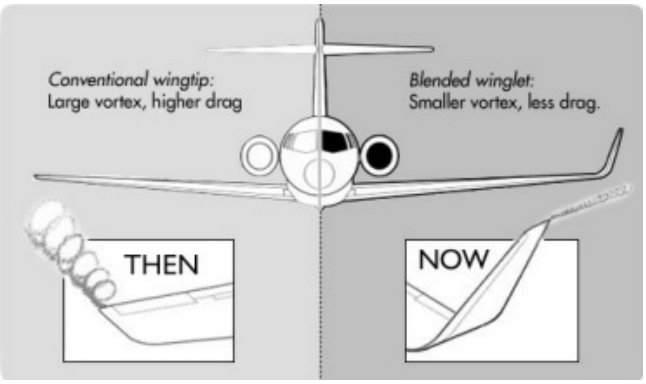

Figure 6.12: Effects of adding Winglets on Tip Vortices [48]

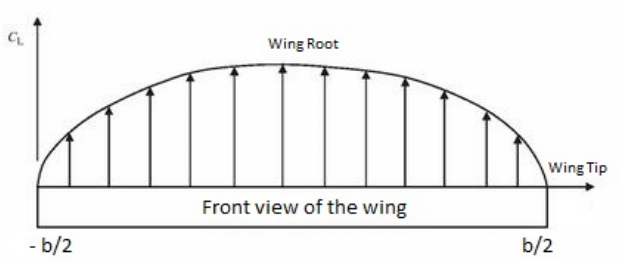

Figure 6.13: Illustration of Lift Distribution over the Span of the Wing

ANALYTICAL C_{D_0}

The following formulas are based on knowledge gathered from "Aircraft Performance Analysis" as made by M. Sadraey from the Daniel Webster College. [49]Drag is the summation of all the forces opposite of the flight direction. Since drag is a function of speed, wing area, air density, and the aircraft configuration, the performance depends on the drag experienced at various flight conditions. To be more specific, the success of AERIS depends on the way it performs without the need of recharging. Which, on its turn, depends on the total C_{D_0} experienced by the aircraft during cruise conditions. Equation 6.14 represents the parameters that can be used to calculate the C_{D_0} in the wing. C_f is the skin friction coefficient which is a function of Reynolds Number. The value of the Reynolds number depends on whether the flow is turbulent or laminar. F_M is a function of Mach Number and so does its value. The S_{wet} is a wetted surface area and f_{tc} is a function of $\left(\frac{t}{c}\right)_{max}$ which is the maximum thickness to chord ratio of NACA 2210. $C_{D_{min}}$ is the minimum profile drag coefficient of NACA 2210. It is also found that the C_{D_0} of fuselage is very small compared to the wing. Hence, using some preliminary values such as initial weight and wing span obtained in the MTR, an initial value of 0.02 is used during the first iteration.

$$C_{D_{0_w}} = C_f \cdot F_M \cdot f_{tc} \cdot \left(\frac{S_{wet}}{b}\right) \cdot \left(\frac{C_{D_{min}}}{0.004}\right)^{0.4} \tag{6.14}$$

The wing is not the only part of AERIS creating drag, there are other parts and components that contribute as well. Since the interference between the wing and the fuselage is a high wing configuration, there is a drag contribution from the interaction of the fuselage boundary layer with that from the lower surface of the wing and because there are two fuselages this happens two times. Also the communication antenna of AERIS is located on the outside of the aircraft, therefore generating additional drag. Also air flowing through small gaps between the control surfaces produces turbulent air and thereby extra drag.

6.6. PROPULSION

This section shows the detailed design of the propulsion system. First of all the basic equations of motion are discussed. Next to that, for part of this design the linear momentum theory is used, this is discussed in the second section. After this the radius of the propeller is determined. To have an efficient propeller the proper airfoil should be selected. Furthermore the most efficient Revolutions per Minute (RPM) is determined together with the angle of twist and the chord distribution. This all is optimized for the cruise condition at which the UAV is flying. This gives an efficiency which is used to determine the power used in cruise and the maximum power required. [50] [51].

6.6.1. BASIC EQUATIONS OF MOTION

To size the propulsion system it is necessary to first take a look at the basic equations of motion. In order to fly, the propulsion system has to overcome the drag. For cruise conditions this is calculated in Equation 6.15.

When ascending or descending, but still remaining equilibrium conditions, the thrust changes due to changes in the density and speed. This is important for the power required. As shown in Equation 6.16.

As can be seen here, the required power increases when the speed increases. Next to that, the drag increases with the square of the speed. When ascending the cruise speed increases to produce enough lift at lower densities. This causes the power required to increase when reaching higher altitudes.

Since AERIS does not use a runway there is no high engine power required during take-off. The maximum available power is therefore determined by another situation, the service ceiling that is located at 4000 [m]. At this point no further climbing

is required. For low speeds the RoC is calculated using Equation 6.17. This shows that the available power is equal to the required power during cruise at the ceiling altitude.

$$T = D \tag{6.15}$$

$$P_r = T \cdot V_0 \tag{6.16}$$

$$RoC = \frac{P_a - P_r}{W} \tag{6.17}$$

6.6.2. LINEAR MOMENTUM THEORY

To be able to determine the radius of the propeller blade, the linear momentum theory is used. This theory comes from the situation drawn in Figure 6.15.

From the momentum theory Equation 6.18 follows. Rewriting this results in Equation 6.19

$$T = \dot{m} \cdot (V_e - V_0) \tag{6.18}$$

$$V_e = \sqrt{\frac{2 \cdot T}{\rho_{air} \cdot 2 \cdot \pi \cdot R^2}} \tag{6.19}$$

The exit velocity is an important parameter when it comes to the propulsive efficiency. This efficiency is determined by dividing the work that is done by the thrust and the energy put in to the flow. Again looking at Figure 6.15 this can be derived to be Equation 6.20. Rewriting yields Equation 6.21.

$$\eta_{prop} = \frac{T \cdot V_0}{0.5\dot{m} \cdot \left({V_e}^2 - {V_0}^2\right)} \tag{6.20}$$

$$\eta_{prop} = \frac{2}{1 + \frac{V_e}{V_0}} \tag{6.21}$$

6.6.3. PROPELLER RADIUS

Substituting Equation 6.19 into Equation 6.21 and using the thrust required in cruise condition at cruising altitude. The most efficient radius can be determined. As can be seen, when the exit velocity decreases, the efficiency increases. This exit velocity decreases when the radius of the propeller increases. This will converge to an efficiency of one. To come close to such a number a huge radius is required. Therefore the radius is selected such that the efficiency will be 0.95 [−]. This is investigated to be a value which gives a reasonable radius.

6.6.4. BLADE DESIGN

To design the propeller blade more detailed, the airfoil has to be selected. For a long endurance aircraft a propeller blade with a high lift over drag ratio is preferred. A common airfoil in the propeller industry is the Clark Y airfoil. [52] To give more insight in this airfoil type, the lift over drag ratio is presented as a function of the angle of attack in Figure 6.14. The Clark Y airfoil is the airfoil that is used in this propeller design.

To determine the total efficiency of the engine, a more accurate way of estimating is dividing the work done by the propeller blade by the brake power produced. As shown in Equation 6.22.

$$\eta_{prop} = \frac{T \cdot V_0}{2 \cdot \pi \cdot n \cdot Q} \tag{6.22}$$

The RPM is an important factor in these calculations. In most engine specifications it is stated per minute, but in the calculations the Revolutions per Second (RPS) is used. From Equation 6.22 it can be seen that if the RPS decreases, the efficiency increases. Therefore a slow turning blade will be most efficient. The RPS of the propeller blade will be sized such that it achieves the lowest possible value but produces enough thrust to overcome the drag. The maximum required RPS is determined by the cruise condition at maximum altitude and the maximum speed at sea level since the velocity is higher here, a higher RPS is required to maintain cruise at both of these conditions.

When looking more closely at a section of the blade, as shown in Figure 6.16. The thrust and torque per element can be calculated. Then by integrating over the entire blade the total thrust and torque can be calculated. The thrust and torque per element are calculated in Equations 6.23 and 6.24 respectively.

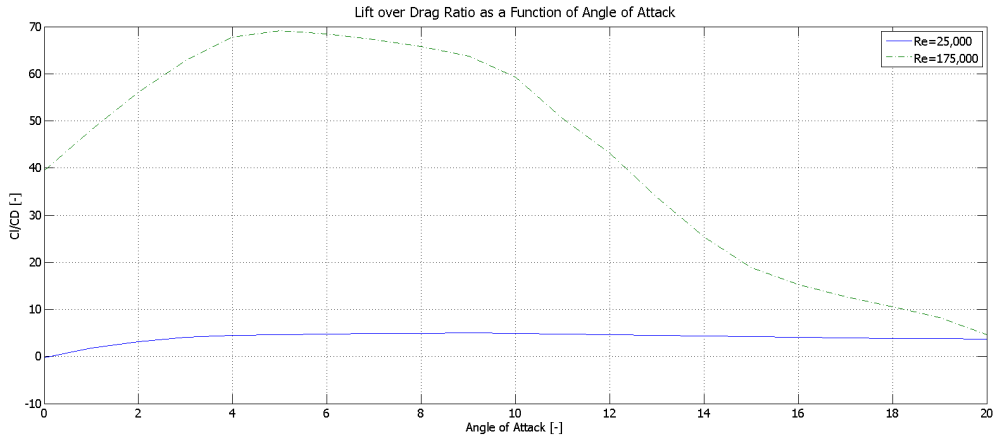

Figure 6.14: The Lift over Drag Ratio of the Clark Y Airfoil as a Function of the Angle of Attack

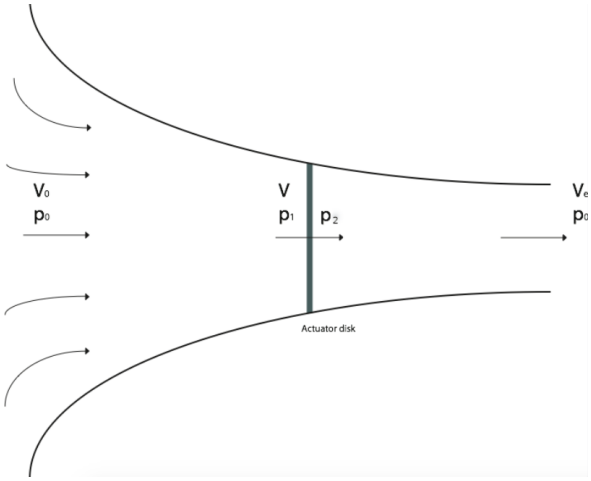

Figure 6.15: Visual Representation of the Actuator Disc

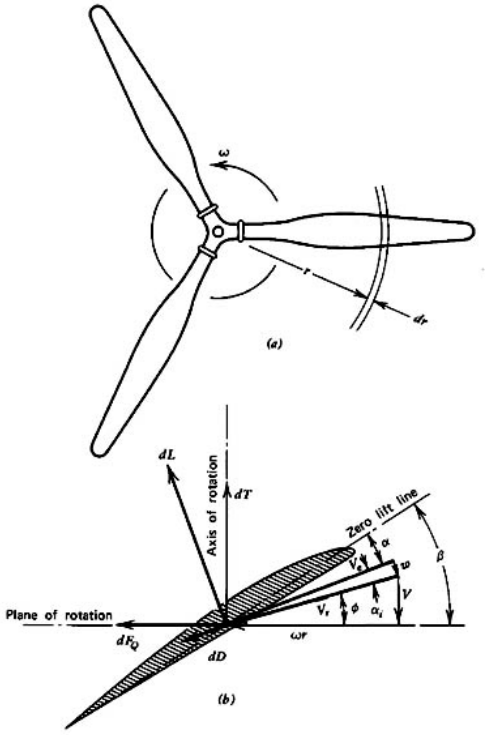

Figure 6.16: Visual Representation of a Propeller Blade Section [50]

$$dT = dL \cdot cos\left(\phi + \alpha_i\right) - dD \cdot sin\left(\phi + \alpha_i\right) \tag{6.23}$$

$$dQ = r \cdot \left[dL \cdot sin\left(\phi + \alpha_i\right) + dD \cdot cos\left(\phi + \alpha_i\right)\right] \tag{6.24}$$

For simplification it is assumed that the induced angle of attack is very small and can be neglected. The lift and drag per section are calculated as shown in Equation 6.25 and 6.26.

$$dL = \frac{1}{2} \cdot \rho_{air} \cdot c \cdot C_L \cdot \left({V_0}^2 + (2 \cdot \pi \cdot n \cdot R)^2\right) dr \tag{6.25}$$

$$dD = \frac{1}{2} \cdot \rho_{air} \cdot c \cdot C_D \cdot \left({V_0}^2 + (2 \cdot \pi \cdot n \cdot R)^2\right) dr \tag{6.26}$$

With the RPS known, the speed per element can be calculated and therefore the angle of incidence per element can be determined. This angle is optimized for the cruise speed at the optimal altitude and it is fixed throughout the entire mission.

The reason for this is that a variable pitch system is heavy and the UAV will spend most time flying at this optimal point. From Figure 6.16 Equation 6.27 follows.

$$\phi = tan^{-1}\left(\frac{V_0}{\omega \cdot r}\right) = tan^{-1}\left(\frac{V_0}{2 \cdot \pi n \cdot r}\right) \tag{6.27}$$

The blade angle per element is the angle of incidence and the angle of attack added to each other. From Figure 6.14 the angle of attack at which the $\frac{C_L}{C_D}$ is highest is 5 $[deg]$. A value of 5 $[deg]$ will be added to each section to determine the blade angle.

Next to the RPS and the blade angle, the chord distribution has to be determined. By taking dummy values it was determined that the most efficient section is at 70% of the blade radius. Next to that by [53] and engineering gut the maximum chord length is taken to be 20% of the blade radius. This maximum chord length is applied at 70% of the blade radius. The first 20% of the blade radius is very inefficient and the chord length has a minimum value of $0.05R$ chord length here. The rest of the sections is sized such that it provides enough thrust to overcome the drag in cruise at the minimum RPS if this is not possible the RPS is increased and the chord distribution is calculated again. Due to this procedure, a very efficient blade is designed.

6.6.5. ENGINE POWER

Now that the RPS, the blade angle, the chord distribution and the radius of the propeller blade are all known. The total efficiency can be determined by Equation 6.22. Using this efficiency the maximum required power and the power consumed in cruise can both be determined as shown in Equations 6.28 and 6.29.

$$P_{cruise} = \frac{P_r}{\eta_{prop}} \tag{6.28}$$

$$P_{max} = \frac{P_a}{\eta_{prop}} \tag{6.29}$$

6.6.6. ENGINE HARDWARE

Now that the blade is designed and the RPM of the propeller has been determined it is time to take a look at the hardware. This has to be done in order to determine the weight and cost of this part.

BLADE

The entire geometry of the blade is now determined. With this data a volume of one blade can be determined. Next to that it is most efficient to have as less propeller blades as possible. But one blade will give an asymmetrical thrust which causes moments in the structure. This is something that should be avoided. Therefore two blades are used on this propulsion system. If a material type is selected the weight of the blades can be determined.

The volume can be determined by dividing the airfoil shape of each blade element in n sections. These sections are evenly divided and running from the leading edge until the trailing edge of the airfoil. The volume is determined using Equation 6.30.

$$dV = \Sigma_{i=1}^{n} \frac{\left((\frac{t}{c})_i + (\frac{t}{c})_{i+1}\right) \cdot c}{2} \cdot c_i \cdot dr \tag{6.30}$$

This is done for every blade element using the chord distribution calculated before.

Most propellers are made out of wood but composite propellers are also available. Using a composite propeller for continuous flight has an advantage: composites are not influenced by corrosion, this perk reduces maintenance. Composite propellers are very complex to produce and the loads on the propeller are in all directions and complex. Therefore manufacturing could get very expensive. Though filling the entire volume with material would cause the blades to be very heavy, therefore a cross section as presented in Figure 6.17 would be most efficient.

From [55] it is found that the density of carbon fibre varies form $1600 - 1900$ $[\frac{kg}{m^3}]$. From [56] it is found that honeycomb structures have a density that varies from $50 - 70$ $[\frac{kg}{m^3}]$. It is assumed that foam is around the same density as honeycomb. Given the current resources there is too little time to calculate the forces present in the propeller blades. Therefore a carbon fibre to honeycomb and foam ratio has to be assumed. It is assumed that the blade consists of 10% carbon fibre and 90% foam or honeycomb. This would result in an average density of around 205 $[\frac{kg}{m^3}]$. This ratio is based on engineering feeling.

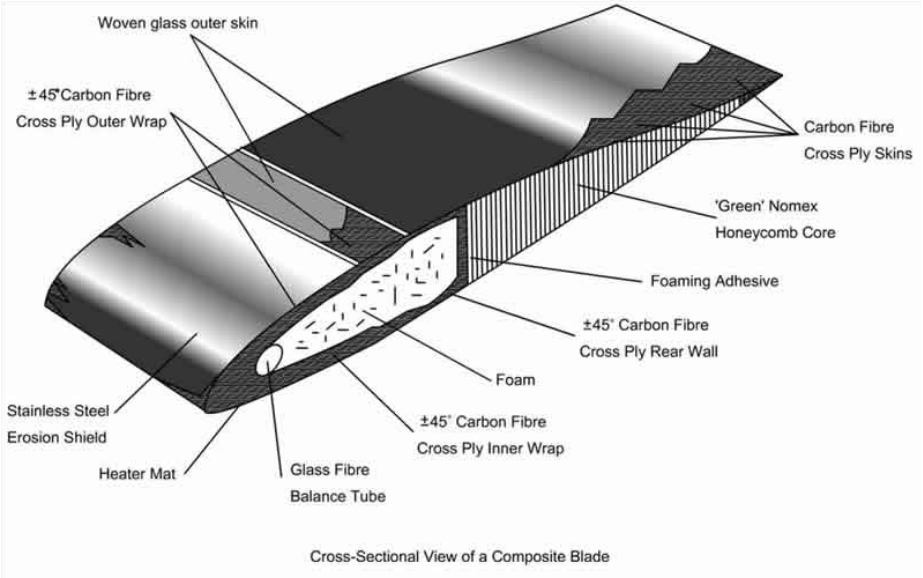

Figure 6.17: Example of a Composite Blade Cross Section [54]

ENGINE

The engine has to be determined as well. As was determined, the propeller has a high diameter and turns at a low RPM for the best efficiency. To achieve these values a gearbox is required. The gear ratio depends on the selected engine and the calculated RPM. This selection is done after the results are found.

Next to the engine the propeller blades are foldable there are two main reasons why this choice is made: The first reason is that without a landing gear the ground clearance is not enough and the engine will be damaged during landing. Secondly a propeller that folds when inactive is aerodynamically more efficient, especially for a glider. The way such a foldable propeller works is that the centrifugal forces push the propeller blades outwards if the engine stops spinning the drag forces will force the blades to fold back to their original position. What still has to be investigated is if the centrifugal forces can overcome the drag forces. This is considered to be out of the scope of this report.

6.7. STABILITY AND CONTROL

This section describes the approach to longitudinal and lateral stability analysis and the preliminary tailsizing. Furthermore the controllability of the preliminary design configuration is analysed. The sizing has been done by a script written in MATLAB. This section will provide a detailed walk through of the scripts and its function while the theory used in the analysis is explained.

The control and stability of the UAV has been based on the following requirements:

1. Ensure moment equilibrium in steady flight (trim condition) during monitoring
2. Ensure stability around this state of equilibrium. In other words: ensure that after sudden disturbance the aircraft restores to its original equilibrium position in relatively short time frame and with acceptable oscillations period and amplitude (ensure adequate damping)
3. Ensure ability to generate forces for manoeuvring, hence, alter the state of equilibrium when required. In other words: controllability in roll, yaw and pitch during flight manoeuvres.
4. Ensure stability and controllability in case of unexpected and inevitable design changes in the last stages of the design
5. Ensure stability and controllability while allowing payload modularity and the change in total mass due to maintenance, structural or hardware updates/modifications

The script has been designed to optimise the tail sizing and balancing of the aircraft for a given configuration of masses, wing, and planform to provide the required performance for a typical mission profile of the UAV. The optimisation has been performed in favour of low drag and minimal weight. Furthermore safety factors and margins have been implemented to allow a shift in the cg range that might occur when UAV experiences hardware updates, repairs or other types of mainte-

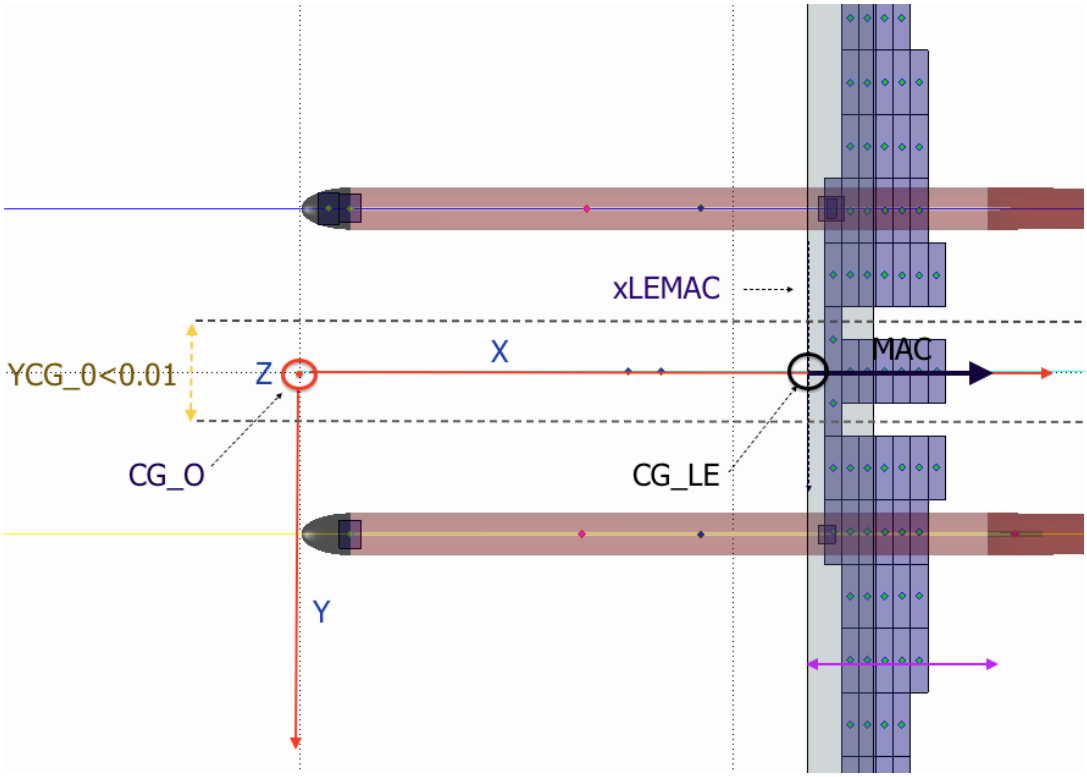

Figure 6.18: Definitions of Two Coordinates Systems Definitions and the Margin Allowed For YCG Location

nance that will either add or reduce the mass.

The script consist of several parts each performing a certain task of the analysis. The end result is achieved when the all of the results are combined.

6.7.1. DETERMINATION OF MASS DISTRIBUTION

This part of the script determines the equilibrium of AERIS in its given mission configuration. Next to that it optimises the battery, systems, and payload configuration locations with respect to the wing position. Furthermore it is used to produce a loading diagram to investigate the effects of changing the payload and battery mass on the cg location.

The scripts starts with taking input on the aircraft dimensions such as wing span, surface area, and the initial masses. It than calculates and stores the cg locations of the components that need a certain fixed location inside the UAV. These are, for example, the payload, located in the nose of the fuselage booms, the safety parachute, and the fuselage booms itself, which are located at a fixed distance with respect to the axis of symmetry. This distance is the propeller diameter times one and a half to ensure safe operation of the engine and also to ensure that the tail stays out of the engine wake.

The locations are defined with respect to two coordinates systems: The UAV overall coordinate system or the fuselage group coordinate system defined as cg_0 and the mean aerodynamic cord leading edge system or the wing group coordinate system defined as CG_{LE}. These coordinate systems are presented in Figure 6.18.

SYMMETRY PLANE AND BATTERY FILLING PROCESS

Once the fixed masses are given together with their positions in the cg_0 coordinate system the script must determine the position of the batteries. The positioning of the batteries is crucial for the location of the y-coordinate of the overall centre of gravity YCG_0. In order to have a symmetry plane in the XZ-plane the UAV need its y-location of the cg to be almost zero. The combination of the payload and the two boom configuration presents a challenge. In a conventional one boom aircraft the payload would most likely be placed in fuselage body. That nearly always is positioned in the symmetry plane (XZ), consequently no additional balancing in y-direction is required. AERIS in contrast has an asymmetric distribution of its payload:

1. A bundle of HSI and IR camera in the right fuselage with gimbal and an additional IR camera for forward vision.

2. Additionally on the left wing tip a special solar panel including heavy cabling needs to be mounted to enable laser charging.
3. Safety parachute placed in one of the two booms
4. Two board computers of different mass and size and a power processing unit distributed over two fuselages

Instead of adding additional dead weight on the opposite side to balance, most logical choice is to shift the batteries to get the desired balance in the y-axis. Therefore, additional effort has been put into designing and algorithm to implement a battery filling an balancing process. Figure 6.19 shows the payload and components on-board AERIS.

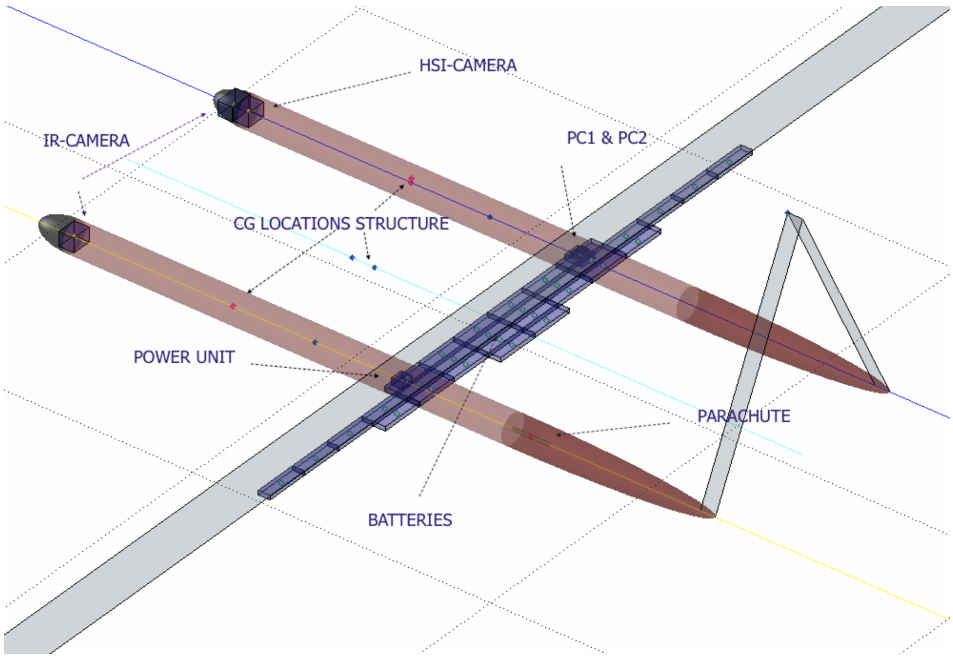

Figure 6.19: Payload and System Components with 20 Battery Packs as an example with the Coordinate System indicated

The algorithm works in the following way; once the wing dimensions are defined, the algorithm defines a space large enough to fit in the wing volume with some margin for cabling and control surfaces. Next, it fills that space with rows of batteries, optimising for stability. The filling process is stepwise, just as a person would fill a box with blocks. The algorithm first fills one row, then checks how many batteries are left and places these on the next row flush to the previous one. The space is defined to have enough thickness such that it will allow additional rows to be placed on top of the first row if the number of rows cannot fit on the first level along the wing cord. Furthermore the batteries are distributed such that the weight is centred around the cg to have a stable moment of inertia while performing turns. Another reason is to prevent flutter of the wings in flight: placing the batteries to far outboard, without adding sufficient weight in the space between may result in flutter or other unwanted motions, introducing high bending and torsional loads on the structure. Figures 6.19 and 6.20 give examples of how the batteries are arranged for different amounts of batteries. They clearly show how the row size reduces going from leading edge to tip, while the number of batteries cascades down.

Once all the batteries are placed, the script calculates the YCG_0 location of the entire UAV and checks if the symmetry plane exists, i.e. if the YCG_0 is around zero. Depending on the sign of this parameter, the script shifts the row either left or right by 0.01 $[m]$ until equilibrium in y-direction is reached. The equilibrium is defined as and absolute value lower than 0.05 $[m]$. This margin is depicted in Figure 6.18.

LOADING DIAGRAM

In the stability analysis, the wing setting plays an important role in sizing the required configuration of the tail. Depending on the wing position, the tail can either have a conventional tail configuration with the tail behind the wing or can be in canard configuration. For AERIS, the conventional tail design was chosen to be the most suitable in terms of payload functionality and drag, which will be touched later in this section. Payload functionality requires the cameras, especially the front viewing safety IR camera to have an unobstructed view. In a canard configuration this might pose additional challenge as the view may be obstructed depending on the angle of rotation of the gimbal.

The wing position is defined as the ratio of x-positions of the cg of the wing, $\frac{X_{cg_{LEMAC}}}{l_f}$, measured from the leading edge mean aerodynamic cord, and the fuselage length, expressed as percentage of the cord length of the mean aerodynamic

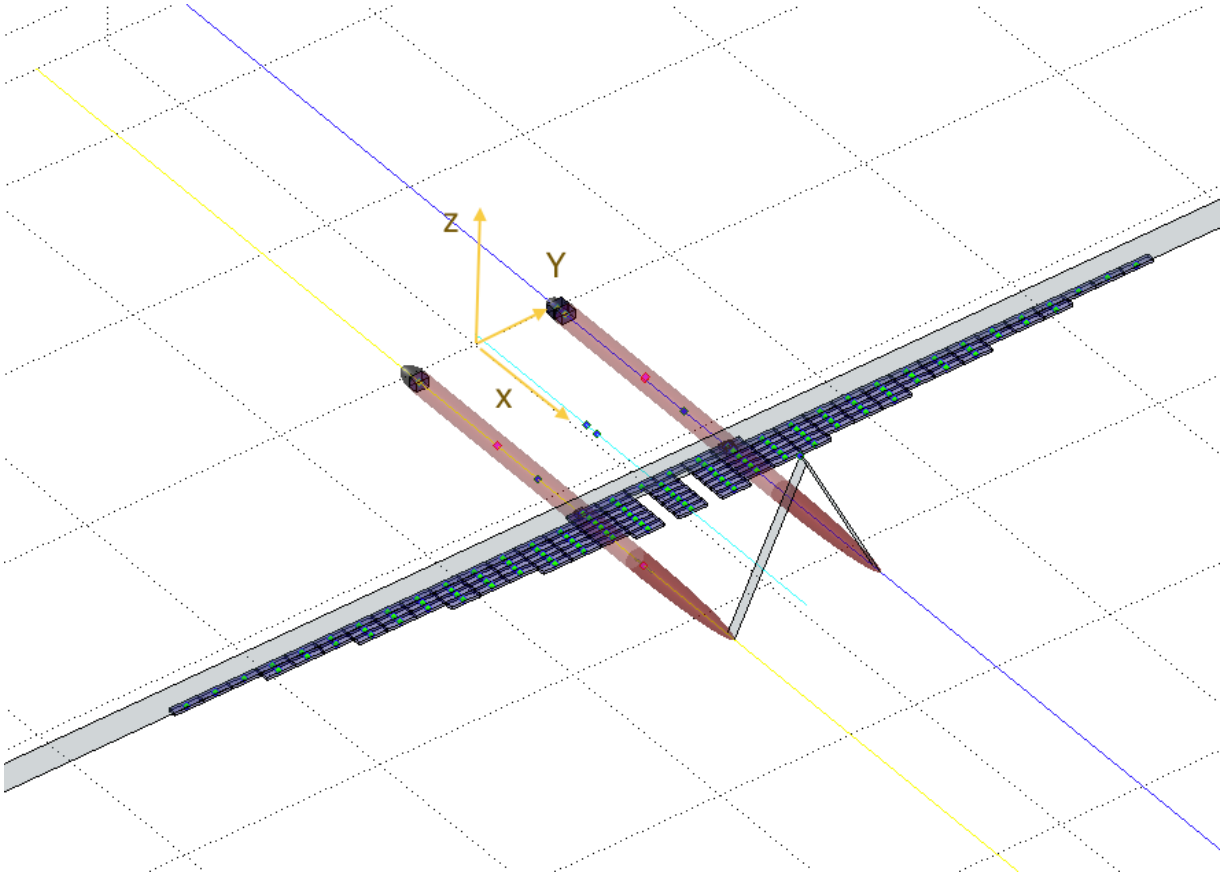

Figure 6.20: 3D MATLAB Plot of the Battery Layout for 39 Batterypacks

cord,$\bar{x}$. This parameter is thus a percentage value, ranging from 20 – 50 and is expressed in the second coordinate system, CG_{LE} as mentioned earlier.

EFFECTS OF MARGINS ON CENTRE OF GRAVITY TRAVEL

The final part of the script is to define the effect of changing the battery and payload weight on the range of x-positions of the cg travel. The parameter cg travel, defines the allowance of the cg to shift from the initial cg location. It sets a limit on the most aft and the most forward cg location (in x) the aircraft is allowed to have while the stability and controllability is ensured. This is, in essence, a safety limit on the weight that may be added or reduced on key locations of the aircraft. This may happen for several reasons:

- Flying with fewer passengers than maximum
- Passengers have different weight and cargo that may change during each flight
- Passengers moving from one end to other (visit to the toilet)
- Added weight from repairs of panels or other parts
- New type of engine or batteries with different weight
- New type of payload (cameras), additional payload to be attached
- Other unexpected design changes in the last stages of the design that add weight

The first cases are not valid for AERIS but the latter ones are a very realistic scenario. During its mission AERIS may experience maintenance on the bottom fuselage due to belly landing for example. These may have to be reinforced with additional material and thus added weight, that must be accounted for in the design. Another example is modularity of the payload that has been mentioned earlier, the camera type might change or additional lenses must be added to the payload to provide what the market needs.

In the AERIS design this has been implemented in the mass of payload and batteries as these are the most likely candidates to be modified once the UAV has been built. A margin of ±25% for both the battery as the payload is used. The battery and payload mass is recalculated again for 25% margin and plotted as the ratio $\frac{X_{cg_{LEMAC}}}{l_f}$ on the y-axis over the location of the cg expressed in percentage of mean aerodynamic chord (m.a.c.). This loading diagram consists of two curves, one is for the

most forward position of the cg the other for the most aft. Their difference is the required cg range that is required for a given wing setting. See Figure 6.22.

6.7.2. TAIL SIZING

This part of the script assesses the required horizontal tail surface, S_h needed to provide longitudinal stability. It runs after the the masses and their locations are determined and compares the results to provide the optimal range of S_v and $\frac{X_{cg_{LEMAC}}}{l_f}$. The analysis is again based on the method provided in the slides of the course System Design III. [57]

LONGITUDINAL STABILITY DERIVATIVE

The whole stability analysis is based on the requirement to provide stability around the cg of the aircraft. The most key conditions are stated in Equations 6.31 and 6.32.

$$C_{m_\alpha} < 0 \tag{6.31}$$

$$x_{n.p.} - x_{c.g.} > 0 \tag{6.32}$$

These two conditions demand that the cg must always stay in front of the neutral point and the moment coefficient around the aerodynamic centre (a.c.) must be negative. The latter case ensures that when the aircraft experiences a sudden disturbance in the form of increased angle of attack, the angle of attack will not increase further, but rather react with an opposing pitch down moment.

The neutral point, is the point where the resultant of the lift forces variations due to a perturbation is applied. These two conditions describe the behaviour of the aircraft with changing angle of attack and are key focus points in this analysis.

PROCESSES OF THE HORIZONTAL TAIL SIZING

The analysis starts with taking the values calculated previously. The assessment of the stability and control is done for two cases:

1. Stability: mission cruise condition, high speed and low lift
2. Control: condition for $C_{L_{max}}$, low speed and high lift

The reason is that for higher speeds, the stability performance goes down, while low speed require a higher degree of control. This behaviour is due to the fact that the position of the aircraft aerodynamic centre is affect by the speed of the aircraft. Consequently its location plays an important role in determining the stability and controllability curves that will help to determine the optimal surface and setting of the wing.

To generate those curves, firstly the lift slopes of both the wing, tail and the wing+fuselage are calculated. The later one include the contribution from the wing to the lift. Since the fuselage body also experience a flow of air it can be considered a lifting surface just as the wings.

Calculation of the lift slopes are performed and for aforementioned two cases and used accordingly.

The equations for the lift slopes used are taken from System Design III slide 4 and 5. They are stated in Equations 6.33 and 6.34. [58] [59]

$$\alpha_h = \frac{2\pi\alpha_h}{2 + \sqrt{4 + \left(\frac{\alpha_h \beta}{\eta_{aero}}\right)^2}} \tag{6.33}$$

$$C_{L_{wf}} = c_{l_\alpha}\left(1 + 2.15\frac{b_f}{b}\right)\frac{S_{net}}{S} + \frac{\pi {b_f}^2}{2S} \tag{6.34}$$

Next, the downwash effect of the wing and the propeller wake are calculated. For this, a wing setting must be chosen. It was decided to have a V-tail for reason explained in the next section. However, direct sizing of a V-tail is not possible with the methods used here. Firstly, the UAV needs to be sized for a horizontal and vertical tail, after which both surfaces shall be converted to a inverted V-tail. T-tail configuration calculation methods provide the best option for converting it into a inverted V-tail as this tail setting experiences least wake from engine and tail. Choosing this setting fixes two parameters. [58]

1. The ratio of horizontal tail speed over vertical, $\frac{V_h}{V}$ becomes 1
2. Lift of horizontal tail: $C_{L_h} = -0.35 \cdot (A_h)^{1/3}$

Then the contributions of the fuselage and the wing to the moment coefficient around the aerodynamic centre are calculated. Once that is done the x-locations of the aerodynamic centre is calculated. Again $x_{w_{ac}}$ has contributions from both fuselage and wing. These parameters are expressed as a percentage of the m.a.c. from the leading edge. For most wings this is usually around 25% from the leading edge. The contribution of the fuselage is calculated using Equation 6.35. [58]

$$\bar{x}_{ac_{wf}} = \bar{x}_{ac_w} - \frac{1.8}{C_{L_{\alpha_{wf}}}} \frac{b_f h_f l_{fn}}{S\bar{c}} \tag{6.35}$$

The fuselage contribution has an additional term which becomes zero in case of unswept wings. [58]

After these parameters are calculated the script generates two curves, the stability curve, Equation 6.36 and the controllability curve, Equation 6.37 as given below, taken from System Design III slide 4 and 5. [58, 59]

$$\bar{x_{c.g.}} = \bar{x}_{w_{ac}} + \frac{C_{L_{\alpha_h}}}{C_{L_{\alpha_{wf}}}} \left(1 - \frac{d\epsilon}{d\alpha}\right) \frac{S_h}{S} \frac{l_h}{\bar{c}} \left(\frac{V_h}{V_\infty}\right)^2 - SM \tag{6.36}$$

$$\bar{x_{c.g.}} = \bar{x}_{w_{ac}} - \frac{C_{m_{ac}}}{C_{L_{wf}}} + \frac{C_{L_h}}{C_{L_{wf}}} \frac{S_h l_h}{S\bar{c}} \left(\frac{V_h}{V_\infty}\right)^2 \tag{6.37}$$

The stability curve shows the limit of the maximum aft location of the centre of gravity to ensure the condition: $x_{n.p.} - x_{c.g.} > 0$. This stability limit is usually shifted back by a certain margin, 5% [58] to ensure a save operational limit. For AERIS a safety margin, Static Margin (SM) of 5% is implemented. This can be seen in Figure 6.22 where the cyan line indicates the limit of neutral point and the red curve is the stability limit with added margin.

These equations represent x-locations of the cg from the leading edge, in the CG_{LE} coordinate system, and are thus expressed in percentage of m.a.c. cord. The bar on top of the symbol represents just that.

COMPARING THE PLOTS AND ITERATING

Next, these x-values are plotted against the ratio of tail surfaces, $\frac{S_h}{S}$ and result in the two curves know as the stability and control curves. An example is provided in Figure 6.22. The plot shows the limits of stability and control as they are defined, everything above the crossing of the two curves is in the safe zone. However we want to find the lowest surface for a given wing setting in order to have the least amount of drag, hence, what we are looking for is to match the optimum cg range with the optimum controllability and stability that will yield in the lightest tail. The trick is to find when the absolute value of the difference of the stability and control curves equals the difference in the most aft and most forward cg location in the loading diagram given in Figure 6.21 and is calculated using Equation 6.38.

$$x_{c.g.aft} - x_{c.g.front} == abs(x_{c.g.control}) - x_{c.g.stability}) \tag{6.38}$$

In other words, when the difference between these two plots are the same. That is exactly what the script performs as a final step.

As mentioned earlier, the stability ans control are assessed at their respective critical limit for speed. These curves are in fact counterparts that set a certain limit to the operational cg range. This is equivalent to the cg travel mentioned earlier for the wing loading. This presents a challenge since we are both trying to optimize for a horizontal surface are as for the position of the wing. The very challenge of stability and control analysis is to find the right balance between all these different parameters that are strongly interlinked. Choosing a certain surface will change the mass assumed for the wing in the first part. This in turn will yield a new optimal position of the wing with respect to the fuselage and when running the script for the tail sizing the downwash gradient, effect of nacelles, lift slopes, and calculations on the aerodynamic centre will change since the calculation required a certain initial input.

Choosing the right set of assumptions is a very important aspect of the design. Poorly chosen assumptions may in fact yield an undersized or oversized tail. The right balance is therefore hard to get and no short cuts exists. The best approach is to iterate over the whole design spectrum of parameters and see what gives the optimum result.

The script written for AERIS is able to cope with a large number of iterations. After each major iteration the script iterates internally and feeds back the values obtained after previous iteration and recalculates until the result converges to a difference of less than 5%. Whilst cruise conditions might have been considered when computing the stability curve of the

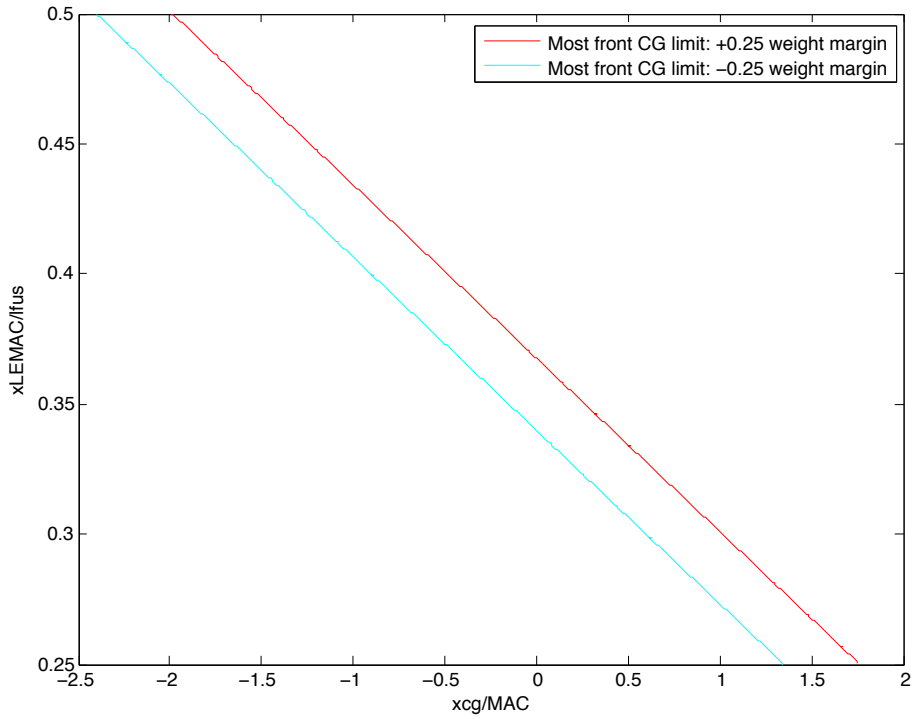

Figure 6.21: Plot Showing Wing Loading Diagram With Most Aft and Most Forward Centre of Gravity Points Resulting From Battery and Payload Weight Margins

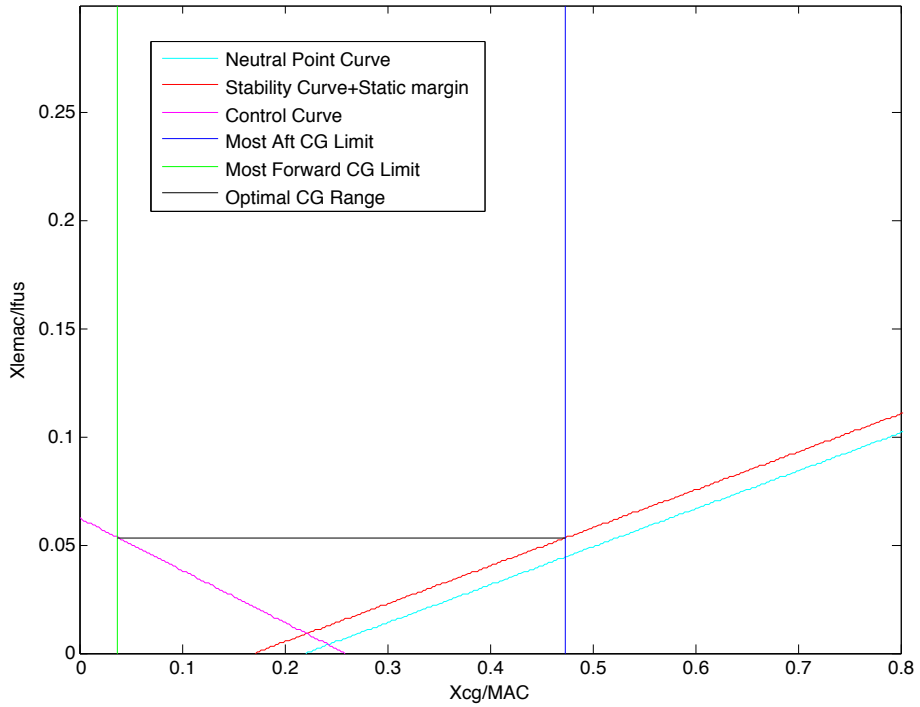

Figure 6.22: Plot Showing The Optimum Wing Setting and Horizontal Tail Surface Area for the Required Centre of Gravity Range

X-plot, the speed at landing condition should be used for the controllability curve (indeed we want to consider the most critical condition of very low speed).

6.7.3. VERTICAL TAIL SIZING

This section of the script is run when most of the UAV configuration has been determined. It combines the results from both the mass determination and the horizontal tail sizing and sizes the vertical tail accordingly. Hereafter the required

horizontal and vertical tail surfaces are combined into an inverted V-tail design. As output it gives the tail surface areas for both V-tail empennages and the ruddervator area along with the trim drag generated by the tail and the force action on it.

LATERAL STABILITY DERIVATIVES

For the longitudinal stability one is primarily interested in C_{m_α} and the pitching motion of the aircraft around the symmetry axis XZ. The lateral stability requires knowledge about the response in yaw and roll. Here is were one makes the transition from 2D to 3D and were other stability derivatives come into play.

There are a number of stability derivatives that describe the complete behaviour of the aircraft in all the degrees of freedom, but for lateral directional stability, the main stability derivative is C_{β_n}. This is the counterpart of C_{m_α} and is also referred to as the weathercock stability. The name already reveals its function: given a positive disturbance in sideslip angle, defined as from the right side of the aircraft, we want the aircraft to rotate in the direction of the sideslip and correct for the disturbance. What this derivative describes is in other words, the response of the aircraft in yaw (moment n around z-axis) to the change in sideslip angle beta.

To have directional stability we want to have C_{β_n}>0. This ensures *static* lateral stability and does not necessarily imply that one has dynamic lateral stability. Dynamic lateral stability involves study of the eigenmotions of the aircraft, which is outside of the scope in this report. The exact dynamic stability is considered to the the very final step in the detail design an can be later achieved, amongst others, by tweaking the surface area of the tail.

Ones the aircraft corrects its attitude by means of rotation about Z-axis due to the force in Y-direction. This force results from the normal 'lift' force of the vertical tail, since the vertical tail is also a lifting surface just as the horizontal tail. It is creating a lift depending on the size and characteristics of the airfoil, but this happens to be in other direction in contrast to the horizontal tail positioned were the normal force is in Z-direction.

The tail of the aircraft is not the only contributor to C_{β_n}, the fuselage shape has an influence as well as the propeller and the wing setting, either high or low. They are defined as contributions $C_{n_{\beta_f}}$, $C_{n_{\beta_p}}$ and $C_{n_{\beta_i}}$. The latter one is the one that still can be changed once the main shape of the aircraft is set. Its contribution ranges from -0.017, 0.012, 0.024 for high, mid and low wing setting respectively. [58] A low wing setting is thus beneficial as we want the C_{β_n} to be positive but setting the wing below the fuselage imposes other difficulties in the aerodynamic flow as the area of wing-fuselage limits the effective surface of the solar panels. The other contributions of the C_{β_n} can be calculated from the fuselage and propeller shape.

SCRIPT FUNCTIONS

The way this part of the script is structures is the following. The script written in MATLAB first calculates the contributions to the C_{β_n} by taking the inputs on the aircraft dimensions, shape of the fuselage, and the properties of the propeller. It then estimated the total tail volume, once a value of $\frac{Svlv}{Sb}$ is determined in order to have directional stability from the quick estimation sizing method described in Torenbeek. [60, fig.9-24] By means of the graph given in Figure 6.23. The value of $\frac{Svlv}{Sb}$ would normally be estimated by manually reading it from the graph. In order to automate the design process and have MATLAB run several design iterations the graph has been digitised and the x and y values have been translated to vectors in MATLAB. After the needed C_{β_n} value (x) is calculated, MATLAB checks what value in x corresponds to the tail volume in y and then finds the vertical tail surface S_v by multiplying the tail volume with the wings span, surface area, and the tail length l_v. The tail length, that is the distance from the wing $a.c._w$ to the vertical tail $a.c._v$ is estimated to be 95% of the horizontal tail arm l_h since $a.c._v$ the vertical tail usually starts at around one vertical cord distance in front a.c. of the horizontal tail. [60]

The digitalised version of the plot from the quick estimation method in Torenbeek is given in Figure 6.24. A comparison between these two will be made in Section 8.1.3.

Once the vertical tail surface is known the script combines the results and calculates the tail surface needed for the inverted V-tail. The reason why a V-tail configuration has been chosen is both for practical as for structural reasons.

For twin boom designs a T-tail is the most common choice since the engine is usually placed in push configuration behind the wing and the elevator surface is lifted up out of the wake of the engine. However, in contrast to one boom configuration the tail has two small vertical tails in stead of one hence two small rudders. The V-tail configuration requires less actuators, only two, against three for the T-tail configuration. The V-tail combines the function of the rudder and elevator in a device called ruddervator. Although the yaw and pitch motions are now heavily coupled, the overall design is lighter and requires less moving parts, wires, and electronic interface. The cross coupling of the yaw and pitch can be resolved by carefully designing the autopilot. The reason to have an inverted V-tail instead of a normal V-tail is due to the placement of the engine

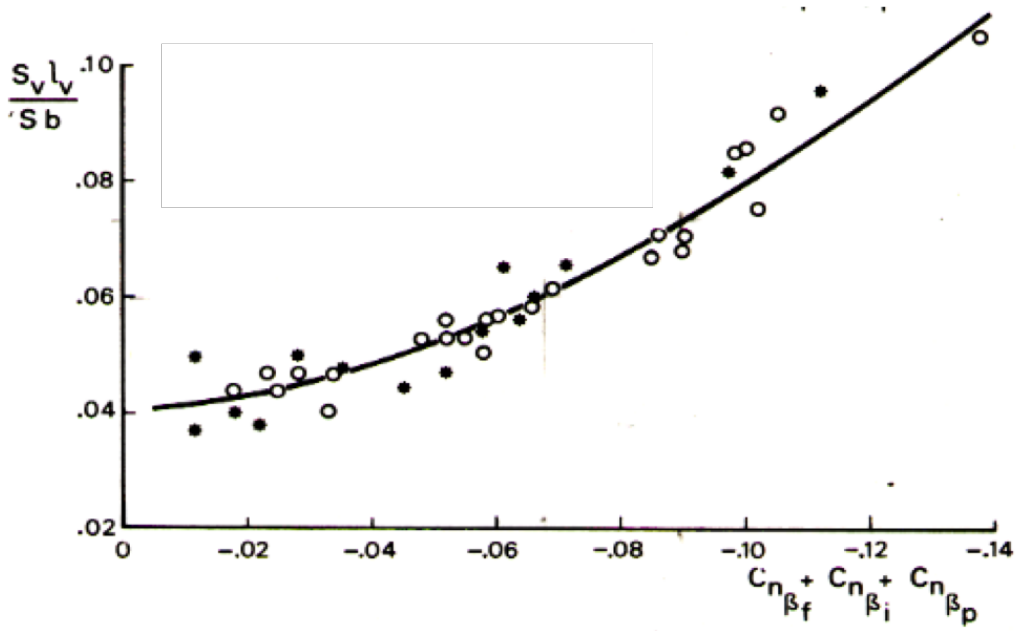

Figure 6.23: Quick Estimation Method of Vertical Tail Volume from Torenbeek [60]

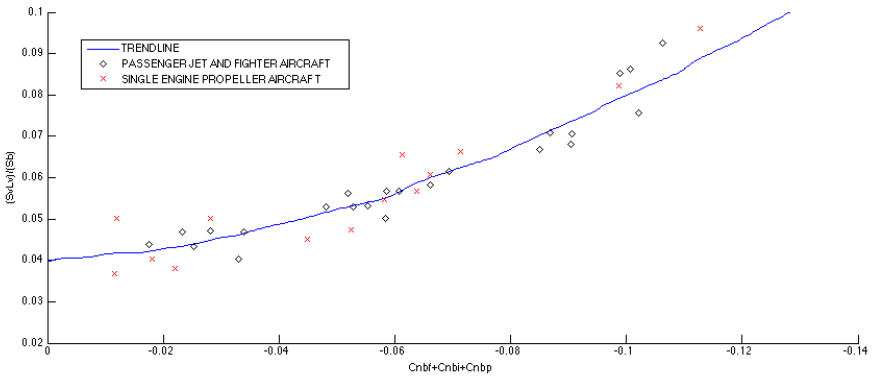

Figure 6.24: Digitalised Version of Fast Estimation Graph from Torenbeek Translated to MATLAB

and the fact that the design includes two booms.

While in a normal one boom configuration the V-tail is usually placed at the end of the fuselage like a dart, the inverted V-tail has two empennages that extend from two booms and meet at a certain height in the symmetry plane of the aircraft. The distance between these empennage tips is determined by the dihedral angle required to have sufficient rudder and elevator control. The angle must provide sufficient height to the V-tail structure in order to be put out of the engine wake. The height of the triangle therefore need to be at least 1.5 times the propeller diameter.

An added advantage of the inverted V-tail is that it forms a rigid structure with the twin boom configuration reducing both flutter from the fuselage as the V-tail, empennages, and the overall structural weight needed.

The V-tail surface and the dihedral angle are calculated using Equations 6.39 to 6.41, which are taken from Systems Engineering II Lecture 4. [58]

$$S_{inv\,total} = S_v + S_h \tag{6.39}$$

$$S_{inv\,1empennage} = 0.5 \cdot (S_h + S_v) \tag{6.40}$$

$$\psi_{inv} = \arctan(\frac{Sv}{Sh}) \cdot \frac{180}{\pi} \tag{6.41}$$

Once the V-tail surface is known, the script calculates the required ruddervator area, that is estimated to be $\frac{1}{3}$ of the total surface area. As a final output, the script also calculates the trim drag in Equation 6.42 and the force exerted on the tail arm in Equation 6.43)and thus the fuselage.

$$D_{trim} = S_v + S_h \tag{6.42}$$

$$L_{inV} = \frac{1}{2}\rho {V_{inV}}^2 S_{inv}\bar{c} \tag{6.43}$$

In order to minimise the tail surface, the tail arm needs to be as long as possible, hence the tail is pushed back all the way to the end of the fuselage. It could, in practice, be extended even further. That would mean that the fuselage must increase in length and must be able to support the bending imposed by the tail force. To limit the complexity of the design the length is therefore fixed.

6.8. POWER SUBSYSTEM

In this section the power subsystem will be sized such that the UAV is provided with sufficient energy. The system consists of several subsystems. First the energy harvesting subsystem will be sized, secondly the batteries will be sized after the power management is done and finally the wires will be sized.

6.8.1. ENERGY HARVESTING

The energy harvesting subsystem consist of two parts, solar cells mounted on top of the wing and a solar panel specifically designed to harvest energy from the laser. The latter is mounted on a winglet.

From Section 6.5 a wing surface area is known. Because we want to make the most use of the free energy from the Sun, 90% of the wing surface will be mounted with solar cells. The cells are made by Alta Devices, the type of cell is a gallium arsenide single solar cell. [9] However the cells need to be mounted to the structure and connected with the PMS. For these tasks, assumptions are made. For the mounting 30% of the solar cell mass is added, for the wires 15%, and for a protective aerodynamic clear coat 90%. The clear coat will be made using fluorine polymer making the airfoil smooth and waterproof. This coating is UV resistant and only 17 [μm] thick. [61] The degradation off the solar cells is about one percent per year and is used to calculate the solar power produced at the end of life. This is the percentage which needs to be more than 20% in order to meet the requirement.

The laser energy send to AERIS needs to be converged to electrical energy to recharge the batteries. The laser operates with a wavelength of 1060 [nm], this in combination with a specially designed InGaAs photovoltaic panel the efficiency is about 50 %. [8] In order to safely use the laser to charge the UAV a laser panel of 0.3 by 0.3 [m] equalling 0.09 [m^2] is needed. This will be sufficient for the laser pointing system to not destroy AERIS. This panel will be mounted on one of the winglets to provide a good angle during a constant turn around the ground station. By placing it on the end of the wing the possibility of hitting the payload is decreased.

In the MTR Peltier elements were considered to regain some of the energy which is transformed into heat by the conversion of the laser beam to electrical power. Calculations showed that adding four Peltier elements would add 260 [g] to the mass while only producing 10 [W] during charging. [62] They would have slightly increased the charging range because a little extra energy would be provided. However, most of the times the batteries will be the limiting factor for charging and not the laser. Therefore, these elements add only an extra mass on the UAV and will not be placed on AERIS. If the efficiency of the Peltier elements increase in the future, it might be reconsidered in next versions of AERIS.

With the solar cells sized the solar percentage is calculated. This is done for three cases; an average winter day, an average summer day, and the yearly average day. Taking the solar cell efficiency of 25% into account the corresponding values are 210, 1240, 710 [$\frac{Wh}{m^2}/day$] respectively. The minimum required solar percentage should be 20% on a yearly average to comply with the requirement.

6.8.2. BATTERY PACK

The battery system is split up in two parts, the normal battery and an emergency battery. The normal battery will be a Lithium Sulfur (LiS) battery while the emergency battery will be a Lithium Polymer (LiPo) battery which is sized in Section 6.3.

The LiS batteries are made by Oxis Energy. [63] The nominal voltage of these cells is 2.1 Volt and contain 10 [Ah]. Since all the subsystems need different voltages there will be a PMS. As the engine is the main power consumer and most efficiently

operates at a voltage in the range of $14 - 18$ volts the battery packs will be made out of eight cells in series. In order to easily change a battery pack if it fails each pack will be made as a $8S1P$ pack (8 series 1 parallel) resulting in a 16.8 $[V]$ and 10 $[Ah]$ battery pack. Each of these packs will have a capacity of 168 $[Wh]$ at Beginning Of Life (BOL). At End Of Life (EOL) this will be approximately 134.4 $[Wh]$, and its mass will be approximately 584 $[g]$. According to the required endurance and the required power extra battery packs will be added. In order to fulfil the endurance at EOL the battery degradation of 20 percent over 2000 cycles should be taken into account. [63] After those 2000 cycles the battery needs to be replaced. When charging approximately twice a day this means that during the design life of five years two battery packs will be used.

To charge the batteries two energy sources are used as explained earlier. When charging using the solar cells there is no problem, but when charging is done using the laser panel the batteries impose a limit. The maximum charge rate is $0.25C$ meaning that the minimum charging time is four hours when the batteries are completely empty. The charge efficiency of LiS batteries is very high, namely 99.5%. [64]

The batteries will be placed inside the wing. The exact location depends on the cg which is calculated in Section 6.7. To minimize the addition of mass for mounting the batteries and in order to easily replace them, if needed, a net structure, made out of ABS, will be printed on the lower side of the fuselage. The height will be such that it reaches the top of the battery pack. When the batteries are placed tape will be used to prevent the vertical movement of the battery.

6.8.3. VOLTAGES

In Section 5.3 it was explained that the supplied power, i.e. voltage and amperage, constantly varies as the intensity of the photonic energy changes over time due to position with respect to the Sun and environmental conditions. To protect subsystems from too many voltage changes that potentially may damage them, the voltage supply has to be regulated. This is done by the PMS. Cable thickness and mass are linearly dependant on the amperage. Although a higher voltage is advantageous as it allows for lighter cables (since the amperage can be lower), the mass of the PMS significantly depends on the input voltage, since the input voltage has to be transformed to the main bus voltage by means of heavy coils. Choosing the voltage is rather arbitrary, since any voltage can be chosen by placing solar cells in series. Typical solar panels produce 12 $[V]$, but as the cable thickness for the cable to the PMS increases significantly with the number of parallel panels, the AERIS team opted for an output voltage of 24 $[V]$ to allow for smaller cables without the need of a heavy voltage conversion system.

Since the individual cells produce 0.96 $[V]$ and 0.223 $[A]$, it is now known that 25 cells need to be connected in series to obtain a solar panel with a voltage of 24 $[V]$ and amperage of 0.223 $[A]$. Dividing the total amount of cells available, which depends on the wing sizing, by 25 gives the amount of panels that are present and thus also the amperage. [9]

The power from the solar cells is then transported to the PMS in which the voltage is transformed as desired for distribution to several systems via the main bus as depicted in Figure 5.5. The voltage that is chosen for the main bus corresponds with the voltage of the battery to eliminate the need of yet another voltage conversion system when transporting power from the battery onto the main bus. This results in amount of 16.8 $[V]$ as indicated in Subsection 6.8.2.

Although most subsystems can handle this voltage, some subsystems need additional components to lower the voltage by means of voltage regulators. These come in the form of resistors, linear regulators and switches. Resistors are by far the easiest and lightest way to alter voltages, but do not offer protection for power surges. Linear regulators and switches do offer this protection, but are not energy efficient and heavier. Table 6.5 provides an overview with all subsystems and their operating voltage. For those systems that have operating voltage ranges that do not include 16.8 $[V]$, one of the power adaptation devices mentioned will have to be implemented. These have been indicated with (!). The CPU is custom build for this UAV and does therefore not require a voltage alteration device. Determining the method of alteration that is used for each subsystems in question is out the scope of this project as sensitivity to power changes will have to be researched for each individual subsystem.

The ground systems are assumed to work with 230 $[V]$ or 400 $[V]$ Alternating Current (AC) , 3-phase power current for the laser. It has not been sized in more detail since there are no mass limitations. For that reason it is assumed that this sizing is outside the scope of the AERIS project.

6.8.4. CABLES

As mentioned in Section 5.3, the sizing of the cables is important. Large cables are both bulky and heavy whereas small cables are dangerous since cables heat up and waste energy as a result of high resistance. In the previous Subsection 6.8.3, it was stated that the sizing of the cables depends on the amperage that is used. Higher voltages and lower amperages allow

Table 6.5: Operating voltages for subsystems

Subsystem	***Operating range*** $[V]$	***Subsystem***	***Operating range*** $[V]$
CPU	Custom	Servo Controller	6 (!)
Antenna	3.3 (!)	lighting Controller	6 (!)
Transceiver	8-48	Emergency Locator Tx	5 (!)
ADS-B +GPS	10-32	Engine Controller	14-18
Parachute, Controller	9-15 (!)	Gyroscope	5-36
HSI+Iris	12 (!)	Gimbal	12 (!)
IR Cameras	5 (!)	Accelero-, Magnetometer	5-36

for smaller cables, but not all subsystems can handle the higher voltage and will need additional components to lower the voltage by means of voltage regulators. Still, using means to alter the voltage at a later stage results in a lighter subsystem than using heavier cables.

In this subsection the cable sizing for the main subsystems is determined. The material used for the cables is copper, and the thickness of each individual cable can be determined with Equation 6.44.

$$q = \frac{0.025(100 - n) \cdot l \cdot I}{n \cdot U} \tag{6.44}$$

Using Equation 6.44, it becomes apparent that a 400 $[W]$ laser panel with one meter wiring and allowable 3% loss needs a wire with 0.79 $[mm^2]$ copper core for 24 $[V]$, whereas a 3.14 $[mm^2]$ cross-section is needed for 12 $[V]$. Table 6.6 indicates the cables that need to be sized using Equation 6.44. Note that the length of the cable is multiplied by two to account for both the negative and positive polarity with a maximum allowable power loss of 3%. The main and emergency bus are located in the wing and run between the two booms. This ensures that the cable length of subsystems can remain as short as possible (not longer than a meter for both polarities combined). The only exception are devices that are located in the wing tip, such as the laser panel, lighting, servos, ELT and parachute. Also, the batteries and solar panels are connected to the PMS. The table includes the respective cable thickness for the connection to the main bus and connection to the emergency bus. These values might differ due to the fact that some subsystems are capable of working on both voltages, affecting the cable surface area that is required.

Table 6.6: Cable Thicknesses for Subsystems

Subsystem	***Length*** $[m]$	***Power*** $[W]$	$V_{mainbus}$ $[V]$	***Cable main bus*** $[mm^2]$	$V_{emergencybus}$ $[V]$	***Cable emergency bus*** $[mm^2]$
CPU	1	10	16.8	0.04	14.4	0.05
Lighting Controller	9	3	6	1.41	6	1.41
Antenna	1	5	3.3	0.01	3.3	0.01
Emergency Locator	4	0.1	5	0.02	5	0.02
Engine + Controller	1	450	16.8	1.80	14.4	2.46
Gimbal	1	7.2	12	0.06	12	0.06
Gyro, Accel & Magnetometer	1	0.8	16.8	0.01	14.4	0.01
Transceiver	1	16.5	16.8	0.07	14.4	0.09
ADS-B + GPS	1	4	16.8	0.02	14.4	0.02
Parachute, Controller	5	5	14.4	0.79	14.4	0.79
HSI+Iris	1	5	12	0.04	12	0.04
IR Cameras	1	5	5	0.23	5	0.23
Servos+Controller	9	10	6	2.83	6	2.83
Main Battery	3	550	16.8	6.62	-	-
Emergency Battery	3	550	-	-	14.4	9.00
Main Bus	3	550	16.8	6.62	-	-
Emergency Bus	3	550	-	-	14.4	9.00
Solar Panel !	4.5	532	24	4.70	-	-
Laser Panel !	7.5	900	24	13.26	-	-

After the cables thickness are known, the size can be standardized. The American Wire Gauge (AWG) standards will be used to do so. The AWG standard defines that 36AWG has a diameter of 0.127 $[mm]$ and 0000AWG a diameter of 11.684 $[mm]$. [65] Using this, the AWG for all cables can be determined which are displayed in Table 6.7;

6.8.5. CHECKS

With the individual parts sized a check is performed to see if the design is possible and complies with the stated requirements. It is checked for the solar power percentage and for the amount of laser power that needs to arrive at the edge of the laser panel. If either of those does not meet the requirements the process will be revisited by re-iteration.

Table 6.7: AWG Cable Sizes

Subsystem	*AWG Normal*	*AWG Emergency*	*Subsystem*	*AWG Normal*	*AWG Emergency*
CPU	31	30	Lighting Controller	15	15
Antenna	37	37	Emergency Locator	34	34
Engine + Controller	14	13	Gimbal	29	29
Gyro, Accel & Magnetometer	37	37	Transceiver	28	27
ADS-B + GPS	34	34	Parachute, Controller	18	18
HSI+Iris	31	31	IR Cameras	24	24
Servos+Controller	12	12	Main Battery	9	-
Emergency Battery	-	7	Main Bus	9	-
Emergency Bus	-	7	Solar Panel	10	-
Laser Panel	6	-			

6.9. STRUCTURES

This section outlines and describes the manufacturing process that has been chosen for AERIS' design as well as the approaches to iteratively design the wing and fuselage structures. The results will be presented in Chapter 7, and their limitations as well as several recommendations for future work in Section 12.7.

6.9.1. MANUFACTURING PROCESS

Manufacturing processes can have a large impact on how one might approach the design of a structure. When designing passenger aircraft, engineers use intricate statistical models to help them size their conceptual designs. Statistical models are useful because, though there have been many significant advances in aircraft design, many existing structures can still be broken down into assemblies of ribs, spars, skins and other structural elements, whose design are in turn dependent on their manufacturing processes - casting, forging, rolling, and extruding (to name just a few).

The first additive manufacturing process - stereolithography - was first commercialized in 1987. [66] Since then, the technology has been developed further and is increasingly accessible and diverse to engineers and even hobbyists. The range of materials that can be print with has also expanded drastically - especially in recent years. One of the biggest advantages of additive manufacturing over most other production techniques is that no material needs be wasted and that structural complexity is "free". In theory, one single machine can produce an infinite number of different designs. Practically speaking, the machines are limited to printing products of certain dimensions with a certain material. When comparing them to a single mould used in a forging process, however, one can quickly understand the power of additive manufacturing. There is still very little advantage, however, to simply print the various aircraft parts to assemble them in the same way of old; structural engineers must instead think outside the box once more, and change their design methodologies accordingly.

One of the reasons that additive manufacturing was chosen as the production method for the wing and fuselage structures is that it allows for their design to deviate from the conventional architectures, like the use of a wing box. For a given material, not only does the amount of material in the final structure decrease, but less material is consumed in its production, making its production far more sustainable than for example machining, where a block of metal is reduced to a final part by removing material. Although one might counter that the left-over material might be recyclable, this production process is limited in the final parts' complexity as it is not able to produce a single hollow part.

At first, the team limited itself to choosing between two relatively widely used molten-deposition materials which are also recyclable: Titanium and Acrylonitrile butadiene styrene (ABS). Titanium has an immense capacity to bear loads and is relatively heavy and expensive; ABS is significantly weaker, relatively light and very cheap. The exact figures can be seen in Table 6.8. The team eventually realized, however, that it might be beneficial to use both materials: Titanium could be used for the higher loads at the roots of the wing and fuselage structures, whilst ABS could be used for the lower loads at the tips (or ends) of those structures. Though the two cannot be chemically bonded together, they can be mechanically bonded in such a way that the loads sustained by the ABS material are gradually transferred into the Titanium as shown in Figure 6.25. Though this concept is feasible according to Dr.ir. O.K. Bergsma, assistant professor at Delft University of Technology, Structures and Materials department, this is a feasible concept. Whether or not it is practical in a commercial environment is a more difficult question to answer; it will at least require a significant number of real tests to validate such an approach. This will be discussed in more depth in Section 12.7.

Table 6.8: Properties of Materials Used for the Structural Design [67]

Material	$\rho_{mat}\ [\frac{kg}{m^3}]$	$\sigma_{max}[Pa]$	$\tau_{max}[Pa]$	$t_{min}[m]$	***Specific Cost*** $[\frac{€}{kg}]$
ABS1	1200	$63 \cdot 10^6$	$31.5 \cdot 10^6$	$50 \cdot 10^{-6}$	25
ABS2	1170	$55 \cdot 10^6$	$27.5 \cdot 10^6$	$30 \cdot 10^{-6}$	25
ABS3	1150	$45 \cdot 10^6$	$22.5 \cdot 10^6$	$100 \cdot 10^{-6}$	25
Titanium1	4410	$1220 \cdot 10^6$	$610.0 \cdot 10^6$	$30 \cdot 10^{-6}$	400
Titanium2	4420	$1155 \cdot 10^6$	$577.5 \cdot 10^6$	$30 \cdot 10^{-6}$	400

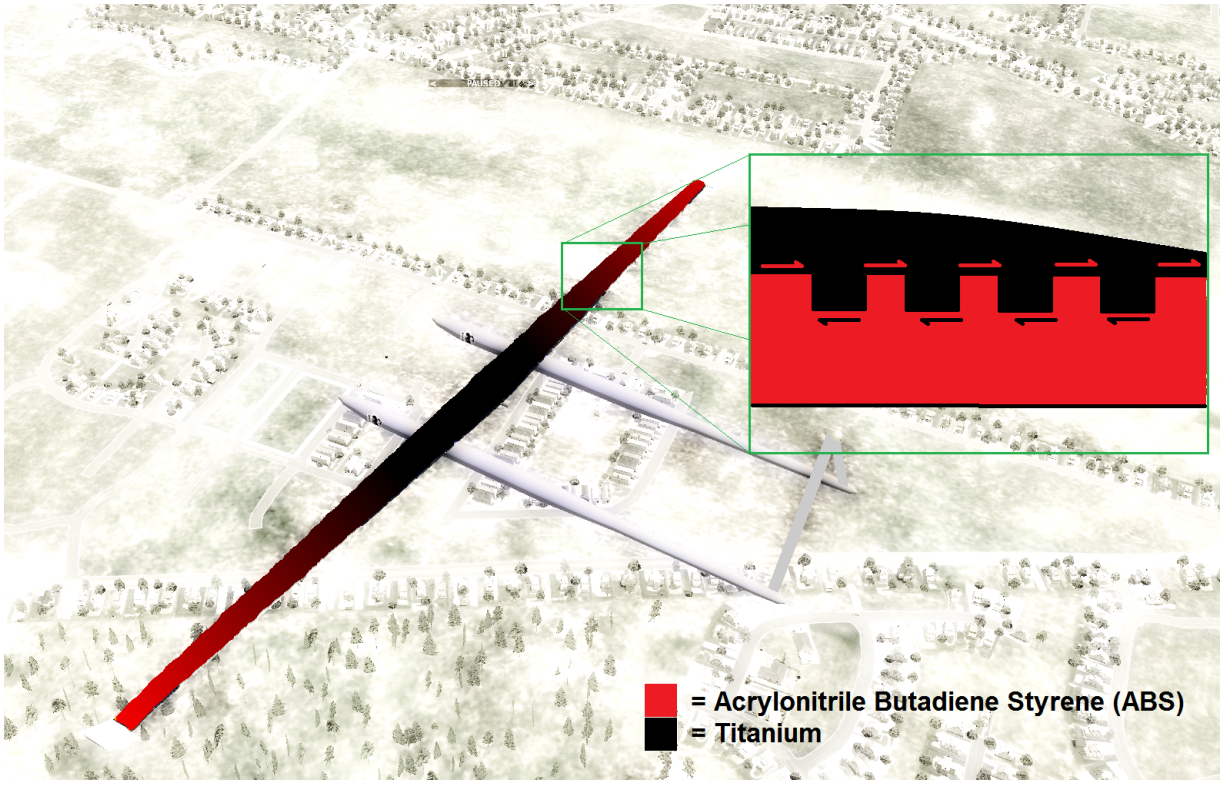

Figure 6.25: Visualization of the Usage of Titanium and ABS

6.9.2. GENERAL APPROACH

The aerodynamics section of the code will generate the required wing geometry, giving an outer boundary for the structure - the main input for the structural sizing of the wing. Meanwhile the size of the various payload and communications components will require a minimum cross sectional area which will be circularized to form an outer shell for the fuselage with the an additional margin of 10%. The reason for this margin will be discussed shortly. Both the wing and the fuselage will be loaded with a variety of point forces and force distributions from the masses inside the structures and the aerodynamic forces acting on the body, giving an overall shear and moment distribution for each structure.

Assuming that the structures are thin-walled, it is allowed to make thin-walled approximations. The MATLAB scripts for each structure gradually add material to the sections suffering the most stress in an iterative process until the loads can be supported. These scripts have been written to give fatal errors should the thicknesses exceed the maximum thickness for thin-walled assumptions to hold true - namely a thickness in excess of 10% of the major dimension of that section. The methods and equations used in the structural analysis of each section come from “Aircraft Structures for Engineering Students, Fifth Edition” and the course “Structural Analysis and Design” as taught at Delft University of Technology by Dr. C. Kassapoglou. [68] [69]

A discussion about the feasibility, limitations and recommendations of this approach will be discussed in Chapters 7, 8 and 12 respectively.

6.9.3. STRUCTURAL DESIGN OF THE WING

From the aerodynamic characteristics, the payload and the weight of the different subcomponents and the loads acting on the wing structure of the UAV can be described in detail. This section describes the methods used to design a safe structure which is as light as possible.

To begin, the internal shear forces S_z and S_x, internal bending moment M_x and internal torque T_y were determined at the root. Once these were known, the loadings in every section were determined from root to tip. Using this, combined with the material properties, the structure of each section could be designed by adding thickness at certain locations within the different cross-sections. A flow chart, describing the structural optimization is shown in Figure 6.26. The structure is assumed to be thin-walled.

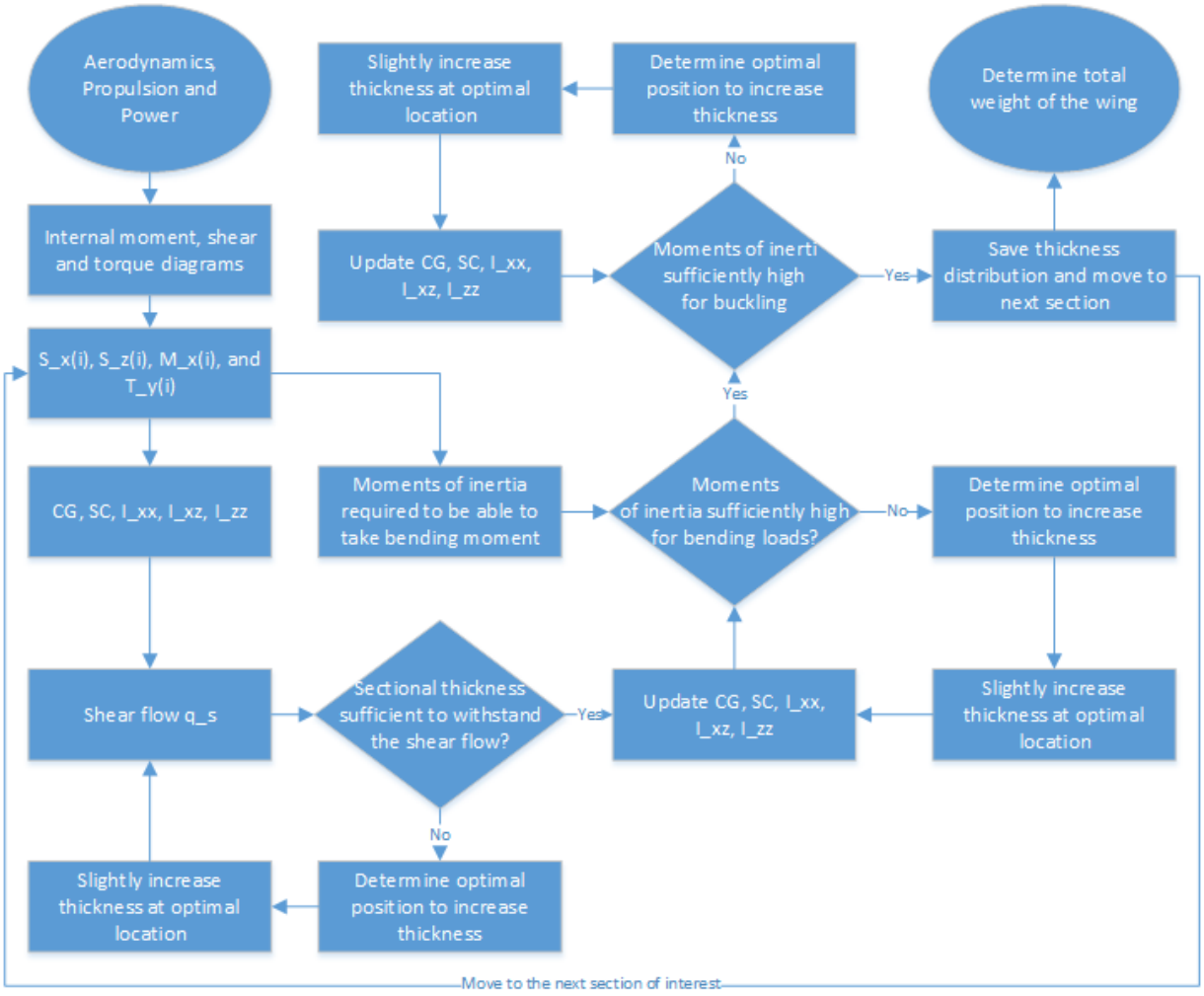

Figure 6.26: Flow Chart of the Structural Optimization

SECTIONAL PROPERTIES

Looking to a single section, many properties could be determined. The cg had to be be defined, hence cg_x and cg_z were determined according to Equations 6.45 and 6.46. The coordinates are in an axis system with the leading point (on the leading edge) of the airfoil as origin. The equations are applicable for a cross-section that exists of different materials, as it includes the density ρ_i for the different sections i.

$$cg_x = \frac{\sum \rho_i A_i x_i}{\sum \rho_i A_i} \tag{6.45}$$

$$cg_z = \frac{\sum \rho_i A_i z_i}{\sum \rho_i A_i} \tag{6.46}$$

After finding the cg, the three relevant moments of inertia I_{xx}, I_{xz}, and I_{zz} are determined according to Equations 6.47 to 6.49, assuming the structure is thin-walled, so only accounting for the Steiner terms. Before this was done, the origin of the

axis system was moved to the centre of gravity of a section because moving the centre of gravity was deemed easier than calculating the moments of inertia around a point not coinciding with the origin.

$$I_{xx} = \sum {x_i}^2 A_i \tag{6.47}$$

$$I_{xz} = \sum x_i z_i A_i \tag{6.48}$$

$$I_{zz} = \sum {z_i}^2 A_i \tag{6.49}$$

To investigate the shear flow and torque acting on the section, the shear centre of the section must be calculated. This, however, increased the time to run the script a lot, since it was found in an iterative way and because it changes every time mass is added to the section. In order to limit the runtime of the script, it is therefore decided to approximate the shear centre by the centre of gravity during the calculations. To validate this, a couple of loops were performed and both the shear centre and centre of gravity were plotted, from which it could easily be seen that the assumption was valid. It seems also logical, because even though an airfoil is not completely symmetrical, it is not very asymmetrical either.

To verify this shear centre assumption, the shear centre, consisting of two components sc_x and sc_z, was calculated in an iterative way. To find the shear centre, an arbitrary load of 1 $[N]$ is applied in both x- and z-direction. A grid of points was generated and for every point, the moment created due to the loading was calculated. First, the shear flow q_s had to be determined using Equation 6.50. The shear centre was then approximated by the point in the grid resulting in the smallest moment. For the NACA 2210 airfoil with ten random thickness distributions, the centre of gravity and shear centre were always located within 5% chord length of each other.

$$q_s = \frac{I_{xx}S_x - I_{xz}\,S_z}{I_{xx}I_{zz} - {I_{xz}}^2}\int_0^s txds - \frac{I_{zz}S_z - I_{xz}S_x}{I_{xx}I_{zz} - {I_{xz}}^2}\int_0^s tzds + \frac{T_y}{2A_{encl}} \tag{6.50}$$

The shear flow in each section can now be determined using equation 6.50 with the right values for S_x, S_z, x and z, starting from the cut and defining the integrals from the the cut up to the section of interest. Adding the constant shear flow due to torque, by using the enclosed area, gives the total shear flow per section. Once the shear flow in every section is known, the thickness per section required to withstand the shear flow across the airfoil can be determined. This thickness will be the starting thickness to calculate where and how much thickness should be added to withstand tension and compression forces due to the internal bending moment. From Equation 6.51, the required moments of inertia to withstand the internal bending moment can be calculated, which, in turn, is compared to the actual moments of inertia to check whether the structure is strong enough or not. If not, an algorithm looks for the most beneficial section to increase the thickness by 0.1 $[mm]$ after which the structure is updated and the whole process is repeated until the moment of inertia of the local airfoil is sufficiently strong to withstand the loads.

Another failure mode to consider is buckling. Buckling is most likely to occur in the upper side of the airfoil because of the positive bending moment M_x, which induces compression in the upper side. To calculated the thickness required to resist against buckling, Equation 6.52 is used.

$$M_x = \int_A \sigma_y z dA = -\frac{Er}{R} \tag{6.51}$$

$$\sigma_y = \frac{\pi^2 I_{xx} E}{A_{cross}{L_y}^2} \tag{6.52}$$

When σ_y exceeds the maximum shear stress σ_{max}, the same trick as for the bending moment is used to add thickness in such a way the stress decreases the most by adding the least amount of mass. This process is, again, repeated until the shear stress σ_y drops below the maximum shear stress σ_{max}.

All this combined results in a detailed structural design for each section, able to withstand all the loads expected during its lifetime, making use of conservative safety and load factors. An example of such a sectional design is given in Figure 6.27.

6.9.4. FUSELAGE DESIGN

In a similar manner to the design of the wing, the fuselage is divided up into the sections in both the direction of the fuselage, and into minute sections around each piece of fuselage. Unlike the wing, however, the outer boundary is defined by what is inside the fuselage: the payload, communications and safety components. Though many of the communications might fit into the wing, the fuselage is sized according to those masses, the payload dimensions require the fuselage to have a relatively large diameter anyway - not much performance is achieved by rushing to shrink the diameter of the fuselage, so

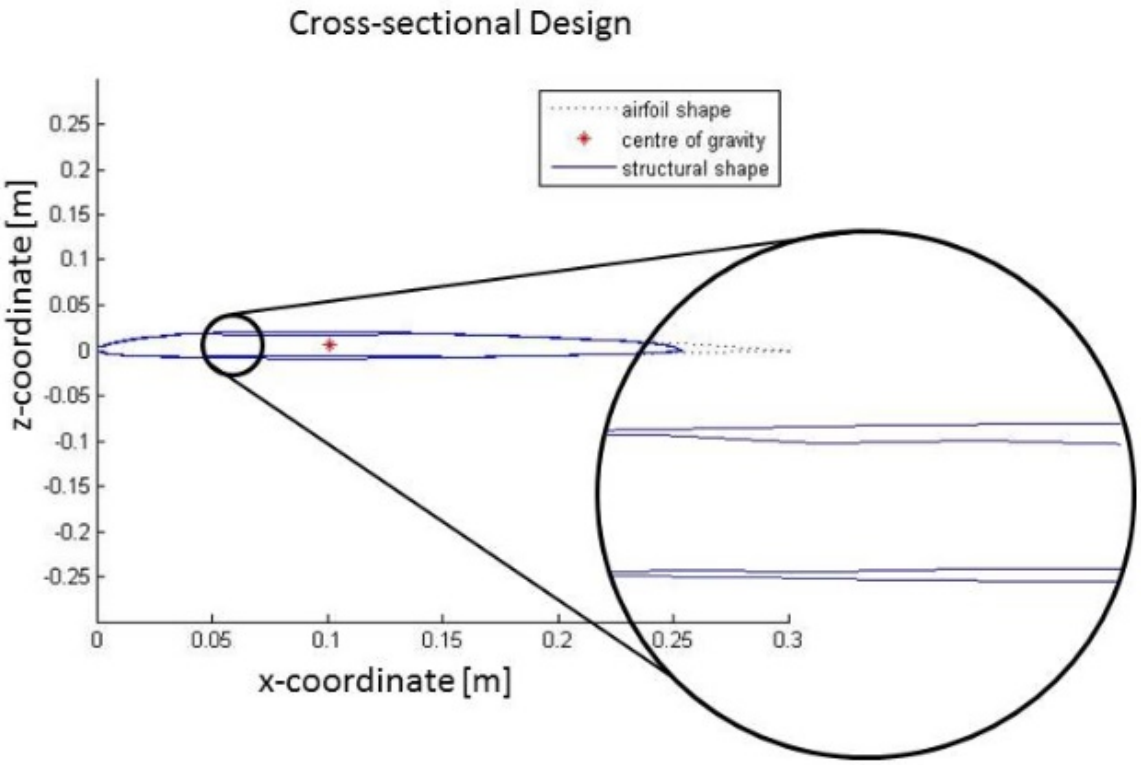

Figure 6.27: Visualization of the Change in the Skin Thickness of the Airfoil

it makes sense to design it conservatively.

The fuselage diameter increases quadratically from the nose. The precise parabolic shape is a function of the payload dimensions, as it must fit and rotate freely within the nose section to observe the ground beneath it. Parabolic sections have a frontal drag coefficient of approximately 0.05. As thickness will be added to the inside of this shape for aerodynamic reasons, the diameter is scaled up slightly by the aforementioned margin of 10% which was further scaled up by a safety factor to ensure sufficient clearance between the payload and the fuselage wall. The fuselage's diameter rounds off at this point to continue as a constant diameter in the cargo section of the fuselage. This is where any components not able to fit in the wing can be placed, or any future components not yet taken into account by the design. From the back end of the cargo section of the fuselage, the diameter decreases with a cosine function along the length of the parachute container, and then further converges to an arbitrary minimum diameter of 7.5 $[cm]$ until the end of the fuselage where it is attached to the tail. If the skin thickness becomes too thick, this minimum diameter is simply scaled up until the thickness is thin enough for the thin walled assumptions to hold. The aerodynamic difference is most likely very small as the skin friction coefficient is assumed to be a conservative 0.004.

6.10. FLIGHT CONTROL

In order to correctly perform the mission AERIS needs to be controlled. For this controllability, control surfaces are required. Since AERIS does not need to land and take-off on a regular basis, no separate high lift devices are used. Instead the choice for flaperons is made. Furthermore, since an inverted v-tail is used, ruddervators are a logical choice. Since the resources provided give too little time, the exact dimensions of the flaperons and ruddervators are not calculated. Instead the dimensions are based on some typical values. Next to that since the exact forces acting in these control surfaces are not determined the right servo to control the surface is not determined. But the weight will approximately be $30-40$ $[g]$ a piece according to. [70]

6.10.1. FLAPERONS

Typically ailerons take up $20\% - 30\%$ of the chord length and $20\% - 50\%$ of the wing span. [71] Using flaperons it is assumed that the control surface needs to be slightly on the large side, since the ailerons also need to function as flaps. Therefore it is determined that the flaperons will take up 25% of the chord length and 45% of the wing span. To provide less of a moment

in the wing, the flaperons are placed near the wing tip in order to increase the roll control.

6.10.2. RUDDERVATOR

Normal elevators are typically spread across the whole span of the tail surface and run from 25% − 45% of the chord. [71] Since these are ruddervators, they control both the pitch and yaw moments instead of only the pitch moment. Next to that, the provided force is under an angle and the surface will be slightly less effective. Therefore, it takes up 40% of the chord length and 90% of the span.

6.11. GROUND SYSTEM

This section discusses the ground system of the AERIS project. The ground system's primary function is the power supply and the data handling of AERIS. The ground station consists of three components. First of all, there is the laser system which will be situated at the top of the EWI-faculty building of Delft University of Technology. Secondly, there is the communication system that consists of an antenna that is required for data communication between AERIS and the ground. Finally, the third part of the ground system is the office. The office is the site where maintenance will be performed, mission control takes place and data will be analysed and send to the customers.

6.11.1. LASER STATION

Locating the laser station on top of EWI optimises the use of the LoS. There are no buildings and trees in the nearby surrounding that are high enough to cause interference with the laser and communications beam. Furthermore, placing the laser on a high building increases the safety, by decreasing the risk of theft, vandalism, accidents and terrorism. The laser and subcomponents require a protection from rain, since, as soon as there is rain or moisture on the lens, water will reflect some of the power from the laser and destroy the laser. An automated system checks the weather, however the office personnel also checks weather data at the laser location and make the final decision if the laser can be activated to make sure no dangerous situations occur. Subsystems of the laser station are presented and discussed in the remainder of this section.

6.11.2. LASER FUNDAMENTALS

Before going into detail on the laser technology that will actually be applied by the AERIS system, the working principle of the laser is examined. LASER is the acronym for light amplification by stimulated emission of radiation. [72] [73] Light in the acronym for laser should be noted as electromagnetic radiation and should thus also include 'invisible' light, such as infrared and ultraviolet light. A main characteristic of laser light is that it is directional which allows the light to be focused on a single spot. This characteristic is used, for instance, to cut through metal and lithography. In the case of AERIS this characteristic is used to focus the energy of the laser beam exactly on the solar panel on the aircraft to charge its on-board batteries.

Also the coherence of laser light is what distinguishes laser-light from other light sources. This coherence can come longitudinal, temporal, or instantaneous. Longitudinal coherency implies the wave to be polarized at a single frequency with a phase correlated over a long distance (coherence length). Instantaneous coherency occurs when the laser light is produced by thermal of incoherent light sources. This results in a very short coherence length. [74]

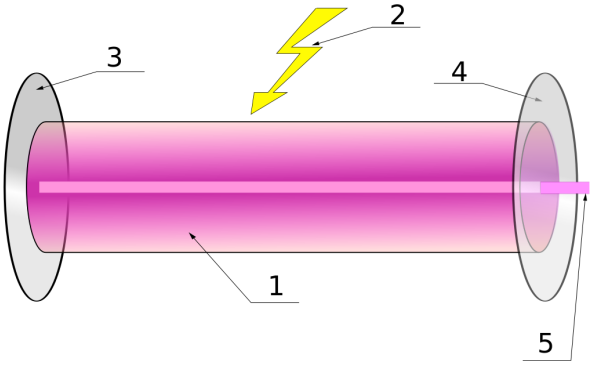

Figure 6.28: Components of a Typical Laser: 1. Gain Medium 2. Laser Pumping Energy 3. High Reflector 4. Output Coupler 5. Laser Beam [72]

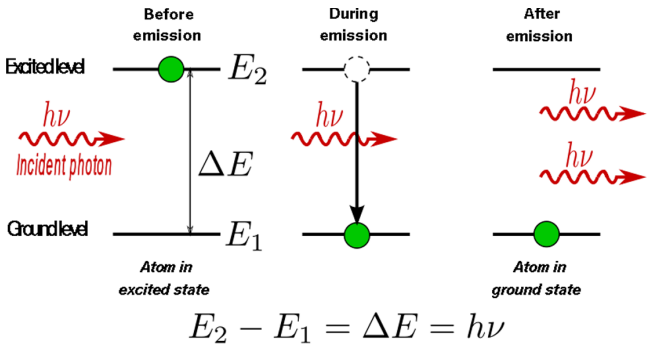

Figure 6.29: Electrons and their Energy Levels around an Atom [73]

In short, a laser consists of a gain medium, a mechanism that supplies energy to it and a part that provides optical feedback. [75] The gain medium is able, when energised, to emit photons of light at a specific wavelength. Furthermore, this gain medium is able to amplify the light that passes through this medium. As can be seen in Figure 6.28, in order to amplify this light it is required to energise the medium. This process is called pumping and with boosts of energy (de-charging

of capacitors for high energy lasers) electrons of the atoms of the material are excited to a higher energy level. When the energised and excited electrons fall back to a lower energy level, photons are emitted. The emission of light by an excited electron falling one energy level down is shown in Figure 6.29. The excitation is commonly introduced by either introducing electricity to the medium or by an other source of light, such as a flash lamp.

Commonly, the laser light is trapped inside the apparatus and is captured between two concave mirrors of which one is able to bleed a bundle of photons. The mirrors allow the photons to pass through the medium several times, amplifying the light every time is passes through. It should be noted that slight changes in the distances between the mirrors, and their shape, caused by temperature shift for instance, can cause noise in the output signal. Furthermore, the flash lamp itself is a cause for slight noises in the laser light. This typically is in the range of maximum 1 $[nm]$. The wavelengths that can be created with current laser technology are varying for the different material of which the electrons are excited. An overview is present in Figure 6.30 where laser types with distinct laser lines are shown above the wavelength bar, below the line lasers are shown that can emit in a range of wavelengths..

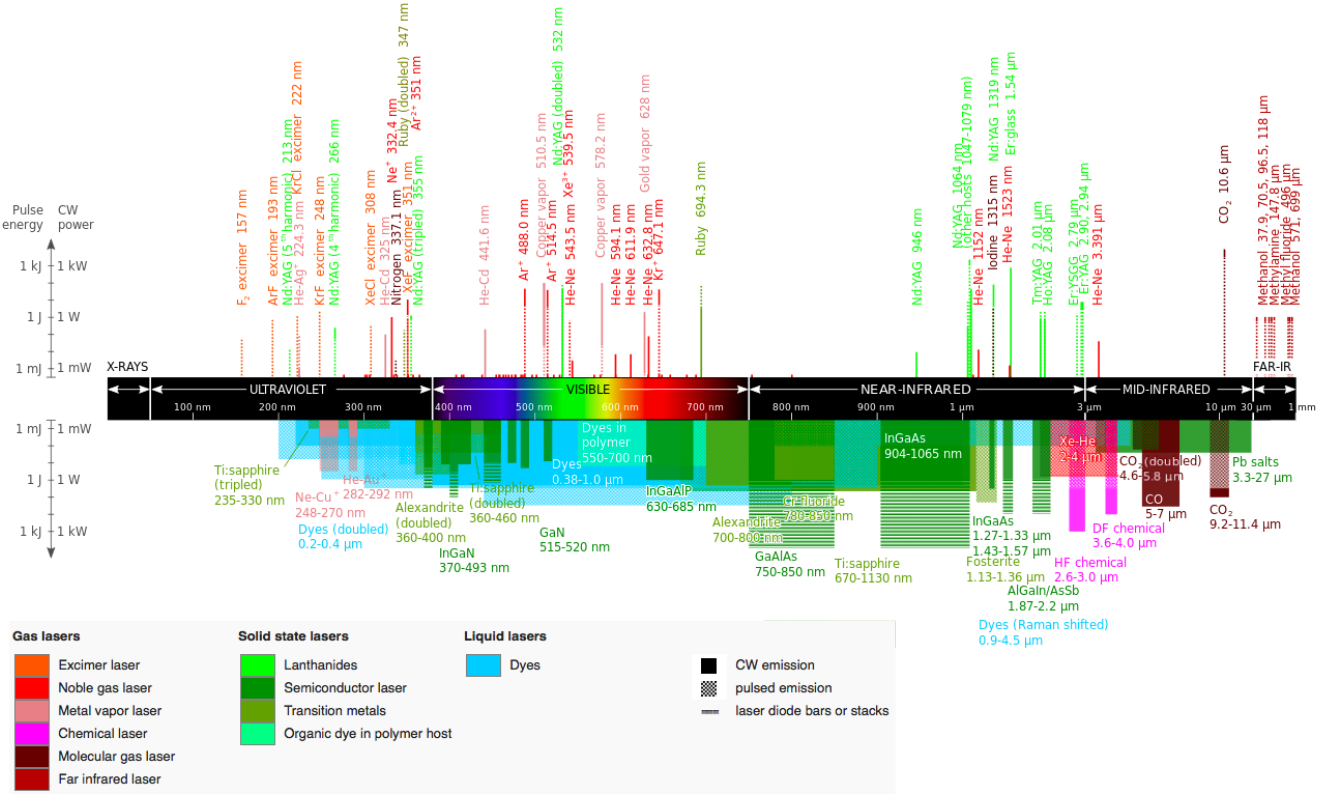

Figure 6.30: Wavelengths of Commercially Available Lasers. [76]

POWER SUPPLY

The laser panel on-board the aircraft is made of InGaAs cells, and are therefore extremely efficient for wavelengths of 1,064 $[nm]$. This specific wavelength sets limitations on the available types of lasers. It has been calculated by means of a MATLAB-script that the minimum power arrival at AERIS to recharge the batteries needs to be 793 $[W]$. However, due to the loss of energy in the atmosphere, the laser power output of the laser needs to be 2 $[kW]$. For sustainability reasons this power source is harvested from a green power source such as a wind energy contractor. One of the leading laser companies in the world state the existence of multiple "disk lasers" that comply with the required calculated specifications. In Table 6.9 these specifications can be found. Although this laser complies with the necessary specifications, there is no pointing system for aerial vehicles includes. It is therefore necessary to modify this laser in such a way that it is able to precisely aim to and track AERIS' laser panel. The system that is able to perform this is proposed in Section 6.11.3.

POWER ARRIVAL

Now the specifications for the laser are known, the power arrival at AERIS must be verified. The formula's and assumptions used below come from several sources and actual values are determined using MATLAB. [8][78]

The laser flux arriving at AERIS can be computed with Equation 6.53.

Table 6.9: Specifications of the Ground Station Laser [77]

Item	*Value*	*Unit*
Wavelength	1064 ± 10	$[nm]$
Laser Output Power	2000	$[W]$
Beam Quality	2 − 8	$[mm \cdot rad]$
Cooling Water Temperature Range	5 − 20	$[deg]$
Width	730	$[mm]$
Height	1375	$[mm]$
Depth	1120	$[mm]$

$$\Phi\left[\frac{W}{m^2}\right] = \frac{3.44 \cdot P \cdot exp(-\epsilon \cdot L)}{\pi \cdot L^2(\sigma^2_{diffraction} + \sigma^2_{turbulence} + \sigma^2_{jitter}\sigma^2_{blooming})} \tag{6.53}$$

Where:

- P = Laser power in Watt
- L = Distance to AERIS in meters
- ϵ = Atmospheric extinction of the beam due to absorption and scattering
- $\sigma_{diffraction}$, $\sigma_{turbulence}$, σ_{jitter} and $\sigma_{blooming}$ are the beamspreading factors for diffraction, turbulence, beam jitter, and thermal blooming

The amount of attenuation of the laser beam caused by absorption (atmospheric molecules) and scattering (molecules and large particles such as water, dust and smoke) is calculated using Equation 6.54.

$$\epsilon = \alpha_{absorption} + \alpha_{scattering} \tag{6.54}$$

In MATLAB, reference data for a wavelength of 1064 $[nm]$ is used. [79] The amount of beam spreading due to diffraction is calculated by making use of Equation 6.55:

$$\sigma^2_{diffraction} = \left(\frac{2 \cdot B \cdot \lambda}{\pi \cdot w_0}\right)^2 \tag{6.55}$$

Where:

- B = Beam quality
- w_0 = Diameter of the waist (smallest) part of the beam
- λ = Laser wavelength

Jitter is caused by vibrations, shaking or other motions of the laser system. In the calculations it is assumed that σ_{jitter} = 6$[\mu rad]$. Furthermore, the impact of thermal blooming does not have a significant influence on the total beam spreading factors, for laser powers below 25 $[kW]$ it is usually less than 1 $[\mu rad]$.

In Table 6.10 a summary is shown of the results from the previous equations. More results can be gathered by running the MATLAB script, where one can input a specific range for several weather conditions, these results are shown in Figure 6.31.

Table 6.10: Total Power Delivery at AERIS for Different Parameters

Visibility $[km]$	***Atm. Att. Coef.*** $[\frac{dB}{km}]$	***Weather***	***P*** $[W]$ ***at R of*** 0.4 $[km]$	***P*** $[W]$ ***at R of*** 0.8 $[km]$	***P*** $[W]$ ***at R of*** 1.2 $[km]$
0.05	78.2	*Fog*	1.49	0	0
0.5	7.8	*Fog*	973	473	230
2	1.26	*Haze*	1780	1584	1410
10	0.166	*Clear*	1970	1940	1910
60	0.02	*Very Clear*	1996	1992	1988

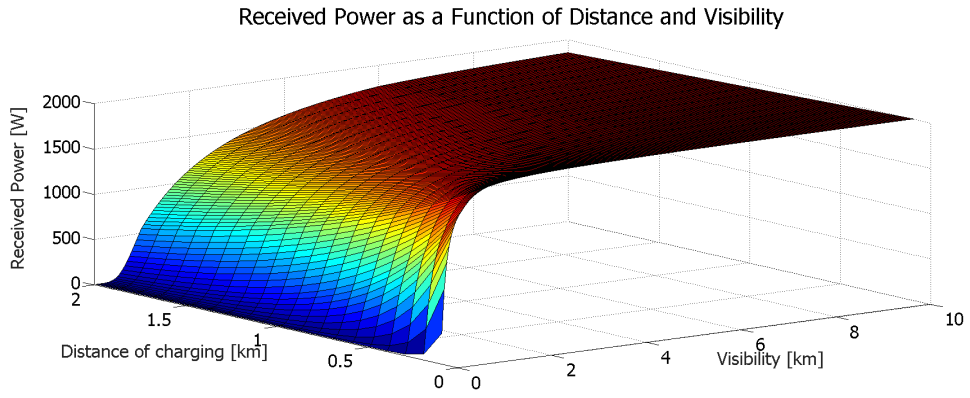

Figure 6.31: Received Power at AERIS for Different Visibilities and Charging Ranges with a 0.09 $[m^2]$ Panel and an Output Power of 2 $[kW]$ with a Wavelength of $\lambda = 1064[nm]$

6.11.3. POINTING AND TRACKING SYSTEM

To achieve a high pointing accuracy the right pointing system has to be selected. An example of a such a system that is already successfully in operation is shown in Figure 6.32. Additional engineering fields that use pointing and tracking systems are the field of astrology where they use trackers to follow and point telescopes on celestial objects. BAE Systems make several different kinds of laser pointing systems with a high pointing accuracy. These systems would provide a pointing accuracy that would be sufficient for AERIS. The system shown in Figure 6.32 is an example of a system the team has in mind. The pointing accuracy required for AERIS is 0.003 $[deg]$ which is equal to 0.052 $[mrad]$, while the pointing accuracy of the given system is set to be 0.05 $[mrad]$. This system pointing accuracy puts the limit of maximum distance from the laser system to AERIS at 1600 $[m]$ with a laser panel size of 0.09 $[m^2]$. Additionally, this system includes a double tracking system. The advantages of this double tracking system is that it is possible to quickly switch between charging two UAVs. Finally, the laser pointing system will be controlled by its own computer and actuators. This computer has a link with the communication system to know where AERIS is flying. The system will be completely autonomous and will move the laser but it will also change the distances between the lenses to focus the laser beam appropriately.

The current systems that are available are integrated pointing and laser systems. At this moment, the lasers provided in these systems do not meet the specifications that AERIS need to charge the batteries efficiently since both the continuity of the laser beam and the wavelength are off. To come up with a system that integrates both the right pointing system and the appropriate laser, a consult has to be arranged with BAE Systems to find an appropriate solution. Under the current conditions and limited resources, arranging such a consult is beyond the scope of this project. The integration of the pointing and tracking system with the appropriate laser is done at a later stage of this project.

Figure 6.32: Example of a Laser with a Pointing and Tracking System. [80]

WILDLIFE AND SECURITY

With a laser output of 2 [kW] in the near IR spectrum with a wavelength of 1064 [nm] there is a certain degree of risk involved for wildlife and aircraft. The danger lies in the fact that the laser is not directly visible but still can inflict harm to eyes. In order to detect objects that potentially cross the laser, LIDAR technology will be used. LIDAR also uses a laser, but uses it to determine distances and is not directly harmful. As soon as the LIDAR detects a distance that does not matches the distance of AERIS, the system will automatically shut down the laser. Hereafter the laser and AERIS lock again, and the laser charging procedure is restarted. [81]

Additionally, the location on top of EWI helps to prevent theft and vandalism as this location is a secured area of the faculty with limited access of personnel. Finally if this security level is breached, the LIDAR system can automatically deactivate the laser as soon unauthorised persons come to close to the system.

COOLING OF THE SYSTEM

The 8 [kW] input of the laser will produce a lot of heat as only 25% is converted into the actual beam. Most of the other 75% will be converted into heat. Therefore the laser needs to be cooled to prevent overheating. This active cooling is performed by means of water cooling. Cold water will be tapped from the buildings and the warm water will be connected to warm water heating system of EWI to warm the building or it will be stored in the reservoir underneath th Library of the TU Delft. Since the laser will mostly be used during the night, heating of EWI during the night phase is a sustainable solution to the warm water product of the cooling system. The reference laser types include an water cooling system. [77]

ALTITUDE OF CHARGING

The maximum slant range for charging is limited at 1600 [m] from the laser, due to the pointing accuracy of the laser system. From Equation 6.56, the altitude, horizontal distance from the ground station, and turn rate can be calculated. The minimum allowed altitude to fly is set by the minimum sector altitude which for Delft is given as 1000 [ft], approximately 350 [m]. Due to placement of the laser at a height of 80 [m] the minimum altitude for AERIS to charge becomes 270 [m], which results in a turn rate of 0.5 [$\frac{deg}{s}$] for a slant range of 1600 [m] and flight speed of 50 [$\frac{km}{h}$]. Again, with Equation 6.56, the maximum altitude measured from the ground station is determined. In this calculation a turn rate of 3 [$\frac{deg}{s}$], which is a rate one turn, was the maximum allowed turn rate. From this it follows that for a slant radius of 1600 [m] the maximum altitude becomes 1577 [m].

The following calculation is done to determine the minimum allowed slant range for the given minimum flight altitude of 270 [m] above the laser with a rate one turn. Using Equation 6.56 it is determined that the minimum slant range becomes 379 [m] above the laser. From these results the horizontal range of the laser is determined. The minimum horizontal distance becomes 266 [m], and the maximum distance becomes 1577 [m]. In Figure 6.34 the two circles indicate the minimum and maximum horizontal distances from which AERIS can be charged while Figure 6.33 gives an schematic overview of the charging distances.

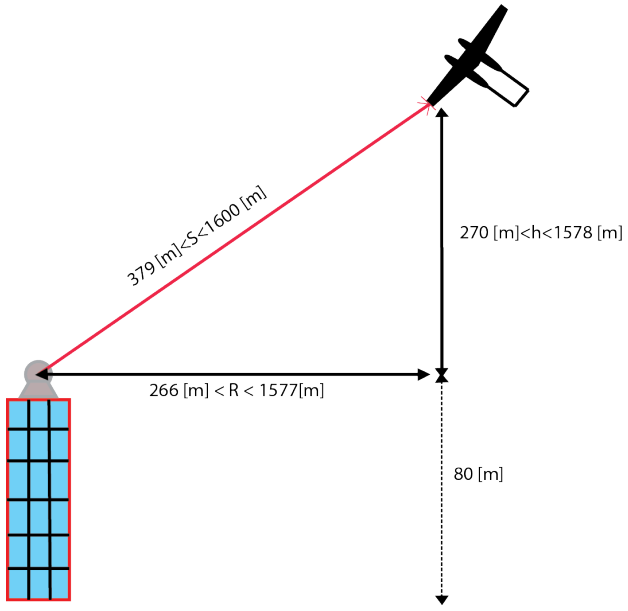

Figure 6.33: Schematic Overview of the Possible Distances of Charging

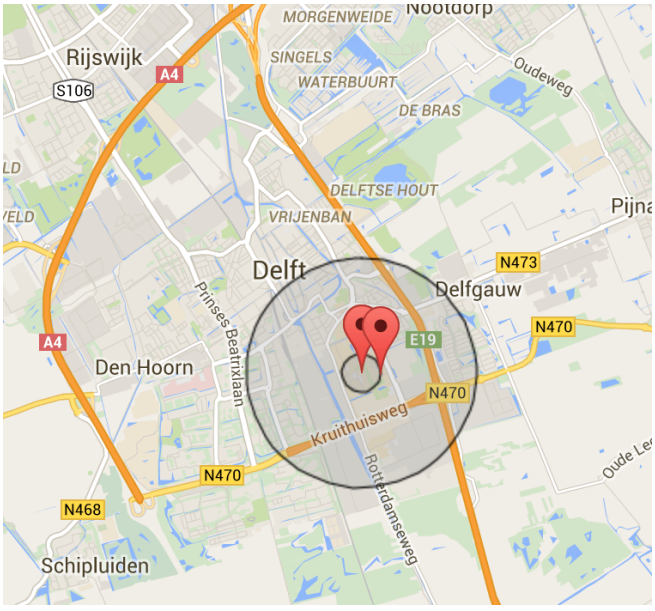

Figure 6.34: Minimum and Maximum Horizontal Range of Charging

$$Turn\ rate = \frac{360^\circ}{\frac{2\pi \cdot \sqrt{S^2 - H^2}}{V}} \tag{6.56}$$

6.11.4. COMMUNICATION

The second system that is situated on top of EWI is the communication system. This is a directional antenna designed and made by UAV Navigation. [39] The antenna will be wired to the same computer as the laser in order to continuously follow AERIS' movements and gather the data it sends. The gathered data will be sent over the internet to the office for further processing and final storage.

Uplink happens via the same communication system as described in the communication section in Section 6.4. Most of the commands will be the desired routes, however in case of an emergency the office will take over control and these commands will be directly send to AERIS. Uplink of commands and downlink of the camera images can happen simultaneously for these emergency services as no hyperspectral imager data is required under emergency situations.

6.11.5. OFFICE

The final part of the whole AERIS mission is the office for the employees. This office preferably lies at the edge of Delft near the Rotterdamseweg. In this way there is water and fields nearby that are suited for emergency landings. This office will have computers for the employees and a place for the pilots to take over control of AERIS in case of an emergency situation. In this control segment of the office a small simulator is necessary, with a joystick to control AERIS. In the flight control computer, there already exists a module that is able to switch between the auto-pilot mode and a mode that is able to control the UAV from the ground station. In order to make the operation as safe a possible, there will be two licensed pilots at the office at all times. These pilots will do the data analysis and maintenance during the time that AERIS is not facing difficulties. The office needs to accommodate for at least ten employees, and there must be enough space to perform maintenance and testing of AERIS.

7. RESULTS: THE BIGGER PICTURE

The previous chapter described the design approach used to create AERIS in detail. There is, however, still a design challenge left, namely interrelating the sizing of the different parts. The different functions are executed following the N^2 chart. Outputs of one script are used as inputs of another as visualized in Figure 6.1. First, the parameters unaffected by the UAV size are discussed (see Section 7.1), after which the iterative sizing process is discussed in Section 7.2, starting from initial guestimates and leading to a final design. At the end of this Chapter, in Section 7.3, the results are discussed and possible ways to improve the accuracy and numerical models are briefly assessed.

7.1. NON-ITERATIVE RESULTS

Although most of the components have masses and properties varying from iteration to iteration during the design phase, there are some that do not change according to the UAV size. These parameters are summarized at the end of this section in Table 7.1 and are of utmost importance when determining the starting point of the iterative process. The unchanging weights are mostly related to payload and communications, of which more details can be found in Sections 6.2 and 6.4 as well as in 7.1.1 and 7.1.2. Apart from these values, the airfoil selection is independent of the UAV size as well. As discussed in detail in Section 6.5, the selected airfoil in an airfoil with good stall properties, namely a NACA 2210 airfoil.

7.1.1. CAMERA OUTPUT

With the equations discussed in Section 6.2, the results of the payload output are discussed and visualised with the figures shown here. Figure 7.1 shows the graphs obtained with the covered equation for the IR camera. The data rate in the speed range, which is limited by the propulsion performance as described in Section 6.6, at the optimum altitude is visualised in Figure 7.1. It can be seen that the data rate increases linearly with velocity, reaching a maximum when the airspeed of the UAV is maximum. Evidently, this is the result of a lower dwell time since the ground is covered in a shorter time span.

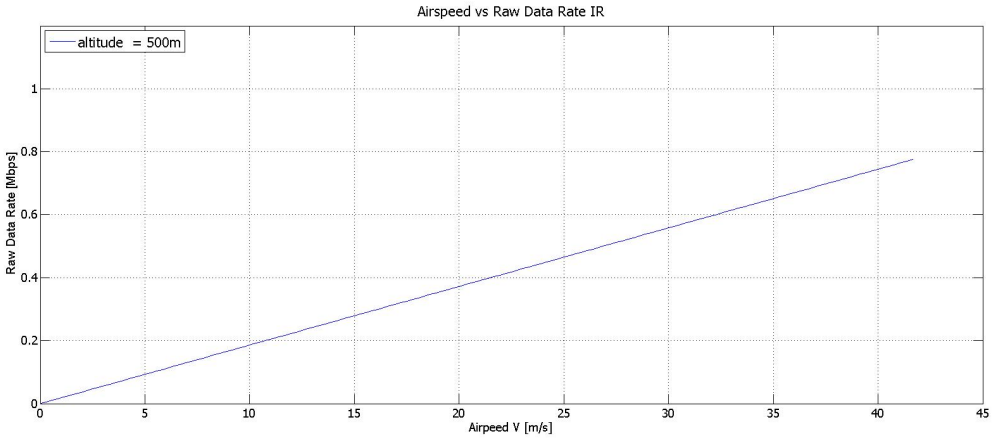

Figure 7.1: IR Raw Data Rate for the Velocity Range at Optimal Height

When the velocity is varied between the minimum and maximum operational velocity at altitudes ranging from 100 $[m]$ to 4000 $[m]$, the resulting data rate is changing as shown in Figure 7.2. As can be seen in the graph at every velocity, the data rate increases quadratically with decreasing altitude. It can also be seen that the critical point for the data rate is at maximum velocity and minimum altitude. Here the ground is passed with shortest dwell time resulting in a data rate of about 5.2 $[Mbps]$. The graph also shows that the data rate increases significantly from an altitude 500 $[m]$ and lower. This result and the average cloud ceiling have been determining the optimum altitude.

Figure 7.3 shows the pixel sizes in the altitude and velocity ranges for the HSI. The graph shows the smallest ground object that can be resolved in the image across the altitude range, that is the pixel size. Thus, the smaller the pixel size, the better the image quality. It can be seen that the critical point is when the velocity and altitude are maximum. This is the result of a high velocity for higher altitude and thus a larger FoV. The pixel size for the HSI at the optimum altitude and cruise velocity is about 12 $[cm^2]$ which is reasonable detailed. In the graph, a constant shutter time of 100 $[msec]$ is assumed. Whenever there is less illumination available from the sun, larger shutter values are needed. This will increase the pixel dimensions and thus lower the resolution. In these situations, it can be decided to change the altitude and/or the velocity. The requirements of all the intended applications define a wide range of specifications. This implies that trade-offs between spatial,

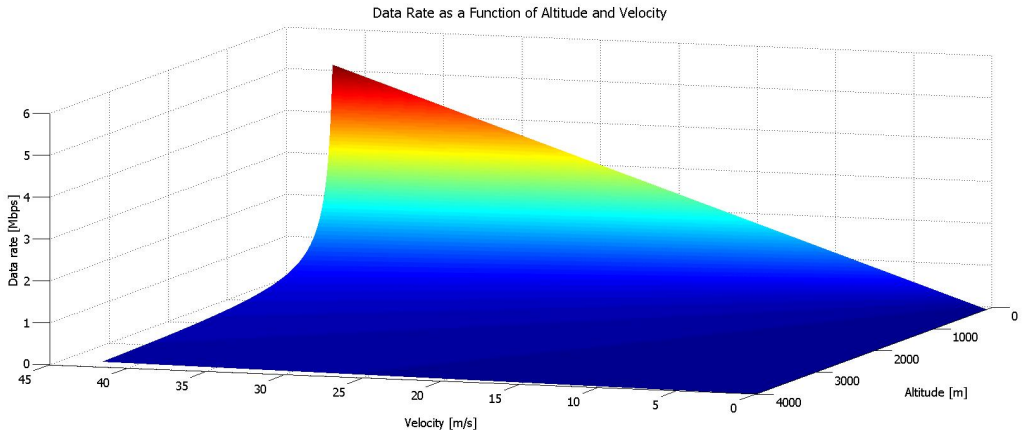

Figure 7.2: IR Raw Data Rate in the Velocity and Altitude Range

spectral and frame rate have to be made.

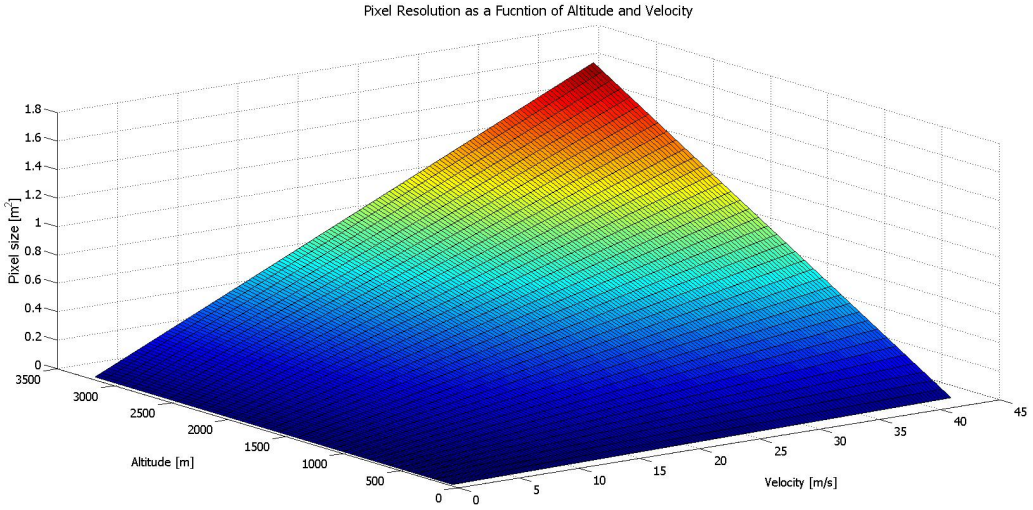

Figure 7.3: HSI Pixel Resolution in the Velocity and Altitude Range

As was shown with Figure 6.7a in Section 6.4, the maximum distance of 69.5 [km] between the ground station and AERIS which allows communication can cover the entire province Zuid-Holland. This means at any point, as long as the signal is not disturbed, AERIS is able to retrieve and send the obtained data.

7.1.2. COMMUNICATIONS

To start with the design of the communications subsystem, the data to be transmitted must be specified. From the payload calculations, the amount of data to be transmitted was determined to be no less than 62 [$Mbps$]. Therefore, a constant data stream is desired, which will be achieved by placing the ground antenna on the EWI building, which is 80 [m] high, to increase the LoS to 69.5 [km]. This LoS will still be the limiting factor to the range of the mission, as AERIS can reach locations much further with its endurance of seven hours.

To transmit this huge amount of data, the data will be compressed with a 3 : 1 ratio, after which it will be sent to the ground station using a link with a frequency of 2.4 [GHz]. Using the customer edition, a power signal of 600 [mW] will be used, offering an operational range without connection loss of about 50 [km]. To send commands to AERIS, a frequency of 430 [MHz] will be used, as the amount of data transferred from the ground to AERIS is limited. An omni-directional 5 [dBi] antenna will be used on-board of AERIS and a parabolic 26 [dBi] Twin Grid Tracking Antenna will be the type of antenna placed on the EWI building. To make the the UAV visible for other aircraft, an ADS-B module is included as well, which periodically broadcasts a signal. More specifications can be found in Section 6.4.

7.1.3. SAFETY

Apart from the parachute, which is dependent on the total mass of AERIS, all systems related to safety do not depend of the UAV size. The back-up battery is partially dependent of it, as it is designed according to a rough estimate of the total mass. Using a 3000 $[mAh]$ Turnigy nano-tech battery, enough power is provided to operate the engine and on-board electronics for about 45 minutes. This, combined with a glide ratio above 30 should be sufficient to find and land on a safe location.

Another on board safety system is an anti-collision flashing LED system, consisting of seven LEDs. Four LEDs are flashing day and night and another three continuously shining LEDs are added at night to partially comply with regulations set by authorities.[32] This results in a total LED mass of 35 $[g]$ while the average power needed for the LED system is 6.1 $[W]$. The planform of the lights is shown in Figure 7.4.

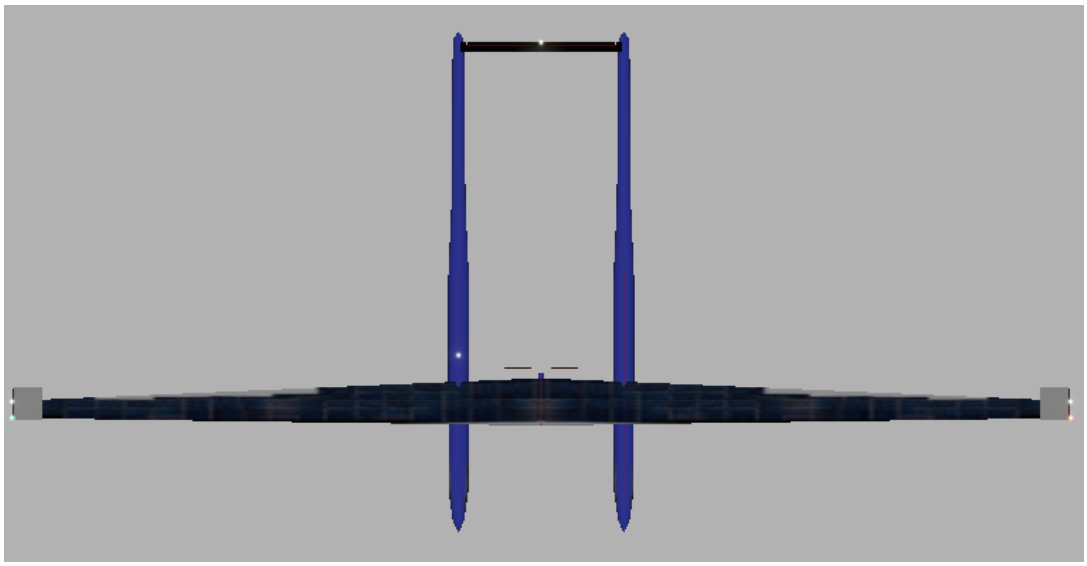

Figure 7.4: Safety Lights Planform

Apart from the LEDs, a GPS tracker of 25 $[g]$ which is able to operate without the help of any other system, as described in Section 6.3, is included. The tracker is able to operate as a stand-alone device without the need of other subsystems since it uses a dedicated communications channel via the cellular network to transmit its location once requested. General aerospace safety margins are found to be 1.5 for conventional calculations and materials, while a safety factor of two is applied on 3D printing and composite structures.

7.1.4. OVERVIEW NON-ITERATIVE PARAMETERS

Below, in Table 7.1, the parameters providing the most important information about the non-iterative part of AERIS are listed. The values are based on the script and the methods stated in Chapter 6. Note that there are three cameras on-board, one HSI, one IR for monitoring and another IR used to avoid collision with other flying object like birds.

7.2. ITERATIVE RESULTS

From the non-iterative values defined in the previous section, the iterative process can start. There are, however, still some parameters that need a preliminary value to run the numerical model. These values are listed in Table 7.2 and are used to find the first iteration. The initially guessed parameters are based on estimations, mass fractions, and the results comming from the MTR. More information regarding the determination of these starting points can be found in Sections 6.1 to 6.11.

7.2.1. AERODYNAMICS

The selected airfoil is the NACA 2210, further details can be found in Section 6.5. Once the airfoil is chosen, the wing characteristics are found. The large aspect ratio of 30 is beneficial for the induced drag, as well as the downwash. A taper ratio of 0.4 is selected in order to obtain a quasi-elliptical lift distribution. From the total mass, the requested lift in cruise is derived, which determines the wing dimensions when combined with the aspect ratio, taper, and C_{L_0}.

LIFT DISTRIBUTION

According to the initial assumption, a taper ratio is used during sizing to approach an elliptical lift distribution over the span of the wing. The iterative process resulted in a tip and root chord of 0.1724 $[m]$ and 0.431 $[m]$ respectively. The lift generated

Table 7.1: Non-Iterative Results

Parameter	*Value*	*Unit*
HSI Mass	0.180	$[kg]$
IR Mass	0.195	$[kg]$
Safety IR Mass	0.115	$[kg]$
Gimbal Mass (2x)	0.150	$[kg]$
Gimbal Power (2x)	7.2	$[W]$
Antenna Mass	0.057	$[kg]$
Radio Data-Link Mass	0.096	$[kg]$
Power for Communications	31.5	$[W]$
Downlink Frequency	2.4	$[GHz]$
Uplink Frequency	430	$[MHz]$
Payload Power	25	$[W]$
Computer Weight	0.520	$[kg]$
Flight Control Computer Mass	0.300	$[kg]$
Attitude Controller Mass	0.059	$[kg]$
Computer Power	30	$[W]$
Safety LED Mass	0.035	$[kg]$
Safety LED Power	6.1	$[W]$
Taper Ratio	0.4	$[-]$
Aspect Ratio	30	$[-]$
Flaperon Forces	± 100	$[N]$
Aileron Location	$70-90$	$[\%c]$
Load Factor	2.5	$[-]$
Safety Margin	1.5	$[-]$
Safety Margin for Composite 3D Printing	2	$[-]$
Maximum Gust	21	$[\frac{m}{s}]$
Optimal Altitude	500	$[m]$

Table 7.2: Initial Parameters

Parameter	*Value*	*Unit*
Starting Mass	5	$[kg]$
Maximum Power Required	450	$[W]$
Maximum Propulsion Power	300	$[W]$
Initial Cruise Speed	13.88	$[\frac{m}{s}]$
Total Drag in Cruise	30	$[N]$
Fuselage Drag in Cruise	9	$[N]$
Tail Drag in Cruie	2	$[N]$
Distance Between Fuselages	1	$[m]$
BOL Endurance	7.8	$[h]$
EOL Endurance	6.2	$[h]$

by the wing should be maximum at the root and should elliptically lower to zero at the tip of the wing. This is done to ensure that the wing root stalls first before the tip. It allows control surface which are situated near the wing tip to remain effective allowing the wing to recover from stall without losing control. Figure 7.5 shows the lift distribution over the semi span of the wing. It can be seen that the lift is maximum at the root and is lowest at the tip. The graph represents a linear relationship and the lift generated at the tip is not equal to zero. The distribution is not elliptical. It is because the wing twist and wing incidence angle are not taken into account which possesses significant impact on the lift distribution and will be addressed in Chapter 12.

7.2.2. PROPULSION RESULTS

The final results on the propeller sizing have a huge impact on the selected engine. In this section first the results of the engine and the shape of the blade are discussed. This is divided in the engine power and the blade dimensions. The next section goes into depth on the engine selection.

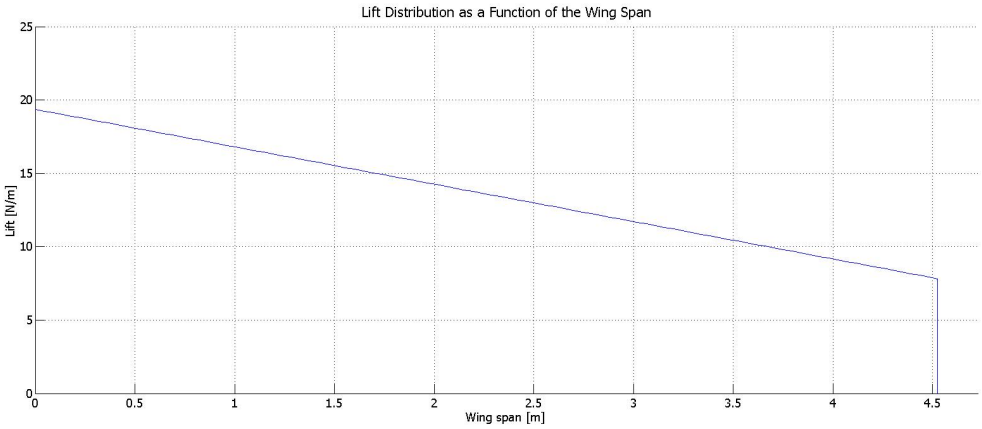

Figure 7.5: Lift Distribution Over the Semi-Span of the Wing

ENGINE

The final design has a required power to maintain cruise flight of 63.268 $[W]$. the angular speed is determined to be 600 RPM and the blade diameter has a value of 1 $[m]$ at a cruise speed of 50 $[\frac{km}{h}]$. The efficiency of the engine is calculated to be 95%. This value implies a engine power of 66.598 $[W]$. A more clear overview of the calculated engine specifications are shown in Table 7.3.

Table 7.3: Non-Iterative Engine Parameters

Parameter	***Value***	***unit***
RPM in Cruise	600	$[\frac{1}{s}]$
Propeller Diameter	1.00	$[m]$
Thrust Produced in Cruise	4.35	$[N]$
Torque Produced in Cruise	1.02	$[Nm]$
Engine Efficiency	0.95	$[-]$
Engine Power in Cruise	63.27	$[W]$
Maximum Engine Power	449.04	$[W]$

The electro engine selected is a currently of the shelf product. Since the angular velocity is very low a gearbox is used. This gearbox makes it possible to select an engine with a higher RPM and lower torque values than the blade itself. Since the electro engine selected for cruise does not deliver to maximum power required and the more powerful engine uses to much power in cruise both engines are used. These are put on to one gearbox with a gear ratio of 10:1. So the engines have an RPM of around 6000. Instead of changing gear ratios, the gearing is done by changing from the gear wheel of one engine to the other. The engine for cruise is the Park 450 brushless outrunner motor with the specifications presented in Table 7.4. The engine used to reach the maximum speed is the power 15 brushless outrunner motor with its specifications presented in Table 7.5. [82] [83]

Table 7.4: Overview of the Park 450 Specifications

Parameter	***Value***	***Unit***
Voltage	$7.2 - 12$	$[V]$
$\frac{RPM}{Volt}$	890	$[kV]$
Mass	0.072	$[kg]$
Continuous current	14	$[A]$

For cruise the voltage needs to be 7.2 $[V]$ so that the engine runs at 6400 RPM this is the closest it can get to 6000 RPM. This a voltage of 7.2 $[V]$ it delivers around 100 $[W]$ of power, which is still a bit too much. This will decrease the end of life endurance of 6.2 $[h]$. Using the specifications and Equation 7.1 it can be checked if the torque in cruise produced by the engine is enough.

Table 7.5: Overview of the Power 15 Specifications

Parameter	*Value*	*Unit*
Voltage	7.4 − 14.4	$[V]$
$\frac{RPM}{Volt}$	950	$[kV]$
Mass	0.152	$[kg]$
Continuous current	34	$[A]$

$$Q = \frac{I_{eng} \cdot V \cdot \eta_{prop} \cdot 60}{n \cdot 2 \cdot \pi} \tag{7.1}$$

Using the values in Table 7.4 and 7.3 the torque is calculated to be equal to 0.13 $[Nm]$ with a gearing ratio of 10:1 it delivers 1.13 $[Nm]$ to the propeller blade which is sufficient to turn the propeller.

BLADE SHAPE

The Blade diameter and RPM are already discussed in the previous section. However another important factor is the shape of the propeller blade. Both the chord length of each element and the angle of twist of these elements determine the shape of the blade. These results are presented in Table 7.6 and 7.7.

Table 7.6: Chord Length of Each Element of the Propeller Blade

Position of Element [% of Radius]	*Chord Length* $[m]$
10	0.025
20	0.025
30	0.042
40	0.042
50	0.042
60	0.042
70	0.042
80	0.075
90	0.042
100	0.025

Table 7.7: Blade Angle of Each Element of the Propeller Blade

Position of Element [% of Radius]	*Blade Angle* $[deg]$
10	90
20	80.9
30	68.3
40	58.0
50	49.8
60	43.5
70	38.6
80	34.6
90	31.4
100	28.9

The chord distribution start small at the root since little thrust is produced here due to low velocities. These low velocities also cause a high angle blade angle at that point since the rotational speed at this element is close to zero. Then the blade start increasing until the 70% point. From there on, it decreases until it is equal to zero at the tip. This is not shown in the table since only the values at the start of each element are presented. The angle of twist keeps decreasing towards the tip since the rotational speeds keep increasing. This can be shown by Equation 6.27 in Section 6.6.

7.2.3. POWER SUBSYSTEM

AERIS has two systems on-board to provide enough energy, namely solar cells, harvesting the free energy of the sun and a solar panel designed to harvest energy from the laser. The energy harvested from the sun changes during the iterative process, as the wings are covered by Gallium Arsenide single junction solar cells for 90% of the wing area. The total solar system

mass, found in Table 7.8 makes use of the assumptions stated in Section 6.8, accounting for mounting methods, wires, and a Fluorine Polymer protective aerodynamic clear coat. All these assumptions result in a weight equal to 235% of the pure solar cells. The laser power that arrives at the UAV has an efficiency of about 50%, so the laser power received should be twice as high as the power arriving. A panel of 0.09 $[m^2]$ is needed to ensure safe power transfer from the ground station.

The energy harvested is transferred to LiS batteries, stored in packages that will deliver 168 $[Wh]$ at BOL, which will reduce to 134.4 $[Wh]$ at EOL, accounting for 2000 cycles. When an endurance of 7.5 $[h]$ is desired, as stated in Table 7.2, the total battery mass iterates to 4.088 $[kg]$. The output voltage is regulated by a PMS, as much variation in amperage and voltage could damage the different subsystems. Next to the PMS in the circuit, the main bus can be found, which operates at 16.8 $[V]$, which is equal to the battery voltage. This is done to reduce the power system weight, because the same voltage on batteries and main bus means there is no voltage converter required in-between the batteries and the bus. When a subsystem requires a voltage deviating from this, resistors, linear regulators, and switchers are used to regulate the local voltage. Details about the operating voltages of the different subsystems can be found in Table 6.5.

An important mass fraction that is often underestimated during the preliminary design is the mass of the cables. The higher the voltage, the thinner the cables, but an additional voltage converter might be required. It was decided to use AWG standards for the cable sizing for both the normal and emergency system. Details on this can be found in Table 6.7. Once this is done, a check is performed to see whether another iteration within the power script is necessary.

7.2.4. STRUCTURES

As described in Section 6.9, both the wing and fuselage structures are iteratively sized to stand the loads exerted on them: a combination of point masses, distributed masses, and aerodynamic forces acting at various points along the wing and fuselage. At first both ABS and titanium were used as materials for the additive manufacturing process, however the MATLAB script could not iterate to a final value for the structure. The ABS exceeded the maximum permissible thickness according to the thin-walled approximation limited, also described in Section 6.9, and the titanium proved to be far too heavy to fly. Instead, a combination of both materials was used to make a composite structure. Titanium was used for the highest stress locations (near the wing and fuselage roots), whilst ABS was used for the lower stress locations. The ABS and titanium parts were mechanically bonded together with a series of "hook and loop"-like joins to efficiently transfer the loads between the parts. The effect of this was that the titanium simply absorbed the major loads, whilst the ABS provided a lighter and sustainable solution to carry the remaining loads, leading to a final wing mass of 2.860 $[kg]$ and a final fuselage mass of 0.524 $[kg]$. The model of this composite is rather simple, and more advanced failure modes should be studied before validating the design before a real production of AERIS. Nevertheless, according to Dr.ir. O.K. Bergsma, assistant professor in the structures department of the Aerospace Faculty of Delft University of Technology, this concept is feasible.

7.2.5. SUMMARY OF THE ITERATIVE PROCESS

The most important parameters changing during the iterative process are shown in Table 7.8. Note that the design converged after eighteen iterations. The results from the first, ninth and last iteration give more insight in the different subsystems and how they affect the complete UAV design. Note that the mass of the parachute does not change. This is because available parachutes are used and are effective in a range of masses. As the total mass remains in one mass category, the parachute used does not change from iteration to iteration. More information on that can be found in Section 6.3.

The final iteration is performed and all the parameters of AERIS are known. The technical drawing of AERIS can be found in Appendix B.

7.3. REMARKS ON RESULTS

This sections describes the remarks that can be made on the final design. Subjects as the take-off and landing procedures and systems that get AERIS in the air and back on the ground are determined and presented in the succeeding subsections.

7.3.1. TAKE-OFF

Now that the dimensions and the mass of the UAV is known the take-off system can be sized accordingly. Based on these results a trade-off is made. This trade-off is shown in Table 7.9.

Table 7.9 presents the catapult system as the optimal solution for our design. The structural impact, safety and re-usability are parameters this team considers to be more important over other parameters. The structural impact should be kept as low as possible since the UAV is not going to take-off and land very often the extra mass which such a system imposes is considered to be dead weight. Next to that, since AERIS will perform its mission in civil areas, safety is an important factor.

Table 7.8: Variation of the Most Important Parameters During the Iterations

Parameter	*First Iteration*	*Ninth Iteration*	*Eighteenth Iteration*	*Unit*
Propulsion Power at Cruise	20.841	61.307	63.268	$[W]$
Maximum Propulsion Power	215.505	435.138	449.044	$[W]$
Wing Span	5.716	8.911	9.054	$[m]$
Wing Area	1.089	2.706	2.732	$[m^2]$
Distance Between Fuselages	0.9	1.5	1.5	$[m]$
Fuselage Mass	0.325	0.509	0.525	$[kg]$
Wing Mass	0.593	2.580	2.860	$[kg]$
Most Aft CG	0.3306	0.3317	0.3356	$[m]$
Most Forward CG	0.0455	0.0740	0.0707	$[m]$
Surface Area Inverted Tail	0.0659	0.1411	0.1507	$[m^2]$
Inverted Tail Angle	55.17	58.53	57.97	$[deg]$
Parachute Mass	0.443	0.443	0.443	$[kg]$
Battery Mass	2.920	4.088	4.088	$[kg]$
Solar Cell System Mass	0.511	1.271	1.283	$[kg]$
Power System Total Mass	4.5498	6.655	6.747	$[kg]$
Average Solar Power Fraction	42.476	65.276	67.089	[%]
Total Power in Cruise	72.141	110.886	114.559	$[W]$
Total Mass	7.742	12.151	12.543	$[kg]$

Table 7.9: Trade-Off Table of the Take-Off System

Trade-Off Parameter	*Weight*	*Runway*	*Couple with Aircraft*	*Catapult*	**Rocket**	**Water Ski Ramp**
Cost	1	6	4	8	6	10
Structural Impact on UAV	5	2	6	9	7	8
Safety	4	9	5	7	4	1
Sustainability	3	5	2	9	1	8
Possibility to Re-use	4	10	5	10	1	7
Total	-	107	80	148	64	106

Although the UAV does not have to take-off and land very often. During certain weather conditions it the UAV is forced to stay on the ground. Therefore the system is preferred to be reusable.

The catapult system that comes out of the trade-off is a rail system which accelerates the UAV while it is locked in a frame until it reaches the right speed to take-off. This catapult system should not impose a high acceleration. The forces of the launch have to be kept low enough such that no extra reinforcement has to be added to the structure. Therefore a slow release system is used which slowly accelerates with $1g$. Since AERIS has a stall speed of 8.05 $[\frac{m}{s}]$ the length of the track should be at least 0.9 $[m]$ and with a appropriate margin set to be 2 $[m]$. Since there are two booms the rail width will be equal to the distance between those booms, which is 1.5 $[m]$. Those booms are clamped into the system and the system lets go of the UAV before the end of the rails.

7.3.2. LANDING

The results and size of the UAV also have an impact on the landing system. With this information again a trade-off can be made. This trade-off of the landing systems is shown in Table 7.10.

Table 7.10: Trade-Off Table of the Landing System

Trade-off Parameter	*Weight*	*Belly Landing*	*Net*	*Parachute*	*Water Landing*	*Runway*	*Inflatable Bouncing System*
Cost	1	7	10	6	9	5	2
Structural impact on UAV	5	7	3	5	3	1	1
Safety	4	8	9	5	7	10	5
Sustainability	3	6	8	3	6	5	6
Possibility to re-use	4	8	8	2	8	10	6
Total	-	124	117	68	102	105	69

The importance rating of the parameters for both the landing system and the take-off system trade-off is equal. These

systems are obviously not the same but the same parameters are valued in both systems. Table 7.10 shows that a belly landing is the best option. With a weight of 12.54 $[kg]$ this should not imply too many risks on the structure. Although with a belly landing the chance of structural failure is always higher than during a landing with landing gear, it still outweighs the other systems as the savings in structural mass compared to the other methods are significantly higher and preferred.

8. System Analysis

Now that the system has been completely sized, it is time to analyse the design in order to see whether the results are logical and according to the desired specifications. This analysis will be performed in a series of logical steps, that consist of the following steps;

- Verification: Used to check whether the sizing tool follows the numerical methods selected.
- Validation: Determine if the numerical methods used correctly represent the real case.
- Sensitivity Analysis: Serves to analyse the uncertainty in the output values of the model.
- Mission Analysis: Serves to analyse and describe a typical mission day for the UAV.
- Performance Analysis: Serves to see if AERIS meets the requirements as set in the RDT.
- Reliability, Availability, Maintainability and Safety (RAMS) Analysis: Serves to see if reliability, availability, maintainability and safety characteristics can be guaranteed.

8.1. Verification

The purpose of code verification is to control that the code does what it is expected to do. The method that is used to verify the code of each subsystem varies. The four main methods of verification are: [84]

- Inspection: A non-destructive inspection of the product. This can be visual, tactile, taste, olfactory or auditory. For coding however, these methods cannot be used.
- Demonstration: A inspection that verifies results by checking if results change as desired when the product is manipulated as intended.
- Testing: Checking whether the product will produce a very specific and predefined output as specified by the requirements when inserting predefined series of inputs.
- Analysis: Using models, calculations and testing equipment, analysis allows to make predictive statements about performance of a system based on the test results of a sample set.

The method that is used for verification for each individual part is described in their corresponding subsection below.

8.1.1. Aerodynamics

This section describes the verification process of the aerodynamics script. This is done by means of analytically solving the governing equations provided in Section 6.5, and comparing those values to the outputs of the code.

The aerodynamics script determines the wing surface first so that the UAV produces just enough lift in cruise. The cruise speed is then changed to increase with altitude and to maintain equilibrium as the air density falls according to the international standard atmospheric model. Following this, the chord distribution is determined using the assumed taper ratio. With this distribution, the approximate lift per section can be determined as well as that sections drag. Summing (integrating) those force distributions along with the re-iterated fuselage and tail drag gives the total lift and drag of the aircraft. The comparison of the analytical and numerical values is shown in Table 8.1. As can been seen, most of the values are exactly the same. The values that differ from each other are due to rounding errors.

Table 8.1: Overview of the Analytical and Numerical Values Calculated of the Aerodynamics Script

Parameter	***Analytical Value***	***Numerical Value***
Surface area	1.66 $[m^2]$	1.66 $[m^2]$
Cruise speed	19 $[\frac{m}{s}]$	19 $[\frac{m}{s}]$
Chord at 4th wing section	0.35 $[m]$	0.35 $[m]$
Lift produced in the 4th wing section	1.03 $[N]$	1.03 $[N]$
Drag coefficient	0.0122 $[-]$	0.0122 $[-]$
Drag	0.49 $[N]$	0.50 $[N]$

8.1.2. Propulsion

In this section, the verification of the propulsion tool is discussed. The method used is the same as in the verification of the aerodynamics code, namely by taking one case and analytically solving this case with the governing equations provided in

Section 6.6 and comparing the results to the results of the code which had been given the same inputs.

In the first part of the code, the required thrust and power is calculated for every speed and altitude - the output of the aerodynamics file. The exit velocities of the propeller are then determined for several blade diameters. The theoretical efficiency of the propeller for every diameter is determined and the blade with an efficiency of around 0.95 is automatically selected. This blade is then divided in to ten elements and their corresponding angular velocities are then calculated, giving the required blade twist per element. The lift and drag of each element is then determined for each of the blade elements as according to its chord length. With this, the thrust and torque per element can be determined. Then the code enters a complicated *while* loop where the angular velocity and the chord length per element is adjusted until it produces enough thrust to counter act the drag in cruise conditions at the design altitude of 500 $[m]$. Following this, the cruise efficiency is calculated according the relevant values for thrust, torque and angular velocity. Hence the engine power in cruise can now be determined. Now that the chord distribution of the propeller is known, the thrust and drag of each element is calculated for each altitude. The angular velocity of the entire propeller is re-iterated such that it produces enough thrust to fly at both the maximum speed and altitude. With this angular velocity the efficiency at this maximum condition is determined; the maximum required engine power is likewise determined. The known airfoil shape and the chord distribution allows one to compute the volume of each section and hence the volume of the propeller. Combined with the density of the material, the mass of the blade is easily determined.

For the analytical solution, a speed of 19 $[\frac{m}{s}]$ is used together with a density of 1.225 $[\frac{kg}{m^3}]$ at an optimum altitude of 450 $[m]$. The drag is set equal to 100 $[N]$. For the radius the first, last and the final selected element is used to verify the code. For the other values, the 4th element is selected. Table 8.2 shows the values of both the analytical and the code's solution.

Table 8.2: Overview of the Analytical and Numerical Values Calculated of the Propulsion Script

Parameter	***Analytical Value***	***Unit***	***Numerical Value***	***Unit***
Required thrust	100	$[N]$	100	$[N]$
Required power	1900	$[W]$	1900	$[W]$
Exit velocity (first/last/selected radius)	145.25/19.15/21.02	$[\frac{m}{s}]$	145.25/19.15/21.02	$[\frac{m}{s}]$
Efficiency (first/last/selected radius)	0.23/0.99/0.95	$[-]$	0.23/0.99/0.95	$[-]$
Selected radius	0.81	$[m]$	0.80	$[m]$
Angle of incidence	0.82	$[rad]$	0.82	$[rad]$
Lift/Drag 4th element	3.21/0.06	$[N]$	3.21/0.06	$[N]$
Thrust/Torque 4th element	2.15/0.64	$[N]/[Nm]$	2.15/0.63	$[N]/[Nm]$
Total thrust for selected RPS and chord distribution	100.01	$[N]$	100.01	$[N]$
Thrust for selected RPS and chord for 4th element	2.87	$[N]$	2.87	$[N]$
Volume of one blade	0.0024	$[m^3]$	0.0025	$[m^3]$
Maximum engine power	1999.4	$[W]$	1999.4	$[W]$
Engine power cruise	1999.4	$[W]$	1999.4	$[W]$

Table 8.2 shows that the code accurately calculates the values as it should. There are slight differences in some values due to rounding errors. Some rounding errors build up during the optimisation processes, but they are sufficiently small as seen in the table above. Since only a finite number of elements is used, the script might skip the actual optimal value and would therefore be different to the analytical value. Another remark is that the maximum engine power and the engine cruise power are the same. This can be easily explained; the speeds that are used are both 19 $[\frac{m}{s}]$, hence there will be no difference in the power since this is both the minimum and maximum speed. The altitude remains constant as well during this verification.

8.1.3. TAILSIZING

In this section, the verification of the tail sizing module is described. The method is rather straightforward. As pointed out previously, the theory behind the stability analysis encompasses many lengthy equations which allow one to easily make mistakes in the code. Though the computer is extremely well suited to making these calculations very quickly, on must take care to verify that the equations have been implemented correctly. This analysis will follow the steps described in Chapter 6 following the equation flow model.

The code was written with the need for verification in mind; several fail-safe checks have been hard-coded into the script at frequent intervals. This has been done by means of an *if* statement to check whether or not certain variables make sense. For example, the script is designed to output a warning when the $C_{L_{\alpha_w}}$ is lower or higher than expected. A value of $2\pi AR+2$ is used as a sanity check since the $C_{L_{\alpha_{wf}}}$ is expected to be in the range of $[5,5-6]$. When running the script with values of

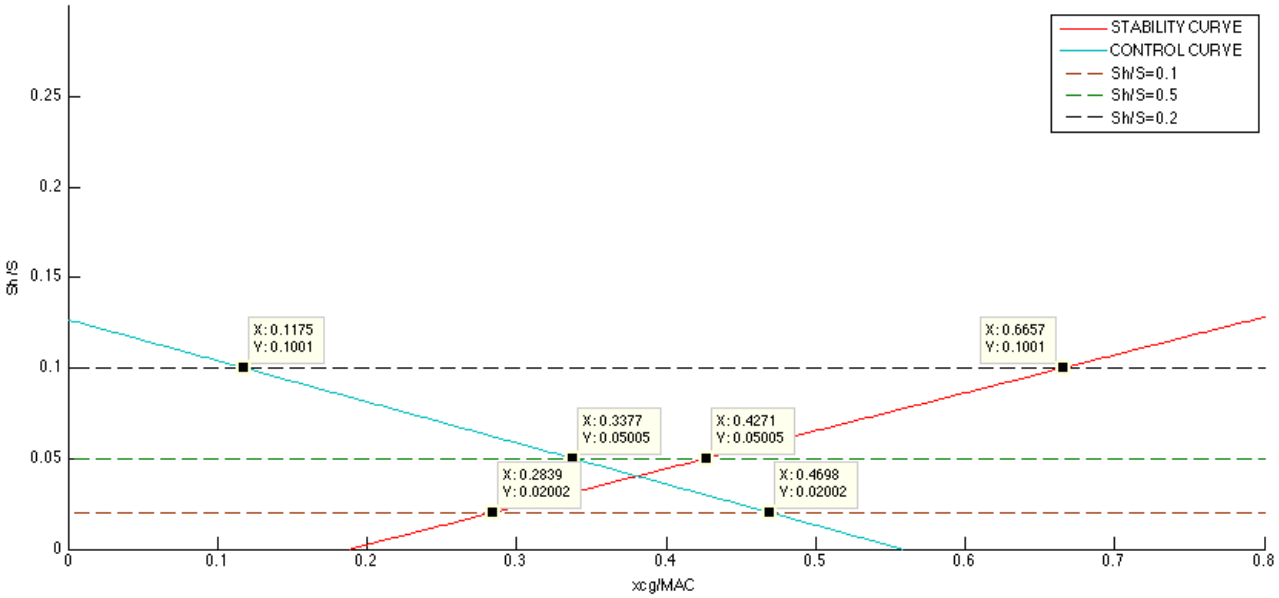

Figure 8.1: Six Data Points on Control and Stability Curves Generated in MATLAB

1000 and −1000 for the aspect ratio, MATLAB did indeed report an error. The lines for C_L and downwash gradient have a similar sanity check to ensure that the values flowing into the stability and control equation are correct.

The actual verification of the code was performed with the input parameters summarized in Table 8.3. The most important output of the first part of the script are the control and the stability curves. MATLAB uses the equations described in Section 6.7 to calculate the $x_{c.g.}$ locations and takes the surface ratio, $\frac{S_h}{S}$, as a running parameter with values of $[0.02, 0.05, 0.1]$. The corresponding center of gravity ranges can be found in Figure 8.1, and are summarized in Table 8.3.

Table 8.3: Verification of Stability and Control Module: Coefficients

Parameter	***Symbol***	***Analytical Value***	***Numerical Value***	***Unit***
Lift Slope H.Tail	$C_{L_{\alpha_h}}$	4.4639	4.4639	[-]
Lift Slope Wing	$C_{L_{\alpha_w}}$	5.6021	5.6022	[-]
Lift Slope Wing+Fuselage	$C_{L_{\alpha_{wf}}}$	5.3855	5.3855	[-]
Downwash Gradient	$\frac{d\epsilon}{d\alpha}$	0.2610	0.2610	[-]
Moment Coefficient	C_m	-0.3832	-0.3833	[-]

Table 8.4: Verification of Stability and Control Module: CG Locations

x-Parameter	***Anal.*** $\frac{sh}{s} = 0.2$	***Num.*** $\frac{sh}{s} = 0.2$	***Anal.*** $\frac{sh}{s} = 0.5$	Num. $\frac{sh}{s} = 0.5$	***Anal.*** $\frac{sh}{s} = 1$	***Num.*** $\frac{sh}{s} = 1$
$x_{c.g.control}$	0.4698	0.4698	0.3377	0.3377	0.1176	0.1175
$x_{c.g.stability}$	0.2838	0.2839	0.4271	0.4271	0.6658	0.6656

Table 8.5: Verification of Stability and Control Module: Coefficients

Parameter	***Symbol***	***Analytical Value***	***Numerical Value***	***Unit***
Wing setting contribution to directional derivative	$C_{n_{\beta_f}}$	−0.01605	−0.01600	[-]
Propeller setting contribution to directional derivative	$C_{n_{\beta_p}}$	−0.000183	−0.001083	[-]
Coefficient of the fuselage dimensions	k_β	0.03616	0.03620	[-]

As explained earlier, the tail volume $\frac{Svlv}{Sb}$ is found from the graph provided in Section 6.7 in Figure 6.23. MATLAB calculates the total C_{β_n} and matches the y value in Figure 6.24. As explained in Section 6.7, the plot shown in MATLAB, Figure 6.24, is the digital form of the plot from Torenbeek. [60] The $[x, y]$ values of this graph have been imported to MATLAB numerically.

The digitalisation of the plot is quite precise, however, due to conversion it is possible to have some deviation. This can be checked by overlaying the two graphs and checking if they match. Figure 8.2 shows the result. It can be seen that the plots match exactly, hence the values that MATLAB produces are exactly the ones of the original plot. Hereby the values of the lateral directional coefficients calculated in MATLAB are verified.

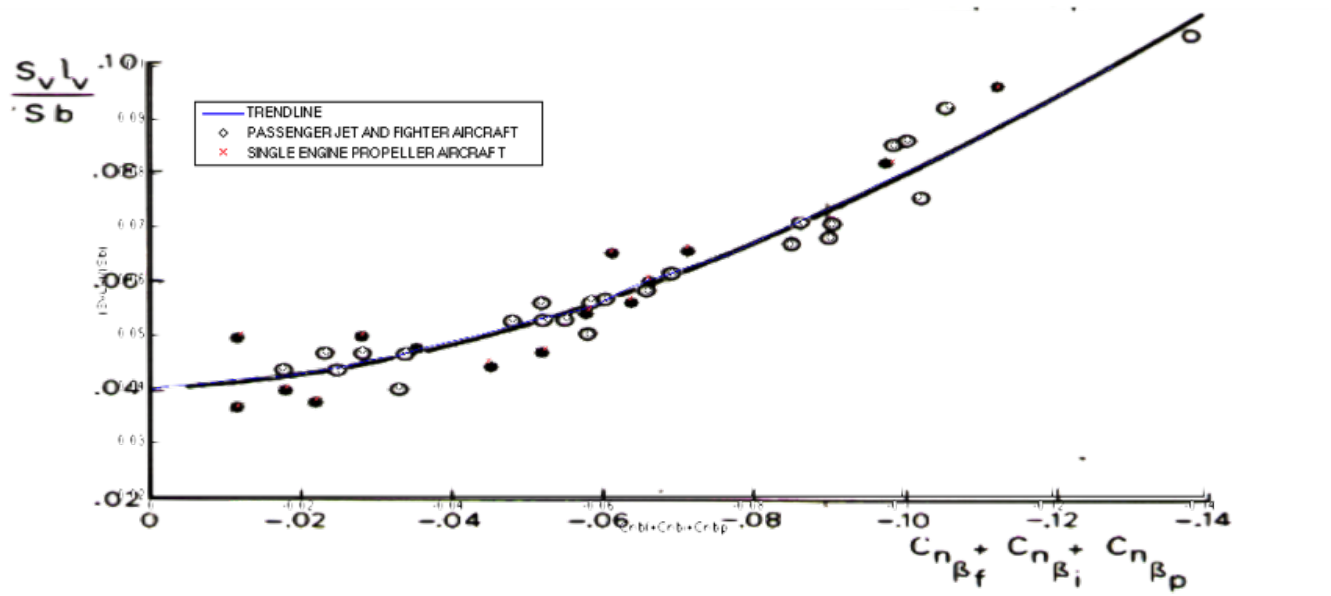

Figure 8.2: Overlay of Two Plots: MATLAB vs Original From Torenbeek [60]

8.1.4. POWER

The AERIS mission is a unique project when it comes down to power subsystem. No other UAV of comparable size has been built with the goal to remain airborne for such a long time. It is for that reason that engineering gut cannot be relied upon to judge if results of the power subsystem are in the right order of size. Testing the script by using a single input and analytically solving the relevant equations as stated in Section 6.6 is not ideal since the sizing tool uses exact formulas without approximation. Therefore the results of such calculations would result in exactly the same answer. Demonstration, however, is possible. By manipulating of the sizing tool input values, it can be verified that results change in a logical manner.

The input values of the sizing tool include:

- Wing surface
- Wing span
- Endurance required
- Engine power in cruise
- Power required of all other systems
- Maximum engine power
- Length of the fuselage
- Lateral boom separation

The output values of the sizing tool include:

- Number of solar cells
- Battery pack mass
- Mass of the total solar subsystem
- Mass of the total power system
- Number of battery packs
- Solar energy share out of total
- Power from laser arriving at UAV

The inputs and outputs are related to each other. Once the dependency is known, it can be seen that the output values of the tool change accordingly with an increase in input value. The dependencies are known to be as follows:

Increasing the wing surface will impact the number of solar cells directly, as the wing is covered with solar cells. The mass of the solar subsystem will increase due to this number of solar cells. Forming only a small percentage of the total energy mass, the total power system mass should increase minimally, whilst the solar system share, battery pack mass, number of battery packs and power from the laser system should remain unaffected.

Increasing the wing span will not affect the number of solar cells as surface area remains the same. The mass of the solar subsystem, solar energy share, mass and number of battery pack and power from laser remain all unaffected. The only mass expected to change is the mass of the total power system, as longer cabling is needed for the lights. This will have a very minor impact.

Increasing the endurance required will not affect the number of solar cells, mass of solar subsystem and power from the laser arriving at the UAV. Note that the battery pack mass will not be affected either, since it only gives the mass of one single pack which in turn is entirely dependent on the chosen voltage, i.e. cells in series. The mass of the total power system and number of battery packs will be affected, and so does the solar share. Reason for the latter is that the amount of solar power generated remains the same, although more power is required that has to be obtained from the laser.

Increasing Engine Power in Cruise affects the endurance. For that reason, the same changes are expected as when changing the endurance required, though less extreme.

Increasing the Maximum Power required affects the ESC that is to be used. When increasing the maximum power required, a heavier ESC is to be used. Since flight at maximum power will not be used often, it is assumed that the endurance remains the same. It is for that reason that only the total mass is expected to increase by a small amount.

Increasing Power required of all other systems affects endurance. For that reason, the same changes are expected as when changing the endurance required, albeit less extreme.

Increasing the Length of the fuselage affects the cable lengths. The same changes are expected as when increasing the wing span, i.e. only the total power system mass will increase by a minimal amount.

Increasing the Boom Separation affects the cable lengths. The same changes are expected as when increasing the wing span, i.e. only the total power system mass will increase by a minimal amount.

Table 8.6 contains all of the inputs and outputs that are mentioned previously. The very first line is the reference or baseline. By increasing the input values one by one and recording the changes, it can be verified that the sizing tool operates as expected. Note that the initial input values for the reference data is arbitrary and does not present the actual data. Also, the solar energy share for an average solar flux is taken. From Table 8.6 it can be noted that the values indeed change as expected, which verifies the power sizing script.

Table 8.6: Verification Values for Power Verification

Item	*# Solar Cells*	*Bat. Pack Mass* $[kg]$	*Solar System Mass* $[kg]$	*Power System Mass* $[kg]$	*# Battery Packs*	*Solar Energy Share* [%]	*Power from laser* $[W]$
REFERENCE DATA	2040	0.5840	1.043	11.8013	16	18.7556	1978
Wing Surface	4080	0.5840	2.087	12.8448	16	37.5113	1978
Wing Span	2040	0.5840	1.043	12.1268	16	18.7556	1978
Endurance	2040	0.5840	1.043	21.6186	32	11.2534	4475
Engine $Power_{cruise}$	2040	0.5840	1.043	18.5507	27	11.2534	3297
Other Power Required	2040	0.5840	1.043	14.8692	21	14.0667	2638
Engine $Power_{max}$	2040	0.5840	1.043	11.8162	16	18.7556	1978
Length Fuselage	2040	0.5840	1.043	11.8283	16	18.7556	1978
Boom Separation	2040	0.5840	1.043	11.8613	16	18.7556	1978

8.1.5. STRUCTURAL VERIFICATION

To verify the code related to the structural design of the UAV, the different parts of the code will be verified separately. First, the shear, moment and torque diagrams will be verified, after which the parts of the code used to locally increase thickness to withstand internal shear forces, internal moments and internal torques will be checked.The analytical and numerical approaches are both based on the equations and concepts described in "Aircraft Structures for Engineering Students, Fifth Edition" and the course "Structural Analysis and Design" as taught at Delft University of Technology by Dr. C. Kassapoglou. [68] [69]

SHEAR, MOMENT AND TORQUE DIAGRAMS

To verify the different force diagrams, a simplified case which shown in Figure 8.3, is calculated analytically and interpreted as inputs to the code. Following this, the results of the analytical calculations and the code are compared and plotted against each other. When they stay within 5% of each other, the code is considered to give reliable results and thus is verified. For the shear force, the analytical solution of the simplified case shown in Figure 8.4 and is calculated by Equations 8.1 to 8.4. The numerical solution is the solution provided by the code. The location of the fuselage in the investigated area can clearly be seen in the shear diagram, as well as the additional weight of the control surface located between 80% and 90% of the

wing span. The numerical model for the shear force in x-direction is similar the one shown in Figure 8.3, but with drag and thrust forces acting on it.

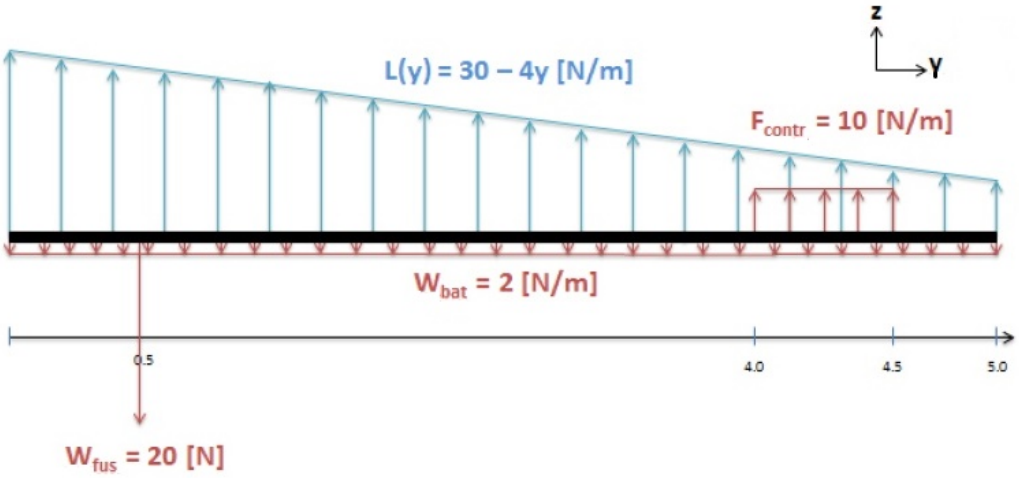

Figure 8.3: Simplified Load Case Used for Structural Verification

$$S_{z1} = \int_0^y (30-4y)dy - \int_0^y 2dy = -2y^2 + 28y - 75 \; for \; 0 \leq y < 0.5 \tag{8.1}$$

$$S_{z2} = \int_0^y (30-4y)dy - \int_0^y 2dy = -2y^2 + 28y - 95 \quad for \; 0.5 \leq y < 4 \tag{8.2}$$

$$S_{z3} = \int_0^y (30-4y)dy - \int_0^y 2dy + \int_4^y 10dy = -2y^2 + 38y - 135 \quad for \; 4 \leq y < 4.5 \tag{8.3}$$

$$S_{z4} = \int_0^y (30-4y)dy - \int_0^y 2dy = -2y^2 + 28y - 90 \quad for \; 4 \leq y < 5 \tag{8.4}$$

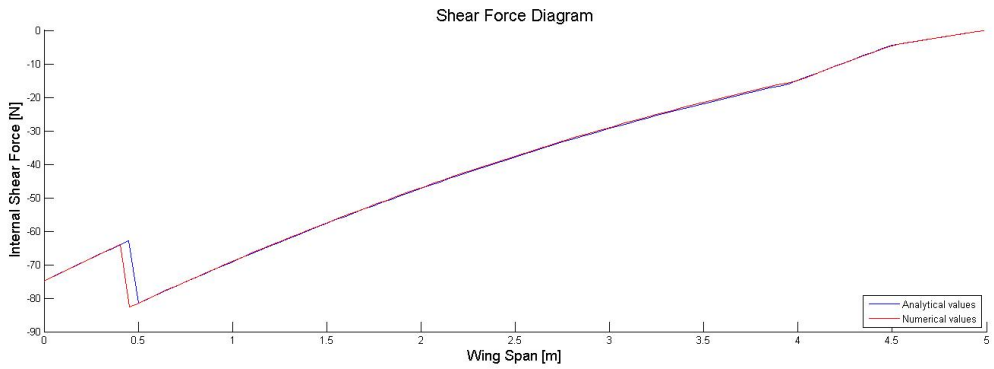

Figure 8.4: Shear Force Diagram Used for Structural Verification

When examining Figure 8.4, it can be seen that the line representing the numerical values is slightly shifted to the right. This is due to the assumption in the numerical model that the internal forces in the first section act in the xz-plane, while they actually act in the middle of the first section, which is half the section width away from the xz-plane. In other words, increasing the number of sections decrease the difference between the model and the reality, making them coincide when the number of sections becomes infinite. Equations 8.5, 8.6, 8.7, and 8.8 are the analytical expressions of the internal moment. The constant values added to the result of the integrals are determined according standard aerospace mechanics of materials values. [85]

$$M_{x1} = \int_0^y -2y^2 + 28y - 75dy = -\frac{2}{3}y^3 + 14y^2 - 75y + 194.5833 \quad for \; 0 \leq y < 0.5 \tag{8.5}$$

$$M_{x2} = \int_0^y -2y^2 + 28y - 95dy = -\frac{2}{3}y^3 + 14y^2 - 95y + 204.5833 \quad for \; 0.5 \leq y < 4 \tag{8.6}$$

$$M_{x3} = \int_0^y -2y^2 + 28y - 135dy - \frac{2}{3}y^3 + 19y^2 - 135y + 284.5833 \quad for\ 4 \leq y < 4.5 \tag{8.7}$$

$$M_{x4} = \int_0^y -2y^2 + 28y - 90dy - -\frac{2}{3}y^3 + 14y^2 - 90y + 183.33 \quad for\ 4.5 \leq y < 5 \tag{8.8}$$

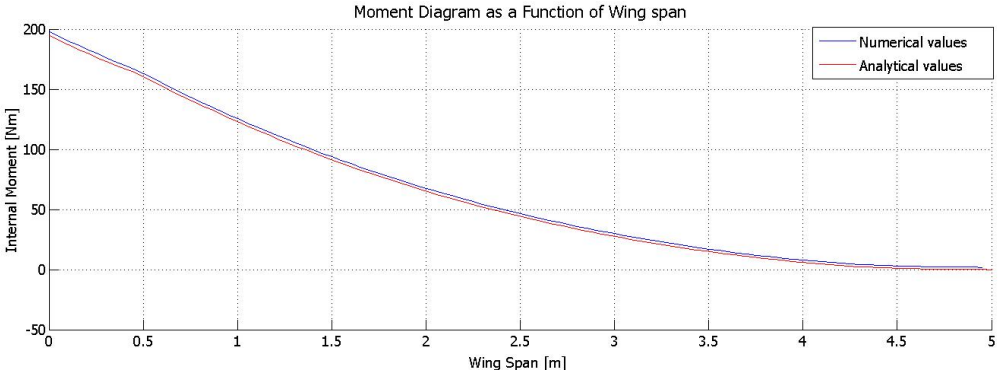

Figure 8.5: Moment Diagram Used for Structural Verification

In Figure 8.5, there is a shift similar to the shift described for the internal shear force. Extending the number of sections to infinity would, again, lead to an exact solution in the code. Because of the small deviation between the curves, it can be stated that using one hundred sections results in a sufficiently accurate model. For torque, the same approach and conclusion follow. The deviation between the code and an analytical model is shown in Figure 8.6. To generate the torque diagram, the control force is pointing down because this generates the highest torque, which is what the structure should be designed for. The influence of the control surface on the torque can clearly be seen in the graph. The location where the loads act is simplified and loaded into the code. The control force, for example, is assumed to act at 90% of the chord length.

Figure 8.6: Torque Diagram Used for Structural Verification

The difference between the numerical and analytical solution for the torque is extremely small. This makes sense, because the location of a section in y-direction has a small influence on the internal torque compared to the influence it has on the internal shear force and internal moments. It can also be seen in the three different diagrams that the forces and moments go to zero at the wing tip. This should indeed be the case, strengthening the confidence in the models.

SHEAR FLOWS, BENDING MOMENTS AND BUCKLING

The forces and moments acting on each of the sections in the spanwise direction are found from the force and moment diagrams. Again, a simplified structure is loaded into the script: namely a simple rectangular thin-walled cross-section, in stead of the complicated airfoil shape. For the root section, the shear flow and bending stresses are calculated, both analytically and numerically according to the formulas found in Section 6.9. The moments of inertia were exactly the same for the analytical and numerical calculations, because thin-walled assumptions were applied to both methods. The numerical shear flows, however, did not completely overlap. Taking the average of the analytical shear flow on every side of the rectangular, however, only gave small deviations, as shown in Table 8.7. Because the non-simplified case uses 100 sections in stead of the four used in the simplified verification model, it can be assumed that, for small sections, the shear flow is nearly constant and close to the average of the shear flow in the section. Therefore, the deviations between the analytical average values and the numerical values are small enough to show the numerical model of the shear flow does what it expected of

it. The code adapts the thickness of each panel. When using this as an input, it was seen that the panel thickness is exactly the thickness required to withstand the local shear flow. The required thickness was calculated using Equation 8.9.

Table 8.7: Shear Flow Verification

Evaluated Panel	***Numerical Value*** $[Pa \cdot m]$	***Analytical Value (avg)*** $[Pa \cdot m]$	***Deviation*** [%]
Front Panel	−36.584	−36.695	0.3
Upper Panel	−17.160	−16.997	0.9
Back Panel	−25.438	−25.618	0.7
Lower Panel	−13.755	−13.581	1.2

$$t_{req,s} = \frac{q_s}{\tau_{max}} \tag{8.9}$$

The next part of the code is the part determining the location where thickness should be added to withstand the bending moment, starting from the moment diagram shown in Figure 8.5. First, it is verified that the selected location is correct by applying a positive and loading the rectangular model again, but partially increasing the height of the upper section. If the code is written right, it should first completely fill in this Next, the code was used until it iterated to a sectional design. This sectional design was analytically checked for it's resistance to bending and resulted in an over sizing of 1.14%, which can be explained by the fact that the thickness added per iteration equals $0.1[mm]$. This will lead to a slightly oversized design, but the more sections are used, the less the over sizing will be.

The last thing to be verified is the occurrence of buckling. To determine this, a section in the middle of the wing is investigated, as well as the root and the tip section. The buckling part of the numerical model is executed and the design that comes out is checked for the buckling requirement. It was found that additional thickness was needed in the root and middle section, while the tip section was fine as it was after designing it to withstand the bending moment. The numerical model outputs an adapted thickness distribution that result in sufficient buckling resistance when calculated analytically. From this point on, it can be assumed that the structural model of the wing is verified.

The verification discussed above is the verification of the wing structure. It was chosen to discuss this verification in detail, as the numerical tool for the fuselage design is basically the same model as the numerical wing design model. The only difference is that, for the fuselage design, it is assumed that there are only vertical loads acting on the structure. The fuselage model is actually a simplified model of the wing model. Loading in the simplified case discussed above into the fuselage model, the results of the fuselage and wing model were compared. It could be concluded that, since the values from the fuselage and the already verified wing model were similar, the fuselage model is also verified.

8.2. VALIDATION

The final design was made in Section 7.2. The verification was performed in Section 8.1 and in this section the validation will be performed. Validation consist of multiple phases. There is subsystem and system validation. One of the most used ways to validate a design is using actual tests, such as a flight test or a structural test. Since AERIS is still a concept, these tests cannot be performed yet. The ways to validate the parts of AERIS will be described in the following sections. First the sub-system tests will be described after which the whole UAV will be validated.

8.2.1. SUBSYSTEM VALIDATION

Some individual subsystems will be separately validated. The descriptions of how these test should be performed will be described in the following sections. The same order as Chapter 6 will be used, although some parts may be left out.

SAFETY

For the safety system of AERIS the parachute needs to be validated.The parachute should slow down the UAV enough to decrease the damage on impact. Since the parachute is not yet fabricated, the test will be performed in the future. If the parachute is constructed it will be tested by attaching a weight, equal to the mass of AERIS, to the parachute. The it will be dropped from an altitude of 100 $[m]$. Doing this test will validate the effectiveness of the parachute and the final impact speed will be known.

COMMUNICATION

The communication system will be validated during flight tests of AERIS. During these flight tests the range and the data rate will be tested. AERIS will fly to the edge of Zuid-Holland to see if the calculations are met. For safety, in case of loss of

control, a mobile control station will be in reach to make sure that, if the communication is lost, AERIS will be send back to a range in which mission control regains the communication link.

AERODYNAMICS

The aerodynamics of the AERIS will be validated using a two step validation. The first step is to test a scale model in a wind tunnel. During these tests major differences between the calculations and the actual data will be noticed and changed before a full scale test plane will be build. This full scale model will go through a flight test program to see if AERIS performs according to its specifications.

PROPULSION

The propulsion consist of the engine and the propeller. As soon as the final engine is sized and the propeller is constructed it will be tested before it will be mounted on AERIS to initiate the flight test program. The propeller needs to be balanced in order to make no disturbances. Each propeller will be balanced before mounting it to AERIS.

TAIL SIZING

Normally XFLR5 would have been used to determine the aircraft's stability at different Reynolds numbers and altitudes. However, since XFLR5 is not able to deal with a double fuselage it is not suitable for AERIS. Therefore the tail sizing needs to be validated by other means, for example during a wind tunnel test with a scale model of AERIS.

STRUCTURES

Since the structure of AERIS will be created using a 3D printer al lot of validation tests need to be performed. First small test samples need to be printed and tested to determine the failure characteristics and other properties of the material. As soon as these properties are known the design might need to be tweaked. After that, parts of the structure will be produced and tested using the limit load of AERIS. After the parts of AERIS are validated the complete structure will be printed. After printing, AERIS will be build up using all the components in order to start the flight test program. During the first phase of these tests, dummy cameras and solar cells will be mounted in order to minimize losses in case of a crash. As the structure is tested AERIS will be completed to continue the flight and certification tests.

FLIGHT CONTROL

The first step of the validation of the flight control is done using X plane. A more detailed description of the flight performance is described in Section 8.2.2. After the simulation is performed the final validation will be done during the flight test program.

8.2.2. FLIGHT PERFORMANCE OF AERIS

AERIS will be created use X plane, in the Plane Maker. [86] After AERIS is created it will be loaded in the flight simulator of X plane. Using the simulator AERIS will be flown at different altitudes, flight speeds, angles of attack, and weather conditions in order to check if al the requirements are met. Furthermore some step inputs will be given to check the eigenmotions such as the phugoid, spiral, Dutch roll, etcetera. These analysis are, for now, the only way to see if the design behaves as the calculations tell us.

DESIGN IN X PLANE

The UAV can precisely be modelled in X plane. Both fuselages are constructed, the electric engine will be mounted with the right amount of power, and the inverted v-tail with ruddervators will be placed. A picture of AERIS as created in X plane can be seen in Figure 8.7. However there are some shortcomings in X plane. One of these is the propeller. This is not a folding prop, but AERIS will have one. Therefore the non powered flight in X plane will be different from real life. Another disadvantage of X plane is that it is designed for normal aircraft which have a higher speed. Therefore the slow speed flight may not be as accurate as desired but for now, it is deemed to be sufficient.

RESULTS OF THE VALIDATION

With the design from Figure 8.7, several flight manoeuvres were performed at different altitudes and power settings in order to check the performance and the cg. Furthermore C_{m_α} and C_{β_n} are determined by X plane.

The Oswald efficiency factor of the wing is 0.93 according to X plane, which is fairly close to the one of an elliptical wing which is equal to one. The moment coefficient derivative C_{m_α} is found to be -0.00004, which is as its supposed to be for stability reasons. The value found for C_{β_n} is equal to -0.00001, which is slightly negative but almost equal to zero. However,

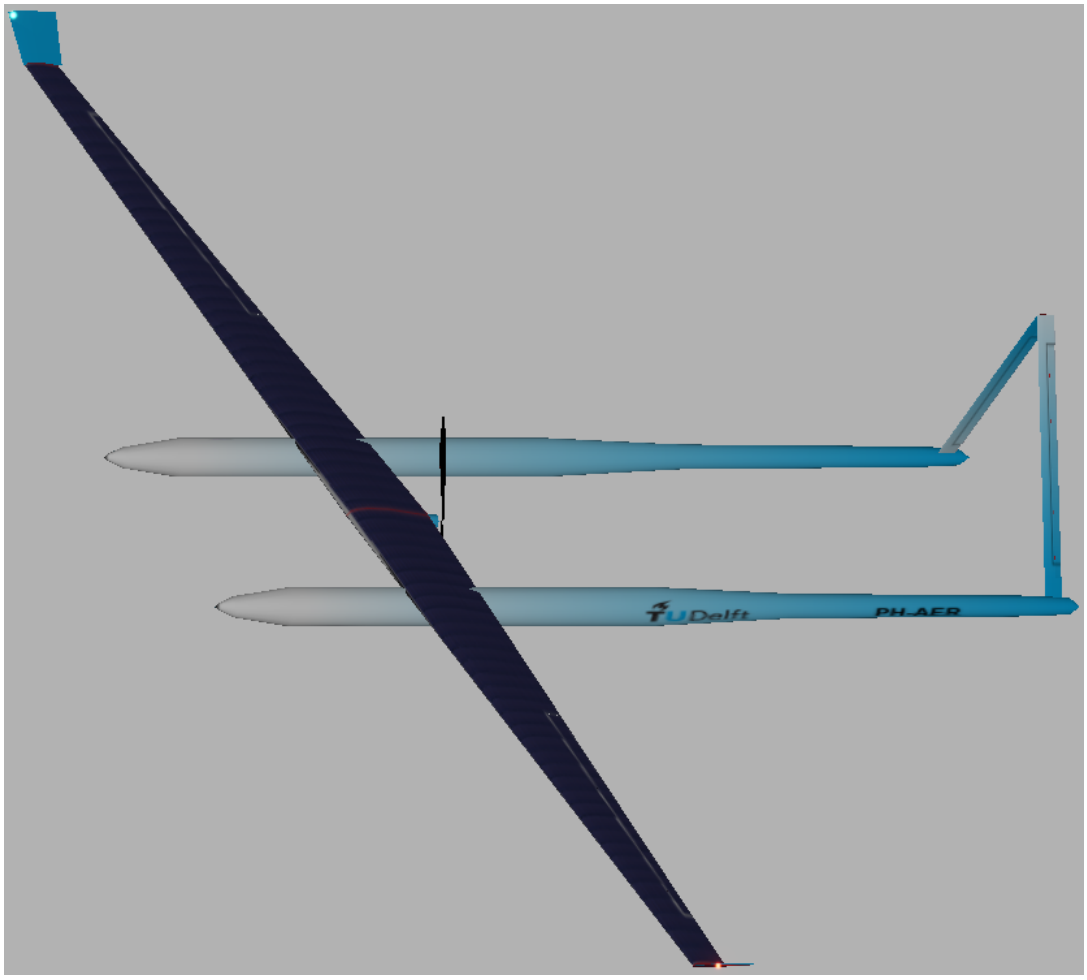

Figure 8.7: AERIS as Created in X plane's Plane Maker

a positive value is desired.

After the determination of the coefficients the spiral mode was tested. During this test an initial roll was initiated after which AERIS was left on its own. Although the recovery is not instantaneous AERIS is able to recover and continuous in steady horizontal flight. When AERIS was stable again the engine was shut down to initiate the phugoid. After a couple of up- and down movements AERIS continuous with a stable, un-powered, gliding flight.

In order to check the glide ratio of the complete UAV the engine is turned off and the speed is reduced to 13.9 $[\frac{m}{s}]$. The vertical speed indicator showed a descent rate of 100 $[\frac{ft}{min}] = 30.48\,[\frac{m}{min}]$. Together with the flight speed a glide ratio of 27.8 is found. This value should be higher because AERIS has a folding propeller but X plane is not able to model that.

8.3. SENSITIVITY ANALYSIS

Sensitivity analyses can be used to identify the variables which might have particularly large impacts on the design and which have a lesser impact, as well as evaluating error functions and developing the model further to give more accurate results. [87] AERIS' design is not at the stage where the theoretical results can be cross-checked with physical data in a validation process, so modelling these error functions at this point is rather difficult and not extremely useful. A sensitivity analysis of slight variations of the main inputs of the design tool, however, can give the team valuable information about the tool, as well as confidence in the design by studying what impact certain errors might have. The most important metric used in the sensitivity analyses in these sections is AERIS' total mass. All analyses were performed with a *brute force approach*: the tool ran through and sized the design for each combination of input parameters. [88]

This sections can be broken up into two subsections. The first subsection discusses the univariate sensitivity analysis of the main variable as they change around the current design point (i.e. the non-varying parameters remain at their designed or "baseline" values). This analysis shows the simple effect that each variable can have on the design; more importantly it

shows how an error in that parameter might affect the entire design. The second subsection deals with a limited multivariate analysis; as it is much more computationally imposing, it has been performed with a much coarser data set. In a multivariate analysis,the team can get a much more detailed view of how a combination of multiple input parameters might affect the design. These analyses will also give the team more insight into future risks and how to manage them, and shall be discussed in Chapter 12.

8.3.1. UNIVARIATE SENSITIVITY ANALYSIS OF THE MAIN INPUT PARAMETERS

The main input parameters and the range in which they were varied are given in the list below:

- Cruise velocity: $50-65$ $[\frac{km}{h}]$
- Aspect ratio: $32-38$ $[-]$
- Endurance: $4-8$ $[h]]$
- Material density: $1500-2000$ $[\frac{kg}{m^3}]$
- Material maximum normal stress: $0.75-1.5$ $[GPa]$

It should be noted that as the maximum normal stresses changethe maximum shear stresses of the material chance an approximated factor two as well. This assumption follows from basic mechanics of materials knowledge obtained in the first year, namely the reduced Von Mises stress calculations.

The univariate sensitivity of the model to changes in the designed cruise speed highly affected the wing mass (the aerodynamic loads become much more imposing), as can be seen in Figure 8.8, closely followed by the size of the power subsystem, total aircraft mass and solar power production percentage. The rate of climb at the design point was largely insensitive to the change in cruise speed. Ignoring the latter performance parameter, this analysis shows that increasing the cruise velocity of the wing heavily impacts AERIS' performance as well as the mass of the wing and hence the overall mass of the aircraft. Direct recommendations are to try and keep the current design speed of 50 $[\frac{km}{h}]$, and to carefully manage AERIS' mission such that it can perform adequately. Small errors in the cruise speed can have a relatively large impact on the design - a total increase in mass of approximately 12% for an increase of just over 8 $[\frac{km}{h}]$. The design did not even converge for designed cruise speeds greater than 60 $[\frac{km}{h}]$. Upon further inspection discrete jumps in mass in the graphs below is due to the script adding additional battery packs.

Figure 8.8: Univariate Sensitivity of AERIS to the Design Cruise Velocity

The sensitivity of the model to changes in the stated endurance directly correlate with the sensitivity to the cruise velocity, as seen in Figure 8.9. The same conclusions can thus be drawn from these analyses.

The sensitivity of the model to changes in the maximum permitted normal stress of the material (and shear stress - the two often differ by a factor of two for reasons given previously) greatly affects the wing mass. The remaining parameters are seen to be rather insensitive in contrast to these stresses, as seen in Figure 8.10. Material choice is obviously an influencing factor: the stronger the material the better. The problem is, in reality, far more complex as one is holding material density constant in this particular analysis. This is the biggest weakness of univariate analysis - the strong dependencies between various parameters cannot be spotted. It is safe to say, however, that using material in the most optimum way truly pays off, and errors here could prove highly problematic for the design. In addition, if safety factors can be reduced with adequate

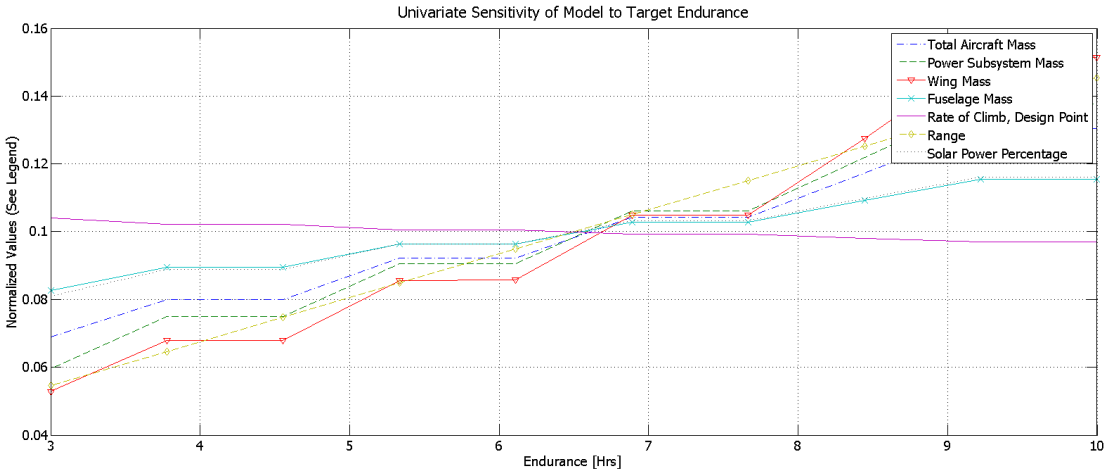

Figure 8.9: Univariate Sensitivity of AERIS to the Design Endurance

testing and/or validation, the total mass of the design would drastically decrease, which is desirable.

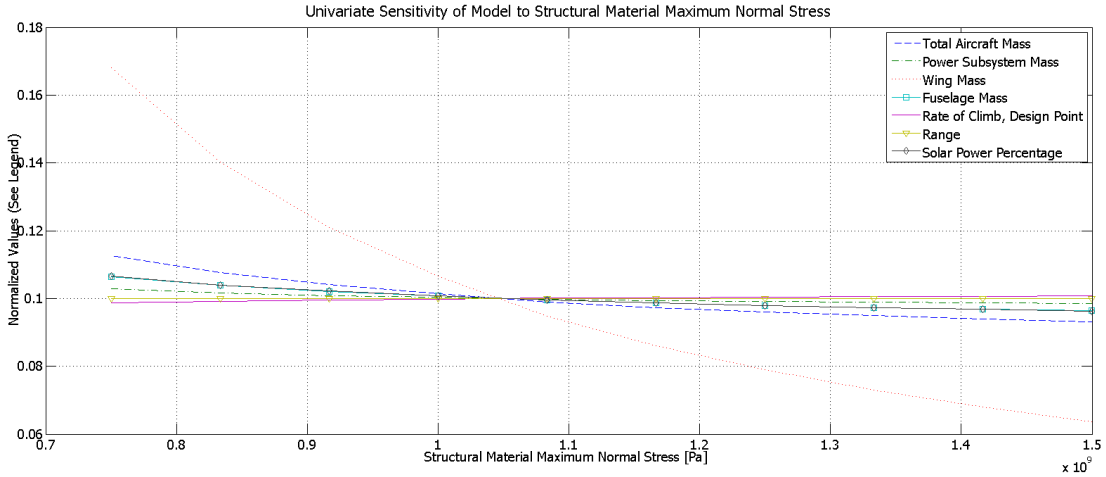

Figure 8.10: Univariate Sensitivity of AERIS to the Maximum Allowable Normal Material Stress

The sensitivity of the model to changes in the wing's aspect ratio was high with regard to changes in wing mass (inversely proportional) and fuselage (directly proportional). The remaining performance parameters were relatively insensitive to changes in the main wing's aspect ratio, as seen in Figure 8.11. The inversely proportional nature of the wing's mass to its aspect ratio can be explained by the torsion that the control surfaces exert on the wing. As the aspect ratio increases (i.e. the slenderness increases), the moment arm of the control forces effectively decreases. Although the graph looks rather dramatic, the overall difference of the wing's mass is just over 2% for a change in aspect ratio of 10.

Finally, the sensitivity to a univariate change in the effective material density is summarized in Figure 8.12. Again, all parameters with the exception of wing mass and fuselage masses are relatively insensitive; the wing and fuselage masses change by 12.4%, and 8.8% for a change in density of 1500 to 2000 $[\frac{kg}{m^3}]$ respectively. Again, one should not attach too much importance to these apparent relationships as they do not take a change in load bearing capabilities into account. In truth, a variety of densities suggest a variety of materials, which in turn will have very different material properties. On the other hand it does show the value of implementing hollowed structures whenever possible - an element not to be forgotten during the manufacturing process is additive manufacturing.

8.3.2. MULTIVARIATE SENSITIVITY ANALYSIS OF THE MAIN INPUT PARAMETERS

As some of the previous results showed (in particular those of the univariate sensitivity to changes in material density and maximum allowable stress), though univariate analyses have their uses by allowing one to clearly see the relationships between input variables and their effects on the design, they do not consider interactions between variables and their com-

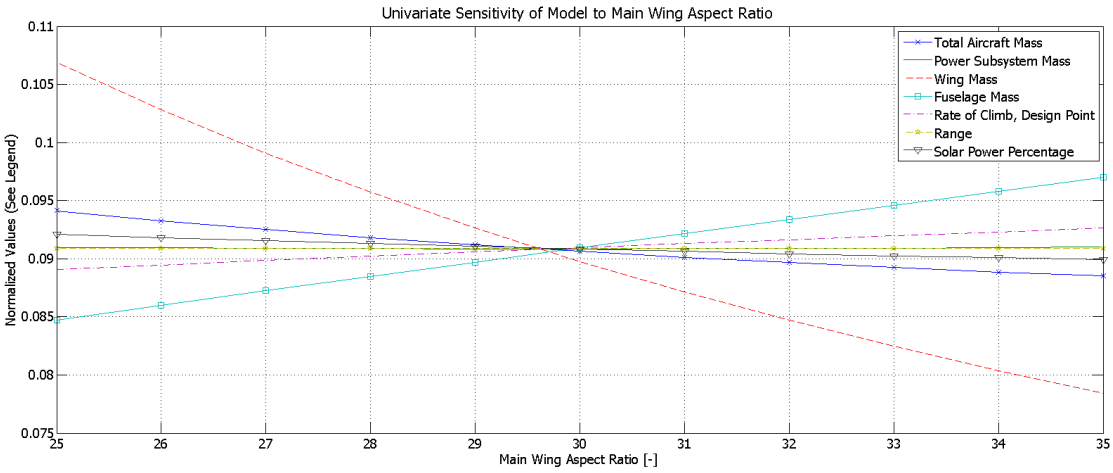

Figure 8.11: Univariate Sensitivity of AERIS to the Main Wing's Aspect Ratio

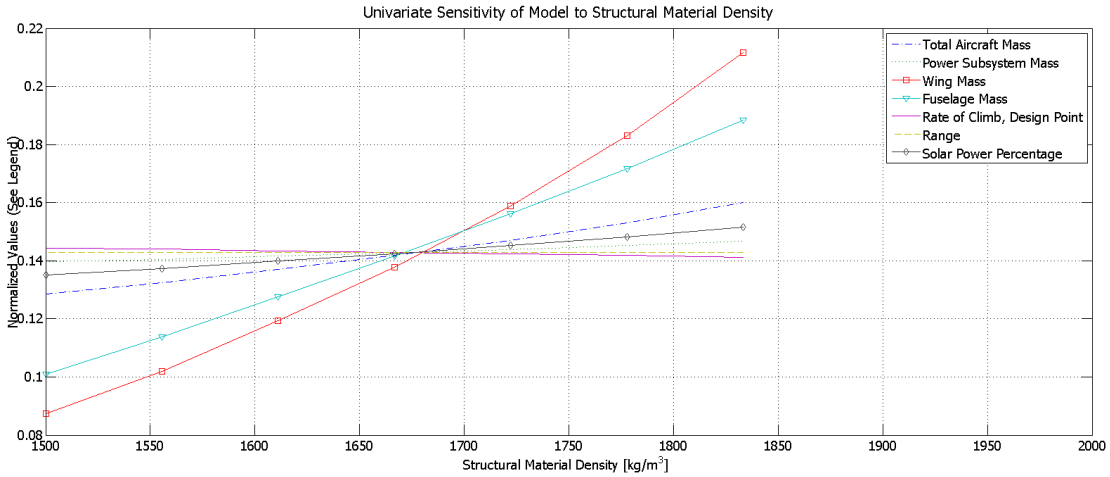

Figure 8.12: Univariate Sensitivity of AERIS to Effective Material Density

bined effect on changing the design. Multivariate analysis is far more computationally heavy than univariate analysis. It is for this reason that the surface responses of the design's mass to changes in input variables is on a less refined mesh of data. The effects of changing the design cruise velocity and the aspect ratio for different endurances were all evaluated in their own plots.

Firstly, the surface and contour responses for various endurances can be seen in Figures 8.13 and 8.14. One can clearly see that the parameters are all interrelated. A pattern can be seen when examining the plots for the various different endurances. In fact, they are all a larger response surface which increases in its variational topography when endurance increases. In simpler terms, the sensitivity of the design increases was endurance increases. This is easily seen in the surface and contour plot with endurances of eight hours at the bottom of Figure 8.14. The significance of this is that errors in either of these input parameters - and likely more - have increasing effects on the design for high endurance designs. One recommendation would be to repeat these plots with a finer data mesh. Upon further inspection of the different AERIS configurations, the sudden jumps in the right-hand surfaces can be explained by the addition of battery packs to the design, giving discrete jumps in the aircraft's mass.

8.4. PERFORMANCE ANALYSIS

This chapter discusses the performance of AERIS. This includes the achievable range of AERIS, the RoC at different speeds and altitudes, the use of solar power, the noise characteristics and the minimum turn radius.

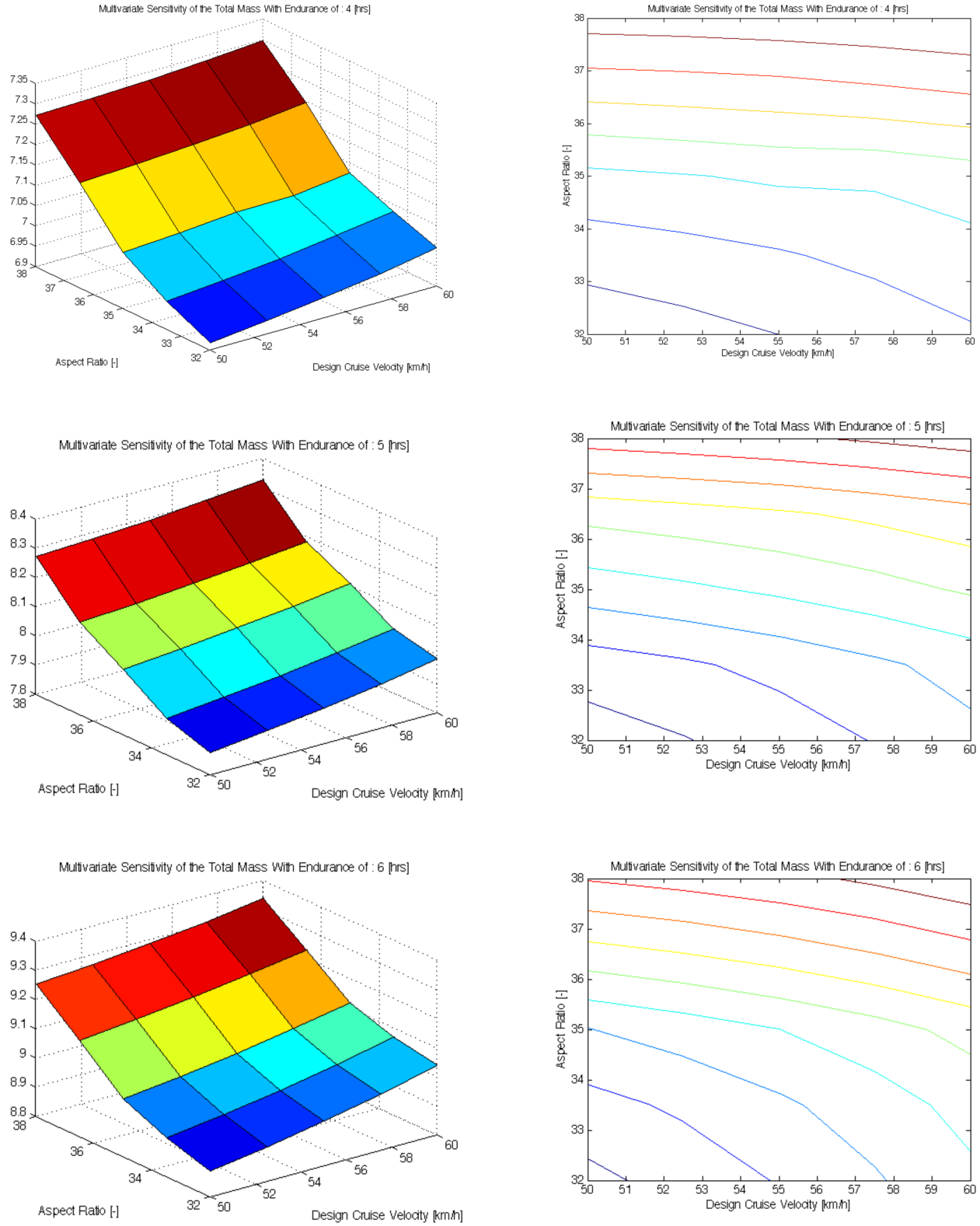

Figure 8.13: Multivariate Sensitivity of AERIS to Cruise Velocity, Aspect Ratio and Endurance (1 of 2)

8.4.1. RANGE

The range is an important factor for of AERIS' mission, as it determines a big part of the mission scope. The range can be calculated by Equation 8.10. [29]

$$R = 3.6 \cdot V_0 \cdot E \tag{8.10}$$

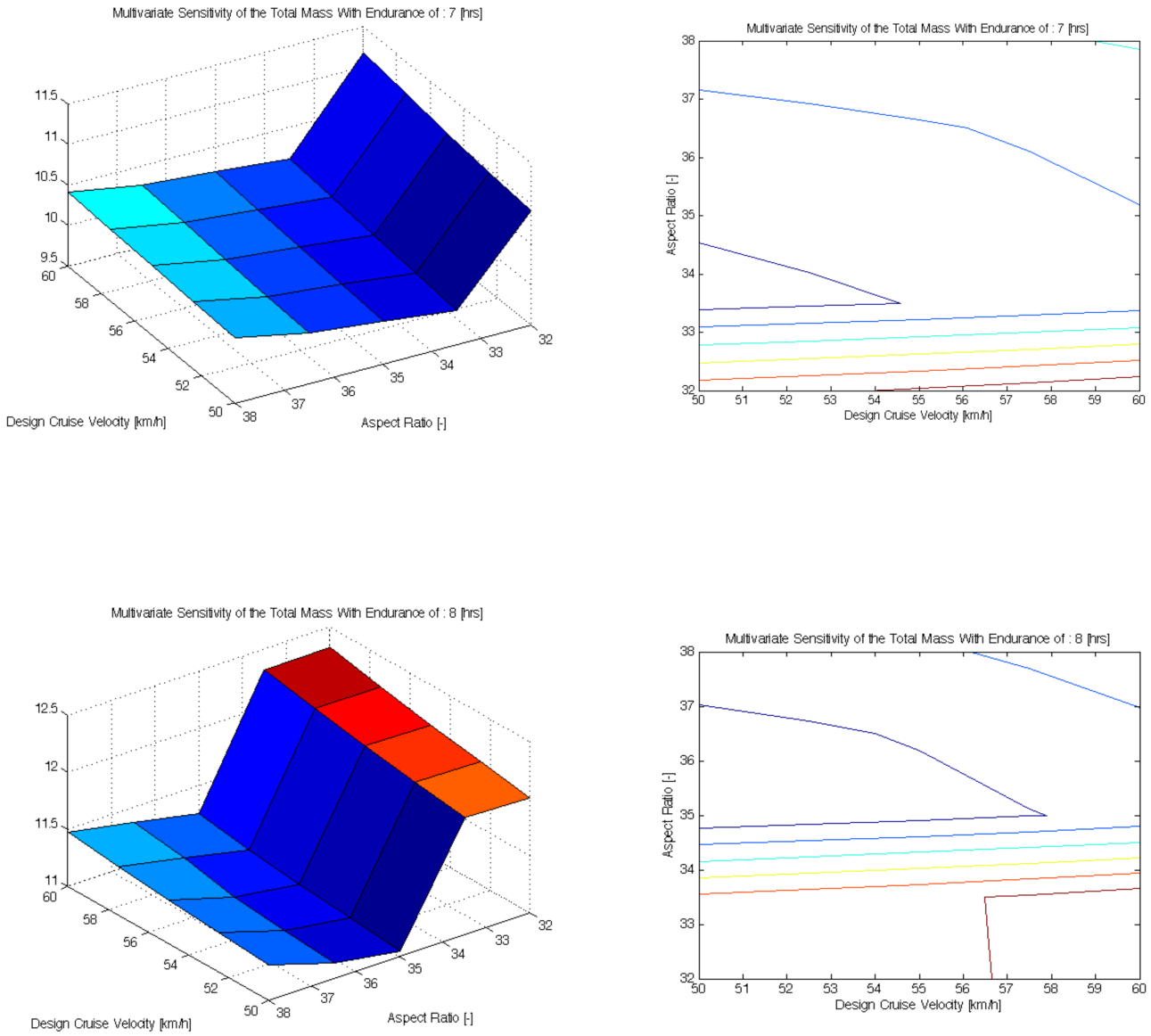

Figure 8.14: Multivariate Sensitivity of AERIS to Cruise Velocity, Aspect Ratio and Endurance (2 of 2)

Since the cruise speed is in meters per second is has to be converted to kilometres per hour to get the range in hours. With endurance at EOL of 6.2 [h] the EOL range is equal to 310 [km].

8.4.2. RATE OF CLIMB

The rate of climb is dependent on the available power that the UAV can deliver. For low speeds, the rate of climb can be determined as shown in Equation 8.11. [29]

$$RoC = \frac{P_a - P_r}{W} \tag{8.11}$$

With the equation known the RoC distribution can be made and is visualised in Figure 8.15.

Taking a close look at Figure 8.15 it can be seen that the climb speed decreases with altitude. But at the ceiling of 4000 [m], the UAV is still capable of performing a climb. The reason for this, as stated in Section 6.6, is not only the available power designed to be able to reach the altitude ceiling; it also has to be able to fly at the maximum speed. This condition implies a bigger power requirement than the maximum ceiling. Therefore, the engines do not operate at maximum power at 4000 [m] altitude.

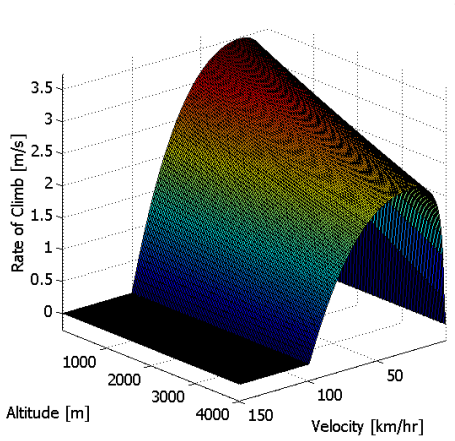

Figure 8.15: Visualisation of the Rate of Climb as a Function of Speed and Altitude

8.4.3. SOLAR POWER

The solar power will be expressed as a percentage of the total energy used. It is calculated using the average yearly influx of solar energy and the solar cell efficiency. [89][9] For the power used, the cruise power is used, after which the power usage of other subsystems is added. Now the total solar power is divided by the total daily power to get too a percentage. This number should be between 20 – 50%. In the design, the solar percentage is 67%, which is not within this range. Since AERIS is not always flying at cruise speed, this percentage will be decreased as higher speeds require more power. Furthermore, full use of all the solar influx is impossible due to banking and the position of the sun, which changes the angle of incidence and decreases the solar cell efficiency. If all these factors are applied, the solar cell percentage will be in the desired range and the rest of the energy will be delivered by the laser.

8.4.4. NOISE CHARACTERISTICS

Part of the performance analysis is determining the noise characteristics. The regulations state that the noise created cannot exceed 80 [dB]. This value is set for both the air segment and the ground segment.

AIR SEGMENT

Two main components on the UAV are responsible for the majority of the sound produced by the UAV, namely the engine and the propeller. Other sound originating from the batteries, servos and lift surfaces is regarded as negligible for the overall sound level for the capability of meeting the set requirement. The final concept will make use of an electric propulsion system, hence an electric engine. These type of engines are known for their low sound level and hardly produce any noise for the same thrust when compared to combustion engines. [90] [91] Looking at the scale of the aircraft (model sized) and the minimum altitude of 100 [m] to be flown at, it is certain that the engines will not produce the level of 80 [dB].

Regarding the propeller, it can be said that the faster it rotates the higher the sound level is. Furthermore, there is a relation between the diameter of the propeller and sound level it produces. [92] [93] The final concept has a propeller diameter of 1 [m] and an angular velocity of 600 RPM. These proportions counteract each other with respect to the sound level they produce. Furthermore, the diameter of the propeller is still small when compared to propeller driven commercial aircraft. When studying similar reference aircraft with respect to their weight, flight speed and propeller size (all electric), it became clear that the 80 [dB] sound level is not reached for these aircraft. Using these facts gives us enough knowledge to ensure that the major sound components of the aircraft will combine to an aircraft that produces less sound than this level. Therefore AERIS will fly according to sound regulations.

GROUND SEGMENT

The second segment of the UAV project that can produce sound is the ground station. It is likely that the ground station is subdivided in a station that houses the laser and an office where all data is processed and mission profiles/routes are communicated with the UAV.

The office will house computers, data processors, and monitors for flight profile control. Chances are negligible that the office will be of a threat for the level of acoustic sound. Regarding the laser, there are several factors that should be accounted for. Initially, for high powered laser, the use of the flash-light that triggers the, for instance, iridium crystal or gas,

as explained in Section 6.11 on the working of the laser, is accountable for a certain degree of noise in the amplitude. Furthermore, the amplitude is also altered by the effect of the changing dimensions of the gain chamber or shape deformations of the mirrors. However, the magnitude of this noise is at most 1 [nm]. This laser noise will not influence the charging of AERIS as it is only very little. Furthermore, in the actuating system, pointing the laser on the aircraft and the lenses focussing this laser beam on the aircraft, small distortions can occur. However, looking at The pointing system that AERIS uses the accuracy will be high enough to limit the scatter to an acceptable level.

The acoustic noise of the laser is no problem either with respect to the requirement of 80 $[dB]$. The de-charging of the capacitor and the flashing of the flash lamp will produce most of the acoustic noise. This sound level will not exceed the requirement, however it is not pleasant to work in an environment where the laser is active in. Therefore, the location of this device should be in a different room than the offices and should be isolated needed. Furthermore, this location should be water tight, so no water is able to reach the system. It can also be considered to place the laser on top of a building and incorporate a shielding device which can protect the laser system during extreme weather conditions. Furthermore, it can be considered to make the system entirely watertight. Before using the laser though, the lens should be clean to make sure that no water droplets are left on the lens. This might have fatal consequences for the laser itself, as some of the energy is reflected back in the device.

In conclusion, when looking at high powered lasers used by the U.S. Navy, it is clear that no noise is made by the actual beam itself when passing through water vapour filled air. Therefore, it can be stated with this initial assessment that it is unlikely that the noise level will exceed the 80 $[dB]$ limit set by requirements by both the air and ground segment of the AERIS mission.

8.4.5. TURN RADIUS

The minimum turn radius is an important aspect in our design. This determines how far from the laser station AERIS can fly in order to charge up and to perform the mission efficiently. The turn radius mainly depends on the load factor and the airspeed. The maximum load factor the UAV can handle is 2.5. The turn radius is based on this value. The load factor is a function of the speed which the UAV is flying at and is shown in Equation 8.12. The radius is both a function of the load factor and the airspeed. The radius is shown in Equation 8.13. With the current specifications, both the load factor and the turn radius can be plotted against the speed as shown in Figure 8.16 and 8.17. [29]

$$n = \frac{0.5 \cdot \rho_{air} \cdot {V_0}^2 \cdot S \cdot C_L}{W} \tag{8.12}$$

$$R = \frac{{V_{turn}}^2}{g_0 \sqrt{n^2 - 1}} \tag{8.13}$$

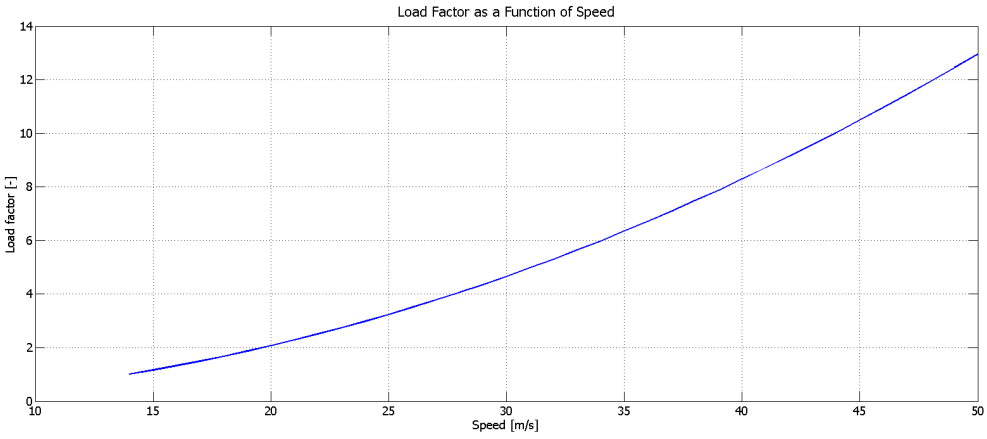

Figure 8.16: The Load Factor Plotter Against the Speed in Meters per Second

Taking a closer look at Figure 8.17 it can be seen that the radius decreases when the speed increases. This is because the load factor increases when the speed increases. Therefore, for the minimum turn radius the load factor has to be the maximum allowable value, which is 2.5. In Figure 8.16 it can be seen that this happens at 22 $[\frac{m}{s}]$. At this, point a turn radius of 21 $[m]$ is achieved. This load factor implies a certain bank angle. This bank angle can be determined by using Equation 8.14. With a load factor of 2.5 this bank angle is equal to 66 $[deg]$.

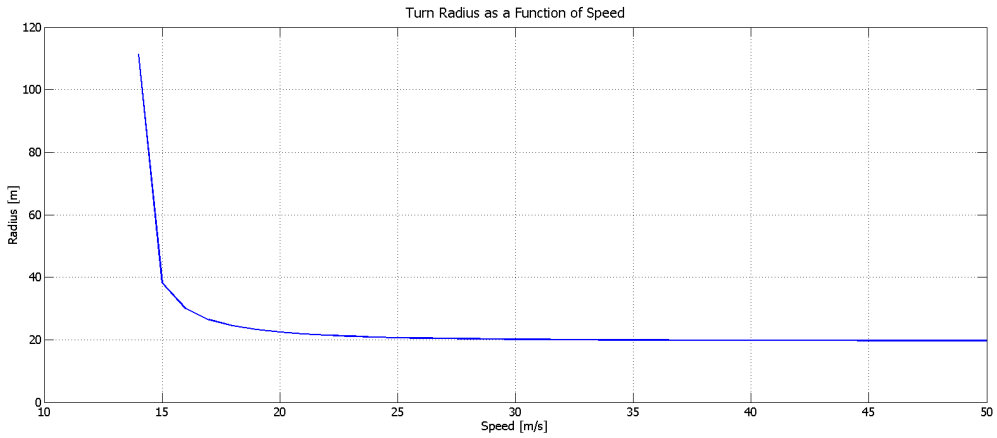

Figure 8.17: The Turn Radius Plotter Against the Speed in Meters per Second

$$\mu = cos^{-1}\left(\frac{1}{n}\right) \tag{8.14}$$

As can be seen in Figure 8.17, the radius does not increase drastically until a speed of 15 $[\frac{m}{s}]$ or lower is reached. Therefore, for safety reasons concerning increased loads caused by for example gust, a normal turn is performed at a lower load factor of 1.5. This gives a turn radius of 26 $[m]$ and a bank angle of 48 $[deg]$ is made.

8.5. MISSION ANALYSIS

This section describes the mission of AERIS. This includes the effect of weather conditions, such as clouds and wind, on the mission. After that, a typical day in the life of AERIS is described, visualising a typical trip around Zuid-Holland.

8.5.1. WIND AND GUST SPEED

As explained in Section 6.3 and the MTR, the maximum designed wind and gust speed AERIS can sustain until a safety landing is required are 50 $[\frac{km}{h}]$ and 80 $[\frac{km}{h}]$ respectively.

Weather data has been obtained from the Koninklijk Nederlands Metereologisch Instituut (KNMI), where the used weather station is located on Rotterdam Airport. The data contains weather information of every day from the 1st of January 2010 to the 1st of January 2015. In this data, the maximum mean wind and maximum gust wind velocities are given. The results are plotted in Figures 8.18 and 8.19. In this figure, the red lines show the maximum designed velocities.

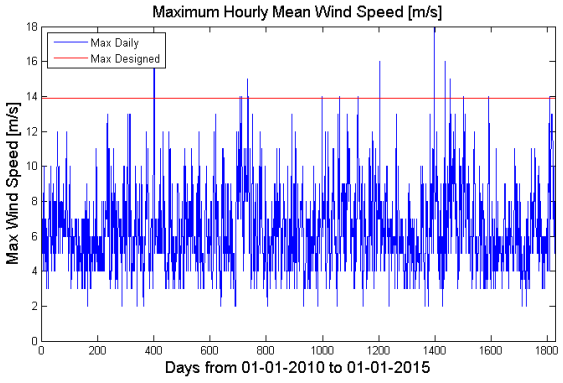

Figure 8.18: Maximum Daily Mean Wind Velocities

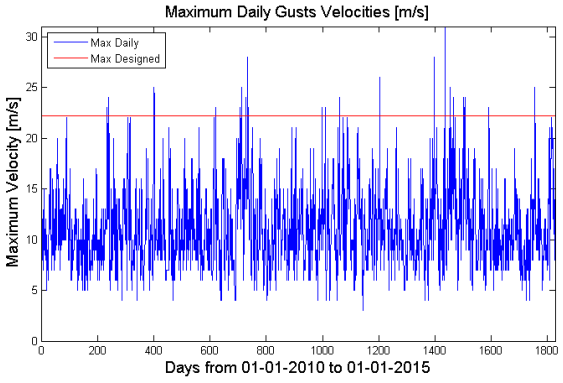

Figure 8.19: Maximum Daily Gust Velocities

From this data set, conclusions can be drawn regarding the amount of safety landings required. For the hourly mean wind velocity, over five years an average of 3.8 times a year the maximum designed value is exceeded and thus safety landings have to be performed. For the maximum gust limit of 80 $[kmh]$, however, 5.4 safety landings are needed in order to comply with the set maximum. As was stated before, the maximum amount of landings per year was anticipated at four times a year

which is equal to the estimated amount. However, these results are based on statistical data and can vary ever year. For this reason, the designed maximum wind and gust speeds are considered acceptable and are verified with actual weather data.

CLOUD CEILING

As explained in Section 6.2.7, clouds can have a significant impact on the picture quality. For this reason, it is important to know at what altitude the clouds are. The cloud ceiling, defined as "the altitude of the lowest layer of clouds that are categorised as broken (mostly cloudy) or overcast (cloudy)" is important as well. [28] Based on weather data, the average cloud ceiling over five years is 540 $[m]$. For this reason, the optimum altitude, and hence the set design altitude of 500 $[m]$ for AERIS to fly at is a good approximation.

SOLAR POWER

Next to the laser, solar energy is the most important energy source for AERIS. Therefore, it is of significant importance to know how much solar radiation the sun is providing every day. In Figure 8.20 the solar radiation per square meter is plotted. Here, five year are shown as can be seen with the sinusoidal shape, where the five peaks represent the summers and the minimums the yearly winters. The mean is shown as well and is equal to 10.3 $[\frac{MJ}{m^2}]$ per day. As was explained in Section 6.8, the average power from the sun per square meter solar cells was determined to be 10.26 $[\frac{MJ}{m^2}]$ per day. With a solar panel efficiency of 25% it was shown to be sufficient to meet the requirement.

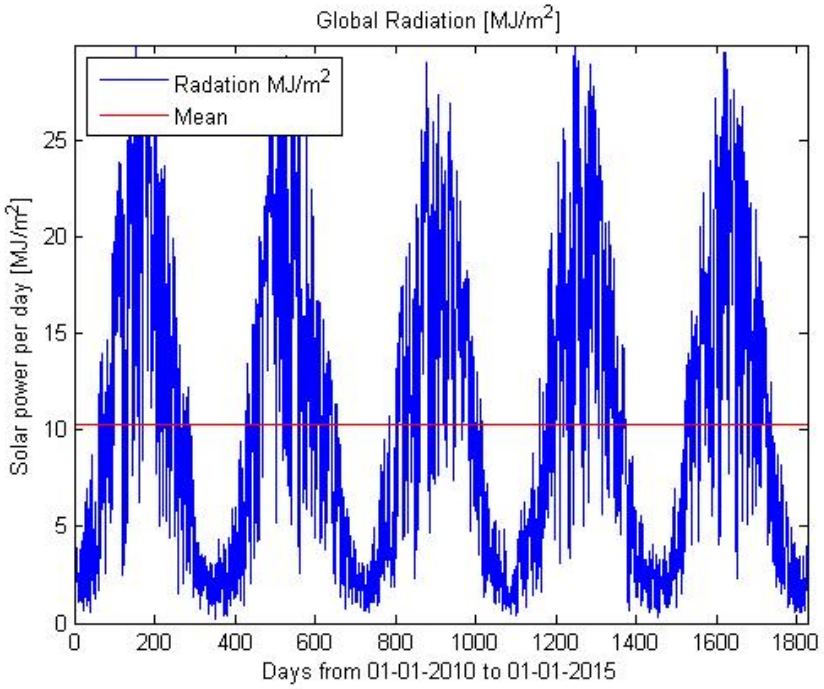

Figure 8.20: Solar Radiation Power $[MJ/m^2]$ over Five Years

8.5.2. A DAY WITH AERIS

At this point, the design has been created and analysed up to a certain point. However, the visualisation of the actual operations of the AERIS has not been made. This section serves to provide an overview of a typical mission day of AERIS. As shown in Chapter 7, the range and endurance at the optimum flying altitude of 500 $[m]$ and cruise velocity of 50 $[\frac{m}{s}]$ respectively, are 350 $[km]$ and 6.2 $[h]$. With these values a day's mission of nine hours daylight is described below. In Figures 8.21, important points of the flight path are shown with the corresponding performance values with the numbers described in Table 8.8.

As light breaks day, AERIS wakes up flying circles around the EWI building after charging during the night and is ready for a full day of remote sensing. The first task of the day is to classify the coastal wetlands for Rijkswaterstaat by mapping the vegetation and the quality of the dunes. The length of the coastline of Zuid-Holland is about 50 $[km]$. With a flight altitude of 500 $[m]$ the FoV on the ground is roughly 200 $[m]$ wide. To cover a significant amount of the coastline and vegetation, AERIS flies two times along the coast, making the flight time two hours. (2-3-2) After performing this mission, the next Rijkswaterstaat mission is awaiting. This requires the aircraft to fly to the port of Rotterdam and monitor the waterways (4). With an annual throughput of 450 million tons of cargo, Rotterdam is the largest port in Europe. [94] This means that

there is a high chance of pollution from ships and cargo. With the data obtained, the water quality can be determined. Oil leakages and other toxic chemicals can be detected and can be reacted upon accordingly if needed. In these situations it can be decided to monitor in a higher resolution by flying at a lower altitude. Next to water quality, data about water depth of rivers and canals can be obtained and used for dredging purposes. [95] The length of the main shipping canal is about 25 $[km]$ with a total port area of 105 $[km^2]$. Flying at an altitude of 500 $[m]$ at cruise velocity this area can be covered in about six hours. Thus, if it is needed to cover the entire port, the batteries will be nearly empty. But if, after three hours of imaging the port, there is an incoming call that a fire has been detected at a factory in the north of the province 30 $[km]$ away. AERIS swiftly stops the remote sensing and starts increasing the velocity to maximum, with a maximum engine power of 428 $[W]$, at an appropriate altitude. In this mode, the target can be reached within approximately 15 $[min]$. (4-5) The target will be observed by making constant turns around it keeping the orientation of the cameras constant. (5) Observations are made with the HSI and IR for temperature data. At maximum banking angle 48 [°] at optimum altitude the fire is 670 $[m]$ away, with a spatial resolution of 12 $[cm]$ and 22 $[cm]$ and a data rate of 62 $[Mbits]$ and 0.32 $[Mbits]$ for the HSI and IR respectively. This data is live streamed to the Rijkswaterstaat if requested.

When the fire is under control and enough data about its progression is known, AERIS leaves the site after one hour. (5-6) For the remainder of the day AERIS stays in the north and creates agricultural images for a commercial client. (6) This client has a delivery time for his data of one week. The farmers requested the most detailed images available so the altitude is lowered to 100 $[m]$. In one hour, an area of 1.2$[km^2]$ can be covered with a HSI spatial resolution of 1 $[cm]$. Since the batteries are almost empty now, it is time for AERIS to return back to EWI and initiate the recharging phase. (6-1) The batteries hold 1176 $[Wh]$ when fully charged. As can be seen in Table 8.8, the total amount of power used is more than the capacity. However, since this value is without solar power which will deliver a significant amount, AERIS is certainly able to fly this mission.

Figure 8.21: The Flight Path Points of AERIS of One Day. [96]

Table 8.8: The Total Distance, Time, Data Rate of Hyperspectral Imager, Power Used and Imager Covered Area per Section Respectively

Section Sequence	***Total Distance*** $[km]$	***Time*** $[min]$	***Data Rate HSI*** & IR	***Power Used*** $[Wh]$	***Imager Covered Area*** $[km^2]$
1-2	20	24	0	46	0
2-3-2	100	120	63	228	23
4	150	180	63	342	35
4-5	30	36	0	258	0
5	60	60	63 + 0.32	114	18
5-6	15	18	63	34	4
6	50	60	63	114	2
6-1	20	24	0	46	0
Total	445	530	-	1186	82

During the night, AERIS is recharging its batteries, which means that during this time missions cannot involve remote

sensing of areas far away. But the option of remote sensing with the IR is there. So when for example a fire has been reported, it can be decided to leave the charging circle and attain information about the fire progression. Or the charging circle can be left behind to start monitoring greenhouses in the Westland area. During the night light pollution of these companies can be measured with the HSI and heat leakage with the IR. This of course can only done when the distance to the fire or the greenhouses is in the range which can be flown with the current battery capacity. Therefore, a trade-off has to made between performing the mission and charging or using the second UAV instead.

OTHER TASKS

Since the HSI is based on the reflectance property, it can be used for measuring air quality. For this, white panels can be installed on the ground which will reflect the incoming sun light. When the reflected light is seized by the HSI it is compared with reference reflectance data. Making use of this, the amount of absorbed light, by certain molecules, is measured from which the amount of air pollution is concluded. With the same principle, AERIS is also able to detect the level of CO_2 in soil, plants, atmosphere, and water. For example, plants can be measured for stress as a result of the amount of induced CO_2 in these plants. [97]

PRIVACY AND LAW

As discussed in Section 8.5, a monthly update is provided to the government. With the cruise velocity at optimum altitude, AERIS is able to cover the 3403 $[km^2]$ of Zuid-Holland area including 585 $[km^2]$ of water in about 25 days. Covering all of Zuid-Holland will certainly include the coverage of private property. As a result, civilians and companies will definitely feel that their privacy is infringed and will bring this up for debate. As stated in the law, the government is allowed to perform observation missions only when a there is a suspicion of offences. [98] Also, only the client and AERIS spectator are allowed to see the obtained data from the client's property. For this reason, violating privacy concerns is an aspect not to be overlooked or dismissed otherwise AERIS is not able to do what it is intended to do.

A solution for these issues is to blur the images where the exact GPS locations of private property is known. Software in the ground station has to detect these parts of the data and make changes. Another way to deal with this is to keep the data under protection without changing the images by encrypting the data as explained in Section 6.4. AERIS will have close relations with the government, as it is the primary client, so licenses will be present making observation easier with the privacy laws and legislations. The issue of privacy in remote sensing is complex since the technology move faster than legislations do, therefore AERIS should constantly revisit the codes of ethics.

8.6. RELIABILITY, AVAILABILITY, MAINTAINABILITY, AND SAFETY CHARACTERISTICS

The RAMS characteristics of the design are crucial for the success of the complete AERIS project. The provided project description specifies a continuous flying vehicle and thereby implies the design to have high reliability, availability, and safety characteristics. Also maintenance should not be complex to increase the availability of the system again. This section will analyse the RAMS characteristics of the concept.

8.6.1. RELIABILITY

When discussing reliability it is important to keep the definition of this term in mind. The definition of reliability is the ability of the product to perform its intended function. Mathematically, it is defined as the probability that an item continues performing its intended function without failure for a specified period of time under its stated conditions. Inherently, production and maintenance are part of the equation when determining the reliability of the item. It should be noted that this item can be the final design, the software running on the ground station, the manufacturing process or even a service. [99] More importantly, one should determine the desired availability of the system to set requirements on the reliability. Overall, reliability is important for: reputation, costumer satisfaction, warranty costs, cost analysis, costumer requirements, and competitive advantage amongst others. Hence a proper reliability analysis is vital.

When glancing at the RDT, it becomes clear that many norms and requirements have a direct consequence on the level of reliability of the system. On the other hand, it is likely that the system will be built by different sub-contractors and components of the different system will come from third parties. Having subsystems in our system from third parties, or manufactured by third parties can increase the risk for the reliability of the system. However, having third parties manufacture parts of the system can also be used to our advantage. For instance, the team has little experience in building lasers, electric engines or propellers. That is why, in fact, the overall performance of the system will go up by using external resources and third parties for these subsystems. Eventually using this to our advantage can have positive effects for the reliability. It is also not unlikely that this will be favourable for insurances/warranty cases. Using existing reliability theories, it can be learned that for many complex engineering processes the quality and the actual expected reliability is difficult to assess. Rather than assessing the reliability of each subsystem, that combined, make up the overall system, a smart practical technique is to prevent failure. [100] Hence, rather than putting a lot of effort in assessing the prediction of reliability, this

team puts most effort in the prevention of failure by improving reliability. A proper risk assessment (strategy) is the basis for this technique. [101]

Ideally there are no unexpected failures in the operation of the system. Failures that are expected should not happen more regularly than predicted. Operations should at least comply with the definition of reliability. In case of AERIS, the reliability is defined as a system to perform operations successfully at all times. In this way, mission performance is optimal and only during storms (wind speeds over 75 [$\frac{km}{h}$]) the mission is temporarily aborted. With little statistical data available on the likeliness of (sub)-system failure, this design will be approached in a critical fail-safe manner. This implies that if a critical system fails, the system is able to survive without complete destruction. In most cases, these failures would refer to a critical failure on the flying subsystem and the aircraft being able to reach the ground safely. Besides this, a second UAV should always be on standby to guarantee the continuity of the mission. In the subsection maintainability, the maintenance aspect of the design will be discussed. It is clear that maintenance of the out-of-order UAV should not take longer. This will increase the availability thereby increases the efficiency of the mission.

Generally, the desired availability determines the requirement on the reliability. However, this should be supported from known reliability specifications from the different systems on-board and on the ground. [102] AERIS will most likely use parts such as batteries, electric-engine, and cameras from the third parties. These primary subsystems provide an important basis for the reliability and availability requirements. For instance, the degradation of the batteries has already been incorporated in the engineering strategies iteration process.

8.6.2. AVAILABILITY

This subsection discusses the availability characteristics of AERIS. Several requirements impose restrictions on the availability. EQ-1: "There shall be a continuous stream of data available during the entire mission" and GEN-1: "In case of failure there shall always be a back-up system on stand-by" have the largest impact on the requirements for the availability of the system. Besides this, the operational lifetime should be five years as set by GEN-3. Aiming to meet these requirements 100% will be very expensive. Failures can always happen unexpectedly and can theoretically result in large number of back-up aircrafts to substitute the broken UAVs. Luckily, it is also possible to increase reliability without stating the exact values on the reliability.

In our case, this means that a lot of effort had to be put in designing an overall system that meets these requirements. Eventually, the extent is limited by economical limitations. In business case, it is expected that clients can rely on our continuous data stream, having this data stream interrupted for failures is undesirable. The data stream will be interrupted for bad weather conditions. It is anticipated that on average, the UAV shall land four times a year. This is because on average, the amount of storms in Zuid-Holland is four per year. [36] More information on back-up and emergency landing systems is provided in the safety subsection of this section.

It has been decided that there will be a back-up UAV available for this case study. This will increase the overall availability and will only be of limited expense, which for the project is acceptable. Besides this, most reliability problems are expected early on during project. Having two UAVs available allows the team to assess small errors that occur after delivery. Thereby it is possible to quickly interchange the two UAVs and update software/hardware. This increases the learning curve and assures that after this pilot project, the team is mature and the efficiency and effectiveness of the team is optimal for future projects. It can be considered, in a more mature stage, to have both UAVs fly at the same time where one UAV serves as the back-up for the other whilst in the air to comply with the continuous flying requirement.

8.6.3. MAINTAINABILITY

Maintenance on the aircraft is only possible at those times when the aircraft is on the ground. This implies that maintenance can only be executed at the time a storm hits. It is defined that it storms as soon as wind speeds reach 75 [$\frac{km}{h}$]. It has been learnt that on a yearly average, storms occur four times in Zuid-Holland and most of them occur in a specific 3 – 4 month window. [36] Since the aircraft is designed to fly a maximum of 100 [$\frac{km}{h}$] landing decision can still be made. Inevitably, the maintenance intervals are not evenly spread. However, it is unpredictable that when the storms will hit, and since maintenance is required, it is decided that at least once every year the aircraft shall land for maintenance. In reality, the opportunity for maintenance is higher due to the hitting storms. However, only during one of these average four storms, maintenance needs to be performed. A second option to do maintenance on the aircraft is to have the second aircraft take-off such that the primary aircraft can land for maintenance. The mission will not be designed for this, but when required, this is an option.

Each landing also implies maintenance to occur from maintenance personnel. With a belly landing, it is expected that the bottom of the UAV experiences wear and tear and the surface of the bottom needs to be made smooth again with polishing

and clearcoat as described in Chapter 6.

All subsystems on the aircraft can be subjected for maintenance during this period. Greasing of actuators, cleaning lenses of the cameras or even replacing malfunctioning batteries should ideally be possible during maintenance. Secondly, since most likely this aircraft is designed for modular payload, this subsystem can easily be interchanged for a different subsystem. Easy interchangeable parts are the cameras and the communication system module. In case of maintenance, this system is therefore quickly fixed when a spare module is on standby. Furthermore, a complete back up aircraft is on standby if maintenance takes longer than the expected storm period. Furthermore, for future projects, with the same flying system, with new payload, more mission can be implemented in the aircraft. As the structure of AERIS will be 3D printed, checking the structure is not possible by visual inspection only. Non Destructive Testing (NDT) methods need to be performed since the behaviour over time of a 3D printed structure which is in contact with the elements $\frac{24}{7}$ is not yet known. Certain safety margins are taken into account during the design but still the need to thoroughly check the UAV is still in there. A possible NDT method is Optical Coherence Tomography (OCT). This method scans the outer layer of the material with a very high resolution. For the small thickness, it will be fine but if the thickness increases, an ultrasound will have be used to test the material. It has a greater penetrating depth but the resolution is less compared to OCT. [103]

The overall system also consists of a ground system. With the aircraft maintenance intervals already discussed, the maintenance of laser is only left. For the laser, however, a different technique is applied. Small maintenance (under seven hours) can be executed after the batteries have been fully charged on-board the aircraft. Any maintenance that takes longer than this, should be performed during sunny days in summer or during storms. On long sunny days, the endurance of the aircraft is higher than in days with less sunlight. Furthermore, in an extreme case, it can be decided to overlap with the back-up aircraft that flies out with fully charged batteries to take over the first aircraft after it has drained the batteries with the laser station still down. This should be planned maintenance and preferable should not happen a lot. When setting a limit on the extensive maintenance, the reliability of the laser should be extensive. With the supplier of the laser strict appointments should be made on the reliability of their system and if maintenance takes longer than expected, and the UAV needs to land, proper appointments need to be made on costs compensation. In extreme situations, using the two UAVs and loading them in turn on the ground is always a backup option.

8.6.4. SAFETY

The risk strategy chapter described earlier in this report presents the AERIS team with a lot of techniques to eventually increase overall safety. In addition, a table was provided of identified risks and for some techniques a treatment was presented. Also some aspects of the applied contingency management strategy, or resilience of the system were discussed. This subsection will focus on some of the applied techniques to increase overall safety that is implemented specific for this system whilst in operation. This includes characteristics of the response and actions of the UAV and laser.

Firstly, the aircraft is autonomous and has the option to be remotely piloted. In the worst case scenario, the aircraft is located at a location that is populated, the single propeller is malfunctioning (possibly due to a bird strike) and aerodynamic properties are distorted making gliding very difficult. In such a worst case scenario, the deployment of an estimated one kilogram parachute will be the applied technique to minimise the consequences of this fatal error. One parachute is the desired option, rather than two smaller parachutes in each end of the boom to decrease overall weight. Since each parachute requires a fixed starting weight for the casing and cabling. The exact dimensions and weight of this rescue device is presented Section 6.3. Since this parachute can be seen as a kind of life insurance for AERIS, the idea is that it will only be needed at most once in its operational life time of five years. The expected probability of actually using this device is minimised but the risks are too high to neglect the risk of not having an emergency back-up system.

Secondly, in a less worst case scenario the emergency 45-minute battery is functioning and able to provide energy to the propeller and other control systems. In this case the aircraft can autonomously fly to a predefined emergency landing zone located by the AERIS team. This might be locations with little to no population, but ideally it is possible to reach the home base and land at the team's location where an emergency landing location is equipped. If necessary, it is possible to land in (fresh) water with a watertight system. After an emergency landing, the emergency localizer starts signalling out to find the aircraft after the crash. Also, the system will directly send a signal to the control station as soon as an error occurs on-board. The last known location is sent and it is also possible to take over the aircraft's control from the ground station. This allows the possibility for a human to assess the risks directly and act accordingly. This requires to have at least two pilot's to be at the ground station at all time. They can have the responsibility over multiple UAVs in a more mature stage of the project. These people will in normal operation be used to assess and process the data of the sensors and design mission profiles for the aircraft, but in an emergency they are able to control the aircraft directly.

Finally, for wildlife protection, the laser will be equipped with a system that recognises interference of the laser beam.

Interference of the laser beam will automatically and directly shut down the laser. This prevents harm to most wildlife in the air. Unfortunately, harm to most small insects can not be prevented with this system.

9. Business Roadmap

This chapter will elaborate the business roadmap envisioned for the AERIS project by means of a five-year plan. The business roadmap is supported by a market analysis performed in Section 9.1. A cost break-down structure in which the costs of AERIS are visualised is presented next in Section 9.2. Hereafter, the revenue model is presented in Section 9.3 which is followed by the five-year plan in Section 9.4. It should be noted that this business roadmap focusses on the case study primarily, but considers the requirement of scalability of the mission to the Netherlands. Furthermore, this section should be considered only as a preliminary estimation. No rights may be derived from the information or calculated values as they are open for change.

9.1. Market Analysis

The main focus of the UAV lies on monitoring of the land and waterways in the province of Zuid-Holland. Since the HSI has many applications, the data stored can be beneficial to large variety of clients. Next to that, the sustainability aspect is getting more and more important. The interest in proper monitoring techniques to check for water, ground and air quality is rising. [104] The use of a HSI allows for monitoring multiple properties of waterways, natural and urban areas in one go. This includes the monitoring of water quality, currents, water heights, temperature, air quality, fire hazards, ground quality and precipitation. The data is collected and stored. Furthermore, combining the forces of a HSI with an UAV allows for continuous monitoring of large areas in a relatively small amount of time. There are different parties which are interested in the data set of the waterways of Zuid-Holland. The market analysis and competitors in this area will be discussed in the next sections.

9.1.1. Market Potential

The market potential of continuous monitoring is large. The Dutch government is a stakeholder with respect to data gathered on its land and waterways. Moreover, there is a business to business potential with respect to farmland and other businesses that are gained from data of AERIS. Zuid-Holland is one of the most industrial provinces in the Netherlands. It implies that this region is subjected to industrial waste. Monitoring of the air, ground and water quality in this province is a very important step to maintain a sustainable environment in the Netherlands. This also fits in the vision of the province of Zuid-Holland. [105]

For the Dutch government alone, penalties accounting for water quality sum up to 1 billion Euros per year. [106] Furthermore, the costs of the measuring system for the ground and groundwater quality used by Rijkswaterstaat are 2.5 million Euros per year. It is also highly desired to switch to one measuring system that is able to measure water quality, ground and groundwater quality all together. [107] Next to that, air quality is also within the range of possibilities to be measured by AERIS with help of some extra ground systems. Zuid-Holland is a big contributor to industrial waste of the Netherlands, with a large contributor being the port of Rotterdam. For this reason, an initial pilot project of the complete system is wise before up-scaling to the full scale size of the Netherlands. To get a substantial market share, scalability of the system to monitor the entire Netherlands instead of only Zuid-Holland is considered. Scaling the project allows the AERIS project to substitute the current measuring system for a lower price.

Next to ecological quality and quantity monitoring, the government can also use the data for fast response to fire hazards and health risks caused by chemical leaks. The UAV will provide the government with a sustainable system that has a broad range of capabilities. These capabilities are even be extended due to the use of an IR camera at night, which gives AERIS the possibility to monitor at night for light pollution.

Although the government is a very trustworthy customer which most probably will not go bankrupt, having only one client will induce the risk of being a one-trick pony. The inspection of waterways is Zuid-Holland is mainly in interest of the government to check if the quality of air, ground and water is according to the European standards. Next to that, climate changes and water heights can also be monitored by the government. Other parties like farmers and the port of Rotterdam might be interested in the detailed data set of the waterways of Zuid-Holland.

Besides monitoring the waterways of Zuid-Holland, it is wise to get into other markets as well. Due to the big range of possibilities of the HSI this should not be a problem, but it goes beyond the scope of this case study.

Considering the growing interest in sustainability, the market for continuous monitoring of certain areas will get more and more important throughout the years. The request of such techniques will grow with the desire for sustainability. Also, because it's more ethical there will be a growing interest in sustainable methods to do this. This being said, it is safe to say the

market for ecological monitoring is in its early stages.

An important feature is to determine the critical and minimal success factors. The minimal success factors determine what is minimally required to buy the product, the critical success factors is what creates the difference in products.

Some important aspect are also considered, for example: the European and Dutch law. Today, drone flying is not legal in the Netherlands whereas the government being a possible client, it may convince itself that they need this system, so the chances of drone monitoring being legal greatly increases. As a company, it might even be possible to get clearance from this restriction which allows for a monopoly in the drone monitoring field.

9.1.2. COMPETITORS

The main competitor is "Landelijk Meetnet Effecten Mestbeleid" which is a product of "Rijksinstituut voor Volksgezondheid en Milieu" and "Landbouw Economisch Institutuut, Wageningen Universiteit en Researchcentrum". This network is currently monitoring the ground and groundwater quality in the Netherlands. The second competitor is "Landelijk Meetnet Water" which also measures the water quality and quantity. Other institutes that measure ground and water quality are:

- Realsense
- Deltares
- Precisionhawk

Realsense provides measuring networks and locations by means of sensors and data loggers. This data is send through Short Messaging Service (SMS) or General Packet Radio Service (GPRS). These systems are applied to meteorology, water management, infrastructural projects, research projects and maintenance projects. They serve customers like: the government, engineering companies, water piping companies and scientific institutes.

Deltares provides measuring of water, air, ground and other ecological data on a broad scale. They do their measuring by means of measuring instruments and sample testing. The measuring instruments are also sold as products for consumer use. Next to their measurements and products they give advice to ecological solutions and project management. They do business on an international level.

PrecisionHawk is a drone company based in the United Stated of America (USA). They provide a drone which can be equipped with either a visual, multispectral, thermal, LIDAR or HSI. The drone is sold to the users and the data can be stored "in the cloud". All data management is within the service the company provides. This system has a broad scope of applications. Although it is not a direct competitor in this case study, it is a competitor that needs to be considered since they are able to penetrate the Dutch market as well. Currently Precisionhawk is able to supply a UAV with an HSI and the full data handling which follows from that. They have a fixed price for the drone with camera of 105,000 American Dollars and an addition of $0.10 - 1.80$ American Dollar per acre for the data handling and storage. This represents roughly 88,000 Euros for the system and an additional $0.04 - 0.75$ Euro per Hectare. [108]

Defining possible competitors shows that there are not plenty of them, from which only two direct ones: Realsense and Deltares of which Deltares provides the ecological monitoring service on a big scale, along with advice and project management. Seeing the size of Deltares, they have considerable grip on the market which means that competing with this company would mean that high amounts of specific knowledge and big financial investments have to be done to get a reasonable part of the market share.

PrecisionHawk has a product that could substitute this project, but they have not penetrated the Dutch market yet. It is important to look out for this competitor and keep track of what steps they undertake.

To compete in this market specific knowledge and big investments are required. Also the system has to be reliable and provide a complete set of data to make the switch of one information system to the other more attractive. Entering this market, therefore, will not be easy. Since the system has no direct substitutes and hyperspectral imaging has such a broad scale of applications it is able to compete with the companies on the current market.

Success factors are that *the product needs to be able to monitor environmental properties accurately* and *the product has to cover multiple areas at once*. It can be seen that all of the competitors comply with the minimal success factors. Though the monitoring of multiple areas is less efficient with ground systems UAVs allow for more efficient and fast monitoring of multiple areas, which is therefore the critical success factor. Deltares and Realsense have equipment which can measure multiple properties with one system, though hyperspectral imaging gives a broader range. Seeing this we have a big step ahead on our competitors in technological advancement.

9.1.3. MARKET TREND

The last couple of years the number of companies involved in UAVs exploded. Currently the market expenditures worldwide are estimated to be 5,4 billion and it will grow in ten years to 11 billion per year totalling up to 77 billion Euros spend on UAVs by 2024. About 65% of the development is done in the United States. The current market split is 89% military UAVs and 11% civil UAVs. This will shift to 86% military and 14% in the next ten years according to the Teal Group. [109]

Currently UAVs are deployed in an increasing number of missions, where several years ago, the only user of UAVs was the army. They used it for Intelligence, Surveillance, and Reconnaissance (ISR) but also for bombing enemy targets.

Nowadays UAVs are in reach for almost everyone. More and more types of UAVs are developed and sold to the public. Some are developed as an alternative for a film helicopter while others are designed for research purposes. Different types of cameras are getting smaller and lighter and so making their way onto UAVs. Some examples of cameras are regular, multispectral, or hyperspectral cameras. The last one will be incorporated in the UAV design.

9.1.4. SWOT ANALYSIS

Part of a market analysis is the Strength, Weakness, Opportunity and Threat (SWOT) analysis. From a SWOT matrix, an opinion can be formed about the attainability of the project. Furthermore, this analysis helps to find the competitive advantage. This SWOT matrix is shown in figure 9.1.

	Helpful	Harmful
Internal origin	• Continuous flight, so a low respond time • Large flight envelope • Good quality camera so usefull data is gathered • Low maintenaince cost • One UAV can be used for multiple purposes at the same time	• Performance depends on weather conditions • Limited payload size and weight • Limited number of basestation due to regulation • Limited speed • No complete coverage due to no-fly zones • Can get really expensive
External origin	• Broad market/applications within reach • Less rules about UAVs making it easier to increase operations • Easy scalability • Multiple UAVs operating around one ground station	• A permit is needed to operate a UAV • Stricter rules regarding UAV operation • Bad weather reduces

Figure 9.1: Strength, Weakness, Opportunity and Threat Matrix

Taking a closer look at the SWOT analysis reveals that there is a large market which can be entered. However, a big threat is the legislation. Currently, it is not allowed to use a UAV for business purposes in the Belgium, Netherlands and Luxembourg (BeNeLux). A permit is needed but the demands that come with such a permit are so high that they prohibit us from flying autonomously. Keeping track of the current changes in the regulations is therefore of utmost important because it can make or break the market for the Netherlands and Europe. On the other hand there exist an opportunity to look for countries

abroad where legislation allows the AERIS project to take place. This, however is beyond the scope of this market analysis.

9.1.5. POSSIBLE EXTENSIONS MARKETS

For this case study, the UAV is designed especially for monitoring of Zuid-Holland. Still, there are a lot of different markets which can be entered without a lot of changes in the design and the business structure. A few examples are displayed in Table 9.1. These ones will get a rating for market size, market potential, and possible competitors when entering the market.

Table 9.1: Extension Markets

Market	***Size***	***Potential***	***Possible competition***
Rode Kruis / Red Cross	Small	Huge, it can be used for monitoring during disasters.	Satellites and high flying, solar powered drones
Environment control	Small	Huge, spilled materials can be detected very soon, also the state of the forests are easily monitored	Satellites, weather balloons, regular aircraft, and UAVs such as the Precision Hawk [110]
Emergency services	Huge	Quicker response times due to the continuous flying characteristic	Normal drones capable of flying for multiple hours, for example the "Ambulance drone" as created by Alec Momont from Delft University of Technology [111]
Oil/gas companies	Normal	Using the hyperspectral camera it is easier to monitor the processes but it can also be used to find new sources of minerals	Helicopters, high flying, solar powered drones, satellites
Farmers	Normal	Farmers can use the gathered data to see if the crops need more water or fertilizer	Normal camera planes, regular drones

Most likely many more markets exist which can be penetrated using only a slightly modified version of the UAV. Hence the modularity of the payload is a great opportunity for the future. Basically every market that uses aerial camera footage for monitoring can be entered. However, most of these markets do not need continuous monitoring. Therefore a rental/leasing service can be introduced in order to facilitate the aerial footage service without the need of a large investment. An example would be a farmer who wants to have his crops monitored once a week, while his neighbour farmer might need it twice a week. Using a UAV which is in the air continuously improves the efficiency of the overall service and thereby allows for a decrease in price or increase in profit margin.

9.2. COST BREAK-DOWN STRUCTURE

The market has been analysed. Hence, it becomes clearer that the potential for this type of product and/or service is great. Therefore, the next step is to get an idea of the development, production and operation costs involved for AERIS. These contributions are treated in the succeeding subsections respectively.

9.2.1. DEVELOPMENT COST

The development costs for the AERIS project are expected to originate mainly from the development of the prototype. It is expected that after the DSE period, an additional period of one year is required for the design to reach maturity before the first aircraft is ready for operations. Hereafter the second UAV will be quickly produced. The development costs are shown in Table 9.2 and are described in the remainder of this section.

Table 9.2: Total Development Costs for the AERIS project

Sub-item	***Total Cost*** [€]
Man-hours	0
Office	0
Licenses	0
Prototype Development	40,000
Total	40,000

Man-hours During the initial development phase of AERIS no salaries are paid to the employees. In this start-up phase of one year ten graduate students will invest parts of their time and money to realise the project.

Office During the first year, the location and offices are sponsored by Delft University of Technology.

Licences The costs for licence related products such as MATLAB and CATIA are sponsored during the development phase of one-year by Delft University of Technology.

Prototype Development The development of the prototype involves expenses for the production of scale models for wind-tunnel testing. The testing itself is sponsored by the university but the production of prototypes is not. Also during this phase, good relations with the future manufacturer of the final product are set up.

9.2.2. PRODUCTION COST

In this subsection, the fixed production cost of AERIS are presented. These costs are subdivided in the costs involved for the aerial segment and the ground segment.

Aerial Segment First, the costs involved for the aerial part of the mission is examined. The costs are given for one aircraft. However, for the case study, two aircraft are required. The total initial subsystem costs of one aircraft for the AERIS project are presented in Table 9.3. It should be noted that only main subsystems are presented in the table. At least 10% margin should be reserved on top of this price to include all details for manufacturing of the subsystems itself such as cabling, control system, small on-board computer, storage and even test flights. Furthermore, it should be noted that the costs of the total aircraft have increased slightly from the MTR. Mainly, this is due to the fact that manufacturing and flight control is included in this estimation. Furthermore, the mission payload has been increased by the two IR imagers to widen the scope of the mission.

Table 9.3: Total Initial Aerial Subsystem Costs for One and Any Extra Unmanned Aerial Vehicle

Subsystem	***Costs for One*** [€]	***Costs for Any Extra*** [€]
Payload	59,000	59,000
Communication	15,737	15,737
Flight Control	1,550	1,550
Power System	25,270	25,270
Propulsion	5,300	2,800
Safety	9,700	9,700
Materials and Manufacturing	18,000	7,000
Total	134,557	121,057

The costs mentioned in this table are given including Value Added Tax (VAT). A detailed description of the estimation of these costs is presented in the remainder of this section. It should be noted that the quality of the estimation differs for each subsystem. When little information are available on a specific part, a rough estimate is made to indicate in the range of costs.

Payload The payload that is carried by one UAV will consists of one HSI and two IR imagers. The costs of a single HSI are around €50,000 as described by Dr. Murali Jayapala of IMEC. The price of one IR imager will be approximately €9,000. [112]

Communication For the communication system, two UHFs are used, separating the commands from the ground station with the valuable data to it. The AERIS aircraft will be equipped with two antennas and the ground station will have a dish antenna. The price of the ground station dish will be included in the total ground station costs. As for the antennas on-board the UAV, this will cost approximately €8,100. [113] Additional communication subsystems are the transceiver which costs €6,637, the ADS-B receiver and compression computer that together cost €1,000. [114] [115] [116]

Flight Control The CPU, which includes the autopilot will be bought to fit the performance requirements. The basic costs are estimated on €1,000. [117] Additionally, the GPS, magnetometer, accelerometer, and gyroscopic-sensors are taken from SBG Systems and are expected to cost €100. [118] Furthermore, the flight servo controller is expected to cost €50 and the four servos cost €100 each. [119] [70]

Power System The power sources of the UAV are subdivided to include the batteries, the solar power harvesting system, and the laser power harvesting system. However to manage all these different power systems, a custom made power management system needs to be manufactured and the costs are expected to be €1,000.

Batteries Looking back in the report at Section 6.8, it can be learned that the battery weight is approximately 2.7 $[kg]$ according to [120]. The price of new generation batteries will lie around $320 - 640$ $[€/kWh]$. The batteries that are assumed to be in the UAV have an energy density of 300 $[Wh/kg]$. This estimate that the batteries will cost around $100 - 200$ $[€/kg]$. With a battery weight of 2.7 $[kg]$, this would result in a maximum battery cost of around €540.

Solar Power Harvesting The solar power harvesting systems largely consist of the actual solar panels. The costs of the solar panels are the main driver of the costs for this subsystem. As mentioned earlier, the solar panels will cover the top surface

of the wings. In Section 6.8, it is stated that the wing surface will approximately be 1.83 $[m^2]$. The price of the solar panels that will be used on-board is found to be 10 $[€/W]$. [120] This is almost equal to 5 cells. To cover 1 $[m^2]$, approximately 1020 cells are required, resulting in a price of 2,040 $[€/m^2]$. With a wing surface of 1.83 $[m^2]$, the costs of the solar panels are estimated to be €3,730.

Laser Power Harvesting The laser power harvesting device consists for a large part of the solar panels that are specifically designed for the applied wavelength. These solar panels cost 200 $[€/W]$. [121] However, this value applies to the energy that will be harvested from the sun. However, the energy inside the laser beam is much more focussed and thus contains more energy per $[m^2]$. This reduces the size of the laser panel, the estimated costs are set at €20,000.

Propulsion For the propulsion system, it is difficult to give an estimation per Watt or kilogram of engine power or weight. Looking at popular web-shops specialised on electric motors, it is fair to say that the propulsion system will cost €200. [122] Additionally to the propeller, a speed control unit of approximately €100 and an engine propeller of approximately €5,000 is needed. The price for one propeller is high, but the second one only costs half of the first since the malls have been made already.

Safety Regarding safety, it is required that an IR imager is carried on the aircraft. This will be the same device as the payload variant. Hence €9,000 should be reserved for it. Furthermore, it has been decided that an ultra lightweight parachute is brought along. The weight is roughly 0.5 $[kg]$ and costs €250. Furthermore, a small emergency beacon will be brought along including a emergency high-energy density battery. This is expected to cost €250. [10][35] Seven led lights are additionally brought along at €12.90 per piece and two smaller servos of €50 to open the hatches of the parachute. [70] [33] This sums the costs for this subsystem to be approximately €9,700.

Materials and Manufacturing The majority of AERIS is 3D-printed. This ensures that the complex shapes of the structure 'come for free'. It is roughly expected that the total manufacturing costs for two UAVs is €25,000, and for one €18,000. This is due to the fact that a custom set-up needs to be made to print the aircraft. Hereafter, the production cost are smaller for the succeeding aircraft to be printed.

Ground Segment The ground segment costs are subdivided into cost of the laser station and costs involved for the office. It is likely that the office is not near the laser station, since the laser will be located at an certain altitude and it is preferred to perform maintenance on the aircraft in a special dedicated area of the office. Furthermore, the costs for the office are estimated for the case study, however with a relatively small increase in costs, the complete Netherlands can be covered with one office space. Prices mentioned include VAT. The total prices are mentioned in Table 9.4.

Table 9.4: Total Initial Ground Station Costs

Subsystem	***Costs for One*** [€]
Laser Station	1,000,000
Office Equipment	42,000
Total	1,042,000

Laser Station This report uses a more accurate estimation of the laser system itself. Sources learn us that it an estimation of 100,000 $[€/kW]$ is accurate when updated for inflation and the maturity of technology. [123] For the 8 $[kw]$ that is required by the laser, this means that €800,000 should be reserved. Furthermore, a pointing system and a safety system to shield the laser from the rain will further increase the costs of the laser with €200,000 which sums op the total to €1,000,000.

Office Equipment Regarding the office, the major costs are involved with the rent of the location and the data storage. However, these costs will be treated in the operational costs section. The only costs that are considered here are actual physical costs such as computers and the remote flight control station. It is expected that a total of €20,000 should be reserved for computers. The remote flight control station will also cost €20,000. This includes monitors, a joystick and flight control system. Finally, other costs such as desks, chairs, and a coffee machine are estimated. The expected costs are €2,000. This sums this part for €42,000.

9.2.3. OPERATION COST

The operational costs consists of all running costs involved for this case study. These running costs are subdivided in several subsections and are the employees, energy costs, maintenance costs, and office costs. The result of the operational cost estimation is presented in Table 9.5.

Employees According to the law, it is required to have two people continuously flying AERIS. However, the law also requires that this control takes place under line of sight. Since this is not possible, it is required to have two persons working at the office at all times. Next to that, maintenance has to be performed occasionally. To be able to fly 24/7 and have people for maintenance, it is assumed that ten people is employed to perform all of these tasks. This also makes it possible to perform the maintenance while having 3 'flying shifts' of eight hours, with two people per shift without being troubled by people who

Table 9.5: Total Operational Costs per Year

Item	*Costs per Year* [€]
Employees	400,000
Energy	5,300
Maintenance	14,000
Laser Station	20,000
Office	40,000
Data Storage	3,000
Permits	0
Licences	10,000
Insurance	50,000
Total	542,300

are ill or need days of. Assuming these people get paid around €40,000 per year, the total annual costs amount to €400,000 per year. These two employees can have the responsibility over a multitude of UAVs.

Energy The energy costs are estimated by assuming the laser needs 8 [kW] of power to create a 2 [kW] laser beam. In this way, enough power is send to the batteries to charge up in four hours. The calculations show that if it is needed to charge up to four hours per day for 365 days per year, it equals to around 23,000 [kWh] per year. Assuming that the price per kWh is around €0.23, the annual costs will be €5,300. [124]

Maintenance Assuming AERIS has an operational life of five years. It is assumed that the maintenance costs are all of the initial costs of a new UAV divided over five years. It means that the maintenance is roughly €14,000 per year and allows us to practically replace one complete UAV during its operational life.

Ground Station Several costs for the ground station are running costs. These costs, for instance, involve the rent of the locations of the office and laser station and data servers. The first ten weeks of this project the location is provided by the Delft University of Technology. Hereafter, eventually this team will move the office to a location where landing the UAV is easily possible. This location allows the team to perform maintenance on the aircraft, processes the data via the data servers and even allows the team to expand. The rent for such a location is €40,000 per year. [125] Furthermore, the location of the laser station will be on top of the EWI-Faculty. This is close to the office location and is at a high altitude to increase line-of-sight communications. The rent is expected to be €20,000 per year.

Data Storage Having learned safe data transfers and storage from FOX-IT experts, the running costs for this are expected to be €3,000 per year. This provides the team with a virtual server and 50 Terra-bytes of storage. [126] [127] This allows us to store all data created by the sensors of the UAV for the case study for two years.

Permits At the moment, permits of operation are predicted to cost no money. The direct stakeholder and client is the Rijkswaterstaat and for the business roadmap, it is assumed the permits of operation are paid by this stakeholder. Obviously, the connections this governmental organisation has with the ILT is beneficial for the success of the permit request. On the other hand, relying to much on the legislation in Netherlands is a large risk so AERIS should be open minded to start operations abroad.

Licences To reduce costs for licences the team will work mostly with open source software such as python. The first year after the DSE period the Delft University licences are still free for one year when the office is on campus, but hereafter a switch needs to be made to other software. Luckily this is achievable for a relatively low cost of approximately €10,000 per year. A good 3D drawing software that allows for finite element methods to take place is Pro/ENGINEER. [128]

Insurance Currently, the insurance are estimated from the experiences of similar high-tech and high risk businesses and are hence expected to be €50,000 per year.

9.3. REVENUE MODEL

This section will elaborate on the revenue model. First the key selling points are listed that provide support to the revenue model and the clients, but also supports the five-year plan of the succeeding section. In this model all expected earnings from governmental and commercial clients are elaborated. This is done because each client type requires a different set and quality of data. This allows us to create a more tailored price for each client. First the government client type is discussed, which is succeeded by the commercial clients.

9.3.1. KEY SELLING POINTS

The key selling points are listed that support the value of the product/service provided by AERIS.

- Continuous flight: low response time and reliable

- Sustainability as integral part of the design with low noise emissions compared to regular aircraft and helicopters
- Large flight envelope
- High quality camera
- Low maintenance cost
- One UAV can be used for multiple purposes at the same time
- Payload modularity
- Broad market/applications within reach
- Scalability of design
- Multiple UAVs can operate around one ground station

9.3.2. GOVERNMENT

The government is a primary client for the AERIS project. The government allows us to perform autonomous flight with the UAV and collect useful data, and in return, the government can make use of a reduced rate for our services. The regular rate will be 780 [€/km^2] with a data delivery time of one week. For the government however, we rate 200 [€/km^2] with a data delivery time of one day. Next to that the government is given a subscription on Live Disaster Detection System (LiDDS). This system allows for direct updates in the case of an emergency. In the occasion of a detected emergency, such as an (oil) spill, wild fire, chemical leaks and floods, the government is alarmed immediately. Also our services to the government include a monthly update about the air quality, water quality (algae), ground quality, climatology and a heat map of the region. [129] Additionally, the government is allowed to reserve one UAV per day per ground station.

The annual fees, based on euros per km^2, of the government per province are presented in Table 9.6.

Table 9.6: Total Cost per Province per Year

Province	***Costs per Year*** [€]
Zuid-Holland	563,600
Noord-Holland	534,000
Zeeland	586,800
Noord-Brabant	983,800
Utrecht	477,000
Gelderland	995,000
Limburg	430,600
Overijssel	684,000
Friesland	1,149,600
Groningen	592,000
Drenthe	536,000
Total	7,532,400

9.3.3. COMMERCIAL

Commercial clients have a rate of 780 [€/km^2], with a data delivery time of one week, as stated before. To reduce this data delivery time the rate increases with 20 [€/km^2] per day sooner. For the regular rate, the client receives information on the air quality, water quality, ground quality and a heat map of the region. Furthermore, the hyperspectral data allows the client to identify mineral sources, fertile ground and information on the quality of their farmland to increase the productivity of their land. Our services allow commercial clients, such as farmers, to increase their revenue by frequent updates on their land respectively. Engineering and construction companies benefit from our services by gaining a hyperspectral insight of their construction site. Early, and continuous identification of soil type and ground quality is essential for the success of projects.

9.4. FIVE-YEAR PLAN

The five year plan gives a brief insight in the planned business activities for the following five year of the AERIS project. In the first year, AERIS expects to have a pilot project for the province of Zuid-Holland for the government. From Table 9.6, it can be learned that for the first year €563,600 is earned. Furthermore, in this first year, AERIS expects to penetrate the farmers market and attain one percent of this market. This amounts to a total of 14 farmers with an average land size of 0.26 [km^2] each. It is expected that farmers require an update at least every week, the costs involved for one farmer results in €10,400 per year and for the province the budget is €135,000 for this year.

In the second year the pilot project is expected to continue. Furthermore, the market share in the farmer industry is expected to grow from one to three percent. This means that the total revenue for the farmers in the second year is €420,000. Also, after a successful first year, the AERIS project expects to expand its horizon to the civil engineering industry by setting up a pilot project with BAM. The pilot project will be similar to the Fiber to Home project that is currently active. [130] The pilot project involves the monitoring of 360 $[km]$ in length with a minimum scanning width of 100 $[m]$ and hence results in a surface area of 36 $[km^2]$. Expecting that BAM requires the data of the sensors within three days, a rate of 860 $[€/km^2]$ is applied and the revenue amounts to €31,000 for this project.

In the third year, an expansion is foreseen for the pilot project for the government is expected. The area grows from Zuid-Holland to include Noord-Holland and Zeeland to include the most important harbour areas of the Netherlands. The revenue for this increase is €1,684,400. This implies to invest in a second laser station and UAV and for each new flying UAV ten extra employees are required. Besides this, it is expected that the market share in the farmers industry in Zuid-Holland increases to five percent. This results in a revenue of €700,000 for this year. Furthermore, the pilot project of BAM has been rounded of successfully. An increase from 1 project to 10 projects for this year is expected with a total revenue of €310,000 per year.

The fourth year the business is focussed on the expansion to covering the whole surface area of the Netherlands for the government. Since the focus is lot on this expansion, no further increase in market share and projects are expected. Hence, the total revenue for this year is the same as in year three.

For the fifth year, the growth to cover the Netherlands is complete which means in total four ground stations are active with each one UAV. After covering the complete surface area of the Netherlands, including all services that were provided in the pilot project of Zuid-Holland will result in a total revenue of €7,500,000. Currently, AERIS has a market share in the total farmers industry of the Netherlands of one percent. This equals a revenue of €1,400,000 per year. Furthermore, it is expected to double the amount of projects in the civil engineering field which will result in an expected revenue of €620,000.

The revenue and costs per year are presented in Table 9.7. The date stamp is at the end of each respective year.

Table 9.7: Total Revenue and Costs for Five Year Plan

Year [-]	***Revenue*** [€]	***Costs*** [€]	***Profit*** [€]
1	703,600	1,837,332	163,900*
2	1,014,600	539,700	474,900
3	2,694,400	2,106,775	587,625
4	2,694,400	985,700	1,708,700
5	9,520,000	4,093,850	5,426,150

*Note that the profit includes an initial investment of €1,297,632. The break even point is currently halfway year four. This same table is visualised in Figure 9.2, with the break even point at year three where the debt is zero.

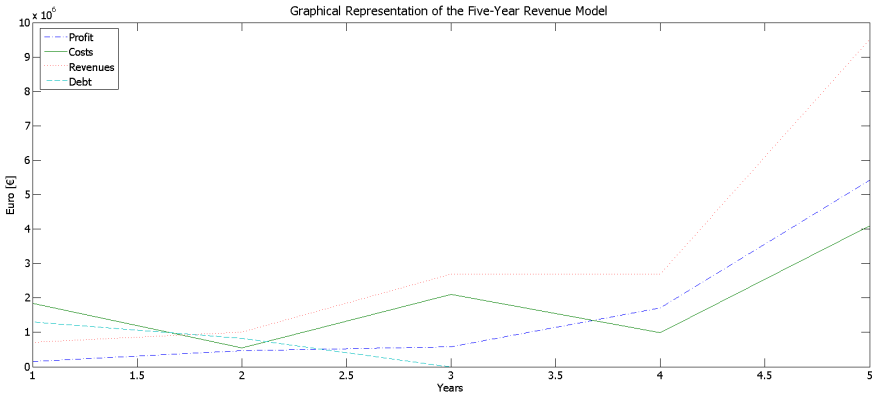

Figure 9.2: Visual Representation of the Revenue Model of the Five-Year Plan

Additionally, a project Gantt chart is provided in Figure 9.3 that visualises all milestones from the first year after the DSE towards the last day of the five-year plan. This Gantt chart distinguishes initial milestones and process and the effort of human resources for the successful completion of this project.

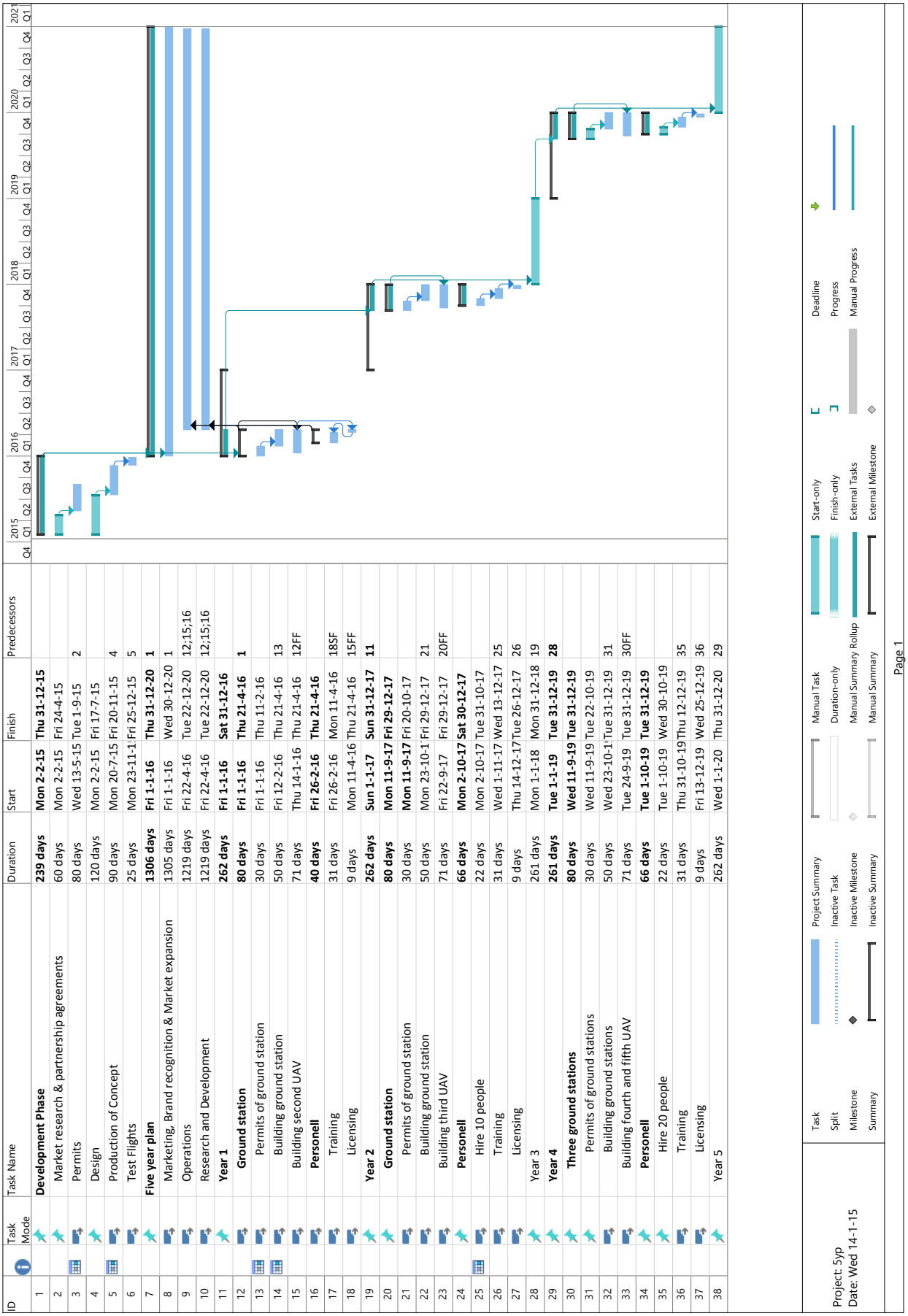

Figure 9.3: Project Gantt Chart for the Six-Year Period after the Design Synthesis Exercise

10. Discussing the Requirements

This chapter provides an overview of the requirements set to the AERIS design. Moreover, the ability of this design to comply with the set requirements as presented in Chapter 2. It should be noted that the requirements compliance is performed on requirements that are set by the AERIS project team and requirements set by the client.

The succeeding sections presents an overview of the compliance of the design to the set requirements. Requirements can either be met fully, partially or not at all. Where necessary, a discussion is present on the compliance. Apart from the requirement division based on norms and values as shown in the RDT, another division can be made. This division classifies the requirements in a more readable overview for the different design teams. This division is in line with the requirement tags presented in the RDT. In this chapter, the compliance of the requirements are discussed according to these categories. All compliance tables are structured by means of stating the identifier, requirements and the compliance respectively. Requirements marked with a "!" are client requirements.

10.1. Management Requirements

The most important requirements for the project management are presented in Table 10.1. Project management related requirements are met in full with an exception on $MG-4$ which is partially met. This requirements shall be extended and completed in full at the completion of this project. In Chapter 9 the fulfilment of requirements $MG-1$ to $MG-3$ was presented.

Table 10.1: Compliance Table on Project Management Requirements

ID	*Requirement*	*Compliance*
MG-1	Employees shall be employed for the whole mission duration	Full
MG-2	The investments shall break even within three years of operation	Full
MG-3	Services shall be within the financial reach of micro-enterprises	Full
MG-4	A manual shall be present, containing all information needed to operate the entire system	Partial

10.2. Sustainability Requirements

The requirements related to sustainable development are listed in Table 10.2. As was presented in Chapter 6 the integrated design of AERIS has been made with sustainable development as an important keystone. The results of this design on a sustainable level have been analysed further in 8.4 and concluded that at this level an significant trade-off has been made towards sustainability. Unfortunately, not all materials will be recyclable and non-toxic, such as the batteries.

Table 10.2: Compliance Table on Sustainable Development Requirements

ID	*Requirement*	*Compliance*
SUS-1	Measures shall be taken to reduce the amount of energy that is used during life-cycle	Full
SUS-2!	At least 20% of the energy used by the system shall come from renewable sources	Full
SUS-3!	The materials used shall be recyclable	Partial
SUS-4	The materials used shall be non-toxic	Partial
SUS-5	The system shall not cause any harm to wildlife	Full
SUS-6	Noise levels shall respect the norms set by environmental institutes	Full

10.3. Equipment Requirements

The requirements related to equipment and payload are displayed in Table 10.3. The requirements have been fully met.

10.4. Safety Requirements

Requirements about safety issues are addressed in Table 10.4. All safety requirements have been met, however this does not mean that it can be guaranteed no accidents shall occur. What can be said is that everything that is possible within reason is done to minimise the risk of safety threats.

Table 10.3: Compliance Table on Sustainable Development Requirements

ID	*Requirement*	*Compliance*
EQ-1	There shall be a continuous stream of data available during the entire mission	Full
EQ-2!	The UAV shall have a high-resolution hyper spectral imager on-board	Full
EQ-3	The data link shall provide sufficient data transfer to sustain a live-stream	Full

Table 10.4: Compliance Table on Safety Requirements

ID	*Requirement*	*Compliance*
SAF-1	The system shall be capable to avoid safety hazards	Full
SAF-2	The position of the system shall be known at any moment during the mission	Full
SAF-3!	The UAV shall have a fail-safe emergency landing mode in case of external power source loss	Full
SAF-4	The power available for the UAV shall not drop below a critical level, making landing on a safe location possible	Full
SAF-5!	The UAV shall have a collision avoidance system	Full
SAF-6!	The system shall be capable of recognizing weather hazardous to the operations	Full

10.5. GENERAL MISSION REQUIREMENTS

Requirements regarding the general mission profile can be found in Table 10.5. The general mission profile requirements have been met.

Table 10.5: Compliance Table on Mission Profile Requirements

ID	*Requirement*	*Compliance*
GEN-1!	In case of failure there shall always be a back-up system on stand-by	Full
GEN-2!	The system shall be capable of monitoring every part of the Netherlands	Full
GEN-3!	The operational lifetime shall be at least five years	Full
GEN-4!	Area monitoring shall be performed by a UAV	Full

10.6. SECURITY REQUIREMENTS

Requirements regarding the security of the entire system can be found in Table 10.6. This is closely related to the management requirements but with the measures taken such as encryption of code and modulation hacking of data is reduced amongst other steps described in Chapter 6. Though steps are taken and there is a level of protection, this does not give guarantees on the threats.

Table 10.6: Compliance Table on Security Requirements

ID	*Requirement*	*Compliance*
SEC-1	The system shall be protected against theft and vandalism	Full
SEC-2	Steps shall be taken to reduce the risk on system hacking	Full

10.7. GOVERNMENT REQUIREMENTS

In order to work conform government legislation, the following requirements are set as shown in Table 10.7. As described, privacy is respected by the system. Currently however the law does not allow operations of AERIS in the Netherlands. This study uses the assumption of flying with a permit granted via the Rijkswaterstaat of the ILT. Additionally, the air and ground segment respect standard levels of noise legislation to comply with the applicable laws as good as possible.

10.8. FLIGHT PERFORMANCE REQUIREMENTS

The requirements related to flight performance and flight envelope is listed in Table 10.8. All requirements have been fully met.

Table 10.7: Compliance Table on Government Requirements

ID	*Requirement*	*Compliance*
GOV-1	The system shall operate according to all relevant laws and regulations	Partial
GOV-2	The system shall respect each and everyone's privacy rights	Full
GOV-3	Stakeholder's privacy shall be respected	Full

Table 10.8: Compliance Table on Flight Performance and Flight Envelope Requirements

ID	*Requirement*	*Compliance*
FPF-1!	The UAV shall fly between 50 and 100 $[\frac{km}{h}]$	Full
FPF-2!	The operational altitude shall be within 100 and 4000 meters above sea-level	Full
FPF-3!	The UAV shall sustain continuous flight in normal operational and meteorological conditions	Full

10.9. ENERGY AND POWERHOUSE REQUIREMENTS

Energy and powerhouse requirements are given in Table 10.9. All requirements have been fully met. The remaining power is coming from additional solar cells that provide enough power to complete the energy household for the successful completion of the mission. This last table completes the compliance check of the requirements set to AERIS.

Table 10.9: Compliance Table on Energy and Powerhouse Requirements

ID	*Requirement*	*Compliance*
ENE-1!	At least 50% of the energy used on-board shall be provided by remote power beaming	Full
ENE-2!	At least 20% of the energy used on-board shall be provided by solar cells	Full
ENE-3!	Remaining power shall come from commonly of the shelf energy harvesting systems	Full

10.10. OTHER REQUIREMENTS

Other requirements are given in Table 10.10. All requirements have been fully met. These requirements have been grouped as other since they consist of requirements not grouped in earlier sections. Also there are requirements presented to the group by the initial project description that are not definitive requirements and are therefore not included in the RDT. These requirements have been directly met and other requirements in the RDT allowed us to do so.

Table 10.10: Compliance Table on Other Requirements

ID	*Requirement*	*Compliance*
GST-1!	Minimise the amount of base stations for remote power	Full
Mass!	As required to meet performance specification	Full
Size!	As required to meet performance specification	Full
Case!	Case study of an UAV performing hyperspectral monitoring of rivers and harbours in Zuid-Holland	Full
Cost!	Roadmap and budget required for bringing technology to market	Full

11. CONCLUSION

This Final Report is the last in a series of four reports describing the design synthesis of AERIS: an UAV capable of continuous flight by using remote power. It succeeds the Mid-Term Report which had considered a variety of different candidate architectures to carry out the mission. Significant progress has been made in the development of the risk strategy, functional breakdown and flow diagrams, system design, and the development of a new design tool tasked with the iterative sizing of AERIS from the subsystem level. This design tool has also been analysed in univariate and multivariate sensitivity analyses to determine the impact of the major tool inputs and hence the effect that yet undetermined errors might have on the system's design.

This project has not only considered how to design a partially laser powered, continuously flying UAV to be used for monitoring urban and natural landscapes, it has done so whilst respecting a framework of wider values which considered sustainable development as a key value. In addition to this, it has fulfilled every client requirement with the exception of requirement SUS-3: "*materials used shall be recyclable*", which was satisfied partially. AERIS started as a "prestige" project investigating the implementation of external laser power in UAV design, but analyses of Western markets showed that there are real niches which can be targeted by AERIS to satisfy the needs of several different clients over a range of different industries. This finding somewhat shifted group priorities and had a major influence on design choices. Throughout the entire project, defining the line between what was feasible and what would be practical in a commercial environment was often difficult. Implementing external laser power is a good example of this.

Reflecting on AERIS' conceptual design, external laser power seemed to pose several performance limits to the design as it is currently not well-suited to long-ranged UAV design. In addition to this, the latest market analysis shows that it would not be especially beneficial to a real design, as it might impose further unnecessary financial risk to potential investors with no outweighing advantage. It is quite clear, however, that external laser power shows a lot of promise in future smaller-ranged UAV design. Not only does it have the potential to broaden the energy mix of future aircraft, it has the ability to drastically reduce the size of those aircraft by eliminating the need of on-board power storage.

AERIS is not only ambitious because of its external power usage, it is also highly ambitious in its extreme endurance, as well as how it explores and attempts to exploit the advantages of additive manufacturing. The team not only moved away from the conventional wing-box and fuselage designs, it implemented a completely novel design technique to give the most efficient structure to bear loads whilst consuming as little material as possible and thereby keeping the weight down.

Despite the name of this report, AERIS' design is far from final. In reality, its structure requires more advanced structural analysis, which was beyond the scope of this course. In addition, significant testing to validate the aforementioned structural design approach is required. Also the justification for a reduction of the rather heavy safety factor of two for additive manufacturing should be investigated. These issues will be revisited and discussed further in Chapter 12.

12. RECOMMENDATIONS

Even though AERIS has been finalised within the scope of the DSE, several parts of the design should be investigated in more detail to fine-tune and improve the design. Most of the recommendations listed in this chapter originate from questions and remarks that arose during the this final design stage of this ten week project. This chapter is divided into several sections, which follows the structure of the N^2 chart, as presented in Figure 6.1.

12.1. SAFETY

The risks involved with the design and operations of AERIS are assessed within the scope of this project, but in order to reduce the risks and increase the reliability of the entire system, a detailed analysis of the events identified as "high-risk" should be performed with more detail. Though this might result in additional constraints, a real company's name stands or falls with the reliability of its system.

Another way to increase the quality of the product is by extensive physical testing of the final product to validate the proposed design methods. When the results of the validation tests are properly examined, it will likely become clear that some parts are heavily oversized due to overly-conservative safety margins. Hence, it might be possible to reassess safety factors and margins, once the understanding of those methods are furthered, which might eventually result in a lighter, higher performing design.

12.2. PAYLOAD

As shown in Section 6.2, several parameters influence the quality of the images obtained from the HSI. In the output estimation, it was assumed that there was perfect light reflection from the ground. However, weather influences these images greatly and will thus influence the operation of the payload - especially its shutter time. Next to this, the yet- un-modelled vibrations in flight will further affect its performance. To cope with all of these factors, an extensive research into corrective algorithms and additional integrated software will be needed to compensate for the noise and random spectral variations as well as the blur for the varying velocities and altitude settings.

12.3. COMMUNICATIONS AND GROUND STATION

From the mission analysis, as learned in Section 8.5, it was found that the limiting factor in AERIS' operational range was the range of the communication system. The system can easily cover the province of Zuid-Holland, which was necessary by the specified case study, but when one considers coverage of the entire area of the Netherlands, this becomes a problem to address. Research must be performed to determine the optimised number and location of additional communication stations. Similarly, the location(s) of ground stations for the lasers should also be investigated. Utrecht would, for example, be one of the most beneficial locations to build a laser station, as it is near the centre of the country.

The laser's performance must be analysed further to consider the laser beam's finer properties - something that was considered to be outside the scope of this project. Doing such an analysis it might show that the required laser is less powerful, that the charge range increases or that using multiple lasers with varying strength could be more sustainable or cheaper. Answering these questions would not only affect the selection of the laser to be used, and could be further influenced by season, desired charge time or weather conditions. This would also give a better indication whether or not it is advantageous to include a laser in the actual final design.

12.4. AERODYNAMICS

In order to increase the climb, roll and stall characteristics of the wing, it is beneficial to investigate the use of a twisted wing as well as the incidence angle of this wing. Wing twist implies a variation in the angle of attack along its span. By implementing wing twist, the wing will first stall at the root, whilst the flaperons would operate in acceptable conditions, keeping the UAV controllable, and giving the complete wing better stall characteristics.

12.5. PROPULSION

Looking back at the design, further investigation regarding engine efficiency and mechanical losses is suggested. The values used in this design are probably optimistic because some minimal losses due to friction are not taken into account.

When the design converged, the propeller had a diameter of one meter at a low RPM. The impact of a propeller of this size on both the *Park* 450 and *Power* 15 engine - are both relatively small engines - has not yet been investigated. [82] [83] It is strongly recommended to calculate the effect of the propeller on these engines, as they might even fail due to high torques due to the inertia of the propeller.

Validating the power usage of the engines thoroughly by performing validation tests on a real scale model of the propeller is also advised. This, combined with the previously mentioned research concerning engine efficiencies should result in a more realistic engine and propeller design.

12.6. POWER SUBSYSTEM

One of the key assumptions made during the calculation of the solar power percentage in the power subsystem sizing script was the negligence of the angle of incidence of the solar rays on the solar panel surface. It was assumed that it always hit the solar panel with a $\pm$ five $[deg]$ at 90 $[deg]$, this made sure that full use was made of the energy and the efficiency of the solar cells was 25%. [9] In real life, the Sun and AERIS will continuously move and therefore the angle is a space-time function. This will most likely decrease the amount of generated solar power and the percentage will drop. Further analysis needs to be performed to check if AERIS still meets the requirements. Furthermore, research needs to be performed to verify the location of the laser panel. This panel requires a lot of relatively thick and heavy cables to be on-board, so it might be beneficial to relocate them to other parts of the aircraft.

12.7. STRUCTURES

One of the points of interest of the structural design of AERIS is the combination of titanium and ABS used to manufacture the wing and fuselages. For now, stress concentrations are reinforced with titanium, while parts under lower loads are made out of ABS. A more thorough analysis, however, might result in an even lighter structure. As titanium is extremely strong, it might be beneficial to use titanium to withstand the shear flow, where the area moments of inertia are of secondary importance and strength normalized to thickness is the driving parameter. To withstand buckling, where the area moment of inertias are strongly influencing the performance of the structure, ABS would could be used to create a sufficiently strong structure.

Apart from the division between titanium and ABS, it is also recommended to investigate a wider range of materials, following the approach used for AERIS whilst implementing the above recommendations. It is likely that there are materials that can be optimally combined in such a way that the total design becomes even lighter. Exploring and then exploiting the relationship between material density and load bearing capability is one of the keys to solving this problem.

Finally, to make sure the structure is able to take the expected loads, it is highly recommended to validate the model by performing extensive real tests on those structures. Tests concerning flutter and fatigue as well as failure due to all failure modes considered in Section 6.9 are also necessary steps to be taken well before considering AERIS' actual production.

12.8. STABILITY

Whilst designing the tail, it became clear that the optimum size of both the horizontal and vertical tail planes required to attain stability and controllability was extremely small. This is because the range in centre of gravity is relatively small - the payload is fixed - and because the push-propeller configuration has strong stabilizing effect on the UAV. The double fuselage configuration is beneficial for the lateral stability as well. To optimize the design, it is therefore recommended to analyse the influence of different tail configurations. As the tail is over-designed, it might be beneficial to decrease the fuselage mass by reducing its length might as it can significantly decrease the total weight as well.

BIBLIOGRAPHY

[1] F. A. Internationale, *Flight endurance record,* http://www.fai.org/fai-record-file/?recordId=16052.

[2] J. Talbot and M. Jakeman, *Security Risk Management: Body of Knowledge* (John Wiley & Sons, Inc., Publication, 2009).

[3] ISO, *ISO 31000 - Risk Management*, Standards (International Organization for Standardization, 2009).

[4] I. L. en Transport Ministerie Infrastructuur en Milieu, *Informatiebulletin lichte onbemande luchtvaartuigen informatiebulletin: lichte onbemande luchtvaartuigen,* www.ilent.nl (2013).

[5] DSE Group 4, *Mid-Term Report: AERIS - Remote Powered UAV*, Tech. Rep. (Delft University of Technology: Faculty of Aerospace Engineering, 2014).

[6] T. Nugent and J. Kare, *Laser Power for UAVs - Power Beaming for UAVs*, Tech. Rep. (LaserMotive White Paper, 2010).

[7] B. DeHoff, D. J. H. Levack, and R. E. Rhodes, *The functional breakdown structure (fbs) and its relationship to life cycle cost,* in *45th AIAA/ASMEJSAE/ASEE Joint Propulsion Conference*, American Institute of Aeronautics and Astronautics (NASA Center for Aerospace Information (CASI), Denver, Colorado, 2009).

[8] R. Mason, *Feasibility of Laser Power Transmission to a High-Altitude Unmanned Aerial Vehicle*, technical report (RAND Corporation, 2011).

[9] Alta Devices, *Technology brief; single solar cell,* http://www.altadevices.com/pdfs/single_cell.pdf (2014).

[10] F. Chutes, *Iris ultra parachute,* http://fruitychutes.com/buyachute/iris-ultra-chutes-30-to-192-c-18/iris-ultra-72-standard-parachute-28lbs-20fps-p-143.html?zenid=X-RTo2zA8BpHSCUN88Rx82 (2014).

[11] The Brundtland Commission, *Our common future,* in *The Report of the World Commission on Environmental Development* (Oxford University Press, Oxford, 1987).

[12] Ecolizer, *Ecolizer,* Booklet; Design Tool (2011).

[13] S. T. Seljebotn, *Continuous autofocus for line scanning hyperspectral camera,* http://urn.kb.se/resolve?urn=urn:nbn:no:ntnu:diva-21101 (2012).

[14] HySpex, *Hyperspectral imaging,* http://www.hyspex.no/hyperspectral_imaging/ (2014).

[15] D. Litwiller, *Ccd vs. cmos: Facts and fiction,* https://www.teledynedalsa.com/public/corp/Photonics_Spectra_CCDvsCMOS_Litwiller.pdf (2001).

[16] Imec, *Hyperspectral imaging by imec,* http://www.imec.be (2014).

[17] Edmund Optics, *Infrared products,* http://www.edmundoptics.com/products/.

[18] FLIR, *Uncooled core,* http://www.flir.com/cvs/cores/view/?id=54717&collectionid=612&col=54727 (2015).

[19] Satellite Imaging Corporation, *Satellite imaging corporation,* http://www.news.satimagingcorp.com (2010).

[20] M. A. Kolodnor, *An automated target detection system for hyperspectral imaging sensors,* Johns Hopkins Applied Technical Digest **27** (2007).

[21] G. A. Shaw and H. hua K. Burke, *Spectral imaging for remote sensing,* Lincoln Laboratory Journal (2003).

[22] CAP Advanced Technologies, *Hyperspectral and high-resolution imagery,* https://tests.capnhq.gov/ops/archer_training/archer_hsi_tech/Hyperspectral%20&%20High%20Resolution%20Imagery.cfm (2015).

[23] e. a. Carol L. Jones, Paul R. Weckler, *Estimating water stress in plants using hyperspectral sensing,* The Society for engineering in agricultural, food, and biological systems (2004).

[24] P. Shippert, *Introduction to hyperspectral image analysis,* Online Journal of Space Communication (2013).

[25] HobbyKing, *Gimbal,* http://www.hobbyking.co.uk/hobbyking/store/__55238__Quanum_Q_2D_Brushless_GoPro_3_Gimbal_suitable_for_Nova_Phantom_QR_X350_and_others_.html (2014).

[26] H. Loewen, *Isolating components from uav vibration,* MicroPilot (2013).

[27] D. Letexier and S. Bourennane, *Noise removal from hyperspectral images by multidimensional filtering*, IEEE Transactions on Geoscience and Remote Sensing **46** (2008).

[28] WeatherSpark, *Weather data from weatherspark*, http://www.weatherspark.com (2014).

[29] M. Voskuijl, *Flight and orbital mechanics*, https://blackboard.tudelft.nl (2014).

[30] Tadiran Batteries, *Tadiran batteries: Better by design*, http://www.tadiranbat.com/index.php/tadiran-batteries-better-by-design (2014).

[31] HobbyKing, *Turnigy nano-tech 3000mah 4s 25 50c lipo pack*, http://www.hobbyking.com/hobbyking/store/uh_viewItem.asp?idProduct=11920 (2015).

[32] Federal Aviation Authority, *Aeronautics and Space: Part 25*, Federal Aviation Authority, 800 Independence Avenue Southwest (2014).

[33] Led-Tech Optoelectronics, *Avago moonstone tri-color power led*, http://www.led-tech.de/en/High-Power-LEDs/Avago-High-Power/Avago-Moonstone-Tri-Color-Power-LED-LT-1511_55_150.html (2015).

[34] Aircraft Spruce and Specialty Co., *Aircraft spruce; everything for planes and pilots.* http://www.aircraftspruce.com/catalog/avpages/kannad406compact.php (2015).

[35] Trax, *Trax gps tracker*, https://traxfamily.zendesk.com/hc/en-gb/articles/200310982-Tracker-specifications (2015).

[36] Koninklijk Nederlands Meteorologisch Instituut, *Klimatologie: uurgegevens van het weer in nederland*, http://www.knmi.nl/climatology/daily_data/selection.cgi (2014).

[37] S. Mithun.K.Thankappan, *Safety margin in aerospace*, Journal of Spacecraft and Rocket **34** (1997).

[38] Dr. Mircea Calomfirescu and Dr. Holger Hickethier, *Damage tolerance of composite structures in aircraft industry*, Presentation (EADS Defence and Security; Military Air Systems (MAS) Manching, Germany, 2010).

[39] UAV Navigation, *Uav navigation*, http://www.uavnavigation.org (2015).

[40] S. Prasad, L. Bruce, and J. Chanussot, *Advances in Signal Processing and Exploitation Techniques*, Vol. 3 (Springer, 2011).

[41] Intel, *Overview of nucboard from intel*, http://ark.intel.com/products/76975/Intel-NUC-Board-D54250WYB (2014).

[42] Tucson Amateur Packet Radio Corp, *Fresnel zone clearance*, http://www.tapr.org/ve3jf.dcc97.html (2005).

[43] i. CelPlan International, *Availability of wireless signal*, http://www.celplan.com/resources/presentations/CelPlan-SmartGridWirelessDesign.pdf (2013).

[44] R. Coude, *Coveragemap*, http://cplus.org/rmw/rmonline.html.

[45] J.-C. Etiemble, *Airfoils*, http://tracfoil.free.fr/airfoils/h.htm (2015).

[46] M. S. Selig and A. Gopalarathnam, *New airfoils for r/c sailplanes*, http://m-selig.ae.illinois.edu/uiuc_lsat/saAirfoils.html (1997).

[47] Ir. D. Steenhuizen, *Aerospace design and systems engineering elements ii ae2101, wing design part 2*, https://blackboard.tudelft.nl (2015).

[48] P. Murphy, *Wingtip Design for a solar aircraft*, Tech. Rep. (Imperical College of Science, Technology and Medicine, 2012).

[49] M. Sadraey, *Aircraft Performance Analysis* (Daniel Webster College, 2009).

[50] *Performance of propellers*, (2015).

[51] P. Sforza, *Theory of aerospace propulsion*, Elsevier Science and Technology , 704 (2011).

[52] E. P. Hartman and D. Biermann, *THE AERODYNAMIC CHARACTERISTICS OF FULL-SCALE PROPELLERS HAVING 2, 3, AND 4 BLADES OF CLARK Y AND R. A. F. 6 AIRFOIL SECTIONS The aerodynamic characteristics of full-scale propellers having 2,3 and 4 blades of clark y and R.A.F. 6 airfoil sections*, Tech. Rep. (NASA, 1938).

[53] R. Eppler and M. Hepperle, *A procedure for propeller design by inverse methods,* http://www.mh-aerotools.de/company/paper_1/epplerhepperle.htm (1984).

[54] E. L. Williams and Dr. I. Turner, *Composite materials and helicopter rotor blades,* http://classroom.materials.ac.uk/caseRoto.php (2015).

[55] ACP Composites, *Composite properties,* http://www.acpsales.com/upload/Mechanical-Properties-of-Carbon-Fiber-pdf (2014).

[56] Hexcel Composites, *Hexweb honeycomb attributes and properties,* http://www.hexcel.com/Resources/DataSheets/Brochure-Data-Sheets/Honeycomb_Attributes_and_Properties.pdf (1999).

[57] Dr.ir. G. La Rocca, *Systems Engineering and Aerospace Design: Weight estimation and iterations in a.c design and Aircraft balance*, Tech. Rep. (Delft University of Technology, 2012).

[58] Dr.ir. G. La Rocca, *Systems Engineering and Aerospace Design: Requirement Analysis and Design principles for A/C stability & control (Part 1) Requirement Analysis and Design principles for A/C stability & control (Part 1) Requirement Analysis and Design principles for A/C stability & control Part 1*, Tech. Rep. (Delft University of Technology, 2012).

[59] Dr.ir. G. La Rocca, *Systems Engineering and Aerospace Design: Requirement Analysis and Design principles for A/C stability & control Part 2*, Tech. Rep. (Delft University of Technology, 2012).

[60] E. Torenbeek, *Syntheis of Subsonic Airplane Design*, Technical Report (Delft University of Technology, 1982).

[61] Power Electronics, *Solar impulse,* http://powerelectronics.com/solar/powered-sun-solar-impulse-takes-flight?page=1.

[62] Custom Thermoelectric, *Teg specification sheet,* http://www.customthermoelectric.com/powergen/pdf/2411G-7L31-15CX1_20140508_spec_sht.pdf (2014).

[63] Oxis Energy, *Lithium sulfur battery,* http://www.oxisenergy.com/ (2014).

[64] Y. Mikhaylik, *High energy rechargeable li-s cells for ev application. status, challenges and solutions,* ECS Transactions **25**, 4 (2010).

[65] ASTM International, *Standard specification for standard nominal diameters and cross-sectional areas of awg sizes of solid round wires used as electrical conductors,* http://www.astm.org/Standards/B258.htm (2002).

[66] T. W. T. Gornet, *History of additive manufacturing*, State of the Industry (Wohlers Associates, 2011).

[67] Senvol, *Material search,* http://senvol.com/5_material-search/ (2015).

[68] T. Megson, *Aircraft Structures for Engineering Students*, 5th ed. (Butterworth-Heinemann, 2012).

[69] C. Kassapoglou, *Structural Analysis and Design*, Tech. Rep. Slides 1-11 (TU Delft, 2013).

[70] Hyperflight, *Servos & accessories - mks servos,* http://www.hyperflight.co.uk/products.asp?cat=Servos+%26+Accessories&subcat=MKS+Servos (2015).

[71] M. Sadraey, *Aircraft Design: A Systems Engineering Approach*, 1st ed. (Wiley Publications, 2012).

[72] Wikimedia, *Laser schematics,* http://commons.wikimedia.org/wiki/File:Laser.svg (2014).

[73] Wikipemia, *Stimulated emission,* http://commons.wikimedia.org/wiki/File:Stimulated_Emission.svg (2014).

[74] RP Photonics, *Coherence and laser light,* http://www.rp-photonics.com/coherence.html (2015).

[75] A. E. Siegman, *Lasers* (University Science Books, 1986).

[76] Wikipedia, *Laser wavelenghts,* http://en.wikipedia.org/wiki/Laser#mediaviewer/File:Commercial_laser_lines.svg (2014).

[77] TRUMPF, *Trudisk laser,* http://www.us.trumpf.com/en/products/laser-technology/products/solid-state-lasers/disk-lasers/trudisk.html (2014).

[78] I. I. Kim, B. McArthur, and E. Korevaar, *Comparison of laser beam propagation at 785 nm and 1550 nm in fog and haze for optical wireless communications,* http://http://www.ece.mcmaster.ca/~hranilovic/woc/resources/local/spie2000b.pdf (2002).

[79] Burle Industries Inc., *electro-optics handbook* (Burle Industries Incorporated, 1974).

[80] BAE Systems, *Laser tracking system lts 2000,* http://esdradar.com/brochures/LTS%202000.pdf (2015).

[81] LaserMotive Inc., *Laser Power Beaming Fact Sheet*, White Paper (LaserMotive Inc., 2015).

[82] E-flite, *Park 450 brushless outrunner motor,* http://www.e-fliterc.com/Products/Default.aspx?ProdID=EFLM1400 (2015).

[83] E-flite, *Power 15 brushless outrunner motor,* http://www.e-fliterc.com/Products/Default.aspx?ProdID=EFLM4015A (2015).

[84] Modern Analyst, *Four fundamental methods of requirement verification,* http://www.modernanalyst.com/Careers/InterviewQuestions/tabid/128/ID/1168/What-are-the-four-fundamental-methods-of-requirement-ve aspx (2015).

[85] R. Hibbeler, *Mechanics of Materials*, 8th ed., edited by S. Fan, Appendix C (Pearson, 2011).

[86] X Plane, *X plane flight simulator,* http://www.x-plane.com/desktop/home/ (2015).

[87] D. A. Tortorelli and P. Michaleris, *Design sensitivity analysis: Overview and review,* Inverse Problems in Engineering **1** (1994).

[88] J. W. Chinneck, *Practical Optimization: a Gentle Introduction* (Carleton University, 2007).

[89] C. Velds, *Zonnestraling in nederland,* (1992).

[90] P. Nyeste and M. S. Wogalter, *On adding sound to quiet vehicles,* Proceedings of the human factors and ergonomics society , 1747 (2008).

[91] M. Robbins, *The effectiveness of emergency vehicle audio warning systems,* Proceedings of the Human Factors and Ergonomics Society **39**, 1004 (1995).

[92] F. Farassat, *Linear acoustic formulas for calculation of rotating blade noise,* AIAA Journal **19**, 1122 (1981).

[93] A. Filippone, *Aircraft noise prediction,* Progress in Aerospace Sciences **68**, 27 (2014).

[94] Havenbedrijf Rotterdam, *Port of rotterdam,* http://www.portofrotterdam.com/de/Hafen/Pages/terminals-und-ladung.aspx (2014).

[95] N. L. Wilson, *Hyperspectral imaging for bottom type classification and water depth determination,* Master's thesis, Rochester Insitute of Technology (2000).

[96] Google, *Google maps,* http://maps.google.com (2015).

[97] L. H. Spangler, *A shallow subsurface controlled release facility in bozeman, montana, usa, for testing near surface co2 detection techniques and transport models,* Environmental Earth Sciences (2009).

[98] G.Vermeulen, *Privacy en Strafrecht* (Maklu-uitgevers N.V., 2007).

[99] ReliaSoft Corporation, *Reliability engineering,* http://www.weibull.com/basics/reliability.htm (2014).

[100] O'Connor and D. Patrick, *Practical Reliability Engineering*, 4th ed. (John Wiley & Sons, New York, 2002).

[101] Federal Aviation Administration, *System Safety Handbook* (U.S. Department of Transportation, 2013).

[102] Blanchard and S. Benjamin, *Logistics Engineering and Management*, 4th ed. (Prentice-Hall, Inc., 1992).

[103] AZoM Staff Writers, *Optical coherence tomography (oct) for industrial ndt (non-destructive testing),* AZOM Materials (2013).

[104] AECOM, *Aecom,* http://www.aecom.com/What+We+Do/Environment/Market+Sectors/Government (2015).

[105] Province of Zuid-Holland, *Zuid-holland milieu,* http://www.zuid-holland.nl/onderwerpen/milieu/ (2014).

[106] H. Lange, *Europa voldoet niet aan eigen normen voor waterkwaliteit,* http://www.prnewswire.co.uk/news-releases/europa-voldoet-niet-aan-eigen-normen-voor-waterkwaliteit-201022961.html (2013).

[107] B. Fraters, B. Beijen, G. Brandsma, H. van Rijswick, J. Reijs, E. Buis, and M. Hoogeveen, *Optimalisatie van het Basismeetnet van het Landelijk Meetnet Effecten Mestbeleid*, Tech. Rep. (RIVM, 2012).

[108] Precisionhawk, *Product & pricing,* (2014), e-mail received from Precisionhawk.

[109] Teal Group, *Teal group predicts worldwide uav market will total $91 billion in its 2014 uav market profile and forecast,* http://www.tealgroup.com/index.php/about-teal-group-corporation/press-releases/118-2014-uav-press-release (2014).

[110] Precision Hawk, *Precision hawk,* http://precisionhawk.com/index.html (2014).

[111] W. Communication, *Tu delft's ambulance drone drastically increases chances of survival of cardiac arrest patients,* http://www.tudelft.nl/en/current/latest-news/article/detail/ambulance-drone-tu-delft-vergroot-overlevingskans-bij-hartstilstand-drastisch/ (2014).

[112] Conrad, *Warmtebeeldcamera,* https://www.conrad.nl/nl/flir-flir-e60-incl-wifi-nieuw-model-met-msx-functie html (2015).

[113] Space Quest, *Communication product price list,* http://static.squarespace.com/static/53fb871ce4b02e1724b07963/t/53fc1953e4b00c4d1bfc8f8d/1409030483463/SpaceQuest+Price+List+2014.pdf (2014).

[114] UAV Navigation, *Uav avionics accessoires: Telem06v,* http://uavnavigation.org/shop/index.php?id_category=18&controller=category (2015).

[115] Sagatech, *Sagatech: Unmanned ads-b solutions,* http://www.sagetechcorp.com (2015).

[116] Intel, *Intel® nuc board d53427rke,* http://ark.intel.com/compare/71620,74484,76975 (2015).

[117] UAV Navigation, *Vector autonomous flight control unit,* http://www.uavnavigation.org/products/uav-autopilot-vector (2015).

[118] SBG Systems, *Miniature high performance ellipse series: Miniature, high performance, inertial sensors,* http://www.sbg-systems.com/docs/Ellipse_Series_Leaflet.pdf (2015).

[119] Pololu: Robotics and Electronics, *Rc servo controllers,* https://www.pololu.com/category/12/rc-servo-controllers (2015).

[120] S. Jaffe, *Next-generation batteries: Problems and solutions,* http://www.batterypoweronline.com/main/blogs/next-generation-batteries-problems-and-solutions/ (2014).

[121] G. Flamand, *High-efficiency multijunction solar cells for Concentrator PV applications*, Tech. Rep. (Technical University, Lyngby, Denmark, 2009).

[122] Neumotor, *Neumotor webshop,* http://www.neumotors.com/Store/page1/page1.html (2014).

[123] G. Verhaeghe, *The fibre laser - a newcomer for material welding and cutting,* http://www.twi-global.com/technical-knowledge/published-papers/the-fibre-laser-a-newcomer-for-material-welding-and-cutting-au (2005).

[124] Milieu Centraal, *Energieprijzen,* http://www.milieucentraal.nl/themas/energie-besparen/gemiddeld-energieverbruik-in-huis/energieprijzen (2014).

[125] Funda in business, *Office space,* http://www.fundainbusiness.nl/kantoor/delft/object-48296612-rotterdamseweg-388-f/fotos/ (2015).

[126] T. de Boer, *Employee at fox-it,* (2014), personal conversation.

[127] Trans ip, *Transip,* https://www.transip.nl/ (2014).

[128] PTC, *Pro/engineer wildfire 5.0,* http://www.ptc.com/community/landing/wf5.htm (2015).

[129] B. van Zonneveld, *Hyperspectrale camera verovert industrie,* http://www.technischweekblad.nl/hyperspectrale-camera-verovert-industrie.307735.lynkx (2013).

[130] BAM Infratechniek, *Fiber to the home valkenswaard en veldhoven,* http://www.baminfratechniek.nl/projecten/fiber-to-the-home-valkenswaard-en-veldhoven?vnc=4f8dadc715ff6f2ce14139e3454c3875&vnp=12 (2014).

A. Risk Matrix

				Consquence ->				
			People	Minor skills impact	Minor impact to capability	Unavailability of core skills affecting services	Unavailability of critical skills or personnel	Protracted unavailability of critical skills/people
				Protracted unavailability of critical skills/people	Injury requiring treatment by medical practitioner	Major injury / hospitalization	Single death and/ or multiple major injuries	Multiple deaths
			Information	Compromise of information otherwise available in the public domain	Minor compromise of information sensitive to internal or subunit interests	Compromise of information sensitive to this organization's operations	Compromise of information sensitive to organizational interests	Compromise of information with significan ongoing impact
			Property & Equipment	Minor damage or vandalism to asset	Minor damage or loss of <5% of total assets	Damage or loss of <20% of total assets	Extensive damage or loss of <50% of total assets	Destruction or complete loss of >50% of assets including intellectual proporty
			Reputation	Local mention only. Quickly forgotten. Freedom to operate unaffected. Self improvement review required.	Scrutiny by Executive, internal committees or internal audit to precent escalation. Short term local media concern. Some impact on local level activities.	Persistent national concern. Scrutiny required by external agencies. Long term "brand" impact.	Persistent intense national public, political, and media scrutiny. Long term "brand" impact. Major operations severely restricted.	International concern, Governmental Inquiry or sustained adverse national/international media. "Brand" significantly affect organizational abilities.
			Financial	1% of Project or Organizational annual budget	2-5% of Project or Organizational budget.	5-10% of Project or Organizational budget.	>10% of Project or Organizational budget.	>30% of Project or Organizational budget.
			Capability	Minimal impact of noncore business operations. The impact can be dealt with by routine operations.	Some impact on business areas in terms of delays, systems quality but able to be dealt with at operational level	Impact on the organization resulting in reduced performance such that targets are not met. Organizations existence is not threatened, but could be subject to significant review or changed ways of operations	Breakdown of key activites leading to reduction in performance (e.g., service delays, revenu loss, client dissatisfaction, legislative breaches). Survival of the project/activity/organization is threatened.	Critical failure(s) preventing core activities from being performed. The impact threatens the survival of the project or the organization itself.
Likelihood ->	Qualitative Likelihood	Quantitative Likelihood		Insignificant	Negligible	Moderate	Major	Extensive
	Is expected to occur in most circumstances	Has occurred on an annual basis in this organization in the past or circumstances are in train that will cause it to happen	Almost Certain	6	7	8	9	10
	Will probably occur in most circumstances	Has occurred in the last few years in this organization or has occurred recently in other similar organizations or circumstances have occurred that will cause it to happen in the next few years	Likely	5	6	7	8	9
	Might occur at some time	Has occurred at least once in the history of this organization or is considered to have a 5% chance of occuring in the next few years	Possible	4	5	6	7	8
	Could occur at some time	Has never occurred in this organization but has occurred infrequently in other similar organizations or is considered to have a 1% chance of occurring in the next few years	Unlikely	3	4	5	6	7
	May occur only in exceptional circumstances	Is possible but has not occurred to date in any similar organization and is considered to have very much less than a 1% chance of occurring in the short term	Rare	2	3	4	5	6

Very High (VH)	Immediate action required by the Executive with detailed planning, allocation of resources, and regular monitoring
High (H)	High risk, senior management attention needed
Medium (M)	Management responsibility must be specified
Low (L)	Monitor and manage by routine procedures
Very Low (VL)	Managed by routine procedures

Figure A.1: General Risk Matrix used for Risk Assessment [2]

B. TECHNICAL DRAWINGS

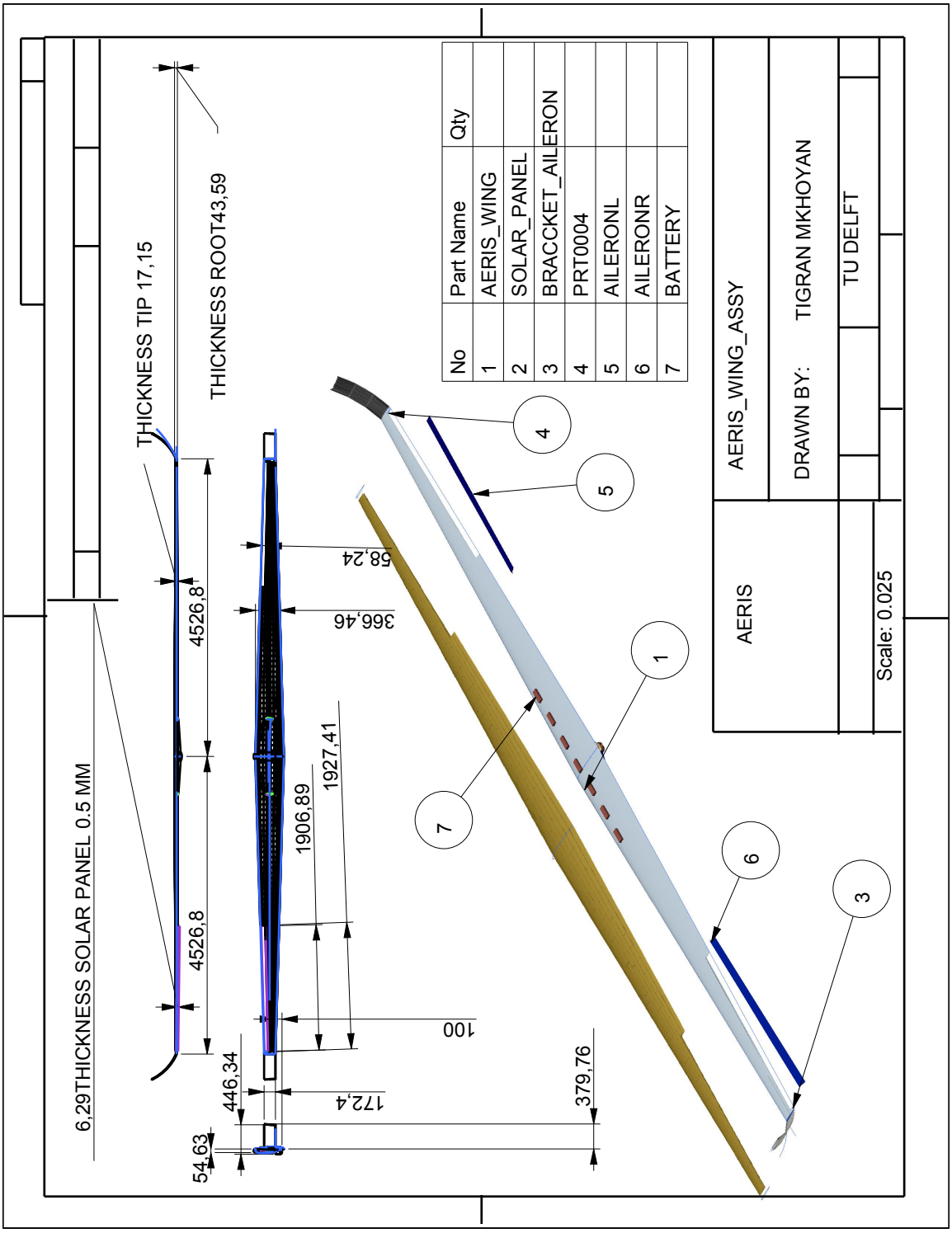

Figure B.1: Technical Drawing of AERIS' Main Wing

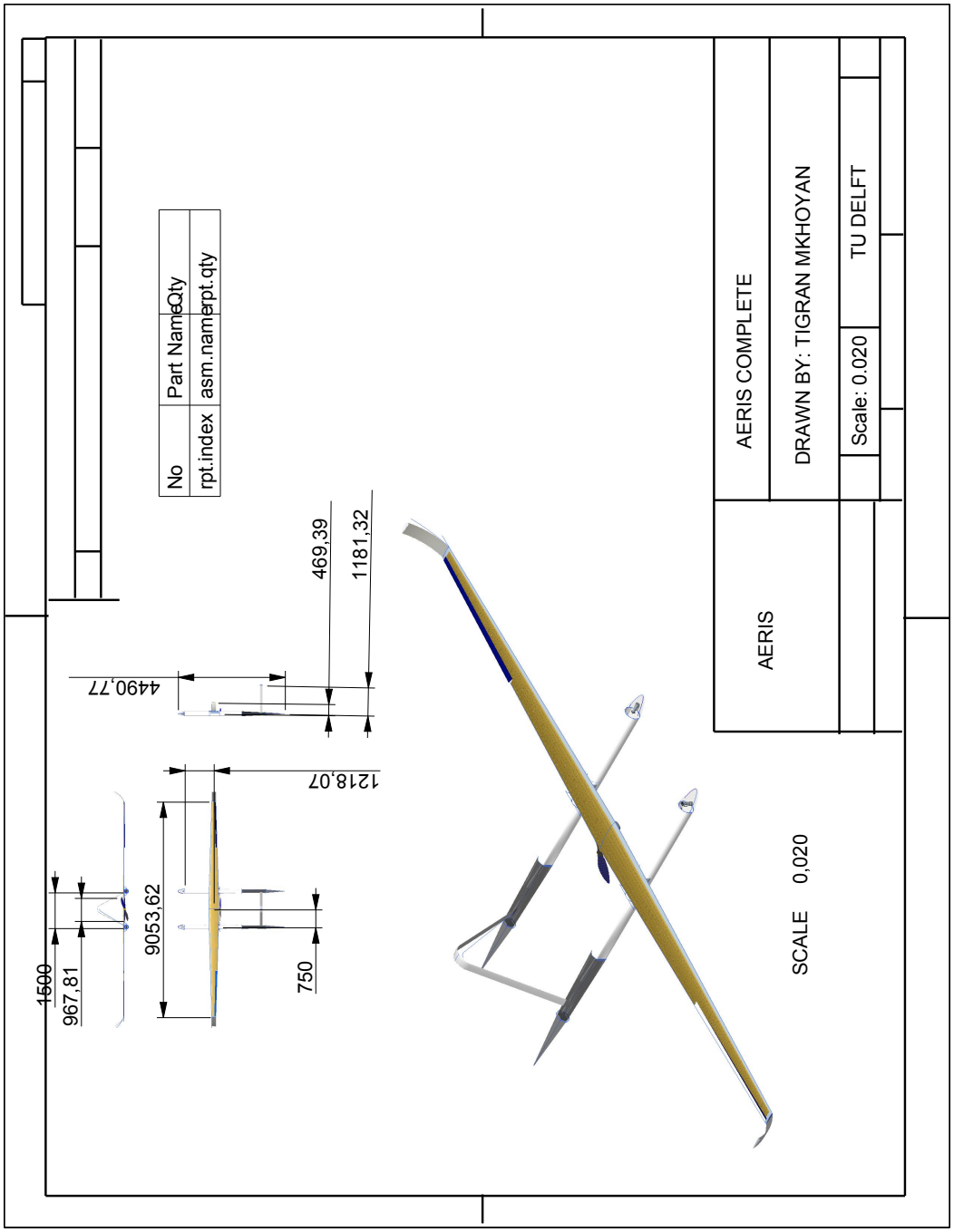

Figure B.2: Technical Drawing of AERIS' Configuration